

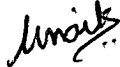
To

Maa, Pappa and Baba

DECLARATION

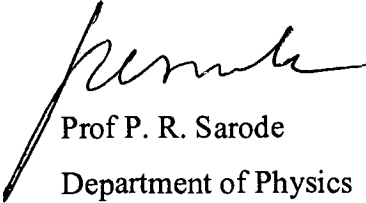
The author, hereby declares that the piece of work presented in this thesis has been carried out by her and that it has not been submitted to any other University or Institution for the award of degree, a diploma or a certificate.

Place: Goa University
Date: 29th May 2009


Ms. Miskil Sachidanand. Naik

CERTIFICATE

I hereby certify that the above Declaration of the candidate, Ms. Miskil Sachidanand. Naik is true and that this thesis represents her independent work.


Prof P. R. Sarode
Department of Physics
Goa University, Goa.

ACKNOWLEDGEMENT

I am deeply grateful to my supervisor, Professor P.R. Sarode, Department of Physics, Goa University, Goa, for the guidance and the freedom to work. His constructive comments, and constant support throughout my research work helped me to complete my work within the time limit.

I would like to express my deep and sincere thanks to Professor R. B. Prabhu for valuable discussion, and spending time to go through the results at every step and his fatherly advice in the progress of my research work.

My thanks go to Prof. J. A. E. Desa, Department of Physics, Goa University, Goa, for his valuable suggestions during entire course of my research work.

I thank Dr. K. R. Priolkar, Senior Lecturer in Physics Department, Goa University, Goa for his valuable advice and friendly help.

My sincere thanks are due to Dr. R.V. Pai, Reader in Physics, Goa University, Goa and Dr. D. V. Borole, Scientist, National Institute of Oceanography for their excellent advice during my research work.

I am grateful to Prof. S. N. Bhatia, Physics Department, Indian Institute of Science, Mumbai and his students and Dr. N. Y. Vasantacharya, Solid State and Structural Chemistry Unit, Indian Institute of Science, Bangalore for providing and helping me in carrying out four probe resistivity measurements at low temperature.

I express my thanks to the Principal and Management of Dhempe College of Arts and Science, Miramar, Goa, for their kind cooperation.

I also express my thanks to Mrs. Sunita Prabhu and Mrs. Mangala Sarode for their moral support and encouragement throughout my research work.

I wish to extend my warmest thanks to my fellow research colleagues Dr. Efrem D'sa, Dr. Preeti Bhoje, and my college colleagues Mr. Sandeep Burye, Mrs. Swati Pawar and Mr. Ram Murthy, for their cooperation.

I would like to thank my uncle, Professor Manguesh G. Korgaonkar, and his family for being kind enough to help me during my stay at I.I.T, Mumbai.

I also wish to thank my parents, and my father in law who taught me the value of hard work by their own example. They rendered me enormous support during the whole tenure of my research.

I also express my thanks to my brother Mr. Gopal Korgaonker and his family for their understanding throughout the course of this work.

Last, but not least I owe my thanks to my husband Mr. Sachidanand Naik for his patient love, inspiration and moral support. Also I owe my daughter Diya for showing patience at the time when she needed my company most. Without their understanding it would have been impossible for me to finish this work.

Finally, I would like to thank all whose direct and indirect support helped me completing my thesis in time.

29th May 2009

Ms. Miskil Sachidanand Naik

Contents

Chapter 1

Introduction

1.1	History of Superconductors	2
1.2	High T_c Cuprates	7
1.3	Crystal and Electronic Structure of Cuprates	9
1.4	Mott Insulator and Magnetism	14
1.4.1	Superconductivity of the Doped Mott Insulator	17
1.5	Various Phases of Cuprates	18
1.6	Charge Stripes in Cuprate Superconductor	21
1.7	Pseudogap in Cuprate Superconductor	24
1.8	Applications of High T_c Superconductors	26
1.9	Scope of Present Work	27
	References	31

Chapter 2

Experimental Technique

2.1	Method of Preparation of Cuprate Compounds	36
2.2	X-ray Diffraction (XRD) Techniques	37
2.2.1	Principle of Powder Diffraction	37
2.2.2	Experimental Set-up for X-ray Diffraction	37
2.3	Iodometric Techniques	42
2.3.1	Determination of the δ value in $YBa_2Cu_3O_{7.8}$ by Iodometric Titration	42
2.3.2	Experimental Procedure	44
2.3.3	Estimation of Oxygen Content	44
2.4	Four Probe Resistivity Measurement	45
2.5	Thermoelectric Power	47
	References	51

Chapter 3

Role of Zn Substitution in $\text{YBa}_2\text{Cu}_3\text{O}_{7-\delta}$ System

3.1	Relevance of Substitution	53
3.2	Structure of $\text{YBa}_2\text{Cu}_3\text{O}_{7-\delta}$	54
3.3	General Consideration of Substitutions	59
3.4	Effect of Zn impurity on Y123 system	60
3.5	Results and Discussion	63
	3.5.1 X-ray Diffraction and Iodometric Titration	63
	3.5.2 Electrical Resistivity	70
	3.5.3 Correlation of T_c with ρ_0 and dp/dT	82
3.6	Conclusion	83
	References	85

Chapter 4

Codoping Effect of Pr and Zn in $\text{YBa}_2[\text{Cu}_{1-y}\text{Zn}_y]_3\text{O}_{7-\delta}$ System

4.1	Introduction	91
4.2	Combined effect of Pr and Zn in Y123 System.....	93
4.3	Results and Discussion	99
	4.3.1 X-ray Diffraction and Iodometric Titration	99
	4.3.2 Electrical Resistivity	109
4.4	Conclusion	128
	References	129

Chapter 5

Doping effect of Ca, Pr and Zn in $\text{YBa}_2\text{Cu}_3\text{O}_{7-\delta}$ system

5.1	Introduction	134
5.2	Role of Ca Doping in Y123 System	135
5.3	Codoping Effect of Ca and Pr in Y123 System	137
5.4	Codoping Effect of Ca and Zn in Y123 System	138

5.5	Results and Discussion	141
5.5.1	X-ray Diffraction and Iodometric Titration	141
5.5.2	Electrical Resistivity	150
5.5.3	Relation between T^*,m with p	153
5.6	Conclusion	163
	References	165

Chapter 6

Summary and Conclusions

6.1	Summary	171
6.2	Suggestions for Future Work	176

	List of Publications	178
--	----------------------------	-----

	Appendix	179
--	----------------	-----

List of Figures

Fig. 1.3.1	K_2NiF_4 type crystal structure of La_2CuO_4	10
Fig. 1.3.2	The CuO_2 planes found in La_2CuO_4 as well as in $YBa_2Cu_3O_7$.	10
Fig. 1.3.3	The ligand field split levels of Cu 3d levels in the octahedral environment	11
Fig. 1.3.4	The Cu $d_{x^2-y^2}$ and oxygen 2p orbitals involved in the relevant electronic band where the Fermi level lies	11
Fig. 1.3.5	The schematic picture of the bonding, non-bonding and antibonding band	12
Fig. 1.5.1	Cuprate phase diagram	20
Fig. 1.6.1	Schematic picture of a stripe-ordered phase	23
Fig. 2.2.1	Geometrical conditions of focusing	39
Fig. 2.2.2	Set up of the X-ray diffractometer	41
Fig. 2.4.1	Experimental arrangement for resistivity	46
Fig. 2.5.1	A layout of the thermopower setup	48
Fig. 2.5.2	A layout of the thermopower sample holder assembly	49
Fig. 3.2.1	Nearest neighbour bonds which shows the puckering of copper – oxygen plane	57
Fig. 3.2.2	Crystal structure of $YBa_2Cu_3O_{7-\delta}$	58
Fig. 3.5.3	X-ray diffraction patterns of $YBa_2[Cu_{1-y}Zn_y]_3O_{7-\delta}$	66
Fig. 3.5.4	Rietveld refined diffraction patterns of $YBa_2 [Cu_{1-y}Zn_y]_3O_{7-\delta}$ with $y = 0$	67
Fig. 3.5.5	Rietveld refined diffraction patterns of $YBa_2 [Cu_{1-y}Zn_y]_3O_{7-\delta}$ with $y = 0.01$	67
Fig. 3.5.6	Rietveld refined diffraction patterns of $YBa_2 [Cu_{1-y}Zn_y]_3O_{7-\delta}$ with $y = 0.03$	68
Fig. 3.5.6(a)	Rietveld refined diffraction patterns of $YBa_2 [Cu_{1-y}Zn_y]_3O_{7-\delta}$ with $y = 0.06$	68

Fig. 3.5.7	Rietveld refined diffraction patterns of $\text{YBa}_2[\text{Cu}_{1-y}\text{Zn}_y]_3\text{O}_{7-\delta}$ with $y = 0.08$	69
Fig. 3.5.7(a)	Rietveld refined diffraction patterns of $\text{YBa}_2[\text{Cu}_{1-y}\text{Zn}_y]_3\text{O}_{7-\delta}$ with $y=0.10$	69
Fig. 3.5.8	Plot of resistivity vs T for $\text{YBa}_2[\text{Cu}_{1-y}\text{Zn}_y]_3\text{O}_{7-\delta}$ samples with different values of Zn concentration	71
Fig. 3.5.9(a)	Plot of resistivity vs T for $\text{YBa}_2[\text{Cu}_{1-y}\text{Zn}_y]_3\text{O}_{7-\delta}$ samples for $y = 0.00$ showing linear fit.....	72
Fig. 3.5.9(b)	Plot of resistivity vs T for $\text{YBa}_2[\text{Cu}_{1-y}\text{Zn}_y]_3\text{O}_{7-\delta}$ samples for $y = 0.01$ showing linear fit.....	73
Fig. 3.5.9(c)	Plot of resistivity vs T for $\text{YBa}_2[\text{Cu}_{1-y}\text{Zn}_y]_3\text{O}_{7-\delta}$ samples for $y = 0.03$ showing linear fit.....	74
Fig. 3.5.9(d)	Plot of resistivity vs T for $\text{YBa}_2[\text{Cu}_{1-y}\text{Zn}_y]_3\text{O}_{7-\delta}$ samples for $y = 0.06$ showing linear fit.....	75
Fig. 3.5.9(e)	Plot of resistivity vs T for $\text{YBa}_2[\text{Cu}_{1-y}\text{Zn}_y]_3\text{O}_{7-\delta}$ samples for $y = 0.08$ showing linear fit.....	76
Fig. 3.5.9(f)	Plot of resistivity vs T for $\text{YBa}_2[\text{Cu}_{1-y}\text{Zn}_y]_3\text{O}_{7-\delta}$ samples for $y = 0.09$ showing linear fit.....	77
Fig. 3.5.9(g)	Plot of resistivity vs T for $\text{YBa}_2[\text{Cu}_{1-y}\text{Zn}_y]_3\text{O}_{7-\delta}$ samples for $y = 0.10$ showing linear fit.....	78
Fig. 3.5.10	Plot of superconducting transition temperature T_c as a function of Zinc content (y) for $\text{YBa}_2[\text{Cu}_{1-y}\text{Zn}_y]_3\text{O}_{7-\delta}$	79
Fig. 3.5.11	Plot of variation of residual resistivity ρ_0 with Zn content y for $\text{YBa}_2[\text{Cu}_{1-y}\text{Zn}_y]_3\text{O}_{7-\delta}$	80
Fig. 3.5.12	Plot of slope dp/dT vs Zinc content (y) for $\text{YBa}_2[\text{Cu}_{1-y}\text{Zn}_y]_3\text{O}_{7-\delta}$	81
Fig 4.2.1	Plot of (a) resistivity vs T (b) T_c vs Pr concentration x . Taken from Ref. [37] for $\text{Y}_{1-x}\text{Pr}_x\text{Ba}_2\text{Cu}_3\text{O}_{7-\delta}$ compound	94
Fig 4.2.2	Variation of the residual resistivity ρ_0 (and ρ_0^{2D} right hand scale) with Zn content in $\text{YBa}_2\text{Cu}_3\text{O}_{7-y}$ with $y = 0.37$ and 0.07 , and in $\text{La}_{2-x}\text{Sr}_x\text{CuO}_4$ with $x = 0.15$ and 0.20 . The solid (dashed) line indicates the unitarity limit with the carrier density $n = x$ ($n = 1-x$).....	98

Fig. 4.3.1	x-ray diffraction patterns of $Y_{1-x}Pr_xBa_2 [Cu_{1-y}Zn_y]_3O_{7-\delta}$ samples with different values of Zn concentration and $x = 0.10$	103
Fig. 4.3.2	x-ray diffraction patterns of $Y_{1-x}Pr_xBa_2 [Cu_{1-y}Zn_y]_3O_{7-\delta}$ samples with different values of Zn concentration and $x = 0.20$	104
Fig. 4.3.3	Rietveld refined diffraction patterns of $Y_{0.9}Pr_{0.1}Ba_2 [Cu_{1-y}Zn_y]_3O_{7-\delta}$ with $y = 0.00$	105
Fig. 4.3.4	Rietveld refined diffraction patterns of $Y_{0.9}Pr_{0.1}Ba_2 [Cu_{1-y}Zn_y]_3O_{7-\delta}$ with $y = 0.01$	105
Fig. 4.3.5	Rietveld refined diffraction patterns of $Y_{0.9}Pr_{0.1}Ba_2 [Cu_{1-y}Zn_y]_3O_{7-\delta}$ with $y = 0.03$	106
Fig. 4.3.6	Rietveld refined diffraction patterns of $Y_{0.9}Pr_{0.1}Ba_2 [Cu_{1-y}Zn_y]_3O_{7-\delta}$ with $y = 0.08$	106
Fig. 4.3.7	Rietveld refined diffraction patterns of $Y_{0.9}Pr_{0.1}Ba_2 [Cu_{1-y}Zn_y]_3O_{7-\delta}$ with $y = 0.10$	107
Fig. 4.3.8	Rietveld refined diffraction patterns of $Y_{0.8}Pr_{0.2}Ba_2 [Cu_{1-y}Zn_y]_3O_{7-\delta}$ with $y = 0.0$	107
Fig. 4.3.9	Rietveld refined diffraction patterns of $Y_{0.8}Pr_{0.2}Ba_2 [Cu_{1-y}Zn_y]_3O_{7-\delta}$ with $y = 0.002$	108
Fig. 4.3.10	Rietveld refined diffraction patterns of $Y_{0.8}Pr_{0.2}Ba_2 [Cu_{1-y}Zn_y]_3O_{7-\delta}$ with $y = 0.005$	108
Fig. 4.3.11	Resistivity vs temperature for $Y_{1-x}Pr_xBa_2 [Cu_{1-y}Zn_y]_3O_{7-\delta}$ samples with different values of Zn concentration and $x = 0.10$	110
Fig. 4.3.12	Resistivity vs temperature for $Y_{1-x}Pr_xBa_2 [Cu_{1-y}Zn_y]_3O_{7-\delta}$ samples with different values of Zn concentration and $x = 0.20$	111
Fig. 4.3.13	Plot showing Superconducting Transition temperature T_c as a function of Zinc content (y) for $Y_{1-x}Pr_xBa_2 [Cu_{1-y}Zn_y]_3O_{7-\delta}$ samples with $x = 0, 0.10, 0.20$	112
Fig.4.3.14(a)	$\rho(T) - T$ curve for $Y_{1-x}Pr_xBa_2 [Cu_{1-y}Zn_y]_3O_{7-\delta}$ samples with showing. linear fit $y = 0.00$ and $x = 0.10$	113
Fig.4.3.14(b)	$\rho(T) - T$ curve for $Y_{1-x}Pr_xBa_2 [Cu_{1-y}Zn_y]_3O_{7-\delta}$ samples with showing. linear fit for $y = 0.01$ and $x = 0.10$	114

Fig.4.3.14(c)	$\rho(T) - T$ curve for $Y_{1-x}Pr_xBa_2 [Cu_{1-y}Zn_y]_3O_{7-\delta}$ samples with showing. linear fit for $y = 0.03$ and $x = 0.10$	115
Fig.4.3.14(d)	$\rho(T) - T$ curve for $Y_{1-x}Pr_xBa_2 [Cu_{1-y}Zn_y]_3O_{7-\delta}$ samples with showing. linear fit for $y = 0.06$ and $x = 0.10$	116
Fig.4.3.14(e)	$\rho(T) - T$ curve for $Y_{1-x}Pr_xBa_2 [Cu_{1-y}Zn_y]_3O_{7-\delta}$ samples with showing. linear fit for $y = 0.08$ and $x = 0.10$	117
Fig.4.3.14(f)	$\rho(T) - T$ curve for $Y_{1-x}Pr_xBa_2 [Cu_{1-y}Zn_y]_3O_{7-\delta}$ samples with showing. linear fit for $y = 0.10$ and $x = 0.10$	118
Fig.4.3.14(g)	$\rho(T) - T$ curve for $Y_{1-x}Pr_xBa_2 [Cu_{1-y}Zn_y]_3O_{7-\delta}$ samples with showing. linear fit for $y = 0.00$ and $x = 0.20$	119
Fig.4.3.14(h)	$\rho(T) - T$ curve for $Y_{1-x}Pr_xBa_2 [Cu_{1-y}Zn_y]_3O_{7-\delta}$ samples with showing. linear fit for $y = 0.002$ and $x = 0.20$	120
Fig.4.3.14(i)	$\rho(T) - T$ curve for $Y_{1-x}Pr_xBa_2 [Cu_{1-y}Zn_y]_3O_{7-\delta}$ samples with showing. linear fit for $y = 0.0005$ and $x = 0.20$	121
Fig.4.3.14(j)	$\rho(T) - T$ curve for $Y_{1-x}Pr_xBa_2 [Cu_{1-y}Zn_y]_3O_{7-\delta}$ samples with showing. linear fit for $y = 0.01$ and $x = 0.20$	122
Fig.4.3.14(k)	$\rho(T) - T$ curve for $Y_{1-x}Pr_xBa_2 [Cu_{1-y}Zn_y]_3O_{7-\delta}$ samples with showing. linear fit for $y = 0.03$ and $x = 0.20$	123
Fig.4.3.14(l)	$\rho(T) - T$ curve for $Y_{1-x}Pr_xBa_2 [Cu_{1-y}Zn_y]_3O_{7-\delta}$ samples with showing. linear fit for $y = 0.06$ and $x = 0.20$	124
Fig. 4.3.15	Variation of residual resistivity ρ_0 as a function of Zn content (y) in $Y_{1-x}Pr_xBa_2[Cu_{1-y}Zn_y]_3O_{7-\delta}$ (a) for $x = 0, 0.10$ and (b) for $x = 0.20$. The dashed line indicates the unitarity limit with the carrier density $n = 0.25$	126
Fig. 4.3.16	Slope $d\rho/dT$ vs Zinc content (y) for different values of $Y_{1-x}Pr_xBa_2 [Cu_{1-y}Zn_y]_3O_{7-\delta}$ for (a) $x = 0, 0.10$ and (b) $x = 0.20$	127
Fig. 5.5.1	X-ray diffraction patterns for $Y_{0.9-x}Pr_xCa_{0.1}Ba_2[Cu_{1-y}Zn_y]_3O_{7-\delta}$ samples with different values of Zn concentration and $y = 0.02$	145
Fig. 5.5.2	X-ray diffraction patterns for $Y_{0.9-x}Pr_xCa_{0.1}Ba_2[Cu_{1-y}Zn_y]_3O_{7-\delta}$ samples with different values of Zn concentration and $y = 0.06$	146
Fig. 5.5.3	Rietveld refined diffraction patterns of $Y_{0.9-x}Pr_xCa_{0.1}Ba_2 [Cu_{0.98}Zn_{0.02}]_3O_{7-\delta}$ with $x = 0.00$	147

Fig. 5.5.4	Rietveld refined diffraction patterns of $Y_{0.9-x}Pr_xCa_{0.1}Ba_2[Cu_{0.98}Zn_{0.02}]_3O_{7-\delta}$ with $x = 0.075$	147
Fig. 5.5.5	Rietveld refined diffraction patterns of $Y_{0.9-x}Pr_xCa_{0.1}Ba_2[Cu_{0.98}Zn_{0.02}]_3O_{7-\delta}$ with $x = 0.1$	148
Fig. 5.5.6	Rietveld refined diffraction patterns of $Y_{0.9-x}Pr_xCa_{0.1}Ba_2[Cu_{0.94}Zn_{0.06}]_3O_{7-\delta}$ with $x = 0.00$	149
Fig. 5.5.7	Rietveld refined diffraction patterns of $Y_{0.9-x}Pr_xCa_{0.1}Ba_2[Cu_{0.94}Zn_{0.06}]_3O_{7-\delta}$ with $x = 0.075$	149
Fig. 5.5.8	Resistivity vs temperature curve for $Y_{0.9-x}Pr_xCa_{0.1}Ba_2[Cu_{1-y}Zn_y]_3O_{7-\delta}$ samples with different values of Zn concentration and $y = 0.02$	151
Fig. 5.5.9	Resistivity vs temperature curve for $Y_{0.9-x}Pr_xCa_{0.1}Ba_2[Cu_{1-y}Zn_y]_3O_{7-\delta}$ samples with different values of Zn concentration and $y = 0.06$	152
Fig. 5.5.10	Methods used for determining T^* of $Y_{0.9-x}Pr_xCa_{0.1}Ba_2[Cu_{1-y}Zn_y]_3O_{7-\delta}$ for $x = 0.075$ and $y = 0.06$	156
Fig. 5.5.11	Plots of T^* against p for $Y_{1-x}Pr_xBa_2[Cu_{1-y}Zn_y]_3O_{7-\delta}$ samples with $Ca = 0$ and for different values of y (a) $x = 0.1$, (b) $x = 0.2$	157
Fig. 5.5.12	Plots of T^* against p for $Y_{0.9-x}Pr_xCa_{0.1}Ba_2[Cu_{1-y}Zn_y]_3O_{7-\delta}$ samples for $y = 0.02$ in Fig(a) and $y = 0.06$ in Fig(b) for varying from 0.00 to 0.15. Here in Fig (b) data from Naquib et al (Ref.63) is reproduced for comparison	158
Fig. 5.5.13	Plot of resistivity vs T of $Y_{0.9-x}Pr_xCa_{0.1}Ba_2(Cu_{1-y}Zn_y)_3O_{7-\delta}$ with $x = 0.075$ and $y = 0.06$ showing extraction of m	159
Fig. 5.5.13(a)	Plot of $\ln(\rho - \rho_0)$ vs $\ln(T)$ of $Y_{0.9-x}Pr_xCa_{0.1}Ba_2(Cu_{1-y}Zn_y)_3O_{7-\delta}$ with $x = 0.075$ and $y = 0.06$	159
Fig. 5.5.14	Phase diagram of $Y_{0.9-x}Pr_xCa_{0.1}Ba_2(Cu_{1-y}Zn_y)_3O_{7-\delta}$ (T^* , m T_c)	160

List of Tables

Table 3.5.1	Rietveld Refinement of XRD data for $YBa_2[Cu_{1-x}Zn_x]_3O_{7-\delta}$. The space group is Pmmm with $Y(\frac{1}{2}, \frac{1}{2}, \frac{1}{2})$, $Ba(\frac{1}{2}, \frac{1}{2}, z)$, $Cu(1)(0,0,0)$, $Cu(2)(0,0,z)$, $O(1)(0, \frac{1}{2}, 0)$, $O(2)(\frac{1}{2}, 0, z)$, $O(3)(0, \frac{1}{2}, z)$, $O(4)(0, 0, z)$. Also shown oxygen content, and transition temperature T_c . The number in the parenthesis are uncertainties in the last digit.	65
Table 4.3.1	Rietveld Refinement of XRD data for $Y_{0.9}Pr_{0.1}Ba_2[Cu_{1-y}Zn_y]_3O_{7-\delta}$. The space group is Pmmm with $Y(\frac{1}{2}, \frac{1}{2}, \frac{1}{2})$, $Pr(\frac{1}{2}, \frac{1}{2}, \frac{1}{2})$, $Ba(\frac{1}{2}, \frac{1}{2}, z)$, $Cu(1)(0,0,0)$, $Cu(2)(0,0,z)$, $O(1)(0, \frac{1}{2}, 0)$, $O(2)(\frac{1}{2}, 0, z)$, $O(3)(0, \frac{1}{2}, z)$, $O(4)(0, 0, z)$. Also shown oxygen content and T_c . The values in the parentheses represents uncertainties in the last digit	101
Table 4.3.2	Rietveld Refinement of XRD data for $Y_{0.9}Pr_{0.1}Ba_2[Cu_{1-y}Zn_y]_3O_{7-\delta}$. The space group is Pmmm with $Y(\frac{1}{2}, \frac{1}{2}, \frac{1}{2})$, $Pr(\frac{1}{2}, \frac{1}{2}, \frac{1}{2})$, $Ba(\frac{1}{2}, \frac{1}{2}, z)$, $Cu(1)(0,0,0)$, $Cu(2)(0,0,z)$, $O(1)(0, \frac{1}{2}, 0)$, $O(2)(\frac{1}{2}, 0, z)$, $O(3)(0, \frac{1}{2}, z)$, $O(4)(0, 0, z)$. Also shown oxygen content and T_c . The values in the parentheses represents uncertainties in the last digit	102
Table 5.5.1	Rietveld Refinement of XRD data for $Y_{0.9x}Pr_xCa_{0.1}Ba_2[Cu_{0.98}Zn_{0.02}]_3O_{7-\delta}$. The space group is Pmmm with $Y(\frac{1}{2}, \frac{1}{2}, \frac{1}{2})$, $Pr(\frac{1}{2}, \frac{1}{2}, \frac{1}{2})$, $Ca(\frac{1}{2}, \frac{1}{2}, \frac{1}{2})$, $Ba(\frac{1}{2}, \frac{1}{2}, z)$, $Cu(1)(0,0,0)$, $Cu(2)(0,0,z)$, $O(1)(0, \frac{1}{2}, 0)$, $O(2)(\frac{1}{2}, 0, z)$, $O(3)(0, \frac{1}{2}, z)$, $O(4)(0,0, z)$. Also shown oxygen content and T_c . The values in the parentheses represents uncertainties in the last digit	143
Table 5.5.2	Rietveld Refinement of XRD data for $Y_{0.9-x}Pr_xCa_{0.1}Ba_2[Cu_{0.94}Zn_{0.06}]_3O_{7-\delta}$. The space group is Pmmm with $Y(\frac{1}{2}, \frac{1}{2}, \frac{1}{2})$, $Pr(\frac{1}{2}, \frac{1}{2}, \frac{1}{2})$, $Ca(\frac{1}{2}, \frac{1}{2}, \frac{1}{2})$, $Ba(\frac{1}{2}, \frac{1}{2}, z)$, $Cu(1)(0,0,0)$, $Cu(2)(0,0,z)$, $O(1)(0, \frac{1}{2}, 0)$, $O(2)(\frac{1}{2}, 0, z)$, $O(3)(0, \frac{1}{2}, z)$, $O(4)(0, 0, z)$. Also shown oxygen content and T_c . The values in the parentheses represents uncertainties in the last digit	144
Table 5.5.3	The values of T_c , T^* , S and p for the underdoped system $Y_{1-x}Pr_xBa_2(Cu_{1-y}Zn_y)_3O_{7-\delta}$ for different values of Zn and $x=0.1$, $x=0.2$	161
Table 5.5.4	Shows the values of T_c , T^* , S and p for the overdoped system $Y_{0.1-x}Pr_xCa_{0.1}Ba_2(Cu_{1-y}Zn_y)_3O_{7-\delta}$ for different values of Zn and for Table(a) $x=0.02$ and Table (b) $x=0.06$	162

Chapter 1

Introduction

1.1 History of Superconductors

Superconductors, materials that have no resistance to the flow of electricity, are one of the last great frontiers of scientific discovery. Not only have the limits of superconductivity not yet been reached, but the theories that explain superconductor behavior seem to be constantly under review. In 1911 superconductivity was first observed in mercury by Dutch physicist Heike Kamerlingh Onnes of Leiden University [1]. When he cooled it to the temperature of liquid helium, (4K) its resistance suddenly disappeared. The Kelvin scale represents an "absolute" scale of temperature. Thus, it was necessary for Onnes to come within 4 degrees of the coldest temperature that is theoretically attainable to witness the phenomenon of superconductivity. Later, in 1913, he won a Nobel Prize in physics for his research in this area.

The next great milestone in understanding how matter behaves at extreme cold temperatures occurred in 1933. German researchers, Walter Meissner and Robert Ochsenfeld [2] discovered that a superconducting material repels a magnetic field. A magnet moving by a conductor induces currents in the conductor. This is the principle on which the electric generator operates. But, in a superconductor the induced currents exactly mirror the field that would have otherwise penetrated the superconducting material - causing the magnet to be repulsed. This phenomenon is known as strong diamagnetism and is today often referred to as the "Meissner effect". The Meissner effect is so strong that a magnet can actually be levitated over a superconductive material.

In subsequent decades other superconducting metals, alloys and compounds were discovered. In 1941 niobium-nitride was found to superconduct at 16 K [3]. In 1953 vanadium-silicon displayed superconductive properties at 17.5 K [4]. And, in

1962 scientists at Westinghouse developed the first commercial superconducting wire, an alloy of niobium and titanium [5]. High-energy, particle-accelerator electromagnets made of copper-clad niobium-titanium were then developed in the 1960s at the Rutherford-Appleton Laboratory in the UK, and were first employed in a superconducting accelerator at the Fermilab Tevatron in the US in 1987[6] .

The first widely-accepted theoretical understanding of superconductivity was advanced in 1957 by American physicists John Bardeen, Leon Cooper, and John Schrieffer [7]. Their Theories of superconductivity became known as the BCS theory - derived from the first letter of each man's last name - and won them a Nobel prize in 1972. The mathematically-complex BCS theory explained superconductivity at temperatures close to absolute zero for elements and simple alloys. However, at higher temperatures and with different superconductor systems, the BCS theory has subsequently become inadequate to fully explain how superconductivity is occurring.

Another significant theoretical advancement came in 1962 when Brian D. Josephson [5], a graduate student at Cambridge University, predicted that electrical current would flow between two superconducting materials - even when they are separated by a non-superconductor or insulator. His prediction was later confirmed and won him a share of the 1973 Nobel Prize in Physics. This tunneling phenomenon is today known as the "Josephson effect" and has been applied to electronic devices such as the SQUID, an instrument capable of detecting even the weakest magnetic fields.

The 1980's were a decade of unrivaled discovery in the field of superconductivity. In 1964 Bill Little of Stanford University had suggested the possibility of organic (carbon-based) superconductors [8]. The first of these theoretical superconductors was successfully synthesized in 1980 by Danish

researcher Klaus Bechgaard of the University of Copenhagen and three French team members [9]. $(\text{TMTSF})_2\text{PF}_6$ had to be cooled to an incredibly cold 1.2K transition temperature and subjected to high pressure to superconduct. But, its mere existence proved the possibility of "designer" molecules - molecules fashioned to perform in a predictable way.

Then, in 1986, a truly breakthrough discovery was made in the field of superconductivity. Alex Muller and Georg Bednorz [10], researchers at the IBM Research Laboratory in Rüschlikon, Switzerland, created a brittle ceramic compound that superconducted at the highest temperature then known 30 K. What made this discovery so remarkable was that ceramics are normally insulators. They don't conduct electricity well at all. So, researchers had not considered them as possible high-temperature superconductor candidates. The Lanthanum, Barium, Copper and Oxygen compound that Muller and Bednorz synthesized, behaved in a not-as-yet-understood way. The discovery of this first of the superconducting copper-oxides (cuprates) won the two men a Nobel Prize the following year. It was later found that tiny amounts of this material were actually superconducting at 58 K, due to a small amount of lead having been added as a calibration standard - making the discovery even more noteworthy.

Muller and Bednorz' discovery triggered a flurry of activity in the field of superconductivity. Researchers around the world began "cooking" up ceramics of every imaginable combination in a quest for higher and higher T_c 's. In January of 1987 a research team at the University of Alabama-Huntsville substituted Yttrium for Lanthanum in the Muller and Bednorz molecule and achieved an incredible 92 K T_c . For the first time a material (today referred to as YBCO) had been found that would superconduct at temperatures warmer than liquid nitrogen - a commonly available

coolant. Additional milestones have since been achieved using exotic - and often toxic - elements in the base perovskite ceramic. The current class (or "system") of ceramic superconductors with the highest transition temperatures are the mercuric-cuprates. The first synthesis of one of these compounds was achieved in 1993 at the University of Colorado and by the team of A. Schilling, M. Cantoni, J. D. Guo, and H. R. Ott of Zurich, Switzerland [11]. The world record of T_c of 138 K is now held by a thallium-doped, mercuric-cuprate comprised of the elements mercury, thallium, barium, calcium, copper and oxygen. The T_c of this ceramic superconductor was confirmed by Ron Goldfarb at the National Institute of Standards and Technology-Colorado in February of 1994 [12]. Under extreme pressure its T_c can be coaxed up even higher - approximately 25 to 30 degrees more at 300,000 atmospheres.

The first company to capitalize on high-temperature superconductors was Illinois Superconductor (today known as ISCO International), formed in 1989. This amalgam of government, private-industry and academic interests introduced a depth sensor for medical equipment that was able to operate at liquid nitrogen temperatures ($\sim 77\text{K}$).

In recent years, many discoveries regarding the novel nature of superconductivity have been made. In 1997 researchers found that at a temperature very near absolute zero an alloy of gold and indium was both a superconductor and a natural magnet [13]. Conventional wisdom held that a material with such properties could not exist. Since then, over a half-dozen such compounds have been found. Recent years have also seen the discovery of the first high-temperature superconductor that does not contain any copper (2000), and the first all-metal perovskite superconductor (2001) [14].

Also in 2001 a material that had been sitting on laboratory shelves for decades was found to be an extraordinary new superconductor. Japanese researchers measured the transition temperature of magnesium diboride at 39 Kelvin - far above the highest T_c of any of the elemental or binary alloy superconductors [15]. While 39 K is still well below the T_c 's of the "warm" ceramic superconductors, subsequent refinements in the way MgB_2 is fabricated have paved the way for its use in industrial applications. Laboratory testing has found MgB_2 will outperform NbTi and Nb_3Sn wires in high magnetic field applications like MRI.

Though a theory to explain high-temperature superconductivity still eludes modern science, clues occasionally appear that contribute to our understanding of the exotic nature of this phenomenon. In 2005, for example, Superconductors.ORG discovered that increasing the weight ratios of alternating planes within the layered perovskites can often increase T_c significantly. This has led to the discovery of more than 35 new high-temperature superconductors, including a candidate for a new world record.

The most recent "family" of superconductors to be discovered is the "pnictides". These iron-based superconductors were first observed by a group of Japanese researchers in 2006 [16]. Like the high- T_c copper-oxides, the exact mechanism that facilitates superconductivity in them is a mystery. However, with T_c 's over 50K, a great deal of excitement has resulted from their discovery. Researchers do agree on one thing: discovery in the field of superconductivity is as much serendipity as it is science.

1.2 High T_c Cuprates

The discovery of superconductivity was followed by a large amount of experimental studies. New superconducting materials were found and their physical properties were studied. As mentioned earlier in 1986, the 75th anniversary of superconductivity was marked by the discovery of new class of superconducting materials. Bednorz and Muller [10] of IBM Zurich discovered superconductivity in the La-Ba-Cu-O system at 40K. The parent compound is lanthanum cuprate, La_2CuO_4 , which has K_2NiF_4 structure. It is an antiferromagnetic insulator containing Cu^{2+} valence state. If one substitutes Ba or Sr or Ca, each having valency 2^+ for La having valency 3^+ to form $\text{La}_{2-x}\text{Ba}_x\text{CuO}_4$ (214) compound, the Neel temperature T_N at the onset of antiferromagnetism is found to be rapidly suppressed as the hole concentration, which is proportional to x , increases. The conductivity increases as the copper ions become mixed valent $\text{Cu}^{2+}/\text{Cu}^{3+}$ and the long range antiferromagnetic ordering becomes frustrated by the presence of doped holes in the CuO_2 planes. The antiferromagnetic phase consists of in-plane antiferromagnetic parent compound, the long range antiferromagnetic ordering is destroyed although short range antiferromagnetic spin fluctuations persist even in the superconducting state.

In early 1987, a group headed by Chu and Wu [17] announced that a compound in Y-Ba-Cu-O system becomes superconducting with its T_c close to 90K, that is above the liquid nitrogen temperature. Attempts were also made to explore superconductivity in non rare earth based oxides The other cuprate families are:

- (i) Bismuth cuprate were discovered by Maeda et-al with composition [18] $\text{Bi}_2\text{Sr}_2\text{Ca}_{n-1}\text{Cu}_n\text{O}_{2n+4}$ where the T_c was shown to increase with n upto 3. For $n=3$, T_c of 100K was found.

- (ii) In 1988, a thallium cuprate was discovered by Hermann and Sheng [19] having composition $Tl_mBa_2Ca_{n-1}Cu_nO_{2+m+2n}$ ($m=1,2$). The T_c shown by this system is found to increase with n upto 3 and for $n=3$ T_c was observed to 125K, and
- (iii) The mercury based cuprates were discovered in 1993 with composition $HgBa_2Ca_2Cu_3O_{2n+2+\delta}$. The T_c (onset) was found to rise to 134K at ambient pressure [20] and 164K at 30GPa.

All above mentioned cuprates are hole conductors. The best example of an electron conductor is $Nd(Ce,Pr)CuO$ having crystal structure identical to $La-Ba-Cu-O$. The parent Cuprate Na_2CuO_4 has tetragonal structure with square planar CuO_4 units. The discovery of non-cuprate superconductors also followed the discovery of cuprates. In this family highest T_c was exhibited by $Ba_{1-x}K_xBiO_3$. Besides ceramic superconductor the physical properties of the materials based on the molecule C_{60} revealed superconductivity with relatively high values of T_c in metal doped C_{60} compounds [21]. This group is called Fullerenes having general formula A_xC_{60} (A-alkali metals) with $T_c = 30K$ has also been discovered. [22,23].

The other superconductors discovered were in a series of compounds with the formula, RNi_2B_2C with a maximum T_c of 16.5K for $R=Lu$ [24,25]. These materials have attracted a great deal of interest because they display both superconductivity and magnetic order and effects associated with the interplay of these two phenomena. The superconducting compound, Sr_2RuO_4 , has the same structure as the $La_{2-x}M_xCuO_4$ ($M=Ba, Ca, Sr, Na$) high T_c cuprate superconductors [26]. While the T_c of Sr_2RuO_4 is only $\sim 1K$, this compound is of considerable interest because it is the only layered perovskite superconductor without Cu. Recently modified cuprate high temperature superconductors with magnetic charge-reservoir block i.e.

$\text{RuSr}_2\text{GdCu}_2\text{O}_8$ (Ru1212) and $\text{RuSr}_2(\text{RE}_{0.7}\text{Ce}_{0.3})_2\text{Cu}_2)_{10}$ (Ru1222), where RE is the rare earth element, were reported to undergo a magnetic transition at ferromagnetic transition temperature T_m followed by superconducting transition at T_s upon cooling. The transition temperatures respectively are (T_m, T_s) (133K, 20-50K) for Ru1212 and (80-180K, 30-42K) for Ru1222 with RE=Eu. Ferromagnetism is believed to coexist with superconductivity in Ru1212 and Ru1222. They may be called as superconducting ferromagnets because of their $T_m > T_s$. Active search for new superconductive materials is still going on.

1.3 Crystal and Electronic Structure of cuprates

The cuprate high T_c superconductors are unconventional superconductors, they do not form the Cooper pairs but are strongly correlated by Fermi liquid. The cuprate high T_c superconductors are quasi –two dimensional conductors containing one or more CuO_2 layers in each unit cell. The copper oxygen layers are separated either by intervening Cu-O chains, or by layers containing other metals or metal oxides (BaO, BiO, TiO), that serves as the carrier reservoir. The CuO_2 layers are believed to be the active component of cuprate superconductors. The original cuprate La_2CuO_4 superconductor described by Bednorz and Muller for which the superconducting phase was found to be crystallised in K_2NiF_4 structure, which is layered perovskite with a strongly anisotropic crystal structure (Fig.1.3.1) The copper atoms are surrounded by an octahedra of oxygen atoms. These octahedra share corners and form a planar square network. These planes are well separated electronically. Thus if one looks at a copper plane it is a simple square lattice of copper atom. There is an oxygen atom between every pair of neighbouring copper atom (Fig.1.3.2). The copper oxygen distance in the plane is $\sim 1.9\text{\AA}$ and that in the vertical distance is $\sim 2.4\text{\AA}$. The copper planes are well separated by about 6\AA

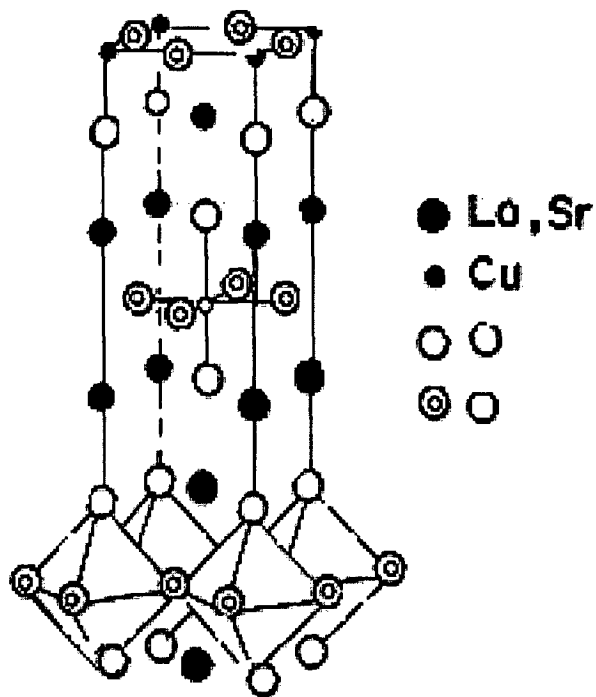


Fig. 1.3.1 K_2NiF_4 type crystal structure of La_2CuO_4

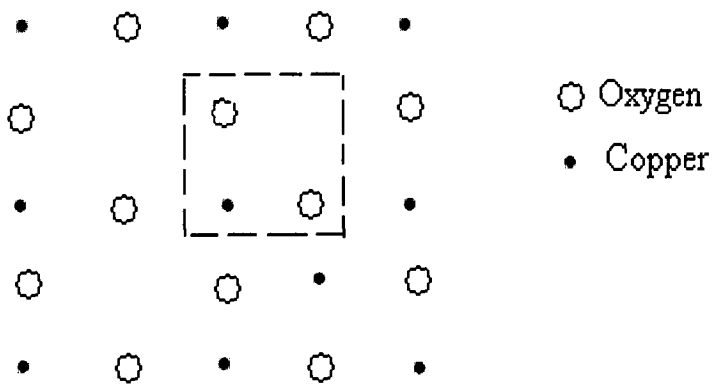


Fig. 1.3.2 The CuO_2 planes found in La_2CuO_4 as well as in $\text{YBa}_2\text{Cu}_3\text{O}_7$

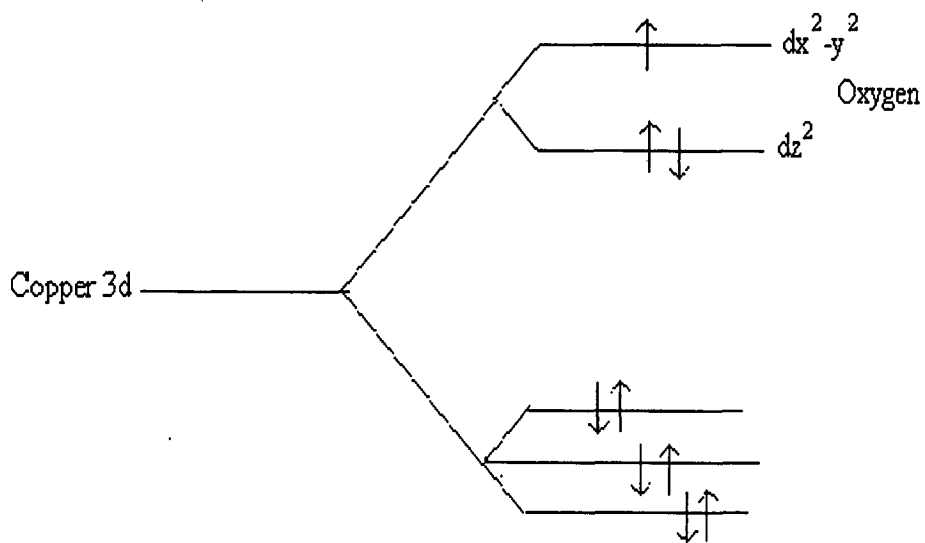


Fig. 1.3.3 The ligand field split d levels of Cu 3d levels in the octahedral environment

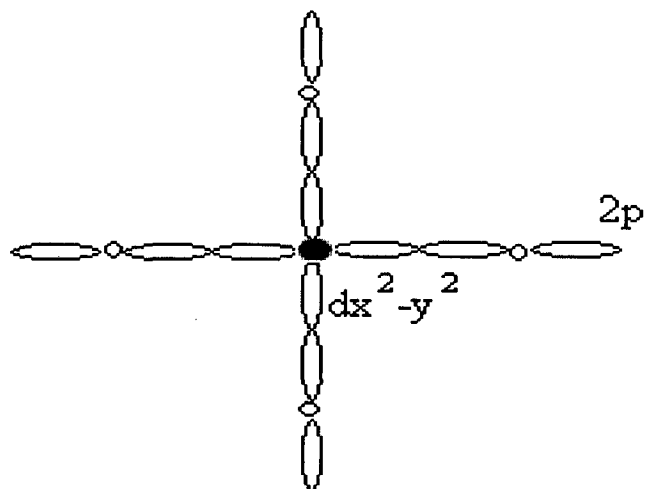


Fig 1.3.4 The Cu $d_{x^2-y^2}$ and oxygen 2p orbitals involved in the relevant electronic band where the Fermi level lies

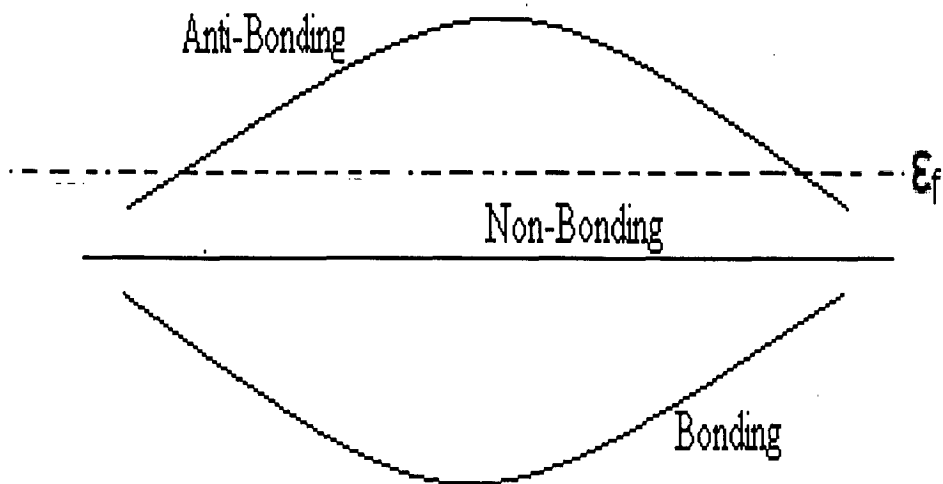


Fig 1.3.5 The schematic picture of the bonding, non-bonding and antibonding bands

La_2CuO_4 is partly ionic and partly covalent in the following sense. There is complete charge transfer of three electrons from La atoms. Even though Cu gives up two electrons and becomes Cu^{2+} , there is a strong covalent binding between the copper $d_{x^2-y^2}$ and oxygen 2p orbitals. A well separated Cu^{2+} ion will be in the electronic configuration $3d^9$ - that is, one hole in the d shell. The 3d level, owing to the covalent bonding and the crystal fields from the oxygen octahedra, is split as shown in Fig.1.3.3. The splitting of the top two levels arises because the octahedron is elongated in the z-direction. There is enough experimental evidence that shows that this large distortion is dominantly arising from packing and electrostatic consideration rather than from Jahn-Teller effect.

Thus in the insulator we have one lone electron in the oxygen $d_{x^2-y^2}$ level. The rest of the levels are far below the Fermi level $d_{x^2-y^2}$. The $d_{x^2-y^2}$ level hybridizes strongly with the four of the oxygen 2p orbitals pointing towards the copper atom Fig.1.3.4 As far as transport and magnetic properties are concerned these orbitals, two oxygen 2p orbitals and one copper $d_{x^2-y^2}$ orbital per unit cell ,(Fig1.3.2) in the plane alone seem to play an important role. Thus we have a simple tight binding model made up of oxygen 2p and copper $d_{x^2-y^2}$ orbitals. In the insulator there are five electrons per unit cell. This tight binding model in which the only non-zero hopping matrix element t is between the copper orbital (of energy ϵ_1) and the neighbouring oxygen orbital (of energy ϵ_2) is easily solved to get the dispersion relation [27]

$$\epsilon_{k_{\pm}} = \frac{-(\epsilon_1 - \epsilon_2)}{2} \pm [(\epsilon_1 - \epsilon_2)^2 + 8t^2(1 + \cos k_x a + \cos k_y a)]^{1/2}$$

$$\epsilon_{k_0} = 0$$

The subscript \pm and 0 denote antibonding, bonding and non-bonding band respectively. The corresponding dispersion is schematically shown in Fig.1.3.5 The bottom band is the bonding band, middle one is the non-bonding band and the top one is the antibonding band. We have three orbitals per unit cell and hence we have 3 bands. Since we have 5 electron per unit cell, the Fermi level lies in the middle of the antibonding band (Fig.1.3.5). The antibonding band is sufficient to understand the magnetic, transport and statistical mechanical properties of the insulator. We consider a simple tight binding model with nearest neighbour hopping between Wannier orbitals centered around the Cu sites. This Wannier orbital has the same x^2-y^2 symmetry as the $d_{x^2-y^2}$ orbital, but has large oxygen 2p orbital component as well. This tight binding model will approximately reproduce the antibonding band of our

original tight binding model. In the case La_2CuO_4 this model contains one electron per site, and the rest of the four electrons being there in the bonding and non-bonding bands.

Pure La_2CuO_4 with one electron per Wannier orbital in the above band is experimentally observed to be an insulator. When a La atom is replaced by Ba or Sr atom, it donates only 2 electrons. Now, one of the oxygen atoms receives one electron instead of two. Oxygen being strongly electronegative grabs one more electron from the copper atoms, making one of the Cu^{2+} into nominally Cu^{3+} . That is one electron from our tight binding band had been removed. Thus, when the doping fraction is x , that is in $\text{La}_{2-x}\text{Ba}_x\text{CuO}_4$, a fraction x electrons, have been removed. Experimentally $\text{La}_{2-x}\text{Ba}_x\text{CuO}_4$ remains an insulator upto $x \sim 0.05$ at very low temperature and then it starts superconducting. The phenomenon of removal of electron from CuO system by the addition of Sr or Ba is called doping. Experimentally T_c is a function of x and T_c is maximum when $x \sim 0.15$. One wants to understand how the insulator arises and how it becomes superconductor on doping.

1.4 Mott Insulator and Magnetism

The tight binding model that we considered above, being half filled, will be a metal according to a simple band theory. But experimentally, it is found to be a good insulator with an energy gap nearly equal to 2eV. Such a band metal can become an insulator if a Fermi surface instability due to perfect nesting of the simple tight binding band in two dimensions occurs resulting in a charge density wave or spin density wave. There is no experimental evidence in existence for this. Thus one should look for an alternate explanation to be an Mott insulators.

Oxides [28] such as NiO, MnO and several other antiferromagnetic insulators can be conducting metals according to simple band picture. Such a picture fails when the energy scale of electron-electron repulsion becomes large compared to the tight binding bandwidth i.e. when we have one electron per orbital, the strong electron repulsion prevents electrons from gaining the delocalization energy thereby localizing one electron per orbital. When we take into account screening, the dominant electrostatic interaction is the outside Coulomb repulsion (the Hubbard U) . This is typically 5 to 10 eV in transition metal oxides. Since the electrons hop between transition metal atoms, only through the oxygen binding orbitals, the hopping integral (t) is low. Hence, delocalization energy of electrons with co-ordination number (z) is small compared to U . This forces the electrons into a Mott-insulator phase.

Any excitation involving charge transfer need an energy nearly equal to $U - zt$ is called the Mott-Hubbard gap. This gap does not arise because of any periodic (self consistent or external) potential as in a band theory. It is a genuine many body effect which escapes explanation even in terms of many “sophisticated” density functional band theories.

The Hubbard Hamiltonian describes a Mott-insulator when U/t is greater than a critical value in two to three dimensions. Even though the charge excitations have a finite gap, the spin fluctuations have no gap. The spin fluctuations which are low lying states are described by an effective Hamiltonian usually referred to as the Heisenberg exchange Hamiltonian. It has been established that spin -1/2 Heisenberg antiferromagnet has long order at low temperatures in three and higher dimensions. In one dimension, quantum fluctuations destroy long range order converting it into a Resonating Valence Bond (RVB) state. RVB state is a quantum liquid of singlet pairs. The fact that singlets have been created in zero momentum state gives phase

coherence among various singlet configurations appearing in the RVB wave function. As Anderson [29] noticed, this phase coherence is exactly the one that appears in superconducting BCS state. What prevents RVB state from becoming superconductor is the absence of any real double occupancy or zero occupancy. Another way of saying this is that it is a BCS state with zero electronic compressibility.

Anderson [30-31] observed that oxides which are $s = \frac{1}{2}$ Heisenberg antiferromagnets rarely have long range magnetic order. Their low temperature magnetic properties are often anomalous and hence he concluded that perhaps antiferromagnetic order is fragile and could easily be destroyed. He constructed, in 1973, the example of 2D triangular lattice where low dimension and geometric frustration resulted in a RVB state.

Much later Anderson et al [32] argued that when less than 1% of holes are introduced in an antiferromagnetic Mott insulator, the long range order is destroyed and the insulator is converted into a RVB liquid. The basic argument is similar to Nagaoka's theorem [33]. The hole wants to delocalize and gain maximum binding energy $\sim tz$. In an antiferromagnetic state, the delocalization energy gain is not the maximum. This is possible only when the bulk magnetic state readjusts itself. This rearrangement costs an energy J . For U/t very large this rearrangement is into a ferromagnetic state (Nagaoka theorem). When $U/zt \sim 1$ to 10, which is the experimentally relevant range, the rearrangement is into a RVB liquid. The transition occurs when the energy loss of the bulk magnetic energy per site Δt becomes comparable to hole delocalisation energy per site $\sim tz$.

Thus Mott insulator can be easily converted into a quantum liquid of singlet pairs with very good phase coherence among the various singlet configurations. Such a state is a potential high temperature superconductor.

1.4.1 Superconductivity of the Doped Mott Insulator

Very soon after the discovery of high temperature superconductivity, Anderson [25] gave a Hubbard model description and provided a qualitative Resonating Valence Bond (RVB) scenario of superconductivity. His basic idea was that the singlet pairs in the RVB insulator are like Cooper pairs. In the Mott insulator, they are neutral owing to the absence of real charge density fluctuation in an insulator. When Ba is added and electrons are removed from Mott insulator, a fraction of pre existing singlet pairs get charged and superconductivity results. Anderson also pointed out that in such a correlated Fermi liquid gapless spin excitations may be still present. He argued that they are the neutral spin -1/2 fermions having their own Fermi surface. This pseudo Fermi surface could remain intact after doping, resulting in a linear low temperature specific heat of the superconductor.

An observation by Kivelson et al [34] brought out a non trivial departure from BCS theory. They argued, by taking analogy from Peierl's and spin Peierl's insulator, that in a doped valence bond system, the charge carriers are "holons" having a charge of $+e$. They behave like bosons and superconductivity results from Bose condensation of holons. A holon is essentially an empty site with the rest of the electrons singlet bonded and resonating among various valence bond configurations in a coherent way. When such an empty state is filled with one electron, we get a spinon, which is a neutral fermion. A spinon is essentially an unpaired spin in a sea of resonating singlet pairs. Thus the holons and spinons are quasi particles of a RVB superconductor.

At low temperatures, the holons have perfect coherence leading to superconductivity. The effective mass of these holons $\sim \hbar^2 / 2a^2 t$, where a is the lattice parameter. in an ideal Bose system, this will set the scale for the

superconducting transition temperature, which will be $\sim 5000\text{K}$. However, the physics in our problem is more complicated. At finite temperatures, spinon pairs are thermally liberated from the RVB sea of singlet pairs. They associate themselves with the holons thereby reducing their boson-like phase coherence. The phase coherence is completely lost when $k_B T \sim J$, at which temperature most of the singlet pairs have been broken. This temperature sets the scale for the superconducting transition temperature.

The holon condensation has dramatic consequences. The important one among them is the magnetic field flux quantization in units of hc/e and not $hc/2e$, as in the conventional BCS superconductors. Experiments show that indeed the flux quantization is $hc/2e$. That this does not contradict RVB theory of superconductivity has been explained by Wheatley et al [35] in the following way. In La_2CuO_4 as well as the Y123 compound, the Cu-O planes as well are well separated and hence electronic conduction is highly anisotropic. The holon condensation in the 2D plane does bring in superconducting Kosterlitz-Thouless type of correlation within the planes. But there is no true off-diagonal long range order. Due to the strong singlet correlations within the plane single electron tunneling is less probable than tunneling of a pair of electrons. This dominant pair tunneling establishes a 2D condensate of $2e$ rather than e . This is consistent with the experimental results on flux quantization and Josephson effect.

1.5 Various Phases of Cuprates

The phase diagram of the cuprates shows a wide variety of different behaviour at different temperatures and levels of doping Fig 1.5.1. All the compounds investigated so far show characteristic changes in almost all their thermodynamic and transport properties as either the temperature, T , or the number of holes per unit cell

of CuO_2 is varied. The number of holes per CuO_2 unit is a convenient parameter that can be used to compare the different cuprates.

The physical properties of the cuprates change abruptly at the superconducting transition (and also at the antiferromagnetic transition). In the other regions of the phase diagram, however, the properties change gradually and there is a “cross-over” region rather than a well defined phase transition.

The antiferromagnetic region is the best understood region in the phase diagram. At zero doping the cuprates are all insulators, and below a few hundred kelvin they are also antiferromagnets (i.e. the electron spins on neighbouring copper ions point in opposite directions). However, when the doping is increased above a critical value (about 5%, although this varies from compound to compound), the antiferromagnetic state disappears and we enter the so-called pseudogap or underdoped region. It is called underdoped because the level of doping is less than the level that maximizes the superconducting transition temperature. Some of the most interesting behaviour observed in the cuprates is observed in this region.

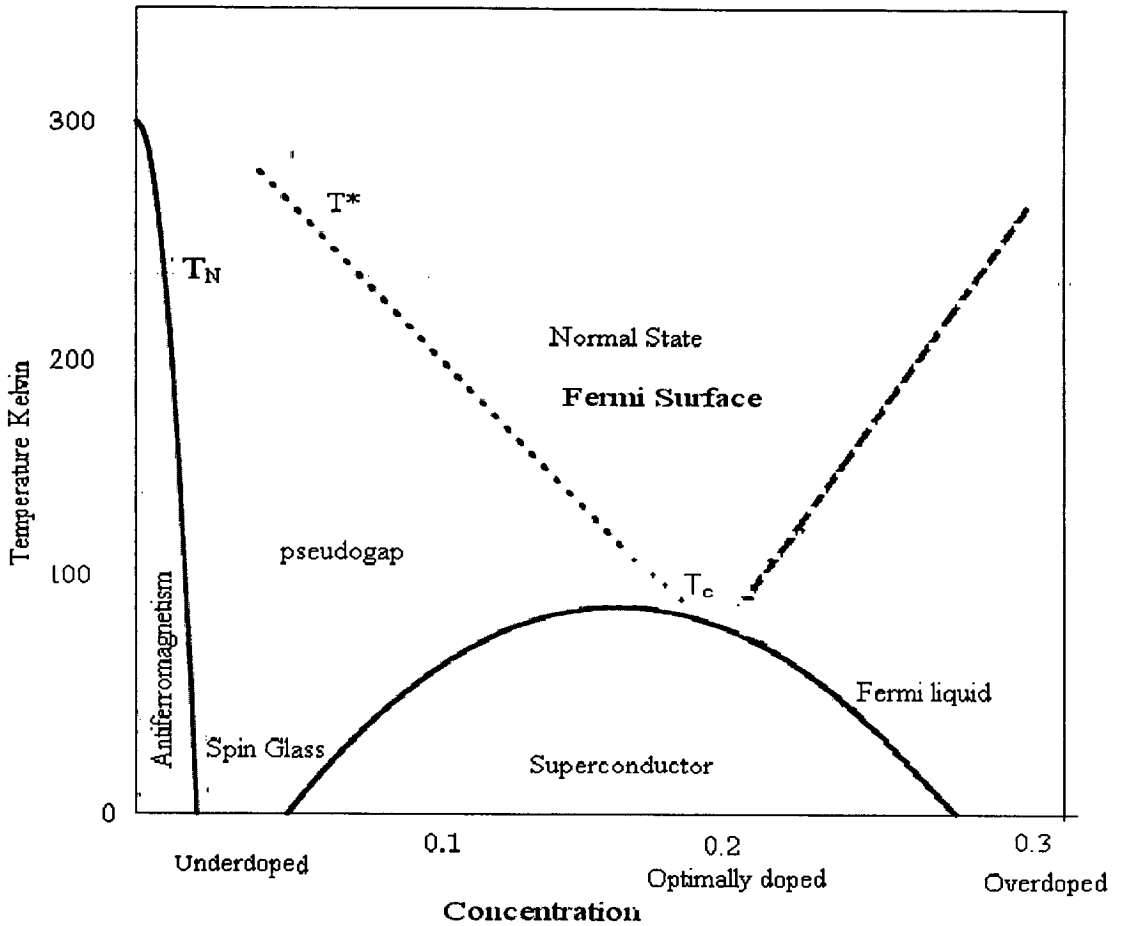


Fig. 1.5.1 Cuprate Phase Diagram

The Fermi-liquid region of the phase diagram is also well understood. One of the central concepts in condensed-matter physics, introduced by Lev Landau [36], is the “quasiparticle”. In a so-called Landau-Fermi liquid the properties of single electrons are changed or “renormalized” by interactions with other electrons to form quasiparticles. The properties of the material can then be understood in terms of the weak residual interactions between the quasiparticles and their excitations. When the quasiparticle approach is valid, there is a well defined boundary between particles and holes in both energy and momentum space at zero temperature. This boundary occurs at the Fermi energy and defines the “Fermi surface” in momentum space. However,

the Landau quasiparticle model can only explain part of the phase diagram of the cuprates.

The best known characteristic of the superconducting region is the fact that the resistivity is zero. However, condensed-matter physicists measure many other properties of superconductors, such as the energy needed to split the Cooper pairs. This is the superconducting energy gap, 2Δ . The pairing process means that there are no single-particle excitations with energies of less than Δ in the superconducting state. Normal metals and Fermi liquids do not exhibit such gaps. Energy gaps show up clearly when the single-particle density of states is plotted - that is when the number of electronic states with a given energy is plotted as a function of energy. Energy gaps are also responsible for semiconductivity, but the mechanism that leads to the formation of the gap is completely different.

The part of the phase diagram between the underdoped and Fermi-liquid regions, and above the area with the highest superconducting transition temperatures, is called the non-Fermi-liquid region. The thermodynamic properties in this region are unexceptional and, within experimental uncertainties, are in fact similar to the behaviour of a Fermi liquid. However, this region is characterized by exceptionally simple but unusual power laws in all of its transport properties as a function of temperature.

1.6 Charge Stripes in Cuprate Superconductor

Superconducting compounds are obtained from the parent cuprates by removing a small but finite density of electrons from the planes by chemical doping with, for instance, strontium for lanthanum. These missing electrons are commonly referred to as holes. If we assume, for simplicity, that each hole is associated with a

copper atom, then an atom with a hole has no unpaired electron and no net spin. An unpaired electron from a neighbouring atom can readily hop onto a hole site, which allows the hole to move through the plane, lowering its kinetic energy. The accompanying rearrangement of the electrons results in clusters of parallel spins, and this costs magnetic energy relative to the antiferromagnetic state. Thus there is competition between the kinetic energy of the holes and the exchange energy of the spins. There is also growing experimental and theoretical evidence that the CuO_2 planes are not doped homogeneously, but instead, hole-rich one dimensional (1D) features “stripes” are formed [36]. This is shown in Fig.1.6.1

The concept of a stripe phase has evolved over the last decade, and which offers a framework for interpreting a broad range of experimental results on copper-oxide superconductors and related systems. These are observed to occur in a class of strongly correlated materials desirable as doped antiferromagnets, of which the copper-oxide superconductors are the most prominent representatives. Stripe phase occur as a compromise between the antiferromagnetic interactions among magnetic ions and the Coulomb interactions between charges (both of which favor localised electrons) and the zero-point kinetic energy of the doped holes (which tend to delocalise charge). Experimentally, stripe phases are most clearly detected in insulating materials (where the stripe order is relatively static), but there is increasingly strong evidence of fluctuating stripe correlations in metallic and superconducting compounds. The existence of dynamic stripes, in turn, forces one to consider new mechanisms for charge transport and for superconductivity. The concept of electronic stripe phases developed for transition-metal oxides is applicable to a broad range of materials [38].

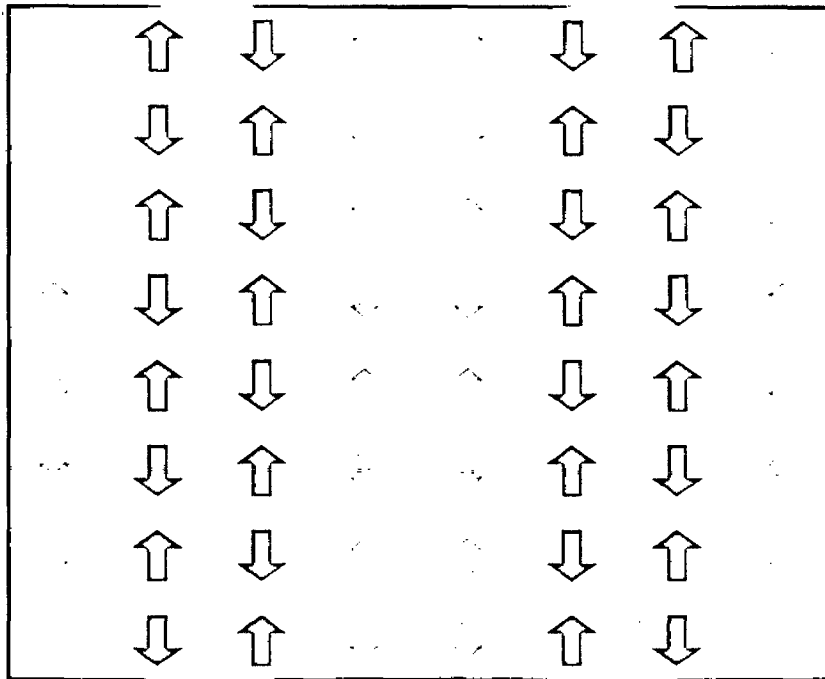


Fig. 1.6.1 Schematic picture of a stripe-ordered phase. The arrows represent the magnetic or spin order, and the blue scale represents the local charge density. Regions of high charge density (stripes) lie between largely undoped regions, where the spin order is much the same in the undoped antiferromagnet. In the figure, the stripes lie along the direction of the nearest-neighbor bonds, which we refer to as “vertical” stripes; when the stripes lie at 45° to this axis, they are to be diagonal.

1.7 Pseudogap in Cuprate Superconductor

It is well known that the properties of high-temperature superconductors vary in an unusual way when a moderate density of holes are introduced into the CuO_2 planes by chemical doping. This is one of the reasons why, despite large experimental and theoretical efforts, the nature of the superconductivity in these materials remains to be explained [39,40]. Correlations show the parent undoped compound to be a Mott insulator and, upon doping, the underdoped compounds display unusual metallic properties with increasing T_c . Doping beyond the optimal level yields normal metals with Fermi liquid behavior and with decreasing T_c .

The discovery of a marked suppression in the density of states of the underdoped cuprate superconductors above the critical temperature has led to a revival of interest in the idea of a pseudogap. This concept was originally introduced by Lee, Rice, and Anderson [41,42] to explain the suppression of the electron density of states associated with order-parameter fluctuations near a charge-density wave instability. According to one school of thought, a similar mechanism may drive the formation of the pseudogap in the underdoped cuprates [43-45]. Many fluctuating order parameters, such as antiferromagnetism [46], charge-density waves [47], and preformed Cooper pairs have been proposed [48].

Pseudogaps are likely to be a widespread feature of correlated electron systems lying close to an instability that causes a gap in part of the Fermi surface, and they have been observed in a wide variety of nested and low-dimensional strongly correlated electron materials, including one dimensional charge-density wave systems [49], vanadium doped chromium [50], colossal magneto-resistance compounds [51], and strontium-calcium and strontium-barium ruthenates [52].

By a pseudogap we mean a partial gap. An example of such a partial gap would be a situation where, within the band theory approximation, some regions of the Fermi surface become gapped while other parts retain their conducting properties and with increased doping the gapped portion diminishes and the materials become more metallic. We view the pseudogap as a fundamental property of underdoped copper oxides. The research on pseudogap was started with the search for the superconducting gap in the newly discovered high temperature superconductors. The energy gap is one of the defining properties of a superconductor, but despite considerable effort, early experiments failed to find one in high- T_c cuprates. Well understood physical properties such as the frequency dependent conductivity, the Raman efficiency or the tunneling conductance did not show the familiar signatures of the energy gap, namely a zero density of excitations below an energy 2Δ [54] appearing abruptly at the superconducting transition temperature T_c . Instead, in the cuprates, the depression of excitations was incomplete and often started well above T_c in the normal state. We now know that this behaviour was not the result of poor sample quality or faulty experimental technique, but a consequence of two basic properties of high temperature superconductors: the d-wave nature of the superconducting gap function varying as the cosine function around the Fermi surface with nodes $k_x = \pm k_y$, and the persistence of this gap into the normal state.

We have attempted to make use of these concepts namely, the charge stripe and pseudogap in the explanation of suppression of transition temperature in the superconducting systems.

1.8 Applications of High T_c Superconductors

There are several areas in which high T_c superconductors have made a considerable technological impact in the last two decades. The impact of critical materials parameters of high T_c superconductors, especially the critical current density and the allowable strain is seen in magnetic applications. Superconducting magnets are the dominant present commercial application of superconductivity. Some of the other important applications of these high T_c superconductors are given below.

- (i) Magnetic-levitation is an application where superconductors perform extremely well. Transport vehicles such as trains can be made to "float" on strong superconducting magnets, virtually eliminating friction between the train and its tracks. Not only would conventional electromagnets waste much of the electrical energy as heat, they would have to be physically much larger than superconducting magnets. A landmark for the commercial use of MAGLEV technology occurred in 1990 when it gained the status of a nationally-funded project in Japan.
- (ii) Superconducting magnets are already crucial components of several technologies. Magnetic resonance imaging(MRI) is playing an ever increasing role in diagnostic medicine. The intense magnetic fields that are needed for these instruments are a perfect applications of superconductors. Similarly, particle accelerators used in high-energy physics studies are very dependant on high-field superconducting magnets.
- (iii) The Korean Superconductivity Group within KRISS has carried biomagnetic technology a step further with the development of a double-relaxation oscillation SQUID (Superconducting Quantum Interference Device) for use in Magnetoencephalography. SQUID's are capable of

sensing a change in a magnetic field over a billion times weaker than the force that moves the needle on a compass (compass: 5e-5T, SQUID: e-14T.). With this technology, the body can be probed to certain depths without the need for the strong magnetic fields associated with MRI's. Superconductors have also found widespread applications in the military. HTSC SQUIDS are being used by the U.S. NAVY to detect mines and submarines. And, significantly smaller motors are being built for NAVY ships using superconducting wire and "tape".

- (iv) In the electronics industry, ultra-high-performance filters are now being built. Since superconducting wire has near zero resistance, even at high frequencies, many more filter stages can be employed to achieve a desired frequency response. This translates into an ability to pass desired frequencies and block undesirable frequencies in high-congestion rf (radio frequency) applications such as cellular telephone systems.
- (v) Superconductors are used to generate very high fields in small volumes, making more widely available analytical techniques which would otherwise be restricted to a few large laboratories having multimewatt motor generators and high field copper magnets.

1.9 Scope of Present Work

A wealth of experimental and theoretical work has been carried out on the normal-state transport properties of high temperature superconducting oxides. The way superconducting and normal state properties respond to substitutional disorder forms their mainstay. The studies have led to a wealth of new insights and information about high T_c behaviour in relation to numerous interlinked aspects, such

as the role of carrier concentration, charge localization, interlayer coupling effects, interplay and coexistence of high temperature superconductivity with magnetic order, formation of pseudogaps and fluctuating stripe phases, etc. The enormous amount of findings thus determined have proved truly invaluable for the basic understanding of the high T_c phenomena.

In the charge-stripe picture, dynamic metallic stripes are thought to dominate the transport properties. So, within this model, one expects a strong influence on the transport properties when, for some reasons, the 1D charge stripes are fragmented and/or pinned. In the presence of stripe fragmentation, charge carriers are forced to hop to neighboring metallic stripes or their fragments passing through the intercalating Mott-insulator areas. This leads to an increased resistivity. The interstripe hopping recovers effectively the 2D transport region and then the low temperature $\ln(1/T)$ increase of the high-field resistivity can be interpreted as weak localization effects, typical for 2D case.

One possible type of pinning centers which might be responsible for stripe pinning and fragmentation is the crystallographic disorder in the CuO_2 plane, in the form of dislocations. These dislocations will also alter the local electronic and magnetic structure in the plane and at low temperatures, when the stripes are less mobile; they can be expected to pin the magnetic domain walls formed by the charge stripes. Moreover, in the case of strong pinning, stripe fragmentation is predicted to occur. Experimentally, the pinning of charge stripes has been seen by neutron-diffraction experiments on the Nd-doped and pure $\text{La}_{2-x}\text{Sr}_x\text{CuO}_4$. The striking result derived from these data is that, although the incommensurate features (i.e., the stripes) are almost identical, the scattering in the pure, near optimally doped, $(\text{La}_{2-x}\text{Sr}_x)\text{CuO}_4$ system is inelastic dynamic stripes whereas in the $(\text{La}_{1.6-x}\text{Nd}_{0.4}\text{Sr}_x)\text{CuO}_4$ system elastic

scattering is observed, corresponding to static stripes. In general, pinning of these stripes is correlated with the onset of an increasing resistivity, although stripe pinning has been found in underdoped samples that are metallic (but close to the metal-insulator transition), suggesting stripe fragmentation to be as important as pinning for the creation of an insulating state.

As mentioned earlier the normal-state and superconducting properties of high- T_c cuprates are extremely sensitive to stoichiometry and the number (p) of added hole carriers per copper oxide plane. In recent years as stated previously one of the most widely studied phenomena in the physics of high-temperature superconductors (HTS) is the so-called pseudogap state which is observed over a doping range extending from the underdoped to the slightly overdoped region. In the pseudogap-state various normal state and superconducting state anomalies are observed which can be interpreted in terms of a reduction in the effective single particle density of states. Existing theories of the pseudogap, which is believed to be an essential feature of HTS physics, can be classified broadly into two categories. The first is based upon a model of Cooper pair formation well above the superconducting transition temperature, T_c , with long-range phase coherence appearing only at $T \leq T_c$. The second assumes that the appearance of the pseudogap is due to fluctuations of some other type, which compete or coexist with superconductivity. These include antiferromagnetic fluctuations, charge density waves, structural phase transition or electronic phase separation on a microscopic scale (e.g., the stripe scenario). Within this second category the concept of a quantum critical point (QCP) has been mooted to explain the HTS phase diagram though its confirmation remains inconclusive.

With these recently developed concepts in mind, we have made an attempt to study the effect of some of the dopant and oxygen stoichiometry in Y123 system by

carrying out measurements on electrical resistivity as a function of temperature in the range 10-300K. In particular, we have prepared the compounds of compositions

1. $\text{YBa}_2[\text{Cu}_{1-y}\text{Zn}_y]_3\text{O}_{7.8}$ with $0 \leq y \leq 0.10$: Zn doping
2. $\text{Y}_{1-x}\text{Pr}_x\text{Ba}_2[\text{Cu}_{1-y}\text{Zn}_y]_3\text{O}_{7.8}$ with $x = 0.1, 0.2$: Zn and Pr doping
and $0 \leq y \leq 0.10$
3. $\text{Y}_{0.9-x}\text{Pr}_x\text{Ca}_{0.1}\text{Ba}_2[\text{Cu}_{1-y}\text{Zn}_y]_3\text{O}_{7.8}$ with $0 \leq x \leq 0.12$: Zn, Pr and Ca doping
and $y = 0.02$ and 0.06

We have selected these compositions such that they lie in the optimally doped, underdoped and overdoped regions in order to see whether pseudogap and charge stripes play any role in the suppression of T_c .

It may be interesting to note that with a single experimental techniques one can get a lot of information on the normal-state and superconducting properties of high T_c cuprates.

References

1. H. Kammerlingh Onnes and Akad Van Wetenschappen ,Proceedings from the section of science s, Amsterdam **14**, 113 and 818 (1911).
2. W. Meissner ,R. chsenfeld, Naturwiss ,**21**,787 (1933).
3. Aschermann ,Friederich , Justi and Kramer, Phys.Z **42**,349(1941).
4. G. F. Hardly and J. K. Hulm, Phys. Rev. **93**,1004(1954).
5. B.D. Josephson, Phys. Rev. Lett.**1**, 125(1962).
6. Fermilab Accelarotor Report No.**10** :The Tevatron..
7. J. Bardeen, L.N. Cooper, and J.R. Schrifferr, Phys. Rev. **106**,162(1957);**108**,1175(1957).
8. W.A.Little, Phys.Rev.**134** ,A1416 (1964).
9. D.Jerome ,A.Mazaud, M. Ribautt,K.Bechgaard, J.Phys.Lett .**41**,L95(1980).
10. A. Bednorz and K.A. Muller ,Z.Phys. B **64**,189(1986).
11. A. Schilling, M. Cantoni, J. D. Guo, and H. R. Ott of Zurich, Nature **363**,56 (1993).
12. L. Gao et al ,Phys.Rev.B**50**, 4260(1994).
13. S. Reshmann,T. Hermannsdorfer and F.pobell ,Phy.Rev.Lett.**78**,1122(1997).
14. T. He.Q. Huang, A.P.Ramirez et al, Nature **411**,54(2001).
15. J.Nagamatsu, N.Nakagawa, T.Muranaka,Y.Zenitani and Akimitsu, Nature **410**,63(2001).
16. Hideo Hosono, Zu –An Ren, New J. of Physics **11**,025003 (2009).
17. M. Wu,J. Ashburn, C. Torng,P. Hor,R.Meng,L.Geo, Z. Huang and C. Chu, Phys Rev. Lett.**58**, 908((1987).

18. M.K.Wu,J.R.Ash burn,C.J.Trong,P.H. Hir, R.L.Meng L.Ga,Z. L.Huang, Y.Q. Wang, C.W. Chu. Phys. Lett. **58**,908(1987).
19. S. Pultin, E.V. Antipov, O. Chmaissen and M. Marezio, Nature **362**, 226, (1993).
20. C.W. Chu, L.Gao, F. Chen, Z. J. Huang, R.L.Meng and Y.Y.Xue, Nature **363**, 323 (1993); L.Gao, F. Chen, Y.Y.Xue,Q.Xiong, R.L.Meng ,D. Ramirez, C.W. Chu, H. Eggert and H.K. Mao ,Physica C **235-240**,1493 (1994).
21. A.F. Hebard, Phys Today, November p.26(1992).
22. M.J. Rosseinsky, A. P. Ramirez, S.H. Glarum, S.M. Zahurak and A.V. Makhija, Phys. Rev. Lett.**66** ,2830(1991).
23. K.Holezer, O.Klein ,S.M. Huang, R. B. Kaner, K. J. Fu, R.L. Whetten and F. Diederich , Science **252**,1154(1991).
24. R. Nagarajan, C. Mazumdar, Z. Hossain, S. K. Dhar, k.V. Gopalkrishnan, L.C. Gupta, C. Godart, B. D. Padalia and R. Vijayaraghavan , Phys. Rev. Lett. **72**,274(1994).
25. R.J. Cava . H. Takagi, B. Battlog,H.W. Zandenbergen, J. J. Krajewski,W. F. Peck,Jr.R.B. Van Dover, R. J. Felder, K. Mizuhasi, J.O. Lee, H. Eisaki and S. Uchida, Nature **367**,252(1994).
26. Y. Maeno, T. Nagata, J. Akimitsu , H. Takahashi, N. Mori and K. Kinoshita, J. Phys. Soc. Japan **65**,2764(1994).
27. L.F. Schnemeyer ,J.K. Thomas, T. Siegrist, B. Bat logg, L.w.rupp,R.L. Opila, R. J.Cava, D. W. Murphy, Nature **335**,421 (1988).
28. J.B.Goodenough, Magnetism and Chemical Bond,Interactive Publishers,a division of John Willey, N.Y.(1963).
29. P.W. Anderson, Science **235**,1196(1987).

30. P.W. Anderson, *Mat.Res. Bull* **8**,153 (1973).
31. P.Fazekas and P.W.Anderson, *Phil Mag.***30**,432(1974).
32. P.W.Anderson, G. Baskaran, z. Zou and T. Hsu, *Phys.Rev.Lett.***58**, 2790(1987).
33. Y.Nagoka,*Phys.Rev.***147** ,392(1966).
34. S.Kivelson,D.Rokshar and J.Setha, *Phys.Rev.***B35**,8865(1987).
35. J.Wheatly, T.Hsu and P.W.Anderson *Phys..Rev.B* **37**,580(1988).
36. L.D.Landau *Zh Eksp.i Teor.Fiz.***30**,1058(1956);*Soviet Phys.JETP***3**,920(1957);
L.D.Landau *Zh Eksp.i Teor.Fiz.***32**,59 (1957);*Soviet Phys.JETP***5**, 101(1957)
37. V.V.Moshchalkov,J.Vanacken and L.Trappeniers *Phys.Rev.B* **64**,2145 (2004)
38. V.J.Emery, S.A.Kivelson , and J.M. Tranquada, *Proc.Natl. Acad.Sci.*, **96** ,
8814(1999).
39. E. V. L. de Mello, E. S. Caixeiro, and J. L. Gonza'lez ,*Phys. RevB*
67,024502,(2003).
40. K. Kitazawa, ,*Physica C* **341-348**, 19 (2000) ,*Proceedings of the IV-M2S HTSC*
conference
41. A. Posazhennikova1, and P. Coleman, *Phys. Rev. B***67**,165109 (2003).
42. P. Lee, M. Rice, and P. W. Anderson, *Phys. Rev. Lett.* **31**, 462,(1973).
43. M. Randeria, in *Proceedings of the International School of Physics“Enrico Fermi” on High Temperature Superconductors*, editedby G. Iadonisi, J. R. Schrieffer, and M. L. Chialfalo (IOS Press, 1998), pp. 53–75 (Varenna Lectures 1997); M. Randeria and J. C. Campuzano, in *Proceedings of the International School of Physics “Enrico Fermi” on High Temperature Superconductors*, edited by G. Iadonisi, J. R. Schrieffer, and M. L. Chialfalo (IOS Press, 1998), pp. 115–139 (Varenna Lectures 1997).
44. T. Timusk and B. Statt, *Rep. Prog. Phys.* **62**, 61 (1999).

45. M. V. Sadovskii, Usp. Fiz. Nauk **171**, 539 (2001) [Phys. Usp. **44**, 515 (2001)].
46. A. P. Kampf and J. R. Schrieffer, Phys. Rev. B **41**, 6399 (1990!);**42**, 7967 (1990);
V. Barzykin and D. Pines, *ibid.* **52**, 13 585 (1995); A. Chubukov, D. Pines, and
B. Stojkovic, J. Phys.: Condens. Matter **8**, 10 017 (1996).
47. V. J. Emery, S. A. Kivelson, and J. M. Tranquada, Proc. Natl.Acad. Sci. U.S.A.
96, 8814 (1999), and references therein.
48. V. B. Geshkenbein, L. B. Ioffe, and A. I. Larkin, Phys. Rev. B **55**,3173 (1997);
V. Emery, S. A. Kivelson, and O. Zachar, *ibid.* **56**,6120 (1997).
49. G. Grüner, Density Waves in Solids (Addison Wesley, Reading,MA, 1994),
and references therein.
50. A. Yeh, Yeong-Ah Soh, J. Brooke, G. Aeppli, T. F. Rosenbaum, and S. M.
Hayden, Nature ~London! **419**, 459 (2002).
51. D. S. Dessau, Y. D. Chuaug, A. Gromko, T. Saitoh, T. Kimura, and Y. Tokura, J.
Electron Spectrosc. Relat. Phenom. **117-118**,265 (2001).
52. Y. S. Lee, Jaejun Yu, J. S. Lee, T. W. Noh, T.-H. Gimm, Han-Yong Choi, and
C. B. Eom, Phys. Rev. B **66**, 041104R (2002);T. W. Noh, Y. S. Lee, J. S. Lee,
K. W. Kim, J. Yu, G. Cao, J. E.Crow, and M. K. Lee, Physica C **364-365**, 480
(2001).
53. Tom Timusk and Bryan Stat, cond-mat,9905219 vo1 (1999).

Chapter 2

Experimental Techniques

2.1 Method of Preparation of Cuprate Compounds

All the polycrystalline samples during the course of this work were prepared by solid-state reactions method. The oxides of Y_2O_3 , $CaCO_3$, $BaCO_3$, CuO , ZnO , Pr_6O_{11} of purity 99.99% were taken in the stoichiometric ratio were thoroughly mixed, grounded and calcined at $920^{\circ}C$ in the Carbolite high temperature furnace in air for a period of 17-20 h. After four intermediate grindings and calcinations in air these precursors were regrounded and pressed into pellets, and sintered in oxygen for 24h at $940^{\circ}C$ and then furnace cooled to below $100^{\circ}C$ with an intervening annealing for 24h at $600^{\circ}C$ [1]. During the course of this work the materials investigated are :

1. $YBa_2[Cu_{1-y}Zn_y]_3O_{7-\delta}$ with $y = 0.0, 0.01, 0.06, 0.08, 0.09, 0.10$.
2. $Y_{1-x}Pr_xBa_2[Cu_{1-y}Zn_y]_3O_{7-\delta}$ with $x = 0.1$, $y = 0.0, 0.01, 0.03, 0.06, 0.08, 0.10$ and $x = 0.2$, $y = 0.0, 0.002, 0.005, 0.01, 0.03, 0.06$
3. $Y_{0.9-x}Pr_xCa_{0.1}Ba_2[Cu_{1-y}Zn_y]_3O_{7-\delta}$ with $y = 0.02$, $x = 0, 0.025, 0.075, 0.1, 0.12$ and $y = 0.06$, $x = 0.0, 0.075, 0.1, 0.12$

These superconducting oxides are then used for

- (i) X-ray diffraction study for determination of crystal structure,
- (ii) Iodometric titration for estimating oxygen content of samples,
- (iii) Four probe electrical resistivity for determination of transition temperature, characteristic pseudogap temperature, impurity scattering and carrier-carrier scattering and
- (iv) Thermopower measurements for finding of hole contents.

2.2 X-ray Diffraction (XRD) Technique

2.2.1 Principle of Powder Diffraction

In the X-ray powder diffraction method, the crystal to be examined is reduced to a very fine powder and is placed in a beam of monochromatic X-rays. Each particle of the powder is a tiny crystal oriented at random with respect to the incident beam. Just by chance, (h00) planes for example can reflect the incident beam. Other particles will correctly oriented for (hk0) reflection. The mass of powder is equivalent in fact to a single crystal rotated, not about one axis but about all possible axis. Consider one particular hkl reflection. One or more particles of powder will by chance, so oriented that their (hkl) planes make the correct Bragg angle for reflection. If one plane is now rotated about the incident beam in such away that θ is kept constant, then the reflected beam will travel over the surface of a cone and the axis of the cone coincides with the transmitted beam.

In the present study the bulk samples were crushed into fine powder in an agate mortar and pestle and the room temperature X-ray diffraction patterns of powdered samples were recorded on the Rigaku D-Max IIC diffractometer with CuK_α radiation source and nickel filter. The patterns were recorded as a continuous scans in the 2θ range of 20° to 80° with a step of 0.02 and a speed of $1^\circ/\text{min}$.

2.2.2 Experimental Set-up for X-ray Diffraction

A diffractometer essentially consists of an X-ray tube, a goniometer and a counter. The X-ray tube, along with the filters produces the required monochromatic radiation. The goniometer is designed to satisfy the focusing condition geometrically and such geometrical conditions are shown in Fig.2.2.1. The focusing circle is a circle on the plane which involves the sample at the centre of the circle and at right angles with the axis of the rotation of the goniometer, and the circle involves axis I of the

focus of the target ,the axis II of the goniometer and axis III of the receiving slit. The radius of the focusing circle is a function of the angle θ formed by the surface of the sample with the extension line of the direct X-ray beam, and the angle formed by the straight line connecting axes II and III is 2θ . This angle is always accurately two times of the angle θ formed by the surface with the extension line of the direct x-ray beam [2].

Since in this goniometer, X-ray beam from the line focus will irradiate on the sample, the greater part of the X-ray beams is irradiated on the sample inclined against the focusing circle plane. When this angle of inclination is large, resolution of the diffracted X-ray beams and accuracy of the measured diffracted angle decreases. To minimize the angle of inclination, therefore, the solar slit is used. The soller slit boxes have the slit holders for insertion of the divergence slit, receiving slit and scatter slit. The divergence slit determines the horizontal divergence angle of the X-ray beams irradiating the sample. The receiving slit is for limiting the width of diffracted x-ray beams entering the counter. Its angular aperture has close relation with the intensities of the diffracted X-ray beams and resolution . The scatter slit limits the scattered x-ray beams incident upon the counter. It forms a pair with the divergence slit.

In the case when curved crystal X-ray monochromator is used ,the positions of the receiving slit and the scattering slit are interchanged. The monochromator is based on the dual diffraction principle of diffraction by a sample and diffraction by single crystal. The goniometer geometrically satisfies the condition of focusing methods and its focal circle becomes the primary focal circle. The monochromator also geometrically satisfies the condition of focusing method.

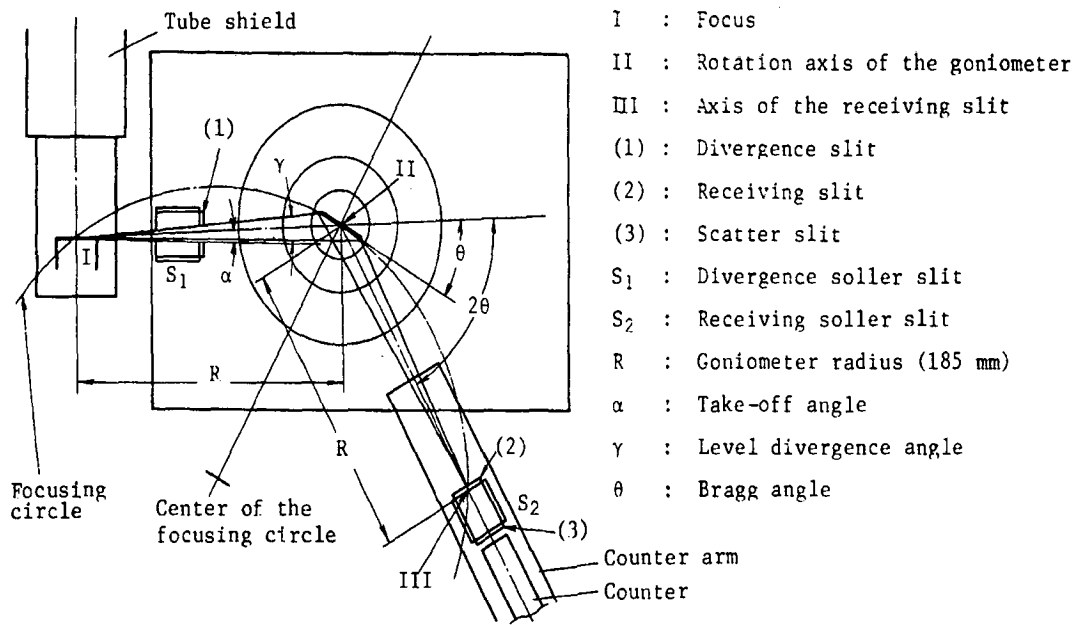


Fig.2.2.1 Geometrical conditions of focusing

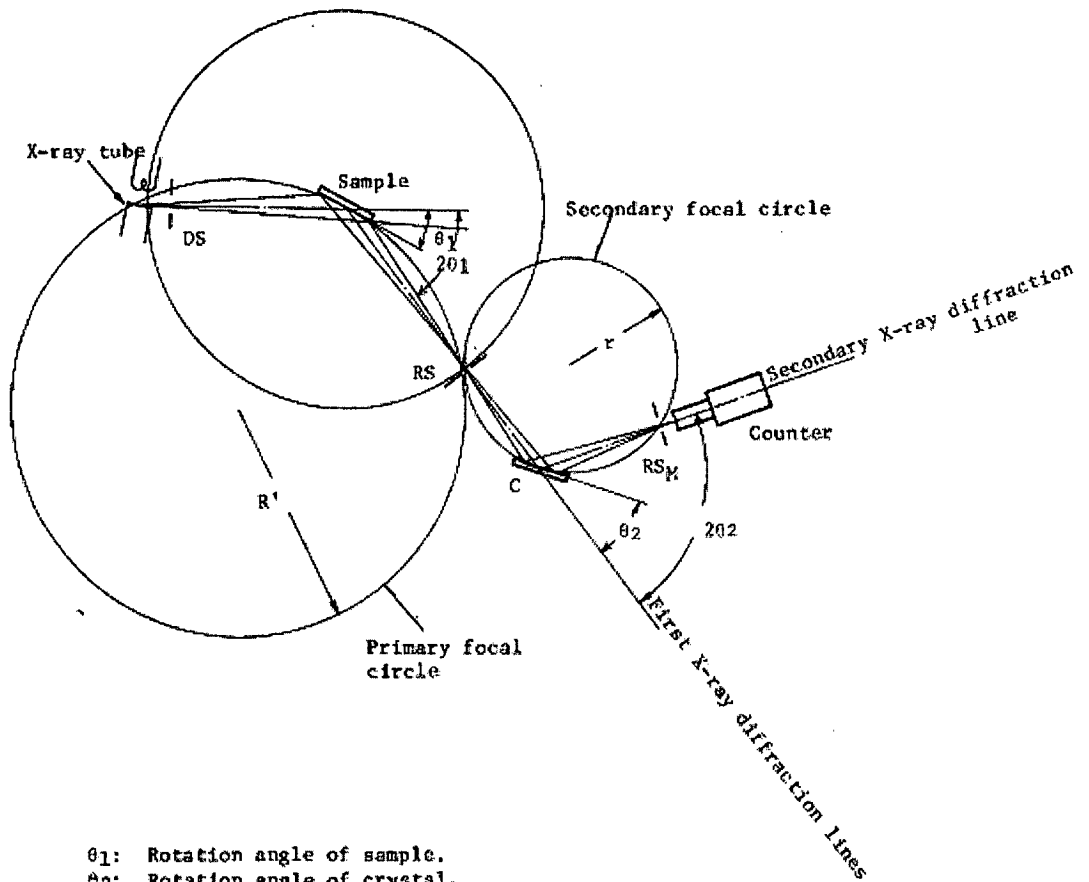
The secondary focal circle, which passes through the three points of the goniometer receiving slit, crystal and monochromator receiving slit, is in the same plane as the primary focal circle and its radius is equal to the curvature of the crystal

Fig.2.2.2

The X-ray monochromator along with the scattering slit and receiving slit is attached to the counter arm of the goniometer. The rotation of the counter through 2θ degrees is automatically accompanied by rotation of the specimen through θ degrees.

The way in which a diffractometer is used to record diffraction patterns depend on the kind of circuit used for measuring the rate of production of pulses in the counter. The pulse rate may be measured in the following different ways:

1. The succession of the current pulse is converted into steady current, which is measured on the counting rate meter, calibrated in such units as counts per second. This gives a continuous indication of the diffracted X-ray intensity.
2. The pulse of current are counted electronically in a circuit called the scalar and the average counting rate is simply by dividing the number of pulses counted, by the time spent in counting. This is the step scan mode.



- θ_1 : Rotation angle of sample.
- θ_2 : Rotation angle of crystal.
- R' : Radius of the primary focal circle (Goniometer radius of 185mm or 250mm).
- r : Radius of the secondary focal circle (Curvature of crystal $\times 1/2$).
- DS: Goniometer divergence slit.
- RS: Goniometer receiving slit.
- RSM: Monochromator receiving slit.
- C: Curved single crystal.

Fig 2.2.2 Set up of the X-ray diffractometer

2.3 Iodometric Techniques

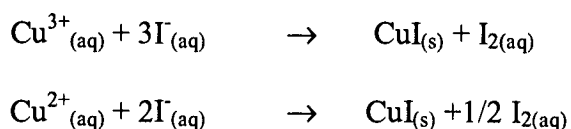
The titration of iodine against sodium thiosulphate, using starch as the indicator, is one of the most accurate volumetric processes. The descriptive term for the procedure depends on which reagent is used as the titrant. If iodine, I_2 , is used as the titrant, the process is termed an iodimetric process. If thiosulphate, $S_2O_3^{2-}$, is used as the titrant, it is termed an iodometric process, which is the procedure used in this analysis.

2.3.1 Determination of the δ value in $YBa_2Cu_3O_{7-\delta}$ by Iodometric Titration

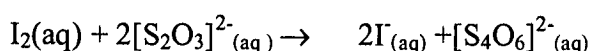
Two titration experiments were carried out to determine the value of δ in the formula of our parent and doped Y123 samples.

Experiment A

$YBa_2Cu_3O_{7-\delta}$ was dissolved in $HCl(aq)$ and then reacts with $KI(aq)$ present as follows:



The liberated I_2 was titrated with standard sodium thiosulphate solution, using starch solution (a added near the end point) as indicator,

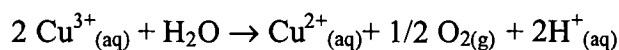


And the volume of $[S_2O_3]^{2-}_{(aq)}$ required was recorded.

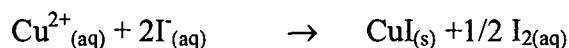
The moles of $[S_2O_3]^{2-}$ required to titrate the liberated iodine are equivalent to $Cu^{2+} + 2 Cu^{3+}$.

Experiment B

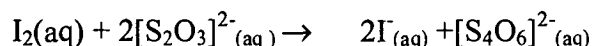
YBa₂Cu₃O_{7-δ} was dissolved in HCL(aq), in which Cu³⁺ is rapidly reduced to Cu²⁺



The total Cu content can then be measured by treatment with iodine.



The titration of the liberated iodine with standard thiosulphate



Each mole of Cu in YBa₂Cu₃O_{7-δ} is equivalent to one mole of [S₂O₃]²⁻.

Experiment B gives the total Cu content of YBa₂Cu₃O_{7-δ} and the difference between results of Experiment A and Experiment B gives Cu³⁺ content. With these two pieces of information, it is possible to calculate the value δ of in the formula YBa₂Cu₃O_{7-δ}.

2.3.2 Experimental Procedure

The procedure for estimation of Cu²⁺ and Cu³⁺ is described below

Experiment A

Weigh 0.025(X1) grams of sample and take in flask A. Add 1.162 grams of KI to the sample (powder) in flask A. Mix the whole mixture thoroughly ensuring that no powder sticks to the flask walls. Add 7ml of 0.7M HCl to flask A, shake well till the sample dissolves in the acid completely and immediately titrate it with 0.01M Na₂S₂O₃ (Sodium thiosulphate)solution. When the colour of the solution fades , add 4-5 drops of starch solution (indicator) to the flask A, the solution turns deep blue.

Titrate till milky colour appears , this is the end point. Read the burette readings as V_1 .

Experiment B

Weigh $0.035(X_2)$ grams of sample and take it in flask B. Add 7ml of 1M HCl to flask B and boil till sample dissolves. Add 1.162 grams of KI to the sample in flask B, and immediately titrate it with 0.01M $\text{Na}_2\text{S}_2\text{O}_3$ solution. When colour of the solution fades ,add 4-5 drops of starch solution (indicator) to flask B, the solution turns deep blue. Again titrate it till milky colour appears, this is the end point. Read the burette reading as V_2 .

2.3.3 Estimation of Oxygen Content

Burette reading for $X_1=0.025$ grams is V_1 ml

Burette reading for $X_2=0.030$ grams is V_2 ml

From four parameters X_1, X_2, V_1, V_2 we calculate two constants A and B as

$$A = V_1 / X_1 \quad \text{and} \quad B = V_2 / X_2$$

As X % of M is being doped at Cu site , the amount of Cu in +2 valence state reduces to $L = 3(1-y) [(A-B) / B]$

The amount of Cu in +3 valence state reduces to $N = 3(1-y) - L$

The oxygen content in $\text{Y}_{0.9-x} \text{Pr}_x \text{Ca}_{0.1} \text{Ba}_2 [\text{Cu}_{1-y}\text{M}_y]_3 \text{O}_{7-\delta}$ compound is given as

$$O(7-\delta) = \{ (0.9-x) \text{ times Oxidation state of Y} + x \text{ times oxidation state of Pr} + 0.1 \text{ times oxidation state of Ca} + \text{Two times oxidation state of Ba} + N(\text{Cu in } +2) + L(\text{Cu in } +3) + (3y/100) \text{ times oxidation state of M} \} / 2$$

2.4 Four Probe Resistivity Measurement

Temperature dependent electrical resistivity measurement on parent and doped Y123 compounds were made using the in-house conventional d.c. four probe setup. Use of a four lead connection for two lead resistive is made so as to avoid voltage drop in the voltage sensing pair that causes measurement error. In two lead measurements the leads that measure sensor voltage are also current carrying leads, the voltage measured at the instrument is the sum of the sensor voltage and voltage drop within the two current leads.

On the sample holder a Teflon tape was spread (so that there is no electrical contact between sample and sample holder) on which the sample was placed. The conducting silver paste was used to attach four copper wires on the sample, out of which two acts as current leads and other two acts as voltage lead. The resistivity data was obtained for various temperature.

The temperature of the sample was monitored using a platinum resistance thermometer (PRT100) in conjunction with scientific solutions CAT601 temperature controller [4]. The data was recorded in the temperature range 300K-10K using closed cycle refrigerator. Current was passed through the sample through a Keithley 224 and the voltage drop in the sample voltage was measured using Keithley 181 nanovoltmeter. For each reading thermal voltage was made zero. The current was passed first in one direction and the voltage was recorded then the current is passed in the reverse direction and the voltage drop was again recorded. The average of the two voltage measurement is taken as the net measured voltage across the sample. After dividing the voltage drop by the current, the numerical value of the resistance of the sample at particular temperature is obtained. The four probe system was interfaced to a computer using Keithley KT-401 GPIB interface card and GPIB cables. The

schematic diagram of this set up is shown in Fig .2.4.The data acquisition and on screen plotting was done with the help of a programme written in Q-basic. The resistivity was then calculated from the measured resistance and the sample dimension. The resistivity ρ in Ohm-cm is calculated using formula

$$R=V/I= \rho/l/A \quad (2.4.1)$$

$$\rho=RA/l \quad (2.4.2)$$

where A is the area in cm. and l is the length in cm.

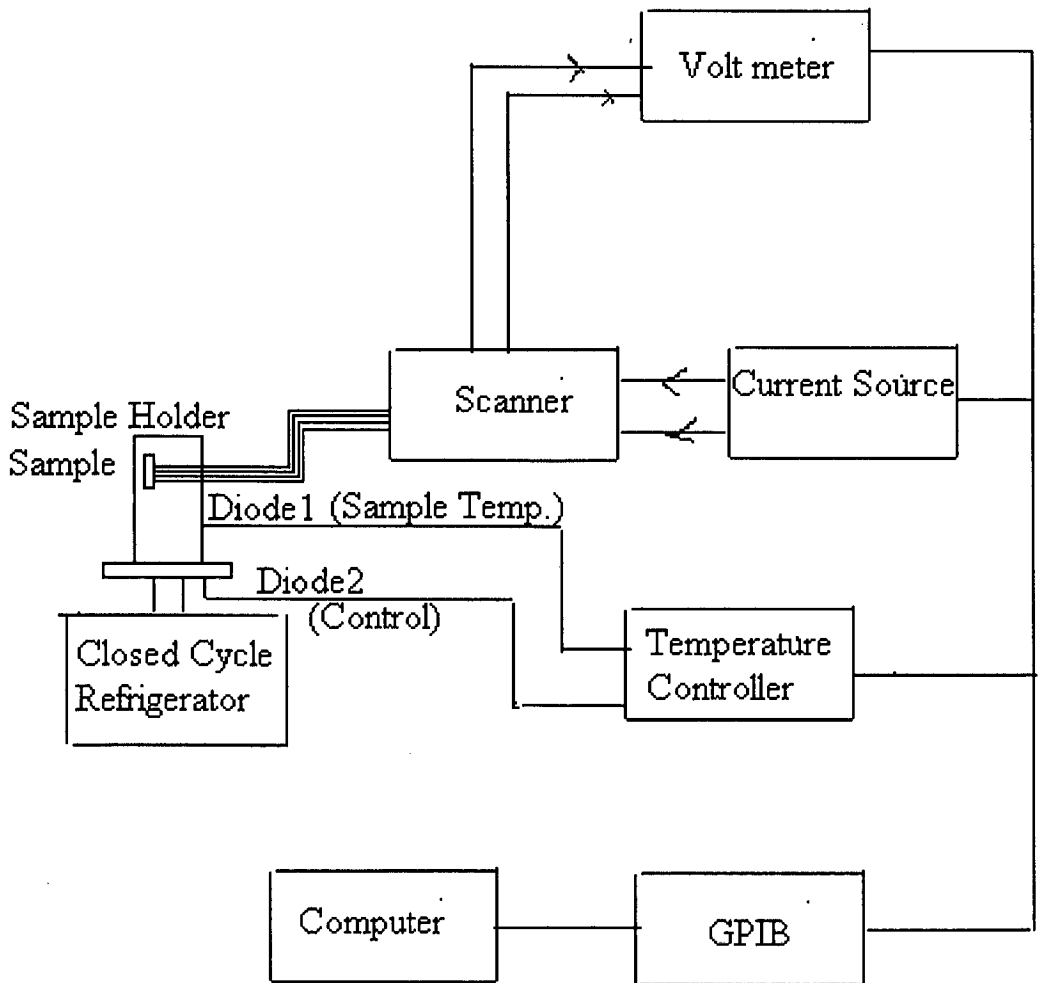


Fig.2.4.1 Experimental arrangement for measurement of Resistivity

2.5 Thermoelectric power

If the two different conductors are joined together at the two ends to form a pair junctions and these junctions are kept at the different temperatures, a thermo emf ΔV is set up between the two junctions, which is proportional to the temperature difference ΔT i.e. $\Delta V \propto \Delta T$ provided ΔT is small. This is known as Seebeck effect. The ratio of the emf to the temperature difference is called the thermoelectric power or thermopower S of the combination which depends on the temperature T i.e.

$$S = \left. \frac{\Delta V}{\Delta T} \right|_{\Delta T \text{ small}} \quad \Delta T \ll T$$

For the measurement of thermopower a standard differential method was used. These measurements were carried out using the setup developed at the Physics Department, Goa University under CSIR project [5]. The experimental set-up and the sample holder are shown in Fig 2.5.1 and Fig.2.5.2 respectively. Here, the sample is kept between the two highly polished copper plates, electrically insulated from the rest of the sample holder. Two heater coils, one on the bottom and the other on the top copper plate, serve to raise the overall temperature of the sample and to maintain a temperature gradient across the length of the sample respectively. The overall temperature of the sample was measured by platinum resistance thermometer (PT-100) while the gradient was monitored by a copper – constantan thermocouple operating in the differential mode. The system is cooled in a liquid nitrogen dewar. The e.m.f. developed across the thermocouple and the voltage across the sample and the temperature is measured using Keithley 2010 digital multimeter equipped with a multiple data scanner card.

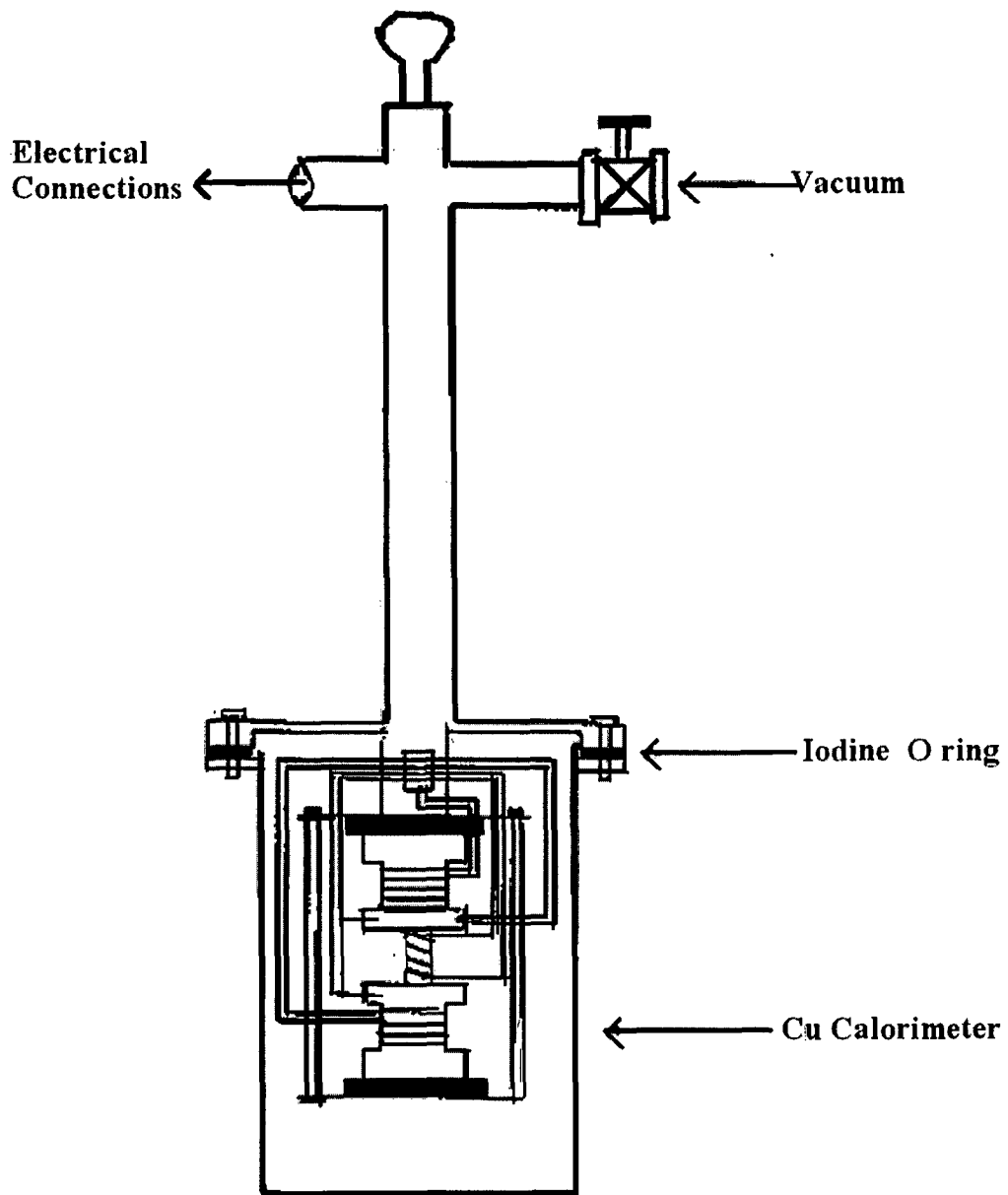


Fig.2.5.1 A layout of the thermopower setup

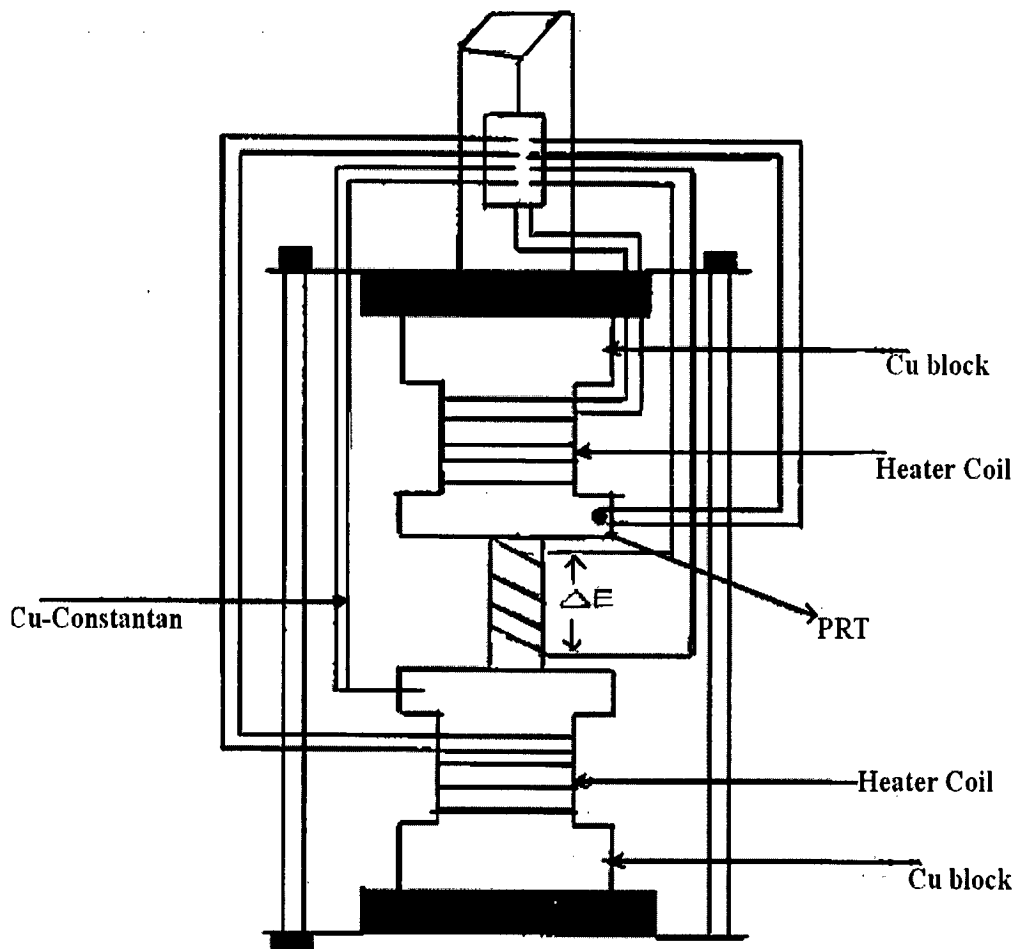


Fig.2.5.2 A layout of the thermopower sample holder assembly

To measure the thermopower S at a particular temperature T , say at 300K, the temperature difference across the sample is adjusted to nearly 0K or $1\mu\text{V}$ (for the copper constantan thermocouple $\sim 40\mu\text{V} \equiv 1\text{K}$ at 300K) by passing current through the two heater coils. The top copper plate of the sample holder is then heated resulting in a thermo emf V_s across the sample. The voltages V_s and that developed across the thermocouple V_{th} are measured for different gradients between the two plates . A graph of V_s versus V_{th} is plotted and its slope ($\Delta V_s / \Delta V_{th}$) is measured . Knowing the slope and the thermopower, S_{th} of the thermocouple at T , thermopower S is obtained.

In the present study, the sample beads were placed between the copper plates and the measurements were carried out at room temperature in the warming cycles similar to that of resistivity measurements.

References

1. A. R. Gupta, R. Lal, A. Sedky, A. V. Narlikar, and V.P.S. Awana, Phys. Rev. B **61**, 11752 (2000).
2. Instruction Manual for Rigaku X-ray Diffractometer System, D MAXII-C model.
3. C. Daniel, E.Marian, and A.Terrell, J.Chem.Educ. **64**, 847 (1987)
4. APD Technical Manual, APD Cryogenics Inc.USA.
5. K.R. Priolkar, P.R. Sarode, and N.Y.Vasantcharya, CSIR Project report January 2003.

Chapter 3

Role of Zn Substitution in $\text{YBa}_2\text{Cu}_3\text{O}_{7-\delta}$

System

3.1 Relevance of Substitution

The significance of substitutional studies can be understood from the fact that the very discovery of these high temperature superconductors owes to various substitutions and dopings carried out in low T_c or even non-superconducting systems. Thus there seems every hope that investigations of substitutional effect might yet pave the way for further enhancement of T_c , the discovery of new high T_c phases and possibly also go a long way in unfolding the mechanism responsible for high T_c superconductivity [1].

Bednorz and Muller's pioneering discovery [2] of La based cuprates containing Ba, and possessing the T_c of about 30K, was the result of a systematic and logical process involving substitutions. Their thinking in this part was essentially based on copper pair formation due to possible stronger electron-phonon coupling in oxides and ensuring Jahn Teller distortion giving rise to polarons. The approach [3] they followed to enhance T_c was more empirical based taking full advantage of the mixed valence character of copper. Their reasoning led them to partial substitution of La^{3+} by Ba^{2+} in La_2CuO_4 , whereby they could change the ratio of $\text{Cu}^{3+}/\text{Cu}^{2+}$ in a controlled way. Thus, in contrast to the non-superconducting metallic perovskite LaCuO_3 (or ABO_3 type) which had only Cu^{3+} and insulating perovskite La_2CuO_4 (having perovskite structure related to K_2NiF_4 structure) having only Cu^{2+} , the substituted material, $\text{La}_{1.85}\text{Ba}_{0.15}\text{CuO}_4$ became metallic, exhibiting superconductivity close to 30K. T_c was raised to 35 K when Ba was replaced by yet another alkaline – earth metal Sr [4]. The marginal increase in T_c may be ascribed to a smaller ionic size of Sr as compared to that of Ba.

3.2 Structure of $\text{YBa}_2\text{Cu}_3\text{O}_{7-\delta}$

The advent of yttrium based superconductors with T_c of about 90K was the result of substitutional studies involving replacement of La by Y in La-Ba-Cu-O system [5-8]. The phase responsible for the transition was found to have a cation stoichiometry of 1Y:2Ba:3Cu. The unit cell dimensions determined by electron and X-ray diffraction identified the structure as being related to a cubic perovskite with one of the cube axis tripled [9-21]. The crystal structure of the new compound so formed was different. The smaller ionic radius of yttrium substitution for lanthanum possibly led to the internal chemical pressure in the crystal lattice resulting in T_c enhancement. In the basic perovskite structure ABO_3 there are two cation sites [22]. The A site lies at the centre of a cage formed by corner sharing anion octahedra and accommodates the large cations in the structure. The B site lies at the centre of anion octahedra and accommodates the smaller cation sites. Hence, it was natural to place the large Y and Ba ions at the A sites and smaller Cu ions at the B site. The tripling of the perovskites unit cell, namely, $\text{BaCuO}_3\text{YCuO}_3\text{BaCuO}_3$ could then be accounted for by ordering the Y and Ba ions in the A sites such that the top and the bottom cells in a streak of three, contained Ba ions while middle cell contained a Y ion. The basic cation arrangement was not only consistent with 1Y:2Ba:3Cu stoichiometry but also provided a reasonable fit to X-ray diffraction data obtained for nearly single phase materials [9-12] and accounted for contrast seen in high-resolution images of the structure [23-26].

There are three anions per unit cell in the ideal perovskite structure, corresponding to nine possible oxygen sites in a tripled perovskite unit cell. Formal balancing of the charges on the cations requires a maximum eight oxygen ions per unit cell if all of the copper is assumed to be in a +3 state and 6.5 and 5 oxygen ions

per unit cell if charges of +2 and +1 are assumed for all the copper cations. It is therefore clear, that Y123 structure was oxygen deficient relative to the ideal perovskite structure. X-ray diffraction from small single crystal extracted from sintered polycrystalline material confirmed the basic positions of the cations and after refinements identified where the oxygen deficiency was accommodated in the structure was identified [27-28]. The X-ray data showed that the Y ion was surrounded by eight oxygen ions rather than by twelve as in the case of ideal perovskite structure. Refinements of the cell parameters in several studies [9-10,12,18-19,28] indicated that the unit cell was orthorhombic with b slightly larger than a.

The effect of oxygen ordering in the basal plane of the structure is to occupy one of the oxygen sites along a cell edge and to leave the other site vacant. The cell edge with the occupied site is thus lengthened relative to the cell edge with the vacant oxygen site, producing an orthorhombic unit cell. The ordering puts the copper ions in the basal plane of the structure at the centre of square arrangement of oxygen ions. The square planar arrangements of copper and oxygen ions are linked together by sharing their corners to form linear chains along the b-axis of the structure. The chains and the planes in the structure are linked through the oxygen that lies at the apices of the square pyramids.

The Y ion, which lies at the centre of the cell, is coordinated by eight oxygen's that form a slightly distorted square prism. The Ba ion is 10-fold coordinated and is shifted towards the Y-ion relative to its position in the ideal perovskite structure as shown in Fig.3.2.1. The crystal structure of $\text{YBa}_2\text{Cu}_3\text{O}_{7-\delta}$ (Y123) compound is shown in Fig.3.2.2. The ordered oxygen vacancies in Y123 structure result in a reduction in the coordination numbers of copper from the ideal six-fold octahedral coordination of

stoichiometric perovskite. The two oxygen vacancies result in four-fold coordinate [Cu 1] and five-fold coordinated [Cu (2)] copper atoms. This compound may be thought of as being made up of layers and chains. The copper [Cu (1)] atoms form linear chains of corner shared square planes oriented along the b-axis and the [Cu(2)] atoms form two dimensional layers of corner shared square pyramids. The O (4) atom from the chain also serves as the apical oxygen atom for the square pyramidal [Cu (2)].

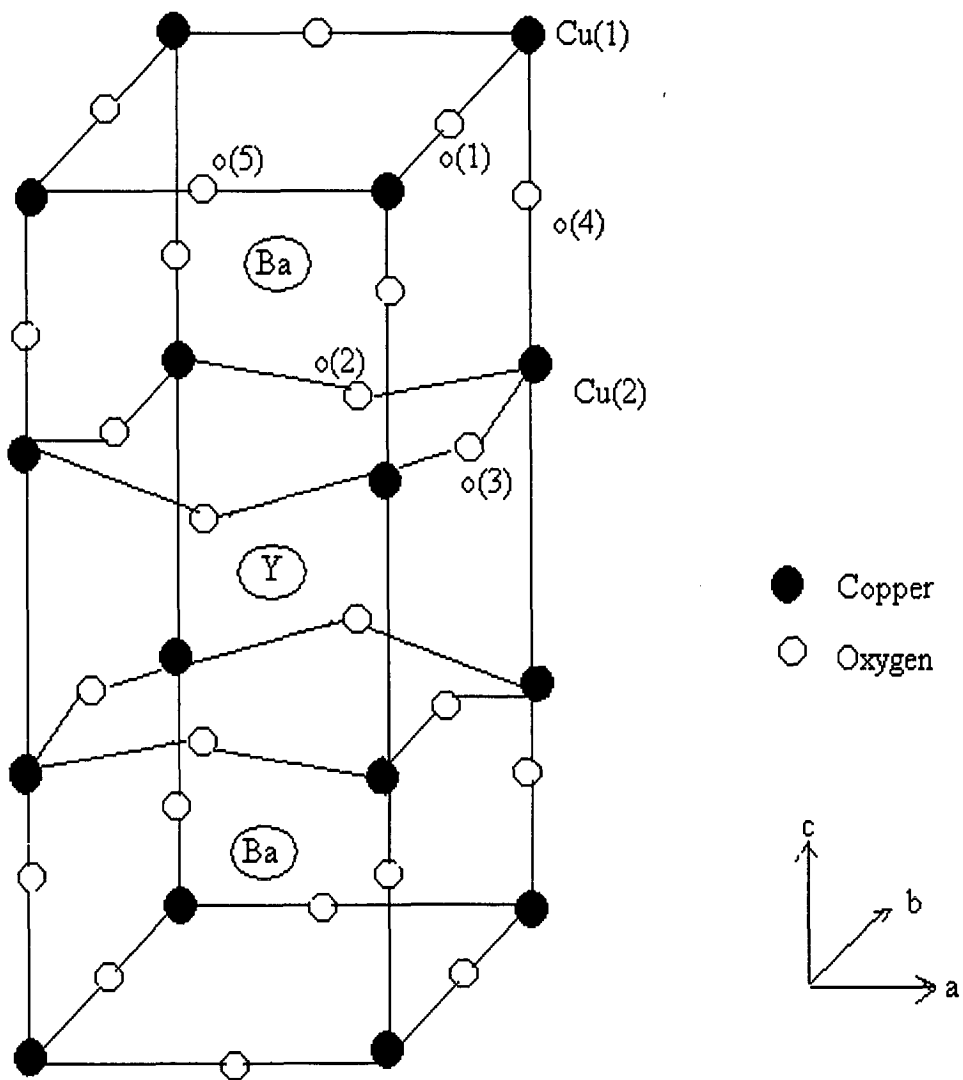


Fig. 3.2.1 Nearest neighbour bonds which shows the puckering of copper-oxygen planes.

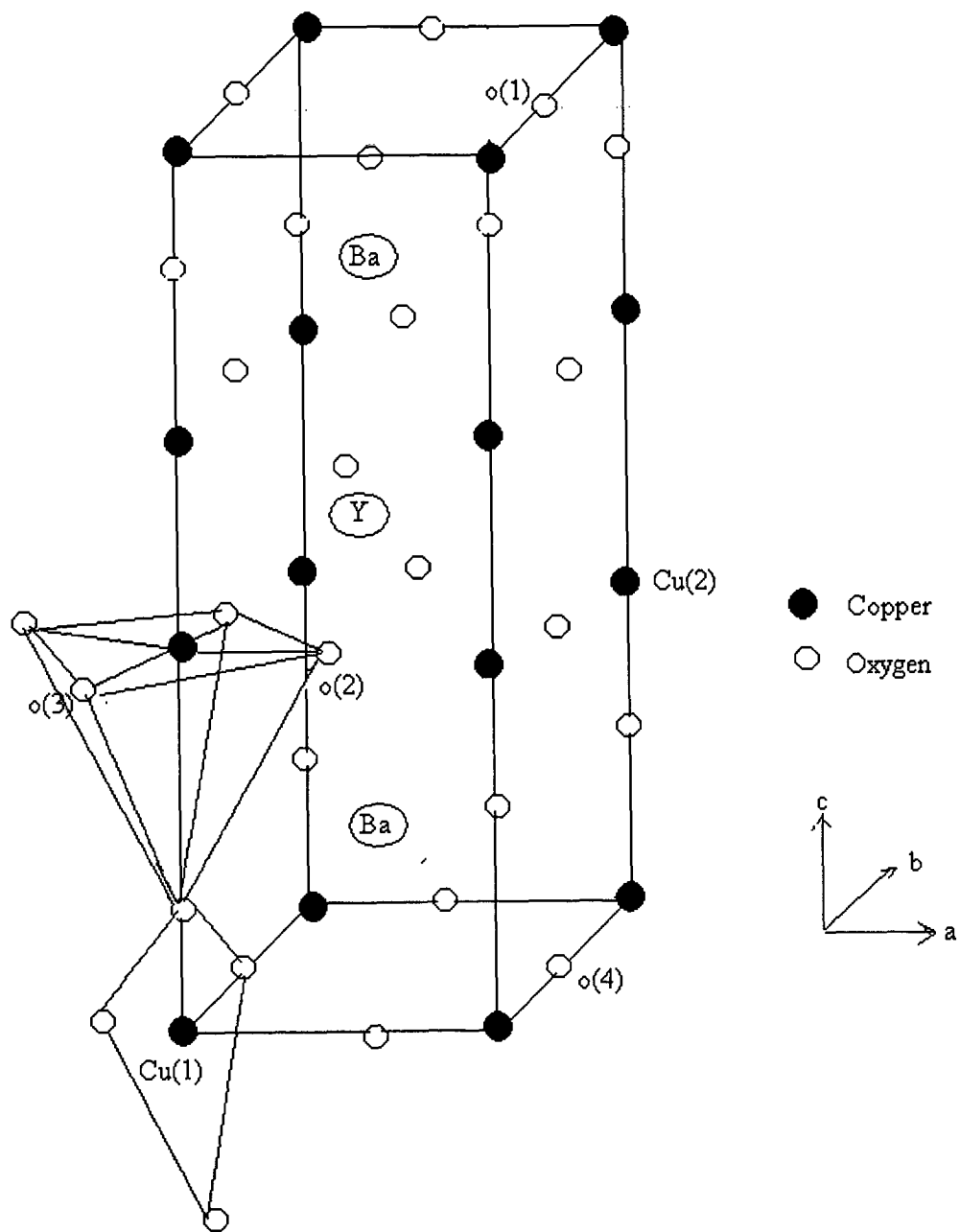


Fig.3.2.2 Crystal structure of $\text{YBa}_2\text{Cu}_3\text{O}_{7-\delta}$

3.3 General Consideration of Substitutions

The substitution of different cations in the cuprate superconductors is an important method for probing the parameters essential for superconductivity. All cuprates possess highly conducting two dimensional Cu-O networks. The Y123 system has in addition one-dimensional Cu-O chains along the b-axis. The low dimensionality in general leads to anisotropy of various properties, namely the range of coherence ξ , the normal state resistivity ρ_0 and the related parameters such as upper and lower critical fields H_{C1} and H_{C2} and the critical current density J_c when measured along, and perpendicular to the a-b plane. Any substitution which directly or indirectly interferes with these Cu-O networks tend to seriously affect superconducting properties of the material. Compared to the Cu-sites, substitutions at the other sites, in general, have lesser effect on T_c . Their role is primarily being to provide the characteristic crystal structures possessing the Cu-O networks. The site occupancy in substitutional studies is primarily controlled by three factors: (i) the ionic radii (ii) the valence state and (iii) the coordination number of the on-site cation.

Complete or partial substitutions of any of the constituents of the parental high T_c systems are in general attempted with the three broad objectives:[1]

- To replace toxic, less abundant or expensive components with less
- Hazardous more abundant or cheaper ones without making any compromise on superconducting property
- To study any anomalous changes in T_c which might give some insight into the mechanism of superconductivity.
- To explore the possibility of forming new superconducting phases of still higher T_c

Some of the prominent features associated with substitutions in the case of the cuprate system is the low-dimensional Cu-O network which is most relevant. The way the superconductivity gets influenced by dopings is essentially the manifestation of how the Cu-O networks would respond to substitutions at various sites. The networks can in general get distorted by: (i) Cation substitution directly at the Cu-sites. (ii) Anion substitution at the O-site and (iii) The aliovalent cation substitution at the non-Cu sites.

Generally, the reasons that reduces T_c are: (i) Orthorhombic to tetragonal transformation, (ii) Change in oxygen stoichiometry, (iii) Pair breaking due to magnetic moment of the dopant, (iv) Decrease in Debye temperature, (v) Disorder effect, (vi) Reduction in the effective carrier concentration and (vii) Localisation of carriers and obstruction of hopping process.

The effect is found to become more significant when the average spacing between the dopants in the network matches with the range of coherence in the a-b plane. When the substituted dopants at the Cu-site or at the non-Cu site is aliovalent, it tends to disturb the oxygen stoichiometry in the Cu-O network between Ba-O planes of the Y123 compound and leads to orthorhombic-tetragonal (O-T) change and T_c depression[1,29].

In all these situations where the gradual incorporation of dopant disturbs or adulterates the Cu-O networks and T_c is lowered, the nature of curve resistance-temperature (R-T) is found to turn from metallic to semiconductor.

3.4 Effect of Zn impurity on Y123 system

The substitution with rare-earth element on the Y site and with transition elements on the Cu site of the high temperature superconductor $YBa_2Cu_3O_{7.8}$

(Y123) is an important method of understanding the mechanism of the occurrence of superconductivity at high temperatures. In $\text{YBa}_2\text{Cu}_3\text{O}_{7-\delta}$ system there are two copper sites Cu(1), the chain site and Cu(2), the planar site. Most researchers found that nominally trivalent elements like Ga, [30-32, 37-39], Fe [30-34, 37, 39-41], Co [30-33, 37, 39-44], Al [32-33, 37, 39] substitutes on the Cu(1) site and cause a moderate reduction in T_c , while divalent dopants like Zn [30, 33-35, 37, 42-44] occupy the planar site and suppresses T_c drastically. The largest rate of reduction of T_c was $\sim 13 \text{ K \%}$ atom for Zn substitution on plane site [30, 37] and 5 K \% atom for Co substitution on the chain site [33, 37]. These results show that Cu(2)-O planes play a more important role than the Cu(1)-O chain in the Y123 superconductor [30, 35, 40-41, 44 - 45].

The valency of Cu fluctuates between $1+$ and $2+$ ($3d^{10}$ and $3d^9$), but divalent Zn having a definite valence state $2+$ and $3d$ levels is not favoured for such fluctuations. As a result Zn on Cu-site serves as an obstacle for charge carriers to move during conduction. Zn is the most widely substituted impurity for Cu in the cuprate superconductors. Only few percent of Zn substitution is sufficient to destroy superconductivity. Some consistent results show that the orthorhombic structure is retained, but the oxygen content is slightly affected. The site occupancy of Zn atom has been investigated by using neutron diffraction [30, 34-35, 46-47], Raman spectra, [48] extended X-ray absorption fine structure analysis [35], X-ray absorption near-edge studies and [40] nuclear magnetic resonance [38-39].

The superconductivity in the cuprate superconductors is controlled by the electronic structure of the two dimensional CuO_2 planes [49-50], and in turn depends upon the antibonding band formed by the interaction between the planar Cu(2) dx^2-y^2 and O(1) p_x , O(2) p_y orbitals. The substitution of a transition metal impurity at the Cu(2) site perturbs the electronic structure of this band and the nature of this band

and nature of this perturbation depends mainly upon the difference in energy between the d level of the impurity and those of the Cu(2) site, is very severe and extended as the d levels of Zn lie far too low in energy, and are fully filled with ($3d^{10}$). This creates the interaction between a Zn impurity and the neighbouring oxygen atoms. Due to this the oxygen orbitals that were previously participating in the formation of antibonding band with a given Cu(2) atom, now no longer participate in the interaction and fall below the Fermi energy to lower energies and charge accommodation occurs at these sites.

The Zn doped Y123 system does not affect the structural properties i.e., the orthorhombic structure of Y123 system doped with Zn remains invariant for various concentration of Zn. Prior to the superconducting transition, the change in the temperature derivative of resistance from positive to negative is indicative of metallic to semiconducting like behaviour occurring with Zn substitution. For larger concentration $x > 0.10$ of Zn the material exhibits semiconducting like behaviour without becoming superconducting. For few concentrations with $x > 0.06$ the resistance shows the tendency to go to zero but actually it is not happened. The overall decrease of T_c with increasing Zn concentration can be understood in terms of its unique electronic structure. In contrast to divalent Cu ($3d^9$) the d-shell of divalent Zn ($3d^{10}$) is completely filled and as a direct consequence of that there is a considerably diminished overlap between the d-orbital of Zn and p-orbitals of O.

There are several advantages of using Zn namely: It mainly substitutes the in-plane, the hole concentration is believed to remain almost unaltered when the divalent Cu(2) is substituted by divalent Zn, enabling one to look at the effects of disorder at almost the same hole content [50]. An impurity disorder at the planar Cu site is found to promote localization of charge carriers, while at the Cu-chain site it affects the

dimensionality and the carrier transport along the c-direction [51]. Zn reduces T_c most effectively and therefore provides a mean to look at the low temperature behaviour of various normal state properties as superconductivity is suppressed.

3.5 Results and Discussion

3.5.1 X-ray Diffraction and Iodometric Titration

The XRD patterns of $\text{YBa}_2[\text{Cu}_{1-y}\text{Zn}_y]_3\text{O}_{7-\delta}$ (YZ123), $0 \leq x \leq 0.10$ are presented in Fig 3.5.1. These patterns are analysed by Rietveld method using the Full Prof programme and is presented in Figs.3.5.4-3.5.7 for some compounds.. The refinement on $\text{YBa}_2[\text{Cu}_{1-y}\text{Zn}_y]_3\text{O}_{7-\delta}$ has been carried out using main $\text{YBa}_2\text{Cu}_3\text{O}_{7-\delta}$ phase as the starting crystal structure model with space group Pmmm. We assume that each refined reflection profile can be described by Gaussian function. The wavelength of $\text{CuK}_{\alpha 1}$ is set as 1.5405\AA . The refinement is performed according to the following group order (1) Scale factor, background, zero point shift, (2) Cell parameters, (3) Preferred orientations, (4) atom position parameters, (5) site occupancies and ,(6) overall thermal parameters. The results of this analysis are summarized in Table 3.5.1 We observe that lattice parameters a, and b remains invariant with Zn doping in Y123 system . However, c parameter is slightly chaged. These values are found close to the values reported in the literature [51(b)] . The position of O(4) atoms is also found to vary. The little change in c parameter makes the O(4) atom to change its position along c axis . It is well known that Zn substitutes at the Cu(2) site [42] and it is evident from the result that Cu(2) positions are also slightly affected by Zn doping . The oxygen content were found using iodometric titration and is presented in Table 3.5.1. along with errors. We see that

with addition of Zn the oxygen content within the errors remains invariant making the system to retain the orthorhombic structure.

For the parent system $\text{YBa}_2\text{Cu}_3\text{O}_{7-\delta}$ the value of T_c is 90.00 ± 0.08 . Most of researchers [33,51(a)] have found this value for oxygen content varying from 6.80 to 6.90 and T_c of about 90K

The influence of oxygen content on superconducting properties, in particular, T_c discussed by Benzi et al [51(b)]. These authors have proposed a simple procedure for determination of oxygen content on the basis of inorganic crystal structure data(ICSD) based on 240 $\text{YBa}_2\text{Cu}_3\text{O}_{7-\delta}$ structures and the $(7-\delta)$ values have plotted as a function of the lattice constant, c , and obtained a relation

$$(7 - \delta) = 75.250 - 5.856 c \quad (3.5.1)$$

The values of oxygen content so obtained using equation (3.5.1) have been tabulated in Table 3.5.1 along with the experimentally determined oxygen content. It is observed that the oxygen content values obtained by above equation in each case is higher than the value obtained by iodometric titration. Furthermore, a comparison between the predicted T_c and experimental T_c was also done by these authors. These experimental results indicate that the proposed method of these authors overestimates the oxygen content .However, the experimental T_c values are in better agreement with the calculated oxygen content with respect to those obtained from iodometric titration indicating that the reliable oxygen content values are obtained from equation (3.5.1). As can be seen from Table 3.5.1, similar results are obtained by us in Zinc doped Y123 compound.

Table 3.5.1 Rietveld Refinement of XRD data for $YBa_2[Cu_{1-x}Zn_x]_3O_{7-\delta}$. The space group is Pmmm with Y ($1/2, 1/2, 1/2$), Ba ($1/2, 1/2, z$), Cu(1) (0,0,0), Cu(2) (0, 0, z), O(1) (0, $1/2$, 0), O(2) ($1/2, 0, z$), O(3) (0, $1/2, z$), O(4) (0, 0, z) Also shown oxygen content, and transition temperature. The number in the parenthesis are uncertainty in the last digit.

	0.0	0.01	0.03	0.06	0.08	0.09	0.1
z(Ba)	0.182(2)	0.182(2)	0.182(2)	0.182(2)	0.182(2)	0.181(2)	0.182(2)
z(Cu2)	0.361(2)	0.359(3)	0.361(1)	0.360(1)	0.358(3)	0.352(5)	0.362(2)
z(O2)	0.367(4)	0.367(3)	0.367(3)	0.373(4)	0.373(2)	0.397(3)	0.381(1)
z(O3)	0.383(3)	0.388(3)	0.388(3)	0.382(3)	0.382(4)	0.387(1)	0.382(4)
z(O4)	0.175(1)	0.172(3)	0.168(4)	0.162(4)	0.160(5)	0.152(5)	0.150(7)
a(\AA)	3.820(3)	3.823(2)	3.822(3)	3.824(2)	3.823(3)	3.824(2)	3.827(2)
b(\AA)	3.881(3)	3.883(3)	3.887(3)	3.888(2)	3.888(2)	3.887(1)	3.887(3)
c(\AA)	11.666(3)	11.672(1)	11.674(1)	11.666(4)	11.667(3)	11.666(3)	11.676(1)
R_{wp}	15.4	17.2	14.3	16.6	15.3	15.13.92	15.8
R_{exp}	12.7	16.4	13.7	15.6	12.7	13.9	12.9
R_{Bragg}	12.29	13.48	11.39	10.95	18.87	12.58	15.84
χ^2	1.48	1.23	1.18	1.74	1.44	1.19	1.20
Oxygen content as obtained from iodometric titration (7-8)	6.66 ± 0.08	6.67±0.05	6.67 ± 0.02	6.67 ± 0.02	6.67 ± 0.03	6.67 ± 0.04	6.67 ± 0.05
Calculated oxygen content from equation 3.5.1 (7-8)	6.933 ± 0.003	6.899 ± 0.001	6.887 ± 0.001	6.933 ± 0.004	6.928 ± 0.003	6.933 ± 0.003	6.875 ± 0.001
T_c (K)	90.00 ± 1.00	65.55 ± 1.00	45.00 ± 1.00	25.00 ± 1.00	19.44 ± 1.00	-	-

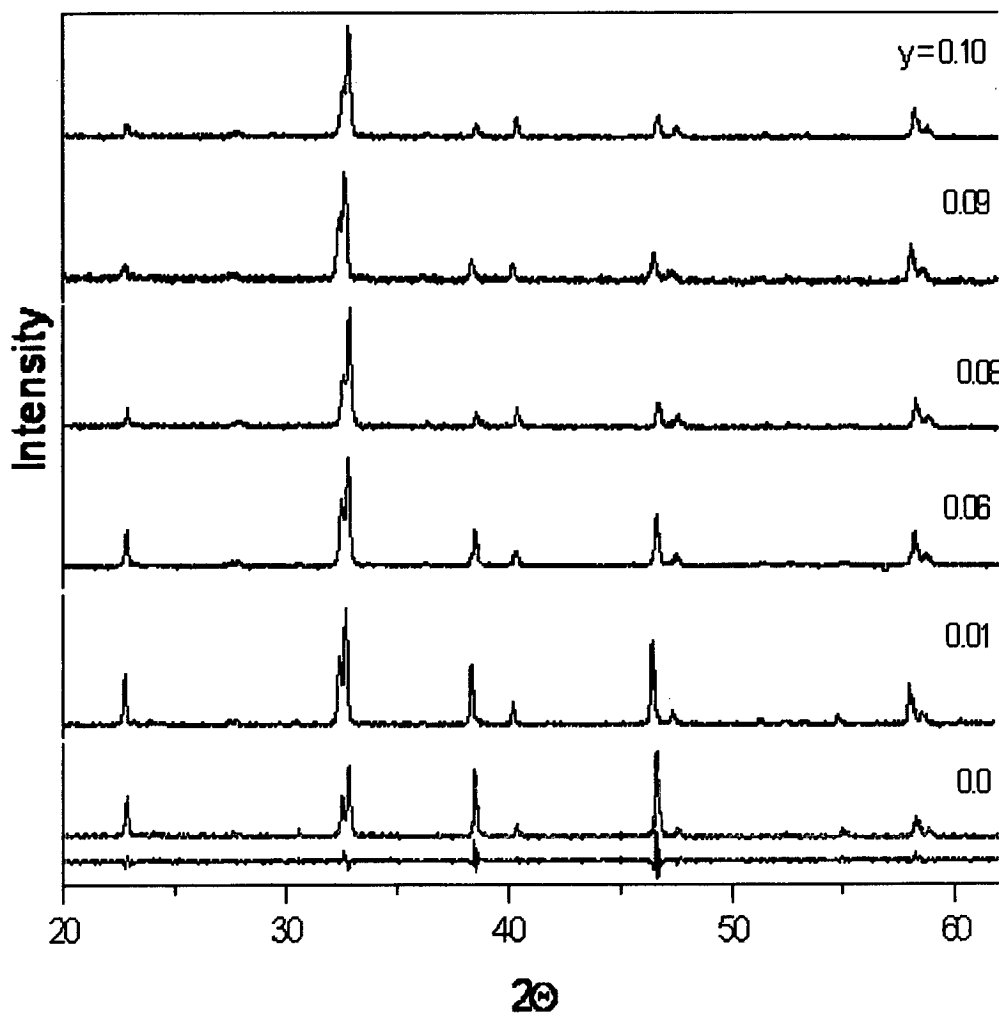


Fig.3.5.3. X-ray diffraction patterns of $\text{YBa}_2[\text{Cu}_{1-y}\text{Zn}_y]_3\text{O}_{7.8}$

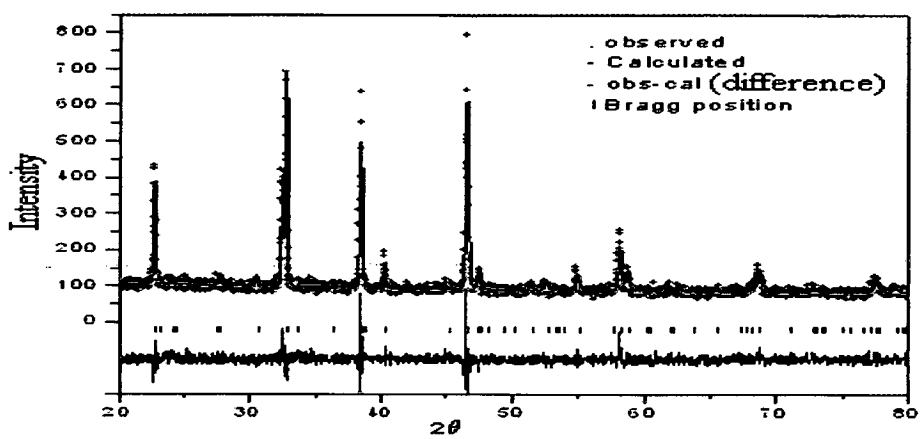


Fig .3.5.4 Rietveld refined diffraction patterns of $\text{YBa}_2 [\text{Cu}_{1-y}\text{Zn}_y]_3\text{O}_{7-\delta}$
with $y = 0.00$

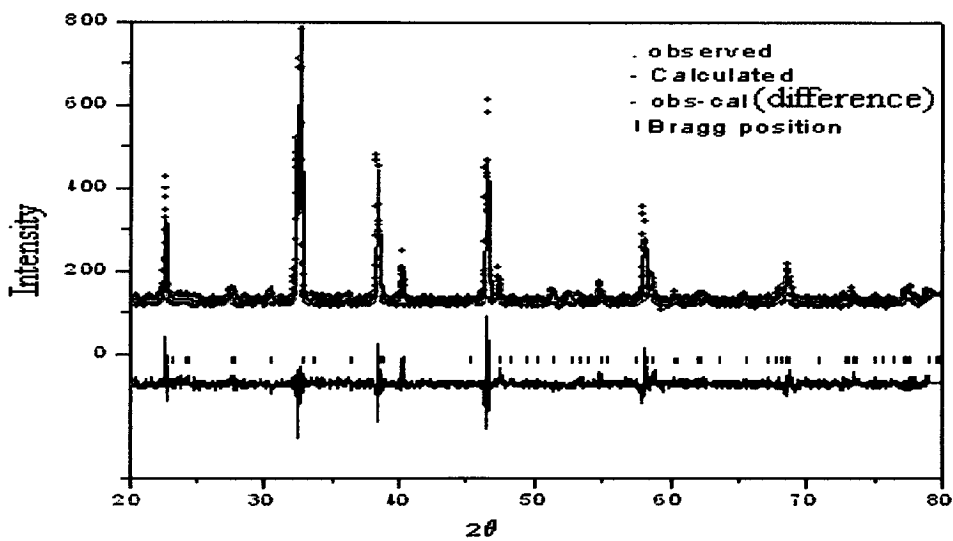


Fig .3.5.5 Rietveld refined diffraction patterns of $\text{YBa}_2 [\text{Cu}_{1-y}\text{Zn}_y]_3\text{O}_{7-\delta}$
with $y = 0.01$

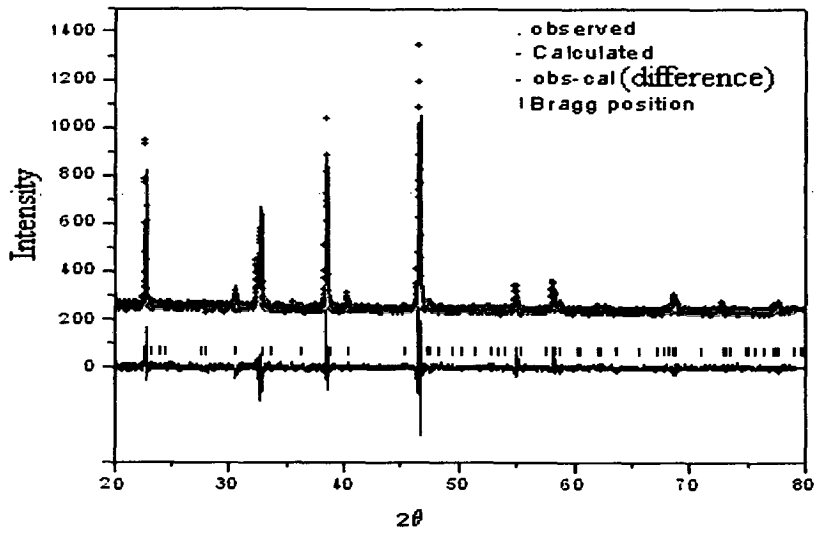


Fig .3.5.6 Rietveld refined diffraction patterns of $\text{YBa}_2 [\text{Cu}_{1-y}\text{Zn}_y]_3\text{O}_{7-\delta}$
with $y = 0.03$

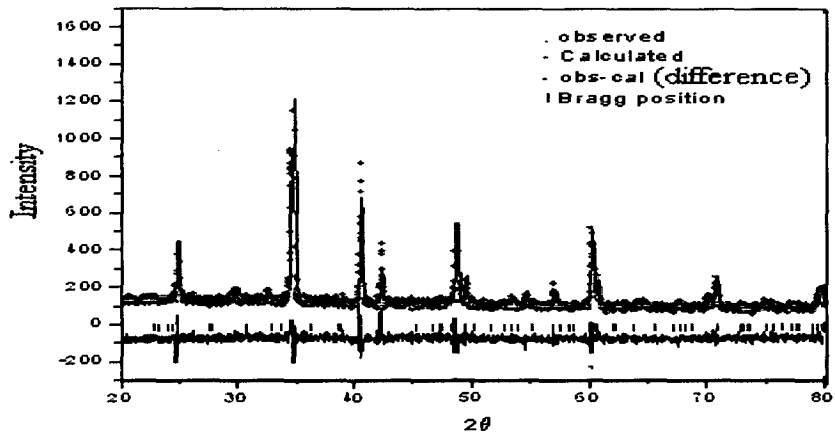


Fig .3.5.6(a) Rietveld refined diffraction patterns of $\text{YBa}_2 [\text{Cu}_{1-y}\text{Zn}_y]_3\text{O}_{7-\delta}$
with $y = 0.06$

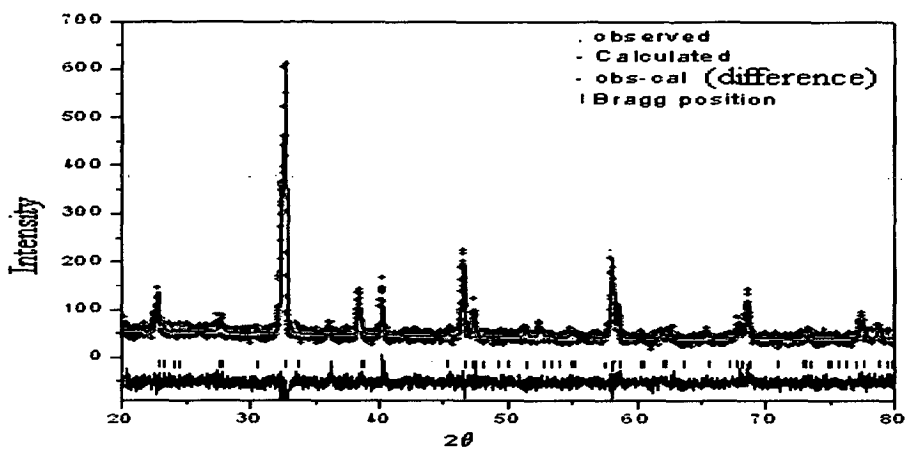


Fig .3.5.7 Rietveld refined diffraction patterns of $\text{YBa}_2[\text{Cu}_{1-y}\text{Zn}_y]_3\text{O}_{7-\delta}$
with $y = 0.08$

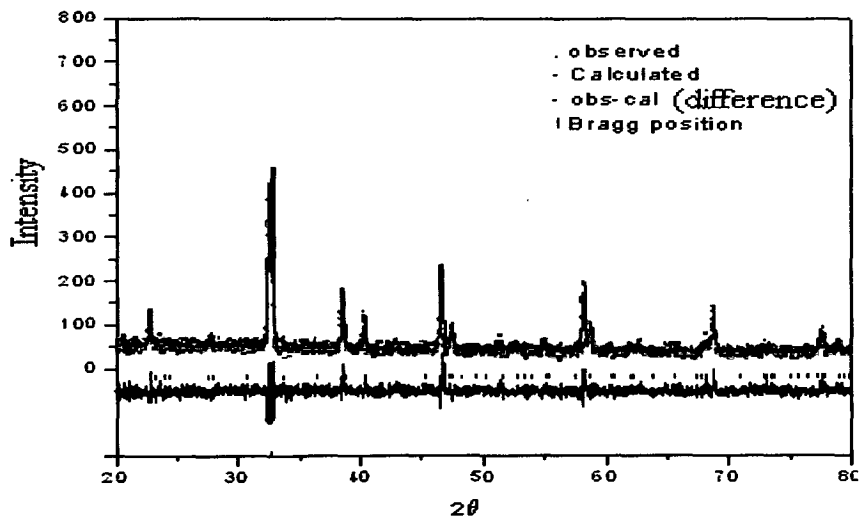


Fig .3.5.7(a) Rietveld refined diffraction patterns of $\text{YBa}_2[\text{Cu}_{1-y}\text{Zn}_y]_3\text{O}_{7-\delta}$
with $y = 0.10$.

3.5.2 Electrical Resistivity

From the electrical resistivity measurements we have obtained the ρ -T data for $\text{YBa}_2[\text{Cu}_{1-y}\text{Zn}_y]_3\text{O}_{7-\delta}$ and the plots are presented in Fig.3.5.8. Part of the ρ -T curves in $\text{YBa}_2[\text{Cu}_{1-y}\text{Zn}_y]_3\text{O}_{7-\delta}$ compound on high temperature side was fitted to a linear equation. This is shown in Fig.3.5.9 (a)-(f) by coloured line for temperature range 175-300K for $y = 0.00$, 200-300 K for $y = 0.01$, 140-200 K for $y = 0.03$, 175-270K for $y = 0.06$, 200-300K for $y = 0.08$, 200-300K for $y = 0.09$ and 165-300K for $y = 0.1$ and the linear curve was extrapolated to $T = 0\text{K}$. From this curve, following the method given in [52], the residual resistivity ρ_0 at $T=0\text{K}$ and the slope, $d\rho/dT$ for each composition were obtained. It can be seen that the linear part of the ρ -T curve has a positive slope $d\rho/dT$. As is known ρ_0 is connected with the impurity scattering and the slope $d\rho/dT$ determined from the linear region of the ρ -T curve is connected with carrier-carrier scattering. The non-linearity in the ρ -T curve starts at $y = 0.06$. Such type of behaviour is observed previously by several researchers [53]. The upturn in the ρ -T curve increases with increase in Zn content (y).

Another feature of this curve is that ρ_0 increases monotonically with increase in Zn content as shown in Fig. 3.5.11. However, the slope $d\rho/dT$ increases gradually with increase in Zn content until $y = 0.03$ where after it starts decreasing. This behaviour is presented in Fig 3.5.12. From Fig 3.5.10 we see that the critical temperature T_c decreases monotonically with increase in Zn concentration. For $y > 0.08$ the ρ -T curves do not show any sign of superconducting drop down to 20 K.

The value of superconducting transition temperature (T_c) obtained from resistivity data are given at the last row of Table 3.5.1 along with the most probable error. Suppression of T_c with Zn concentration (y) becomes large or small depending upon the corresponding change in ρ_0 . Larger the value of ρ_0 smaller is the T_c of the

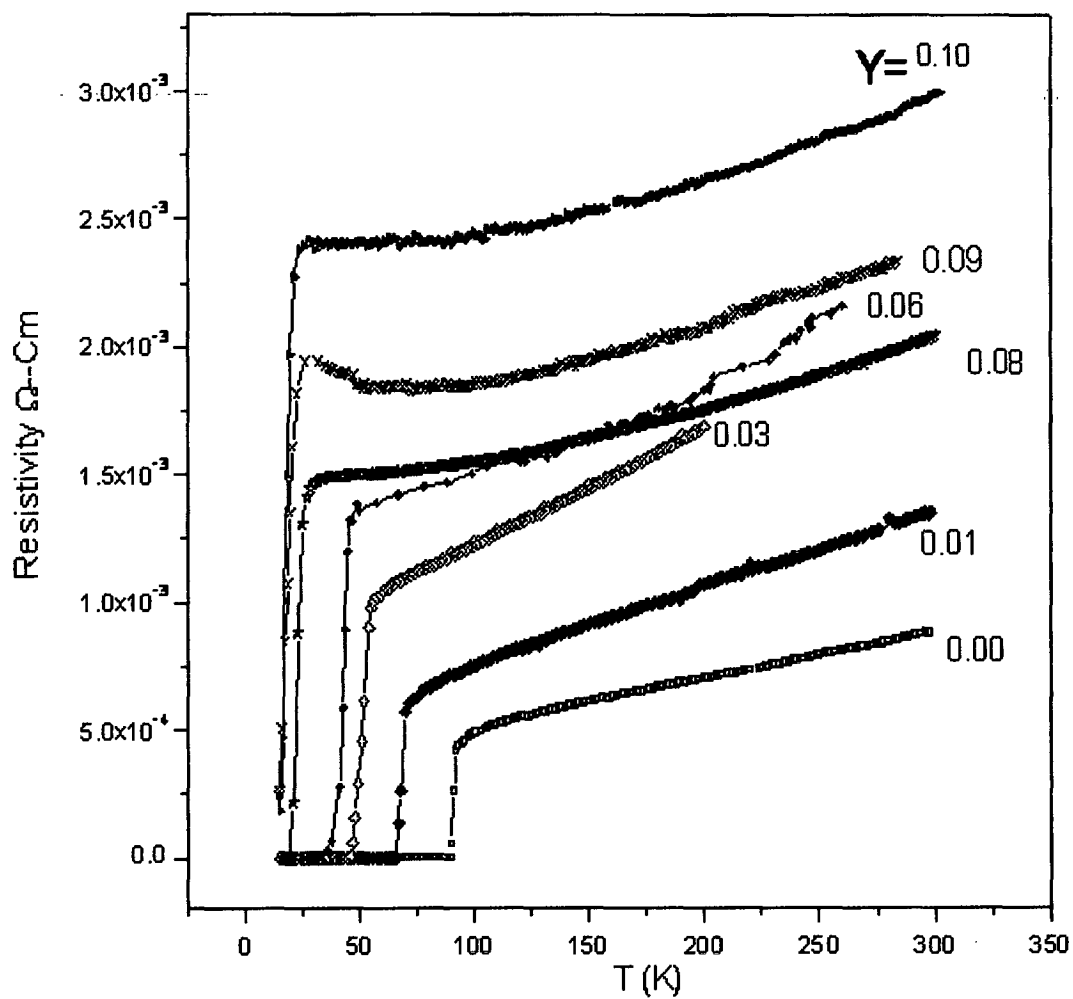


Fig. 3.5.8 Plot of resistivity vs (T) for YBa₂[Cu_{1-y}Zn_y]₃O₇ sample with different values of Zn concentration

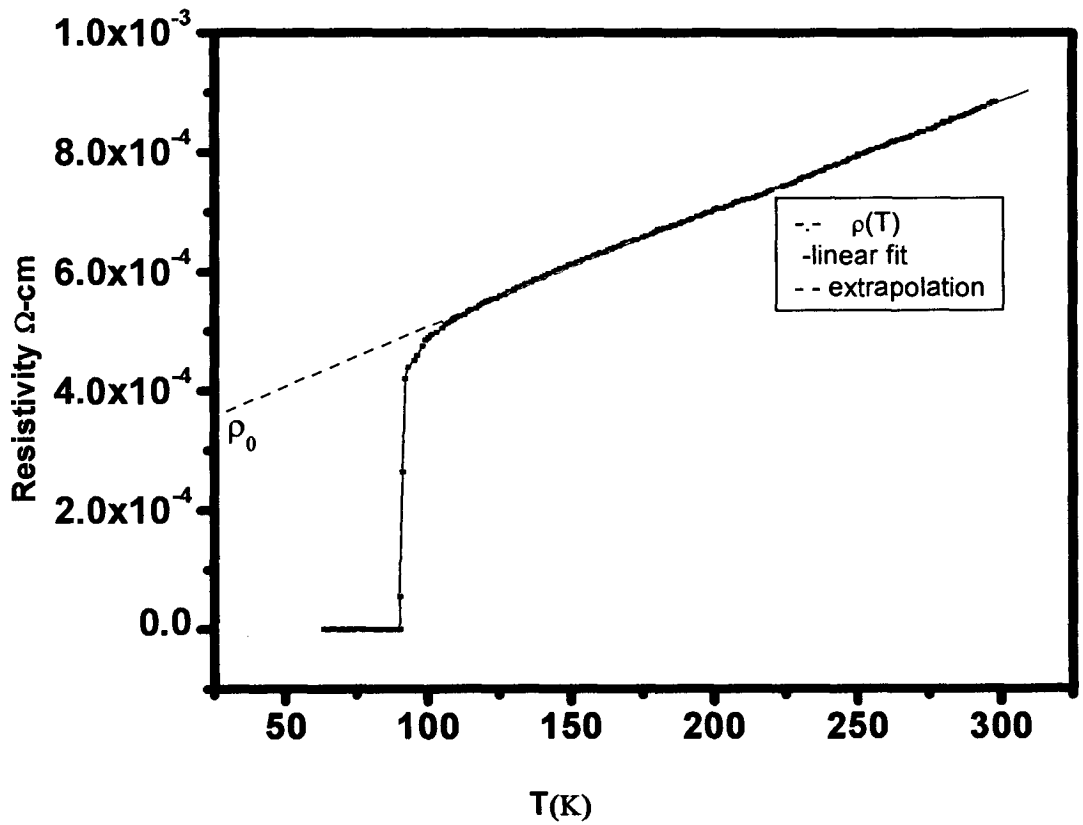


Fig 3.5.9 (a) Plot of resistivity vs T for YBa₂ [Cu_{1-y}Zn_y]₃O_{7.5} for y = 0.00 showing linear fit .

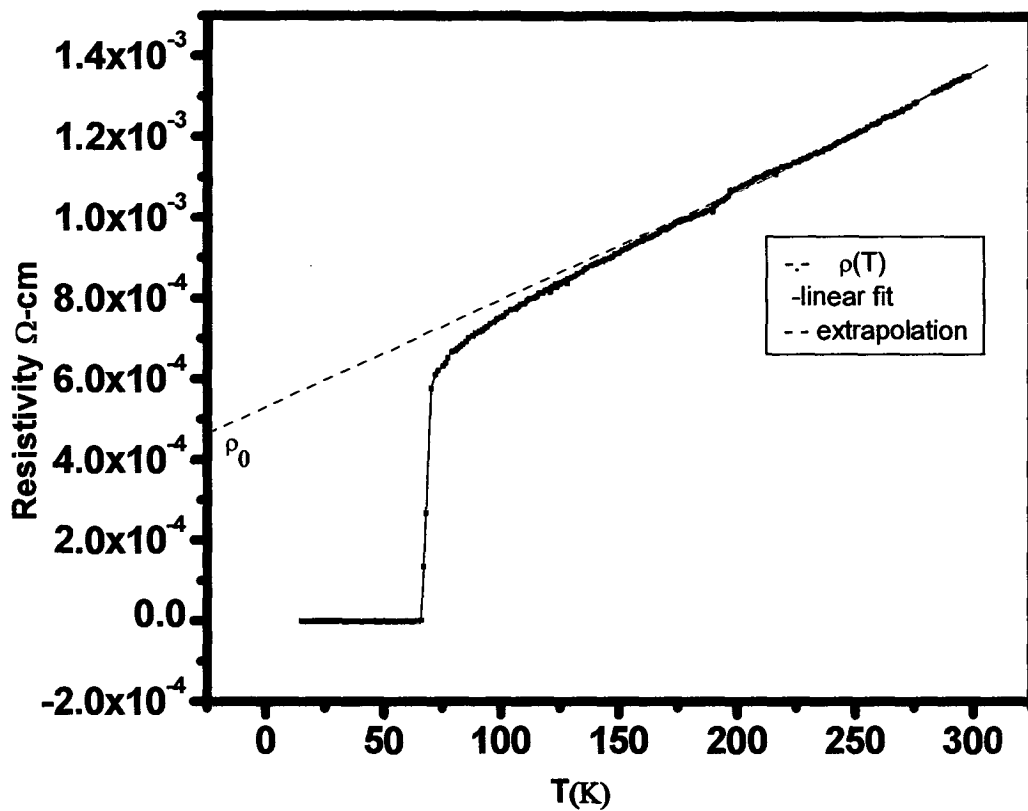


Fig 3.5.9 (b) Plot of resistivity vs T for $\text{YBa}_2[\text{Cu}_{1-y}\text{Zn}_y]_3\text{O}_{7.8}$ for $y = 0.01$ showing linear fit .

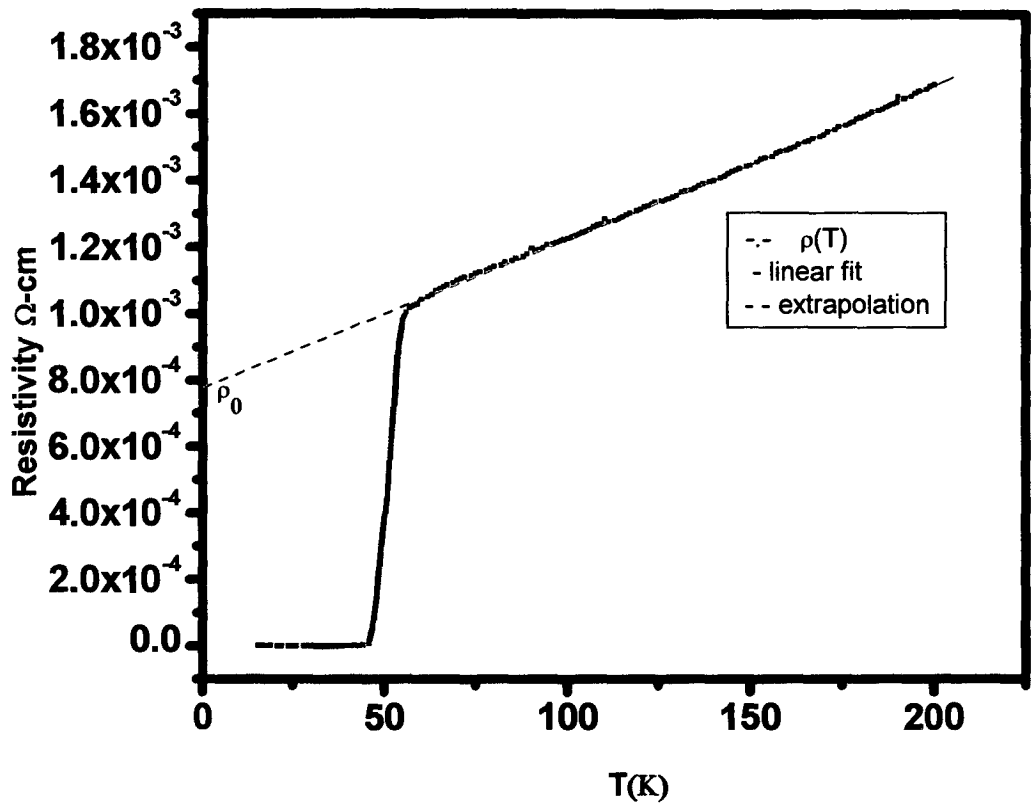


Fig 3.5.9(c) Plot of resistivity vs T for $\text{YBa}_2[\text{Cu}_{1-y}\text{Zn}_y]_3\text{O}_{7-s}$ for $y = 0.03$
 showing linear fit .

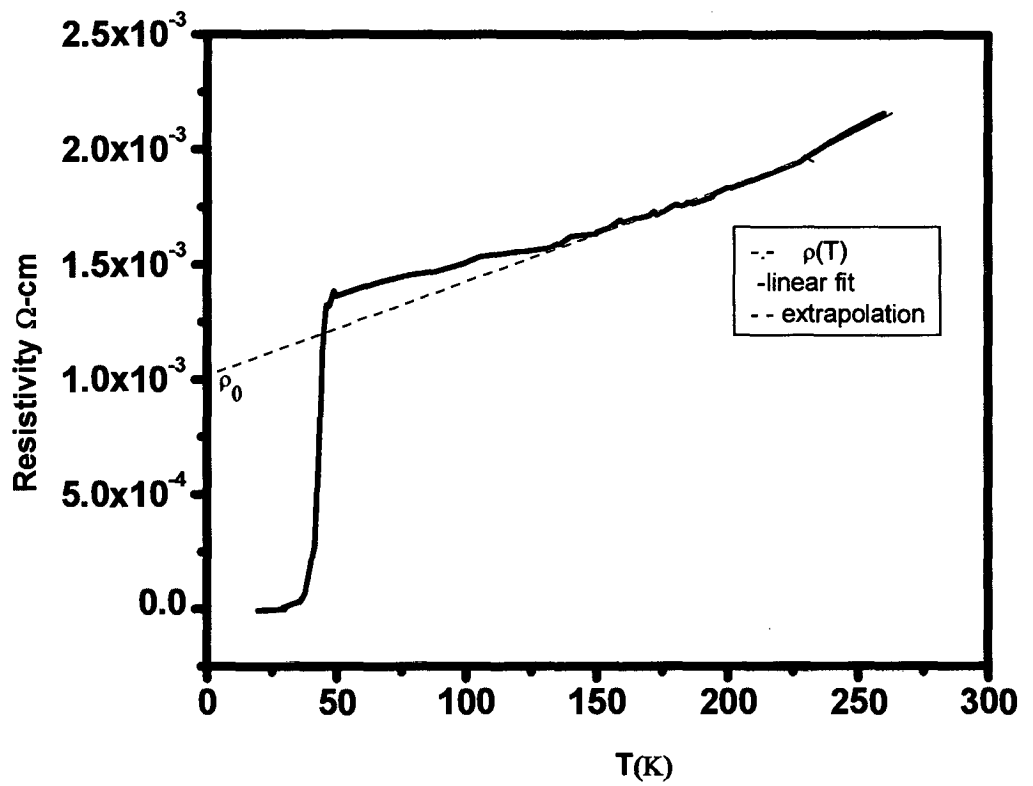


Fig 3.5.9(d) Plot of resistivity vs T for $\text{YBa}_2[\text{Cu}_{1-y}\text{Zn}_y]_3\text{O}_{7.8}$ for $y=0.06$ showing linear fit .

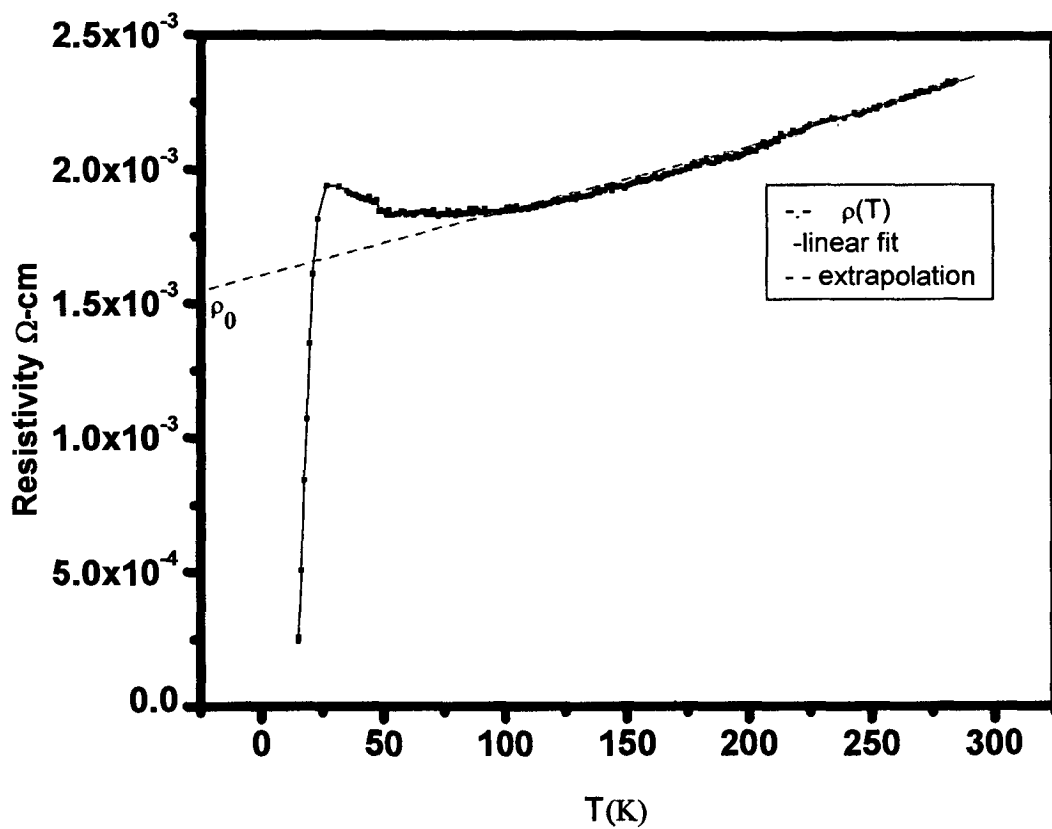


Fig 3.5.9(e) Plot of resistivity vs T for $\text{YBa}_2[\text{Cu}_{1-y}\text{Zn}_y]_3\text{O}_{7-\delta}$ for $y = 0.08$ showing linear fit .

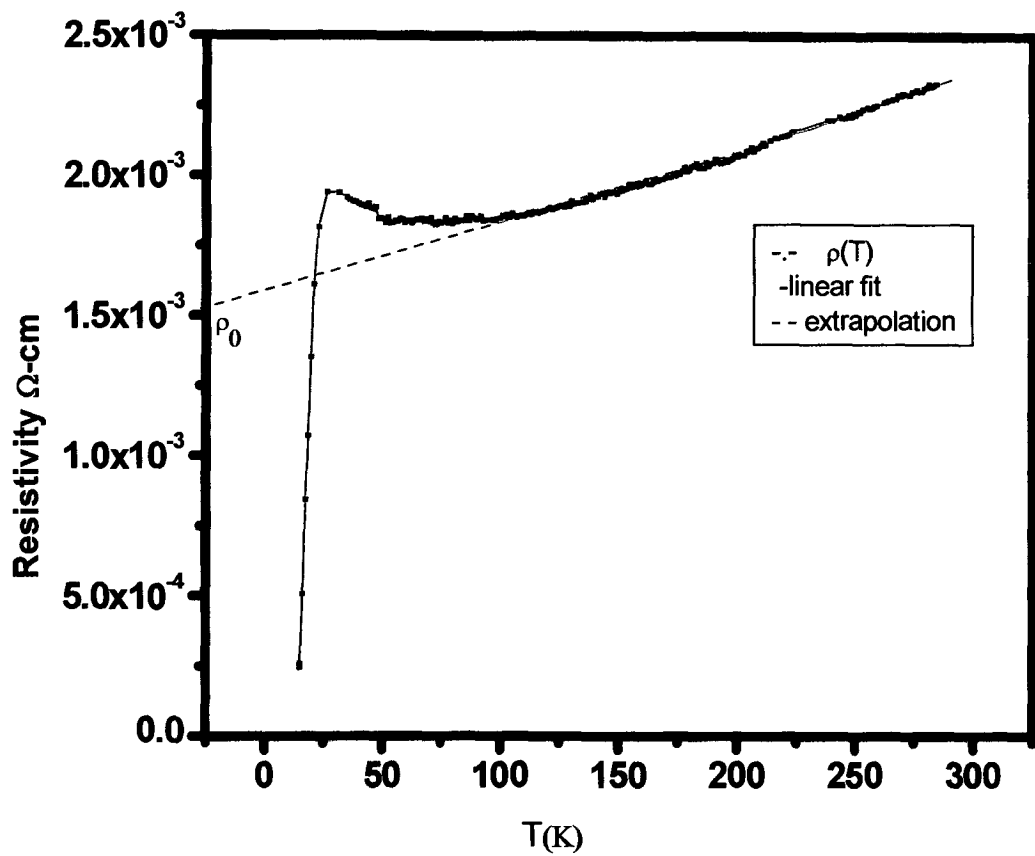


Fig.3.5.9(f) Plot of resistivity vs T for $\text{YBa}_2[\text{Cu}_{1-y}\text{Zn}_y]_3\text{O}_{7.8}$ for $y = 0.09$ showing linear fit .

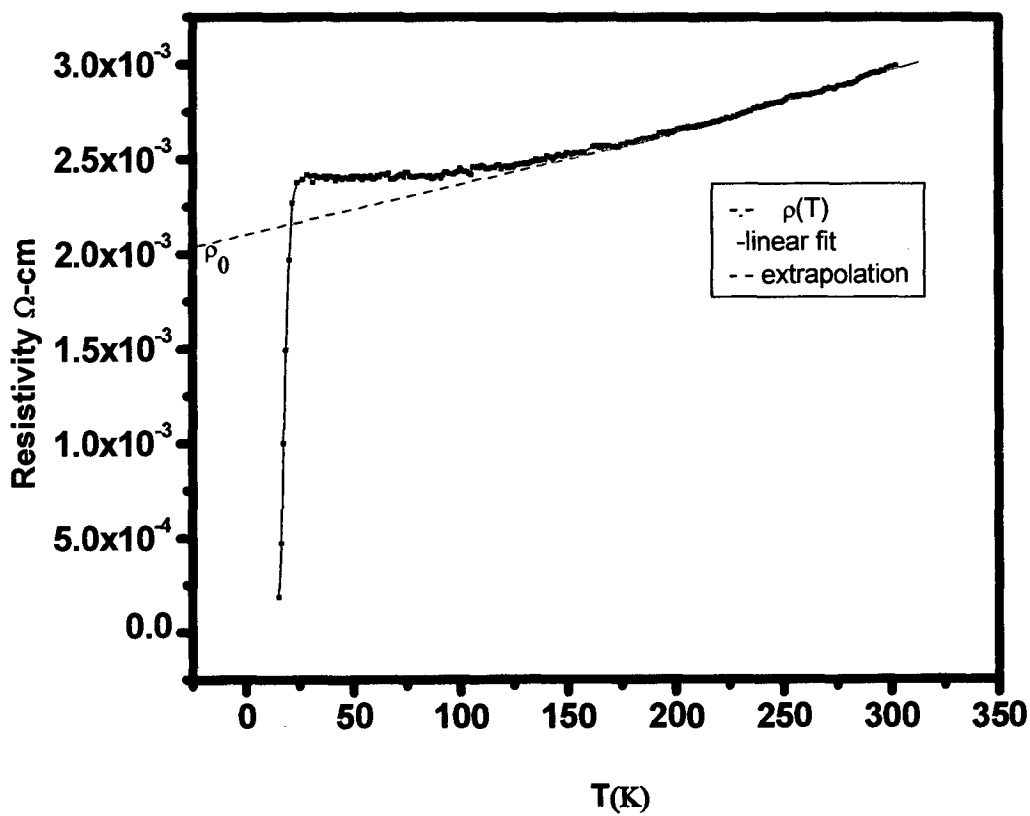


Fig 3.5.9(g) Plot of resistivity vs T for $\text{YBa}_2[\text{Cu}_{1-y}\text{Zn}_y]_3\text{O}_{7.8}$ for $y = 0.10$ showing linear fit .

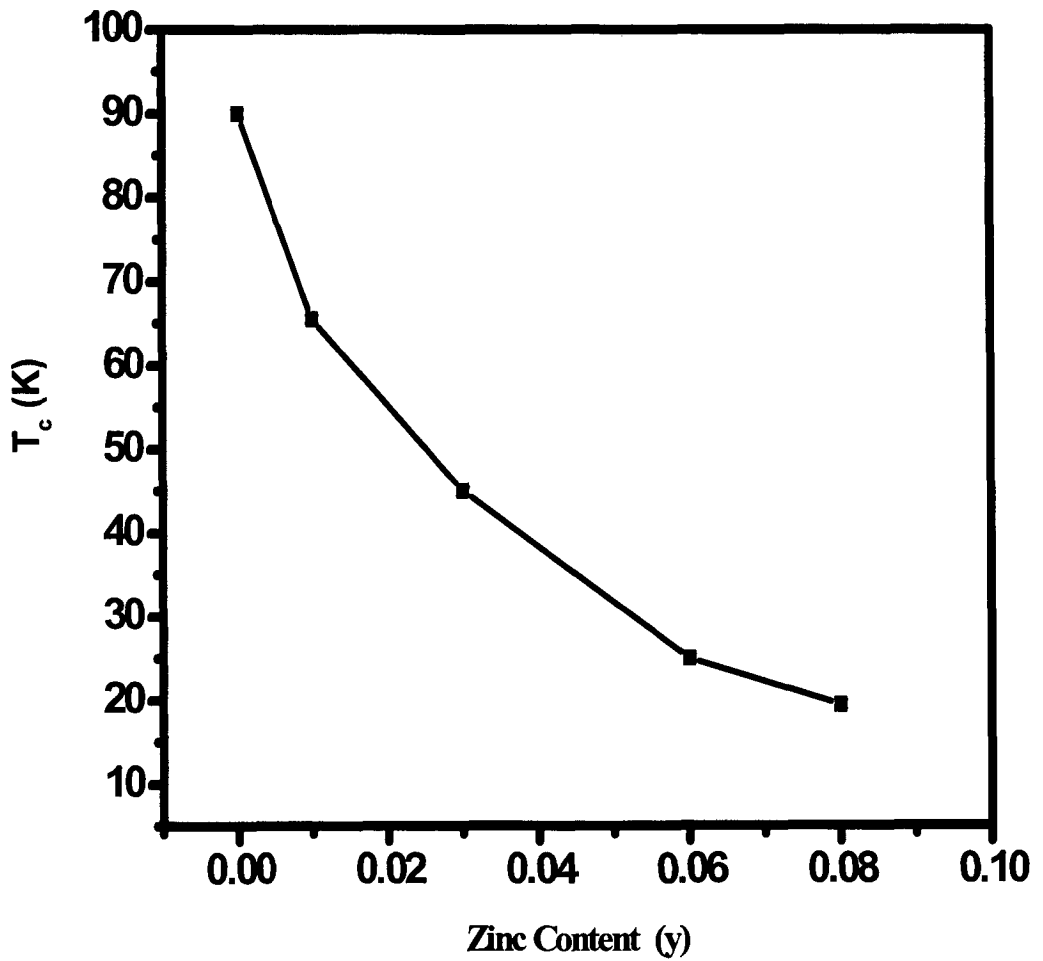


Fig.3.5.10 Plot of superconducting transition temperature T_c as a function of Zinc content (y) for $\text{YBa}_2[\text{Cu}_{1-y}\text{Zn}_y]_3\text{O}_{7-8}$

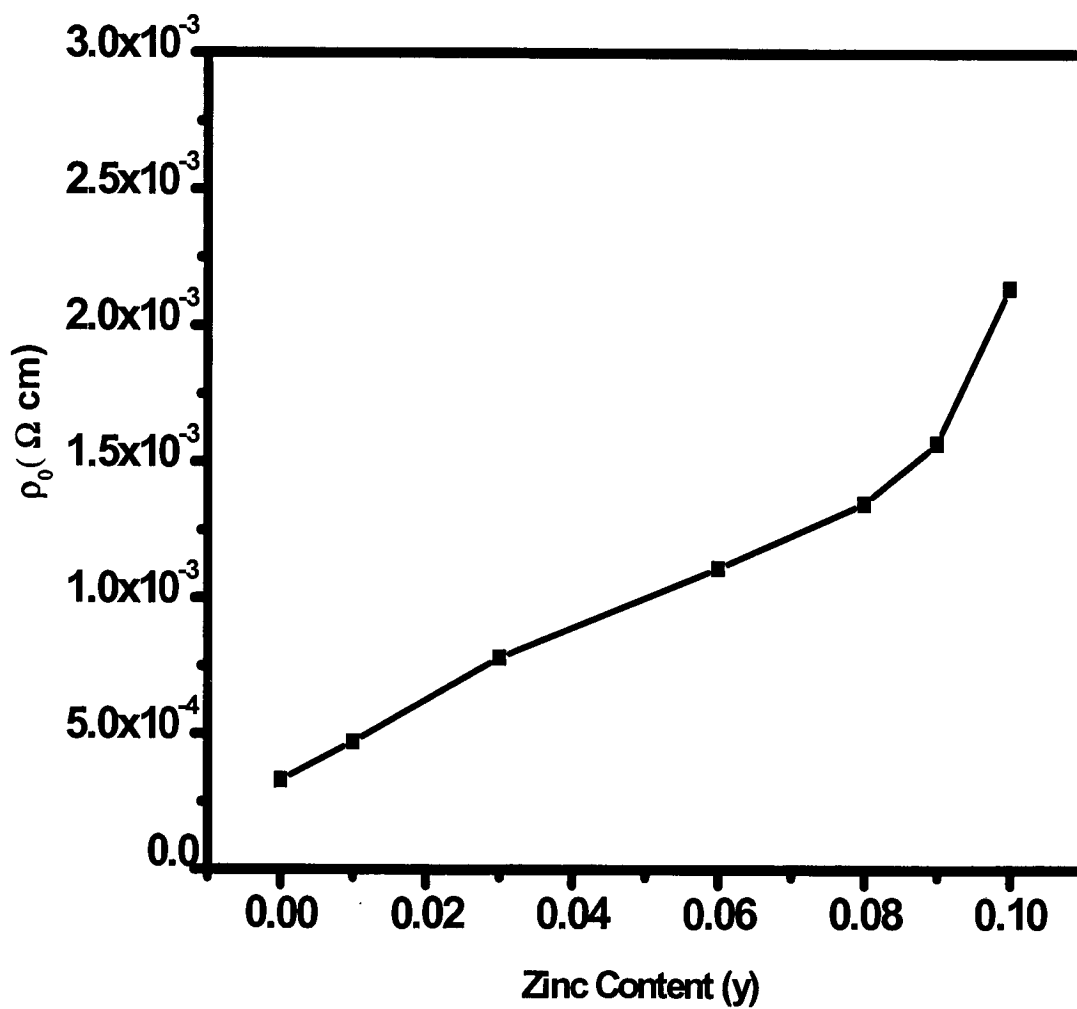


Fig. 3.5.11 Plot of variation of residual resistivity ρ_0 with Zn content y for $\text{YBa}_2 [\text{Cu}_{1-y}\text{Zn}_y]_3\text{O}_{7-\delta}$

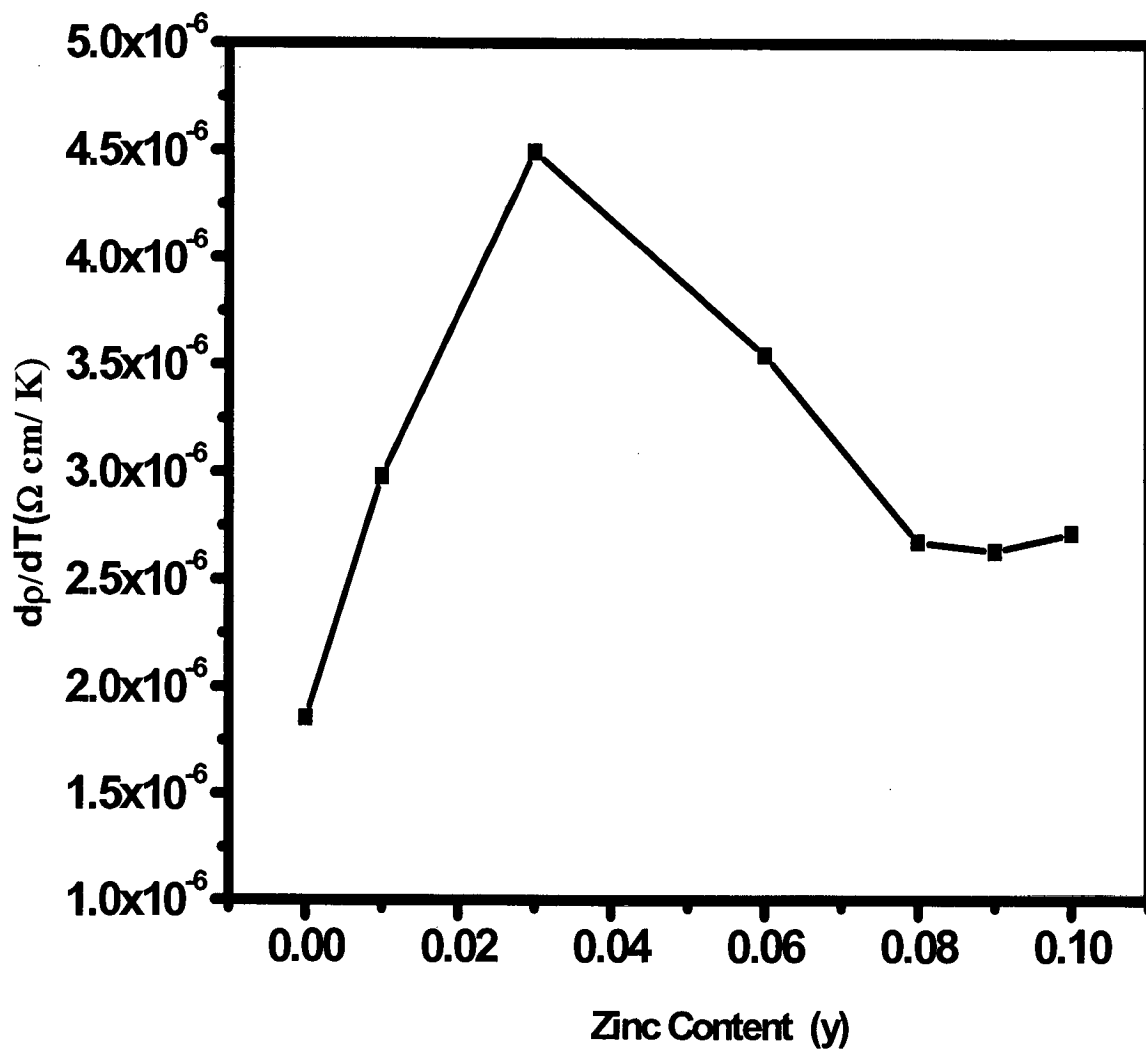


Fig. 3.5.12 Plot of slope dp/dT vs Zinc content (y) for $\text{YBa}_2[\text{Cu}_{1-y}\text{Zn}_y]_3\text{O}_{7-8}$

sample. On the other hand from the correlation of T_c with $d\rho/dT$, we find that just below maximum of $d\rho/dT$, the rate of decrease of T_c reduces and for values of Zn content corresponding to region after maximum of $d\rho/dT$, the T_c tends to vanish rapidly.

3.5.3 Correlation of T_c with ρ_0 and $d\rho/dT$

From the earlier section we see that increasing ρ_0 tends to degrade T_c , while increasing $d\rho/dT$ enhances T_c . This kind of effect of ρ_0 on T_c may be explained in the following ways. (1) According to Laughlin [54] the cuprate superconductors are mainly d-wave superconducting systems. So potential scattering will lead to pair breaking. Since the potential scattering is proportional to ρ_0 , increasing ρ_0 implies enhanced pair breaking. Thus T_c will reduce with increasing ρ_0 . (2) Reduction of T_c with increasing ρ_0 lies in the pinning of the dynamically fluctuating striped phase. It has been suggested by Liu et al, Zhou et al, Hasselmann et al [55-58] that the pinning of the dynamically fluctuating striped phase leads to the suppression of superconductivity in cuprate superconductors. Our result that increase in ρ_0 suppresses T_c corroborate theoretical consideration put forth by Liu et al, Zhou et al, Hasselmann et al.

It may be noted that the correlation of T_c with both ρ_0 , and $d\rho/dT$ simultaneously cannot be explained on the basis of the potential scattering. The physical origin of correlation of $d\rho/dT$ with zinc content lies in the carrier- carrier scattering. In fact we do not expect a T- dependent resistivity from carrier –impurity scattering. There may, however, be a T-dependent contribution to the resistivity from electron- phonon scattering. But in cuprate superconductor such a contribution is

significantly weaker than the contribution due to carrier-carrier scattering. Therefore we may overlook the electron-phonon scattering rate as compared to the carrier-carrier scattering rate. So, the increase in dp/dT implies increase in carrier-carrier scattering rate unless there is change in carrier density / density of state at the Fermi level. Cu valence (p^+) obtained from the charge neutrality conditions do not show any significant difference compared to optimum value of $p^+ = 2.11$ for our Y123 system. So we may thus assume that substitution of Zn does not change charge carrier density. This is supported by earlier studies of Williams et al [59] on high T_c superconductors, where in the case of Zn substitution in the Y123 system no change was observed in carrier density and density of state at the Fermi level. So, the view point that Zn doping increases dp/dT implies enhanced carrier-carrier scattering rate does not hold good. This contradicts our above mentioned observation on dp/dT suggesting depinning stripe phase. The possible solution for such discrepancy is that, suppression of T_c due to Zn arises due to pinning of dynamically striped phase. So, ρ_0 signifies the extent of pinning of the striped phase. These findings in Zn doped Y123 do not agree with the findings of Gupta et al [53]. This might be due to the presence of two doping ions such as Zn and Fe in Er123 system studied by these workers.

3.6 Conclusion

In this Chapter we have studied the effect of Zn substitution for Cu in the $YBa_2Cu_3O_{7.8}$ superconductors. Based on the XRD measurements and its refinement by Rietveld method, we find that for all the compositions, these superconductors retain the orthorhombic structure.

We have also reported our results of electrical resistivity vs temperature behaviour for Zn doped Y123 system. From $\rho - T$ curves we have obtained the

values of residual resistivity , resistivity slope corresponding to carrier- carrier scattering and critical temperature T_c .An attempt has been made to understand the observed correlation of ρ_0 and $d\rho/dT$ with Zn content .It is found that the critical temperature T_c is suppressed when ρ_0 increases .Whereas increase in $d\rho/dT$ enhances T_c . On the basis of generally acclaimed belief that the cuprate superconductors are d-wave superconductors it has been argued that potential scattering is not adequate for explaining the correlation of T_c with ρ_0 and $d\rho/dT$ simultaneously. Lowering of T_c can, therefore, be understood from the fact that the pinning of dynamically fluctuating stripe phase is by impurity scattering , rather than the weak depinning effect shown by carrier carrier scattering.

References

1. A. V. Narlikar, C.V. Narsinha Rao, S. K. Agarwal, Substitutional Studies on High temperature Superconductors Vol.1 , p.341.
2. J.G. Bednorz, K.A. Muller, Z Phys B **64**,187 (1986).
3. M.K. Wu,J.R. Ashburn, C. J. Torng, P.H. Hor , R.L. Meng, L.Gao, Z.J. Huang, Y.Q. Wang, and C.W. Chu, Phys.Rev. Lett. **58**,908 (1987).
4. H. Takagi, S. Uchida, K. Kitazawa, and S Tanaka, Jap. J. App. Physics **26**,1,123(1987).
5. W. K. Wu, J.R. Ashburn, C.J.Tong, P.H.Hor,R.L.Meng, L.Gao,Z.H. Huang,Y.Q. Wang ,C.W. Chu, Phys.Rev.Lett. **568**, 908(1987).
6. P. G.Anguly, R.A. MohanRam,,K. Sreedhar, C.N.R. Rao, Pramana J. Phys.**28**, L321 (1987).
7. J.M. Tarascon, L.H.Greene, W.R. McKinnon,G. W. Hull,Phys. Rev. B **35**, 7115 (1987).
8. S. J. Hwu, S. N. Song, J. Thie, K.R. Poeppelmeier, J. B. Ketterson, A. J. Freeman. Phys. Rev. B **35**, 7119 (1987).
9. R.J. Cava,B. Batlogg, R.B.VanDover, D.W. Murphy, S.Sunshine, T. Seigris, J.P.Remeika,E.A. E.A.Reitman,S. Zahurak, G.P.Espinoza, Phys Rev. Lett. **58**,1676 (1987).
10. P.M. Grant, R.B. Beyers, E.M. Engler, G. Lim, S.S.P. Parkin, M. L. Ramirez, V.Y. LeeA.Nazzal, J.E. Vazquez,R.J. Savoy,Phys. Rev. B **35**, 7242 (1982).
11. R.M. Hazen,,L.W. Finger, R. J. Angel, C. T. Prewitt, N.L. Ross, H. K. Mao, C. G. Hadidiacos, P. H. Hor, R.L. Meng, C.W. Chu, Phys.Rev.B **35**, 7238 (1987).

12. W.R. Mckinnon, J.M. Tarascon, L.H. Greene, G.W. Hull, D.A. Hwang, *Phys. Rev. B* **35**, 7245 (1987).
13. W. J. Gallagher, R. L. Sandstrom, T.R. Dinger, T. M. Shaw, and D. A. Chance, *Solid State Commu.* **63**, 147 (1987).
14. D. G. Hinks, L. Soderholm, D. W. Capone II, J.D. Jorgensen, I.K. Schuller, *Appl. Phys. Lett.* **50**, 1688 (1987).
15. Y. Kitano, K. Kifune, I. Mokouda, H. Hamimara, J. Sakurai, Y. Komura, K. Hoshino, M. Suzuki, A. Minami, Y. Maeno, M. Kato, T. Fujita, *Jpn. J. Appl. Phys.* **26**, L394 (1987).
16. T. Hatano, A. Matsushita, K. Nakamura, K. Honda, T. Matsumoto, and K. Ogawa, *Jpn. J. Appl. Phys.* **26**, L374 (1987).
17. M. Hirabayashi, H. Ihara, N. Teada, K. Senazaki, K. Hayashi, S. Waki, K. Murata, M. Tomumotao, Y. Kimura, *Jpn. J. Appl. Phys.* **26**, L476 (1987).
18. E. Takayama-Muromachi, Y. Uchida, Y. Matsui, K. Kato, *Jpn. J. Appl. Phys.* **26**, 1476 (1987).
19. Y. Syono, M. Kikuchi, K. Oshishi, K. Hiraga, H. Arai, Y. Matsui, N. Kobayashi, T. Sasaoka, Y. Muto, *Jpn. J. Appl. Phys.* **26**, L498 (1987).
20. K. Semba, S. Tsurumi, M. Hikita, T. Iwata, J. Noda, and S. Kurihara, *Jpn. J. Appl. Phys.* **26**, L429 (1987).
21. S.B. Qadri, L. E. Toth, m. Osofsky, S. Lawrence, D.U. Gubser, and S.A. Wolf, *Phys. Rev. B* **35**, 7235 (1987).
22. J. B. Goodenough and M. Longo, in *Londolt-Bornstein*, K.H. Hellwege and A. M. Hellwege eds. Group II Vol.4a, Chap 3a, Springer- Verlag, New York, (1970).

23. A. Ourmazd, J. A. Rentschler, J.C.H. Spence, M. O’Keeffe, R. J. Graham, D.W. Johnson Jr., and W. W. Rhodes, *Nature* **327**,308 (1987).
24. E. A. Hewat, M. Dupuy, A. Bourret, J.J. Capponi and M. Marezlo, *Nature* **327**,400 (1987).
25. Y. Matsui, E. Takayama-Muromachi, A. Ono, S. Horiuchi and K. Kato, , *Jpn. J. Appl. Phys***26**,L777 (1987).
26. K. Hiraga, D.Shindo, M. Hirabayashi,M. Kikuchi, K. Oh-Ishi, Y. Syono, , *Jpn. J. Appl. Phys***26**,L1071 (1987).
27. T. Siegrist, S.Sunshine, D.W. Murphy, R.J. Cava and S. M. Zahurak, *Phys. Rev. B* **35**,7137 (1987).
28. F.P. Okamura, S. Sueno, I. Nakai, and A. Ono,*Mat. Res. Bull* **22**,1081(1987)
29. B. Jayram, S. K. Agarwal, C. V. Narsimha Rao,A.V. Narlikar,*Phys. Rev.***B38**,2903 (1988).
30. G. Xiao , M. Z. Cieplak, A. Garvrin, F. H. Streitz A. Bakhshai and C. L. Chien , *Phys. Rev. Lett.***60**,1446,(1988): G. Xiao et al *Nature* **332** ,238 (1988):*Phys.Rev. B***35**,8782 (1987).
31. Y. Maeno , T. Tomita, M. Kyogoku, S. Awaji, Y. Aoki, K. Hoshino, A. Minami, and T. Fujita, *Nature* **328**, 512 (1987).
32. Youwen Xu, R. L. Sabatini, A. R. Modenbaugh, and M. Suenaga, *Phys. Rev. B* **38**, 7084 (1988): Youwen Xu et al, *ibid* **39**,6667 (1989): *Physica C* **169**, 205 (1990).
33. J.M. Tarascon, P. Barboux, P.F. Miceli, L.H. Greene, G.W. Hull, M.Eibschutz, and S. A. Sunshine , *Phy. Rev. B* **37**,7458(1988): J.M. Tarascon et al, *ibid***36**, 8393 (1987): P.F. Miceli et al *ibid* **37**,5932 (1988).

34. M. Mehbod, W. Biberacher, A. G. M. Jansen, P. Wyder, R. Deltour and P.H. Duvigneaud , Phys. Rev. B**38**,11813(1988); M. Mehbod et al, *ibid* ,**36**,8819 (1987).
35. H. Maeda A. Koizumi, N. Bamba, E. Takayama-Muromachi, F.Izumi, H. Asano, K. Shimizu, H. Moriwaku, H. Maruyama, Y. Kurada, and H. Yamazaki, *Physica C* **157**,483 (1989).
36. N. W. Shafer , T. penney, B. L. Olson, R. L. Greene, and R. H. Koch, *Phys. Rev. B* **39**,2914 (1989).
37. T. J. Kistenmacher, *Phys. Rev. B* **38**, 8862 (1988).
38. H. Alloul, T. Ohno, H. Casalta, J. F. Marucco, P. Mendels, J. Arabski, G. Collin and M. Mehbod, *Physica C* **171**,419(1990);P. Mendels, H. Alloul, J. F. Marucco, J. Arabski and G. Collin,*ibid* .**171**, 429 (1990).
39. R. Dupree, A. Gencten and D. McK. Paul, *Physica C* **193**, 81 (1992); A . Gencten, R. Dupree, and D. McK. Paul *ibid* .**216**,491 (1993).
40. C. Y. Yang, A. R. Moodenbaugh, Y. L. Wang, Y. W. Xu, S. M. Heald, D.O.Welch, M. Suenaga, D. A. Fischer,and J. E. Pennerhahn, *Phys. Rev. B* **42**,2231 (1990).
41. R. S. Howland et al. *Phys. Rev. B* **39** ,9017 (1989).
42. Y. Shimakava, Y. Kubo, K. Utsumi,Y. Takeda, and M.M. Takano, *Jpn. J. Appl. Phys.***27**,L1071 (1988).
43. T. Kajitani, K. Kusaba M. Kikuchi, Y. Syono,and M.Hirabayshi, *Jpn. J. Appl. Phys.***27**,L354 (1988).
44. E. Takayama-Muromachi, Y. Uchida and K. Kato, *Jpn. J. Appl. Phys.***26**,L2087 (1987).R. Liang, T. Nakamura, H. Kawaji,M. Itoh, *Physica C* **170**,307 (1990).

45. C.S. Jee, D. Nichols, A. Kebede, S. Rahman, J. E. Crow, A. M. Ponte Goncalves, T. Mihalisin, G. H. Meyer, I. Perez, R.E. Salomon, P. Scloftmann, S. H. Bloom, M.V. Kurie, Y.S. Yao, and R. P. Guertin, *J. Supercond.* **1**, 63 (1988).
46. J.L.G.Munoz, X. Obradors, S.H. Kilcoyne and R. Cywinski, *Physica C* **185-189**, 1085 (1991).
47. G. Roth P. Adelman, R. Ahrens, B. Blank, H. Bürkle, F. Gompf, G. Heger, M. Hervieu, M. Nindel, B. Obst, J. Pannetier, B. Raveau, B. Renker, H. Rietschel, B. Rudolf, H. Wühl *Physica C* **162-164**, 518 (1989).
48. B.Roughani, L.C. Sengupta, J.L.Aubel, S. Sundaram and W.C. Joiner, *Physica C* **171**, 77 (1990).
49. R.P.Gupta and M.Gupta *Phys. Rev. B* **44**, 2739 (1991)
50. R.P.Gupta and M.Gupta *Phys. Rev. B* **59**, 3381 (1991).
51. H. Alloul, P. Mendels, H. Casalta, J.F. Marucco, J. Arabski, *Phys. Rev. Lett.* **67**, 3140, (1991).
- 51(a). K. Westerhott, H.J. wuller, H. Bach, P. Stauche *Phys. Rev. B* **39**, 11680 (1989)
- 51.(b) Paola Benzi, Elena Bottizo, Nicoletta Rizzi *Journal of Crystal Growth* **269**, 625 (2004)
52. S.Zagoulaev, P. Monod, J. Jegoudez, *Phys rev. B* **52**, 10474 (1995)
53. Anurag Gupta Ratan Lal, A. Sedky, A.V. Narlikar and V.P.S. Awana, *Phys. Rev. B* **61**, 11752 (2001).
54. R.B. Laughlin, *Phys. Rev. Lett.* **80**, 5188 (1998).
55. G.D. Liu, Z.X. Zhao and G. Che, *Solid State Commun.* **109**, 495 (1999).
56. J.S. Zhou, J. B. Goodenough, H. Sato and M. Naito, *Phys. Rev. B* **59**, 3827 (1999).
57. R.F. Service, *Science* **283**, 1106 (1999).
58. N. Hasselmann, A. H. Castro Neto, C. Morair Smith and Y. Dimashko, *Phys. Rev. Lett.* **82**, 2135 (1999).
59. G.V.M. Williams, J.L. Tallon and R. Meinhold, *Phys. Rev. B* **52**, 7034 (1994).

Chapter 4

Codoping Effect of Pr and Zn in

YBa₂ Cu₃O_{7-δ} System

4.1 Introduction

The substitution of Y by trivalent rare-earth elements in orthorhombic $\text{YBa}_2\text{Cu}_3\text{O}_{7-\delta}$ yields a superconducting phase with T_c identical to Y123 [1] except for Ce, Tb, Pm, and Pr. The insensitivity of the superconducting properties to the substitution is presumably due to their layered structure and the nearly complete lack of interaction between rare-earth and CuO_2 sheets [2]

Although crystallographically identical to all the other rare-earth-based superconductors, $\text{PrBa}_2\text{Cu}_3\text{O}_{7-\delta}$ inhibits the superconducting and metallic behavior [3–5]. The $\text{Y}_{1-x}\text{Pr}_x\text{Ba}_2\text{Cu}_3\text{O}_{7-\delta}$ system is particularly interesting since it is isostructural to Y123, yet the superconductivity is strongly suppressed as a function of Pr concentration. The suppression of T_c by Pr doping in $\text{Y}_{1-x}\text{Pr}_x\text{Ba}_2\text{Cu}_3\text{O}_{7-\delta}$ has been attributed to several possible mechanisms. The first mechanism involves the filling of holes (hole filling) in CuO_2 sheets due to the substitution of Pr ions with its valence greater than +3 and, hence, implies the suppression of superconductivity and metallic behavior, arising from a reduced number of carriers (holes) in CuO_2 sheets. Indeed, magnetic susceptibility,[4–6] Hall measurements [5], thermoelectric power [7], muon spin resonance [8], neutron diffraction [9], specific-heat measurement [10], and x-ray-absorption spectroscopy [11] are consistent with a Pr valence substantially larger than 3+. Superconductivity observed in $\text{Pr}_{0.5}\text{Ca}_{0.5}\text{Ba}_2\text{Cu}_3\text{O}_{7-\delta}$ film [12] strongly supports this mechanism. Based on the spin-polaron model, Wood [13] obtained an agreement with experimental data for a Pr concentration dependence of T_c in the $\text{Y}_{1-x}\text{Pr}_x\text{Ba}_2\text{Cu}_3\text{O}_{7-\delta}$ system. According to electron energy-loss spectroscopy measurement [14], the total number of holes on O sites was shown to be independent of Pr concentration (x). It suggests that Pr ions are trivalent and localize, rather than fill, the mobile holes on CuO_2 planes. The localization leads to the suppression of

superconductivity and induces a metal-insulator transition. In fact, most experimental results supporting hole filling would also support hole localization.

The second mechanism for T_c suppression involves the spin-flip effect of the pairing electrons (pair breaking). It is based on Abrikosov-Gor'kov (AG) theory [15], which has been used widely and successfully for interpretation of conventional alloy superconductors with paramagnetic doping. This model suggests that Pr ion acts as a strong magnetic pair breaker [6,16–18]. The close correspondence of T_c vs x data with results based on AG theory has been interpreted as an evidence for pair breaking [16–18]. Spin-polarized electronic band-structure calculations [19] for $\text{R}\text{Ba}_2\text{Cu}_3\text{O}_{7-\delta}$ (R=Y, Gd, and Pr) also confirms the pair-breaking mechanism. AG theory successfully explained the basic features of experiments, but it is difficult to explain the metal-insulator transition at larger Pr concentration in $\text{Y}_{1-x}\text{Pr}_x\text{Ba}_2\text{Cu}_3\text{O}_{7-\delta}$ [3,4,6,16,20] on the basis of this theory

The relatively satisfactory models [21] for the explanation of the T_c suppression are that of Fehrenbacher and Rice (FR) [22] and Liechtenstein and Mazin [23]. The FR model assumes hole depletion in the CuO_2 planes, not because of higher Pr valence, but because of transfer of the holes from the Cu-O (d) band into the $\text{O}2p\text{-Pr}4f$ hybridization state. FR suggested that the p-f hybridisation bandwidth is small due to the orthogonality of the involved orbital on shared O sites of neighboring Pr cubes. The combination of the small bandwidth with a strong coupling to spin degree of freedom and with a potential disorder renders the p-f band localized. They assumed that the CuO_3 chains are intrinsically metallic, and ascribed the absence of metallic conductivity to oxygen disorder. This has been supported by experiments [24]. Although the FR model has been supported by many experiments, and resolves the controversy on the different valence values of the Pr ion obtained from different measurements [25], it still fails to explain some experimental observations. One of the failures of the FR model is that it cannot explain the R-ion-size dependence of the T_c suppression [22].

4.2 Combined effect of Pr and Zn in Y123 system

It is known that Zn substitutes at Cu(2) sites in the CuO₂ plane [26-31]. It is a non-magnetic impurity and degrades T_c by potential scattering [32-34] which results in pinning the charge stripe [35,36]. On the other hand Pr substitutes at the Y site and is responsible for forming a narrow band called FR band [36] near the Fermi energy. This band grabs holes from the p-d band in the plane resulting in T_c degradation [21].

There are three regions in terms of Pr concentration x. For 0 < x < 0.1 the system is in the vicinity of overdoped to optimally doped state and T_c as a function of x decreases very slowly. For 0.1 < x < 0.5 the main process is hole depletion and T_c decreases faster. For x > 0.5 [21] there is additional process of magnetic pair breaking and T_c goes to zero rapidly. This is shown in Fig 4.2.1 where the T_c's plotted are taken from Ref.[37].

In this work we present resistivity versus temperature results for varying Zn concentration y for two values of Pr concentrations x = 0.1 and x = 0.2 and study the codoping effects in the first two regions mentioned above.

Zn substitution in YBa₂ [Cu_{1-y}Zn_y]₃O_{7-δ} superconductors has a strong influence on the critical temperature T_c and offers an opportunity to characterise the high T_c superconducting state. Many experimental efforts have been made to explain the T_c depression in relation with a normal impurity in the d-wave pairing state [38,39]. Since a small concentration of Zn impurities introduced into the CuO₂ plane produces a significant change in the low-energy spin fluctuations as evidenced by the NMR [38,40] and neutron scattering [41] experiments, Zn in the CuO₂ plane is itself a nonmagnetic impurity with a closed d shell and is expected to be a strong potential scatterer for charge carriers.

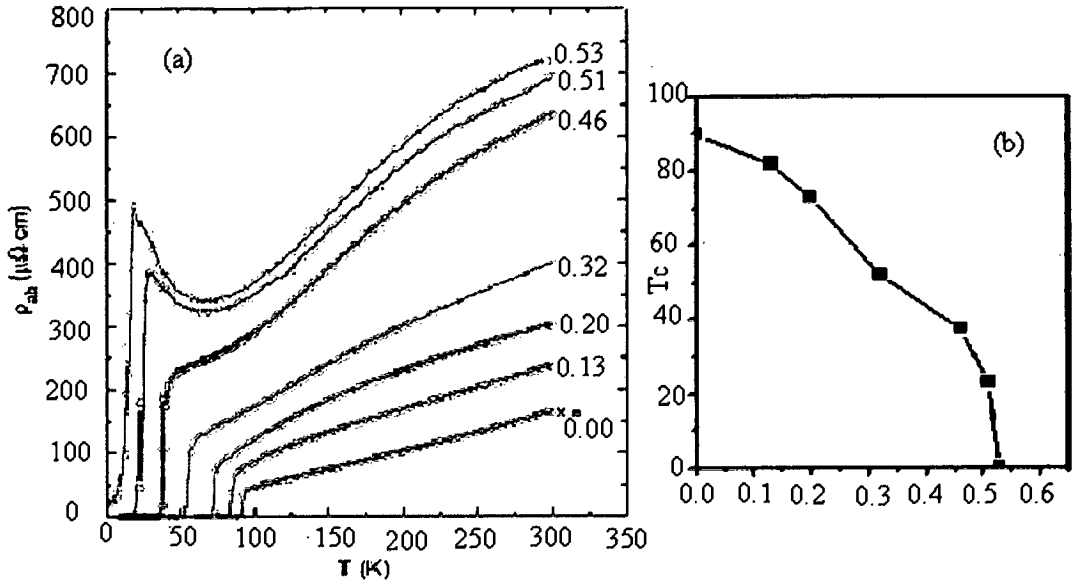


Fig 4.2.1 Plot of (a) Resistivity vs T (b) T_c vs Pr concentration x . Taken from Ref.[37] for $\text{Y}_{1-x}\text{Pr}_x\text{Ba}_2\text{Cu}_3\text{O}_{7-\delta}$ compound

Recently, Chien et al [42] have investigated the Zn-substitution effect on the normal-state charge transport in $\text{YBa}_2\text{Cu}_3\text{O}_{7-\delta}$ and estimated a large scattering cross section of the Zn impurity. As the scattering cross section of Zn impurity is related with the parameters characterising the electronic state of the high- T_c cuprates, Zn is expected to be an effective probe for detailed study of the evolution of the electronic state with doping.

Uchida et al [43] have carried out resistivity measurements on the single crystals of Zn-substituted $\text{YBa}_2\text{Cu}_3\text{O}_{7-y}$ (YZ123) and $\text{La}_{2-x}\text{Sr}_x\text{CuO}_4$ (La214) with different levels of hole doping. These authors have demonstrated how the Zn-induced residual resistivity varies with hole density and established that the depairing relation between T_c and the two-dimensional resistance which would serve as a constraint for the various theoretical models. It is highlighted that Zn probes a remarkable

difference in the electronic state between underdoped and highly doped superconducting regime.

The temperature dependence of the resistivity was studied by these authors for $z = 0.37$ and 0.07 of YZ123 with Zn content ranging up to $z = 0.04$. The compound with $z = 0.37$ shows Zn-substitution effects typical of underdoped cuprates. The effects of Zn- substitution are two fold (i) T_c is rapidly reduced and the superconductivity disappears at $z_c \cong 0.03$. (ii) A large T -independent component ρ_0 (residual resistivity) adds to the T-dependent resistivity. Notably the $y = 0.37$ compound becomes insulating when the superconductivity is destroyed, and a superconductor-insulator (SI) transition occurs at $\rho_0 \sim 400 \mu\Omega\text{cm}$. This value corresponds to the two dimensional (2D) resistance (ρ^{2D}) $\sim 6.8 \text{ K}\Omega/$ per CuO_2 plane and is close to the universal value $h/4e^2 \simeq 6.5 \text{ K}\Omega/$ which is predicted to separate superconducting and insulating behavior at $T = 0$ in 2D[44,45].

On the other hand the highly doped superconducting compounds studied by these authors show a contrasting behavior. For $x = 0.20$ in $\text{La}_{2-x}\text{Sr}_x\text{Cu}_{1-z}\text{Zn}_z\text{O}_4$ (La-214) [46], the material remains metallic even after the superconductivity disappears at $z = 0.04$ where the residual resistivity is by a factor of 4 smaller than the critical value observed for $x = 0.10$ and 0.15 . The 90K Y123 ($y = 0.07$) would behave in the same manner, when more Zn could be introduced as the linear extrapolation of the ρ_0 - z curve to $z = 0.08$ reach only 1/3 of the critical value.

These author show how the in-plane resistivity varies with changing doped hole density for fixed z . The magnitude of the residual resistivity is fairly large in the underdoped regime ($x = 0.10$ and 0.15 for La214 and oxygen content 6.68 and 6.73 for Y123) and is rapidly reduced for higher hole density. Using the results from ρ -T plots, these researchers obtained the values of T_c which are normalized to the value T_{c0} for

the Zn-free compound and then plotted it against against ρ_0^{2D} for the two systems with various z and $x(y)$. These plots show another aspect of the universal T_c depression in the underdoped cuprates. Irrespective of the doped hole density, the data for the underdoped cuprates merge into a single pair-breaking curve which points toward the universal 2D resistance $h/4e^2$ as $T_c \rightarrow 0$.

The highly doped cuprates La214 with $x = 0.20$ and Y 123 with oxygen contents 6.93, 6.88, and 6.83 show quite distinct $T_c - \rho_0^{2D}$ curves which are strongly dependent on the doped hole density. As the hole density increases, the T_c degradation speeds up as a function of ρ_0^{2D} and the $T_c - \rho_0^{2D}$ curve appears to end up at ρ_0^{2D} considerably lower than $h/4e^2$.

A possible explanation for this nonuniversal behavior would be that the highly doped material being three-dimensional (3D) superconductor. Certainly, it is a general trend that the magnitude of the anisotropic resistivity (i. e. the ratio of the resistivity between the CuO₂ planes ρ_c to that of the in-plane resistivity ρ_{ab}) decreases with increase of dopant concentration [47,48]. However, the recent c-axis optical and transport study has demonstrated that a truly 3D state is realized in the overdoped nonsuperconducting region [49].

An alternative explanation, suggested by Fukuzumi et al [46], though highly speculative, is that the nonuniversal behavior in the highly doped regime may result from some inherent inhomogeneity such as phase separation or strong fluctuations of the amplitude of the order parameter, that is, an appreciable density of normal carriers may coexist in the highly doped superconducting compound. The density of the normal carriers increases as the nonsuperconducting overdoped region is approached. If one supposes that overdoped domains in which the electrons are not easily localized due to Zn impurities forms a parallel circuit with underdoped domains

which readily lose superconductivity and become insulating for Zn substitution at $z = z_c$. The superconductivity then would disappear at resistivity appreciably smaller than the critical value ($\sim 400 \mu\Omega\text{cm}$) observed in the underdoped regime and the material would keep metallicity due to much more conductive normal fluid. In this model the apparent critical resistivity or the slope of the $T_c - \rho_o^{2D}$ curve would depend on how much the normal metallic phase is mixed in. The result of Fukuzumi et al for highly doped compounds shows a trend just expected from this model.

For the Zn-substitution effect in the normal state, they determined the residual resistivity ρ_o (or the corresponding ρ_o^{2D}) determined from the nearly parallel shift of the $\rho(T)$ curves and /or from the zero-temperature intercept of the T-linear part of ρ and it is plotted as a function of Zn content for Y123 and La 214 in each system. The plots for two representative compounds in each system are shown in Fig. 4.2.2. Following the analysis made by Chien, Wang, and Ong [42], the resistivity arising from *s*-wave impurity scattering in 2D is

$$\rho_o^{2D} = \frac{4\hbar}{e^2} \frac{n_i}{n} \sin^2 \delta_0, \quad (4.2.1)$$

where n_i is the impurity concentration and δ_0 is the *s*-wave phase shift. The straight line (dash lines) in each plot is the value of unitarity limit $\delta_0 = \pi/2$, the carrier density $n = x$, the doped hole density per planar Cu. For Y123 these authors assumed that $x \sim 0.23$ for $y = 0.07$ and $x = 0.14$ for $y = 0.37$ [50] and that Zn atoms are substituted only on the plane Cu sites such that $n_i = 3/2z$ [38,40].

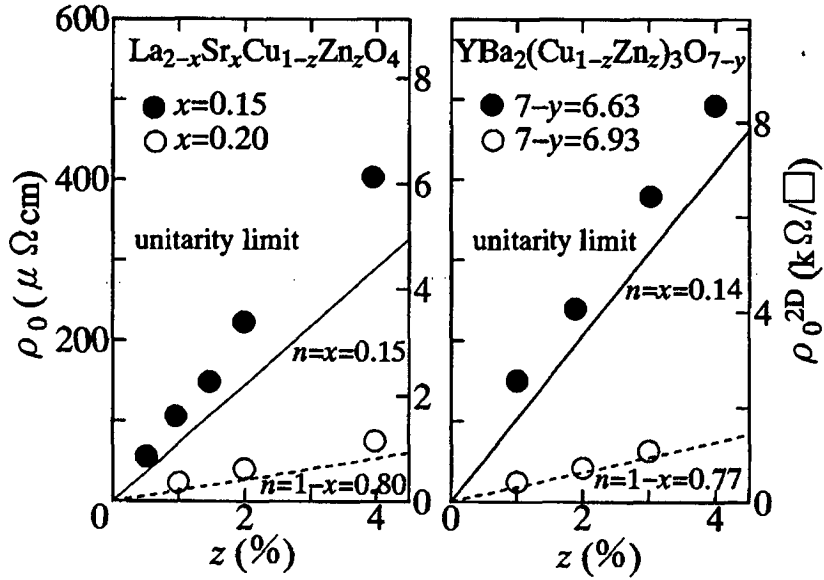


Fig.4.2.2 Variation of the residual resistivity ρ_0 (and ρ_0^{2D} right hand scale) with Zn content in $\text{YBa}_2\text{Cu}_3\text{O}_{7-y}$ with $y = 0.37$ and 0.07 , and in $\text{La}_{2-x}\text{Sr}_x\text{CuO}_4$ with $x = 0.15$ and 0.20 . The solid (dashed) line indicates the unitarity limit with the carrier density $n = x$ ($n = 1-x$).

It turns out that the experimental values of ρ_0 for the underdoped materials are close to (or even larger than) the unitarity limit with $n = x$. The carrier density in the underdoped regime should thus be identified with the density of doped hole number. Here one should check the assumption that Zn is a potential scatterer. Zn is itself a nonmagnetic impurity, but it induces a localized magnetic moment in the CuO_2 plane. The magnitude of the induced moment is as large as $0.8 \mu_B$ (μ_B is the Bohr magneton) for the underdoped cuprates, and is reduced in the highly doped regime, $\sim 0.2 \mu_B$ in 90 K Y123 [51]. Borkowski and Hirschfeld [52] have shown that a scattering rate Γ_S from the induced magnetic moments in the 90 K Y123 is much smaller than the potential scattering rate Γ_N . This should be the case also with the 60 K Y123. Since the carrier density or the density of states $N(0)$ should be smaller in 60 K Y123, and $\Gamma_N \sim N(0)^{-1}$ whereas $\Gamma_S \sim N(0)$, Γ_N still outweighs Γ_S with the decreased $N(0)$ compensating the increased magnetic moment.

The residual resistivity for the highly doped materials is remarkably smaller than the unitarity limit ($n = x$) but is near the unitarity limit with $n = 1 - x$. Then, the decreased ρ_0 is ascribable either to a decrease in δ_0 or to an increase in n toward $1 - x$. The fact that the value of ρ_0 for overdoped ($x = 0.30$) La214 is near the value in the unitarity limit with $n = 1 - x$ which is expected in a Fermi liquid state gives evidence for the increase in n while δ_0 remains to be $\pi/2$. Using the above mentioned data Fukuzumi et al plotted the variation of ρ_0^{2D} for 1% Zn with doped hole density (x) per planar Cu atom. Even if one admits ambiguity in estimating x in Y123 [50] it is evident that a rapid increase in carrier density or a rapid crossover from $n = x$ to $n = 1 - x$ is taking place when x exceeds ~ 0.17 . This result is indicative of a radical change in the electronic state of the CuO_2 plane with increase of doping. The crossover region just corresponds to what we call a highly doped region.

4.3 Results and Discussion

4.3.1 X-ray Diffraction and Iodometric titration

X-ray diffraction patterns of samples of composition $\text{Y}_{1-x}\text{Pr}_x\text{Ba}_2 [\text{Cu}_{1-y}\text{Zn}_y]_3\text{O}_{7.8}$ with different values of x and y with $x = 0.1$ and 0.2 and $0 \leq y \leq 0.10$ were recorded on Rigaku X-ray diffractometer D MaxII-C with $\text{CuK}\alpha$ radiation at room temperature. These patterns are shown in Figs.4.3.1- 4.3.2 . The structural parameters were refined by Fullprof program. The refined profiles are presented in Figs.4.3.3- 4.3.10 . The present investigation was undertaken in order to see whether the crystal structure parameters play any role in the suppression of superconductivity. In particular, the attention was paid to the changes in the lattice constants as well as the atom positions.

The structural analysis shows that all the samples are of orthorhombic symmetry. This can be confirmed by the visual examination of the diffraction patterns and comparing them with reported orthorhombic Y123 structure [53]. The Rietveld analysis was carried out for the space group Pmmm. The refined cell parameters and the atom positions are presented in Tables 4.3.1-4.3.2. We find from this table that the lattice parameters a, and b do not change much however, c parameter is slightly affected thereby slightly affecting the O(4) parameter which is responsible for keeping the structure to be orthorhombic. With Zn substitution the parameter O(2) increases whereas parameter O(3) decreases thereby suggesting the changes in the Cu-O₂ plane. It may be noted here that this is a new series of high T_c cuprate superconductors with Pr at Y site and Zn at Cu site. Since no structural data is available, no comparison of lattice parameters and other structural parameters extracted from X-ray diffraction patterns in our study can be made with reported in literature.

Looking at the results on oxygen contents obtained from iodometric titration method, described in Chapter 2, it is seen that the oxygen content remains almost constant. The values of oxygen content are given in Table 4.3.1 and Table 4.3.2 along with error for x = 0.1 and 0.2 concentration. In these tables we also show the calculated values of oxygen content using equation 3.5.1. It is observed that the calculated values of oxygen content are higher than those determined from iodometric titration.

Table 4.3.1 Rietveld Refinement of XRD data for $Y_{0.9}Pr_{0.1}Ba_2[Cu_{1-y}Zn_y]_3O_{7-\delta}$. The space group is Pmmm with $Y(\frac{1}{2}, \frac{1}{2}, \frac{1}{2})$, $Pr(\frac{1}{2}, \frac{1}{2}, \frac{1}{2})$, $Ba(\frac{1}{2}, \frac{1}{2}, z)$, $Cu(1)(0, 0, 0)$, $Cu(2)(0, 0, z)$, $O(1)(0, \frac{1}{2}, 0)$, $O(2)(\frac{1}{2}, 0, z)$, $O(3)(0, \frac{1}{2}, z)$, $O(4)(0, 0, z)$. Also shown oxygen content and T_c . The values in the parentheses represents uncertainty in the last digit.

	y = 0.0	y = 0.01	y = 0.03	y = 0.06	y = 0.08	y = 0.10
z(Ba)	0.182(3)	0.182(3)	0.182(3)	0.182(3)	0.178(3)	0.178(3)
z(Cu2)/z(Zn)	0.361(2)	0.360(2)	0.361(2)	0.361(2)	0.359(2)	0.362(2)
z(O2)	0.366(4)	0.367(4)	0.396(2)	0.383(2)	0.379(2)	0.378(2)
z(O3)	0.388(1)	0.388(1)	0.355(4)	0.370(3)	0.336(5)	0.336(5)
z(O4)	0.160(2)	0.163(2)	0.159(4)	0.159(4)	0.156(4)	0.158(4)
a(Å)	3.820(2)	3.820(2)	3.823(2)	3.824(2)	3.826(2)	3.827(2)
b(Å)	3.884(3)	3.884(3)	3.883(3)	3.887(1)	3.888(1)	3.889(1)
c(Å)	11.663(1)	11.663(1)	11.665(1)	11.658(2)	11.668(1)	11.669(1)
R_{wp}	16.0	15.0	12.6	15.4	15.6	15.
R_{exp}	14.0	12.0	13.6	13.5	14.4	13.8
R_{Bragg}	12.67	12.91	11.4	9.96	16.27	13.99
χ^2	1.22	1.29	1.27	1.30	1.18	1.18
Oxygen content as obtained from iodometric titration (7- δ)	6.67 \pm 0.03	6.67 \pm 0.05	6.67 \pm 0.06	6.67 \pm 0.03	6.67 \pm 0.07	6.67 \pm 0.06
Calculated oxygen content from equation 3.5.1 (7- δ)	6.951 \pm 0.001	6.951 \pm 0.001	6.940 \pm 0.001	6.980 \pm 0.002	6.922 \pm 0.001	6.916 \pm 0.001
T_c (K)	77.05 \pm 1.00	61.78 \pm 1.00	26.10 \pm 1.00	19.49 \pm 1.00	13.16 \pm 1.00	-

Table 4.3.2 Rietveld Refinement of XRD data for $Y_{0.8}Pr_{0.2}Ba_2[Cu_{1-y}Zn_y]_3O_{7.8}$. The space group is Pmmm with $Y(\frac{1}{2}, \frac{1}{2}, \frac{1}{2})$, $Pr(\frac{1}{2}, \frac{1}{2}, \frac{1}{2})$, $Ba(\frac{1}{2}, \frac{1}{2}, z)$, $Cu(1)(0, 0, 0)$, $Cu(2)(0, 0, z)$, $O(1)(0, \frac{1}{2}, 0)$, $O(2)(\frac{1}{2}, 0, z)$, $O(3)(0, \frac{1}{2}, z)$, $O(4)(0, 0, z)$. Also shown oxygen content and T_c . The values in the parentheses represents uncertainty in the last digit

	y = 0.0	y = 0.002	y = 0.005	y = 0.01	y = 0.03	y = 0.06
z(Ba)	0.182(3)	0.182(3)	0.181(3)	0.182(3)	0.182(3)	0.182(3)
z(Cu2)/z(Zn)	0.361(2)	0.360(2)	0.359(2)	0.360(2)	0.361(2)	0.361(2)
z(O2)	0.366(5)	0.396(5)	0.396(4)	0.396(4)	0.396(4)	0.383(6)
z(O3)	0.388(1)	0.354(6)	0.354(6)	0.354(6)	0.354(6)	0.357(6)
z(O4)	0.160(2)	0.157(3)	0.159(3)	0.159(3)	0.160(1)	0.159(3)
a(\AA)	3.820(3)	3.829(1)	3.830(1)	3.825(3)	3.830(2)	3.823(5)
b(\AA)	3.884(6)	3.888(1)	3.888(1)	3.886(2)	3.888(3)	3.887(1)
c(\AA)	11.663(4)	11.667(1)	11.665(2)	11.666(2)	11.669(1)	11.668(1)
R_{wp}	16.0	14.0	15.0	14.2	15.5	16.4
R_{exp}	14.0	8.76	13.5	12.5	13.4	14.3
R_{Bragg}	12.67	15.99	16.4	14.51	22.27	25.22
χ^2	1.19	1.20	1.12	1.25	1.20	1.14
Oxygen content as obtained from iodometric titration (7- δ)	6.67 \pm 0.05	6.67 \pm 0.01	6.67 \pm 0.03	6.67 \pm 0.05	6.67 \pm 0.02	6.67 \pm 0.05
Calculated oxygen content from equation 3.5.1 (7- δ)	6.951 \pm 0.004	6.928 \pm 0.001	6.940 \pm 0.002	6.933 \pm 0.002	6.916 \pm 0.001	6.922 \pm 0.001
T_c (K)	37.08 \pm 1.00	31.99 \pm 1.00	29.4 \pm 1.00	15.96 \pm 1.00	-	-

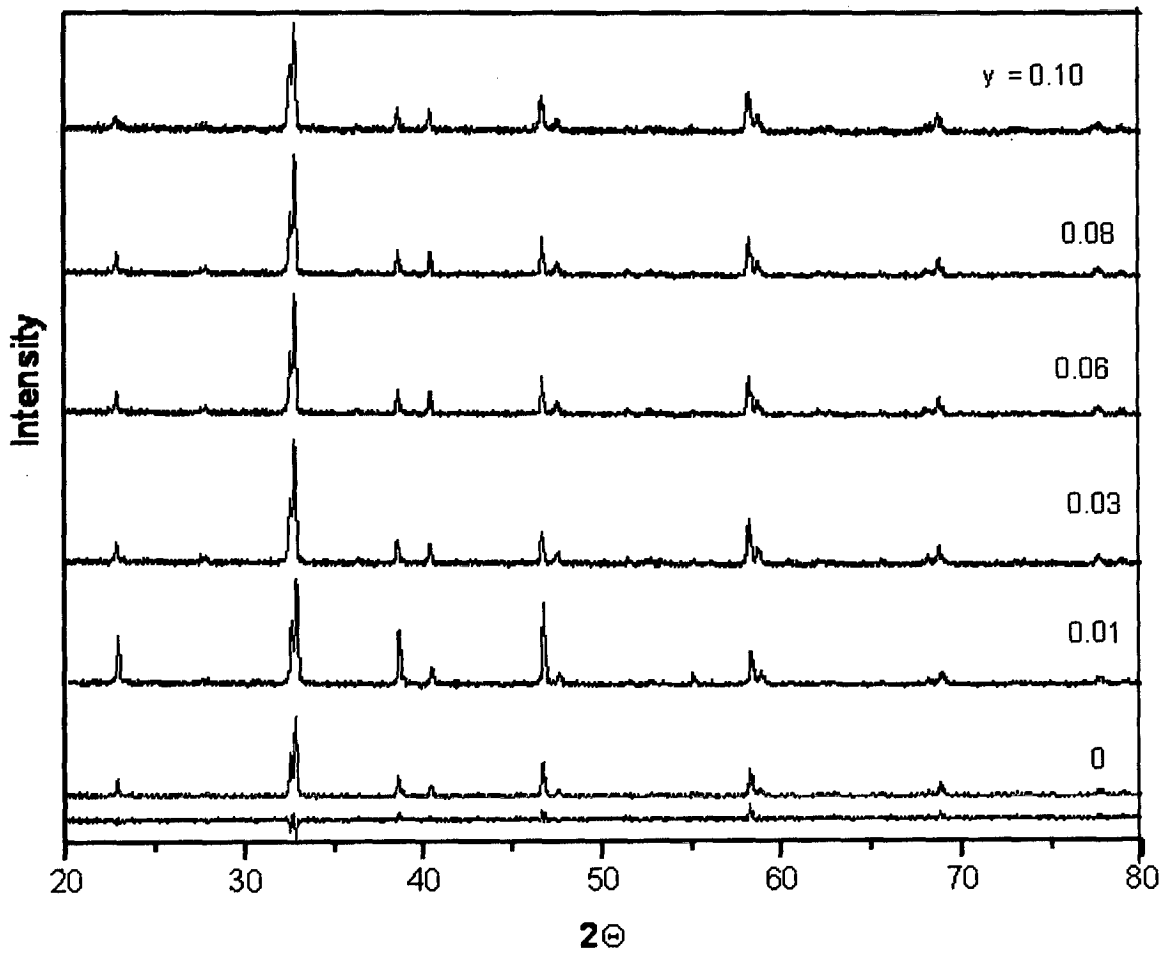


Fig. 4.3.1. x-ray diffraction patterns of $Y_{1-x}Pr_xBa_2[Cu_{1-y}Zn_y]_3O_{7-\delta}$ samples with different values of Zn concentration and $x = 0.10$.

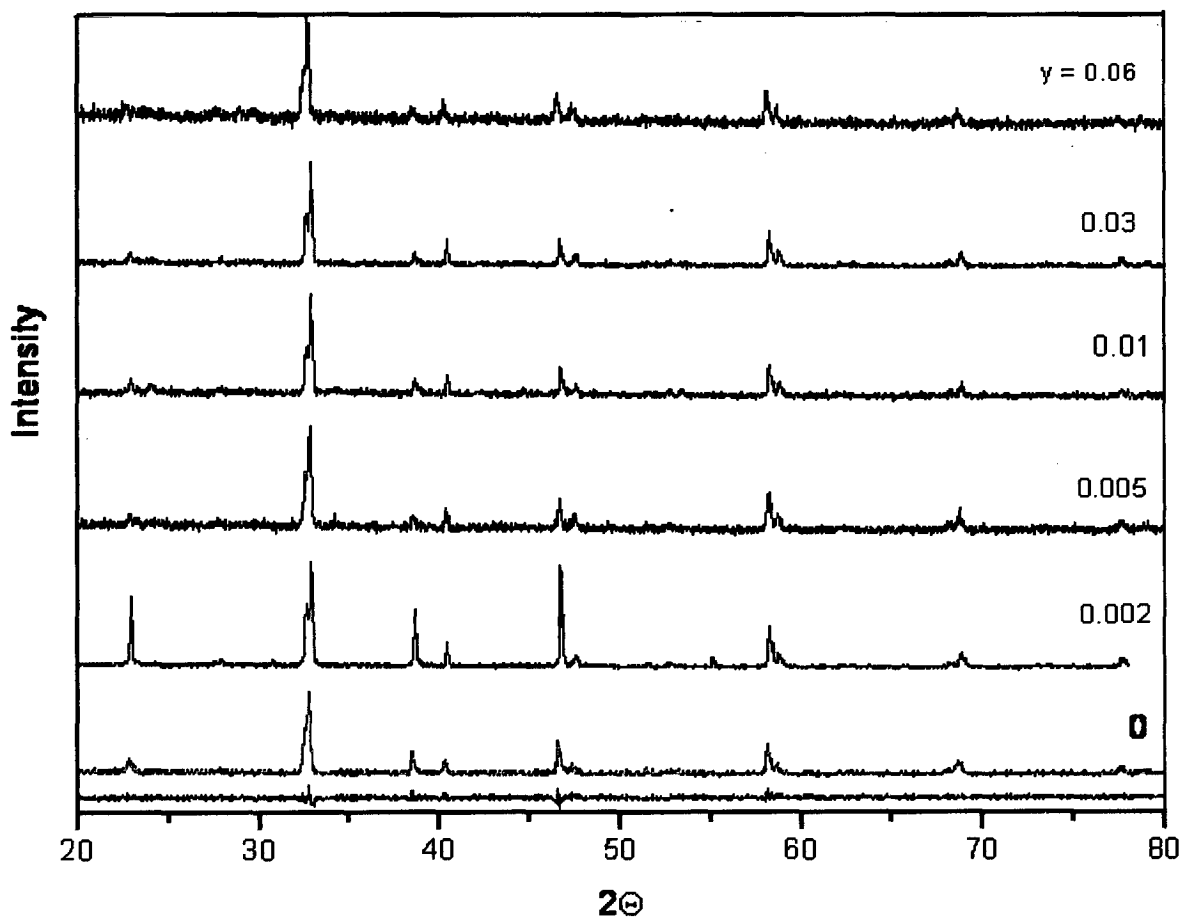


Fig.4.3.2. x-ray diffraction patterns of $Y_{1-x}Pr_xBa_2[Cu_{1-y}Zn_y]_3O_{7-\delta}$ samples with different values of Zn concentration and $x = 0.20$

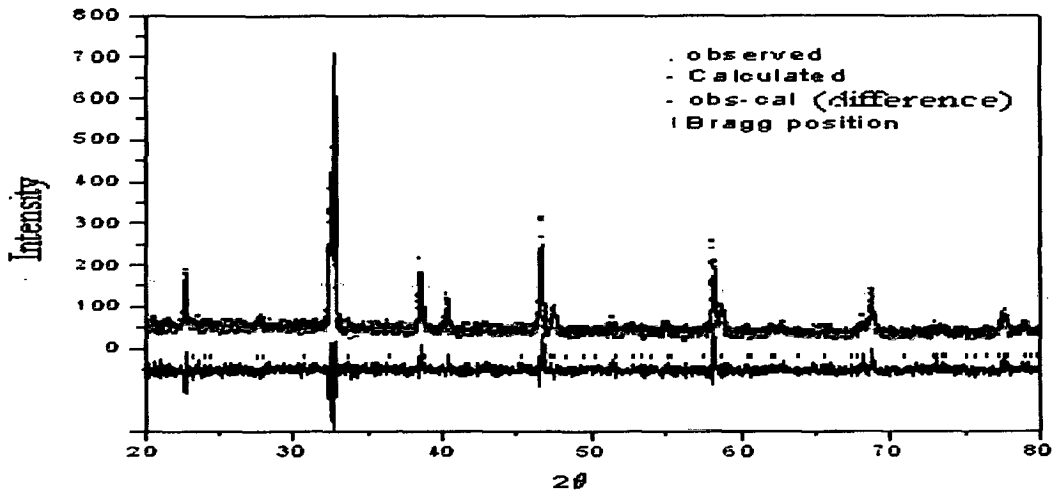


Fig .4.3.3 Rietveld refined diffraction patterns of $Y_{0.9}Pr_{0.1}Ba_2 [Cu_{1-y}Zn_y]_3O_{7.8}$ with $y = 0.00$

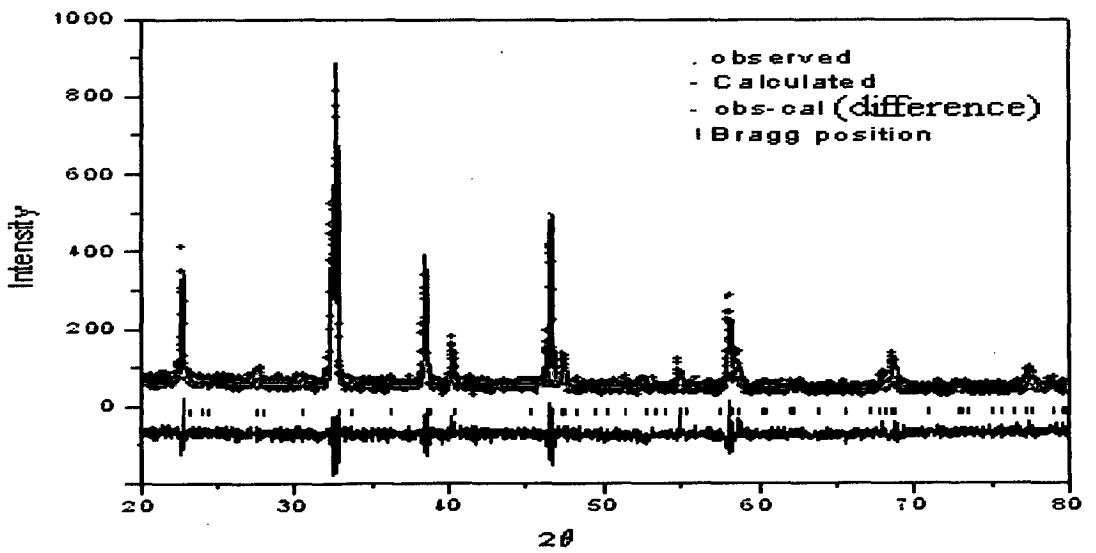


Fig .4.3.4 Rietveld refined diffraction patterns of $Y_{0.9}Pr_{0.1}Ba_2 [Cu_{1-y}Zn_y]_3O_{7.8}$ with $y = 0.01$

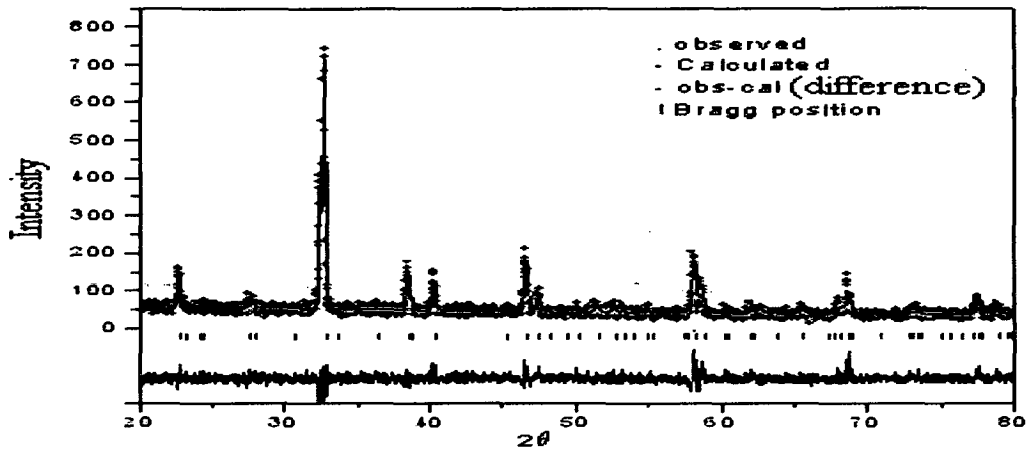


Fig. 4.3.5 Rietveld refined diffraction patterns of $Y_{0.9}Pr_{0.1}Ba_2[Cu_{1-y}Zn_y]_3O_{7.5}$ with $y = 0.03$

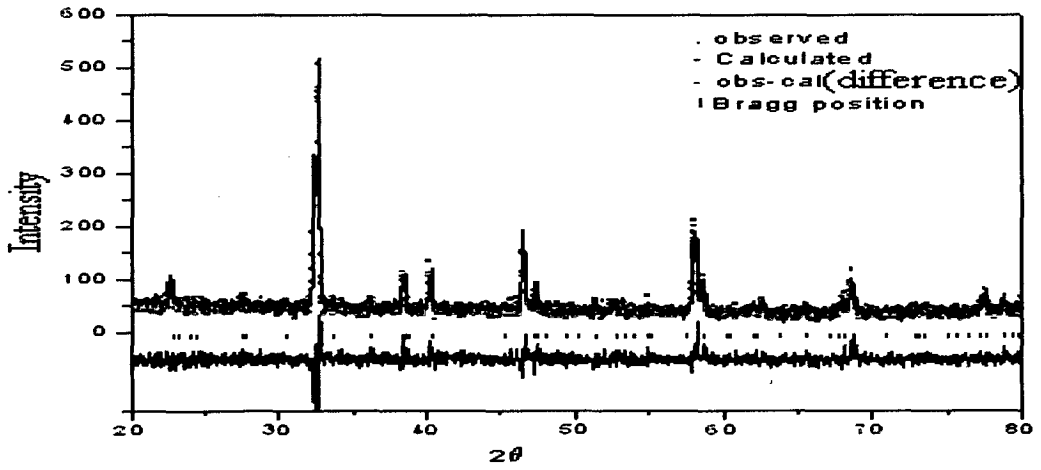


Fig. 4.3.6 Rietveld refined diffraction patterns of $Y_{0.9}Pr_{0.1}Ba_2[Cu_{1-y}Zn_y]_3O_{7.5}$ with $y = 0.08$

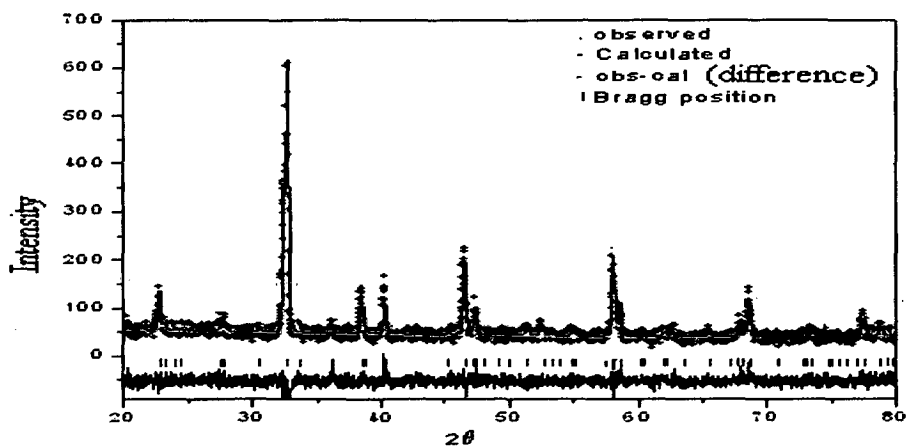


Fig .4.3.7 Rietveld refined diffraction patterns of $Y_{0.9}Pr_{0.1}Ba_2[Cu_{1-y}Zn_y]_3O_{7.5}$ with $y = 0.10$

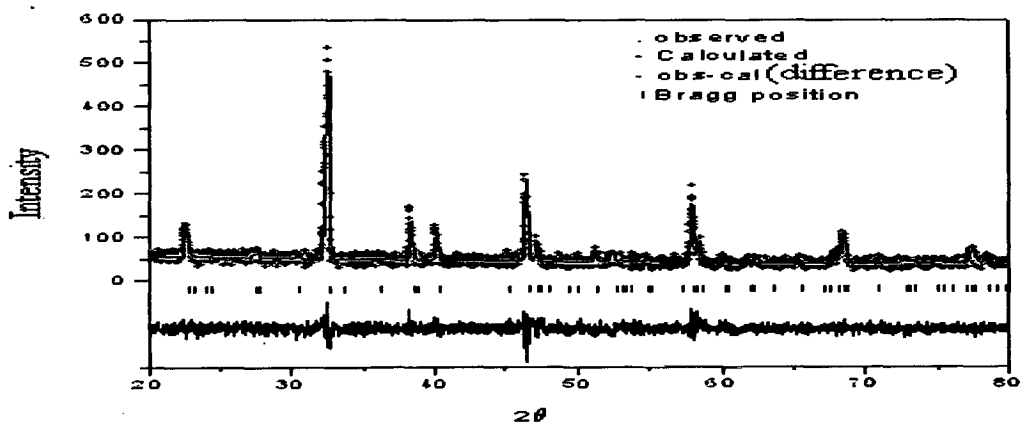


Fig .4.3.8 Rietveld refined diffraction patterns of $Y_{0.8}Pr_{0.2}Ba_2[Cu_{1-y}Zn_y]_3O_{7.5}$ with $y = 0.0$

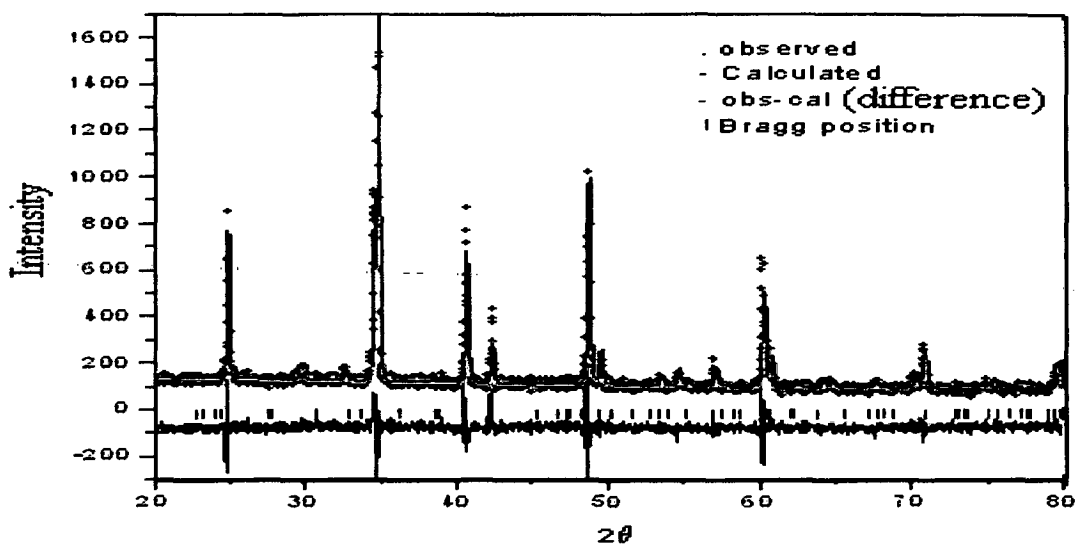


Fig .4.3.9 Rietveld refined diffraction patterns of $Y_{0.8}Pr_{0.2}Ba_2 [Cu_{1-y}Zn_y]_3O_{7.5}$
with $y = 0.002$

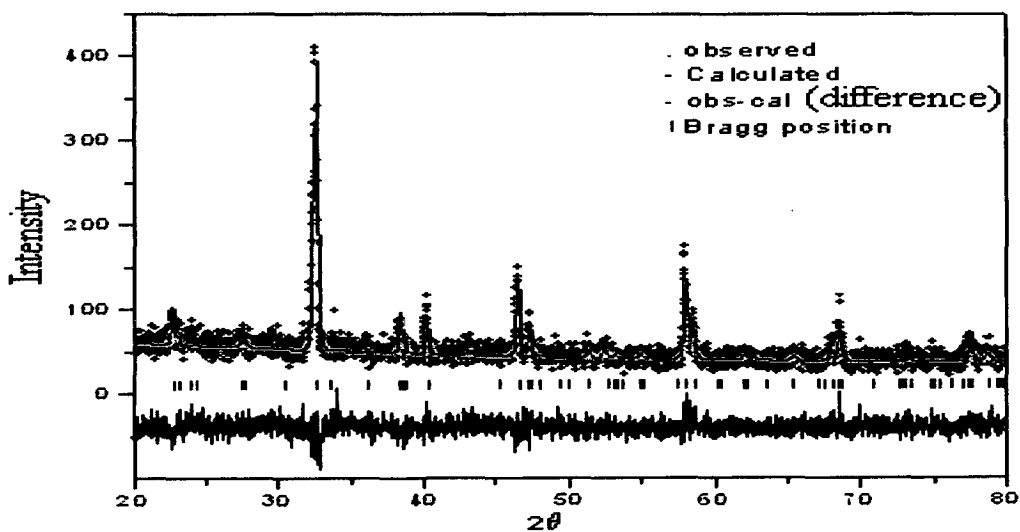


Fig .4.3.10 Rietveld refined diffraction patterns of $Y_{0.8}Pr_{0.2}Ba_2 [Cu_{1-y}Zn_y]_3O_{7.5}$
with $y = 0.005$

4.3.2 Electrical Resistivity

From Fig 3.5.8 (in the earlier chapter) one can see that for $x = 0$ T_c seems to disappear at $y = 0.1$ but the linearity in the curve above 100K is retained. Whereas for $x = 0.1$ in Fig 4.3.11 $\rho(T)$ curve shows non-linear behaviour at $y = 0.10$ and for $x = 0.20$ in Fig.4.3.12 the non-linearity in $\rho(T)$ curve starts for $y = 0.03$. The behaviour of T_c for different concentration of Zn and Pr is presented in Fig.4.3.13. The linear part of ρ -T curve is fitted by equation $\rho = \rho_0 + \rho_1 T$, for the range 175-300K for $y = 0$ and $x = 0.10$, 200-300K for $y = 0.01$ and $x = 0.10$, 190-300K for $y = 0.03$ and $x = 0.10$, 175-300K for $y = 0.06$ and $x = 0.10$, 175-300K for $y = 0.08$ and $x = 0.10$, 220-300K for $y = 0.10$ and $x = 0.10$, 175-300K for $y = 0$ and $x = 0.20$, 200-300K for $y = 0.002$ and $x = 0.20$, 200-300K for $y = 0.005$ and $x = 0.20$, 180-300K for $y = 0.01$ and $x = 0.20$, 175-300K for $y = 0.03$ and $x = 0.20$, 200-300K for $y = 0.06$ and $x = 0.20$. This is presented in Figs. 4.3.14(a)-(l). The intercept ρ_0 (residual resistivity) corresponds to the impurity scattering that leads to the pinning of charge stripe [53] and the slope ρ_1 (that is $d\rho/dT$) of this linear part gives the carrier-carrier scattering. Fig. 4.3.15 shows the behaviour of ρ_0 as function of y for only Zn, and Zn plus Pr impurities. Fig.4.3.16 shows that $d\rho/dT$ for both only Zn and Zn plus Pr impurities. We analyse the data for $x = 0.1$ and $x = 0.2$ separately.

Fig. 4.3.15(a) shows that for $x = 0.1$ Pr has a very small effect on ρ_0 upto $y = 0.09$ and hence on the pinning of charge stripes. For only Zn, $d\rho/dT$, Fig.4.3.16(a), shows a rise upto $y = 0.03$ and then a fall implying that there is no overall depinning effect is seen in Fig.4.3.13 (showing T_c vs x curve). The values of T_c obtained from $\rho(T)$ -T curve is presented in Table 4.3.1 along with most probable error. T_c falls more or less uniformly as x increases. However, when Pr is present Fig.4.3.16(a) shows that $d\rho/dT$ rises more sharply from $y = 0.03$ to $y = 0.06$. Then Fig 4.3.13 shows

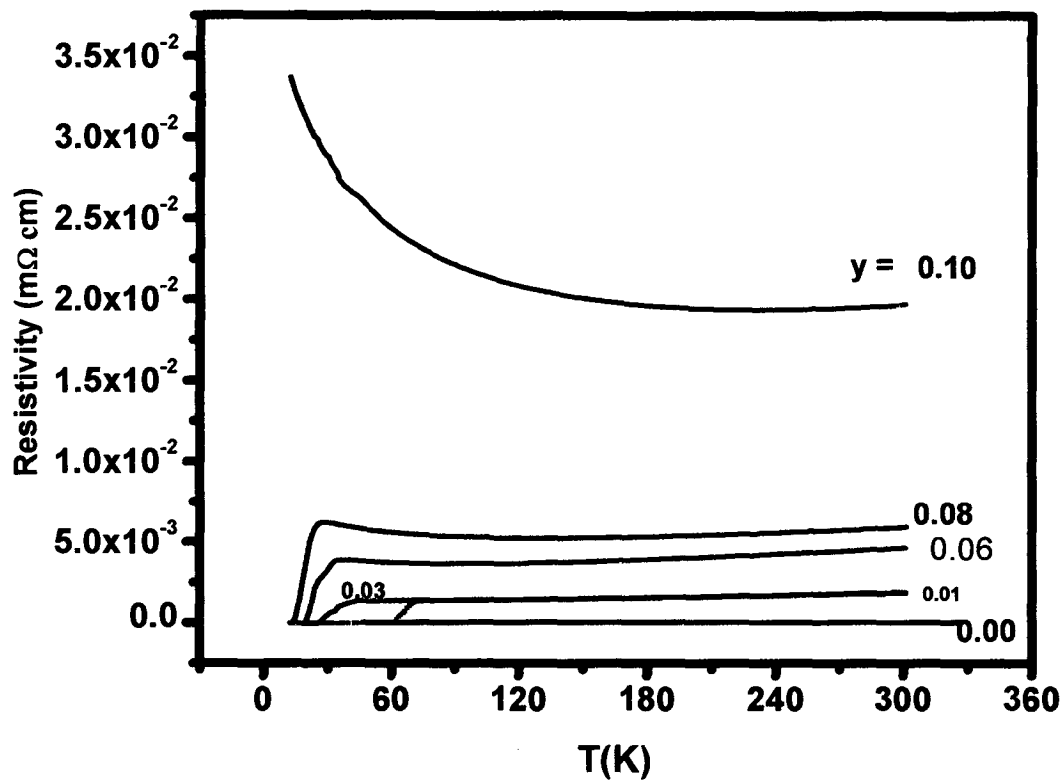


Fig.4.3.11 Resistivity vs temperature for $Y_{1-x}Pr_xBa_2[Cu_{1-y}Zn_y]_3O_{7-\delta}$ samples with different values of Zn concentration and $x = 0.10$.

[All the curves are separately shown in Fig 4.3.14(a)-(f)]

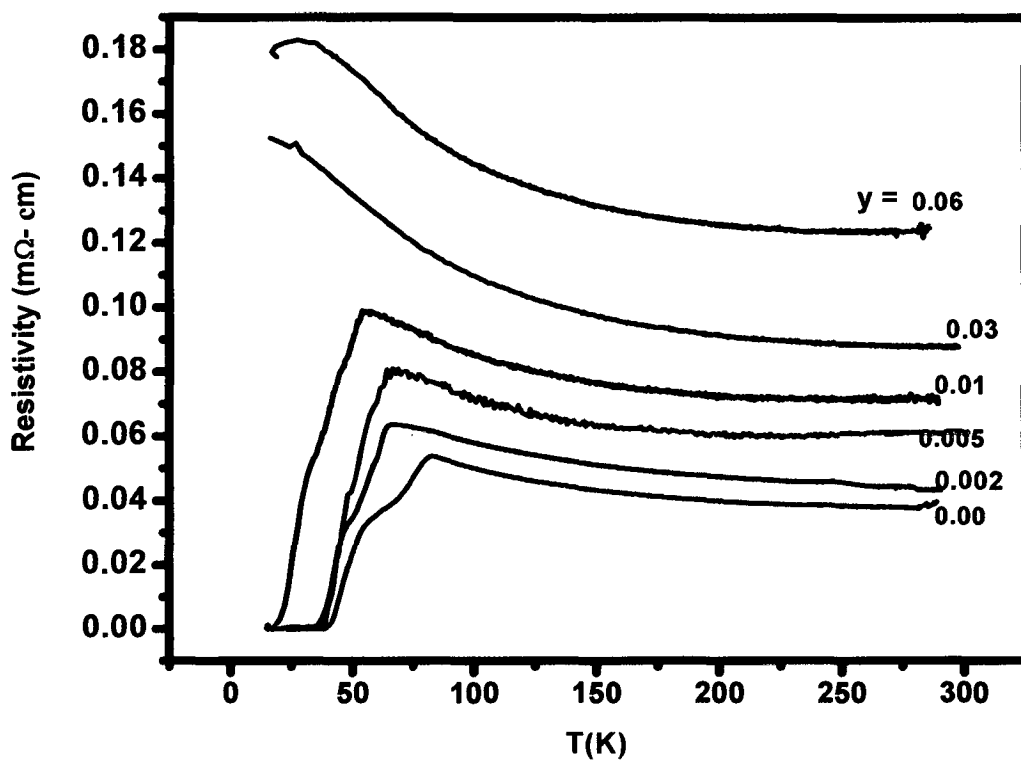


Fig.4.3.12. Resistivity vs temperature for $Y_{1-x}Pr_xBa_2 [Cu_{1-y}Zn_y]_3O_{7-\delta}$ samples with different values of Zn concentration and $x = 0.2$

[All the curves are separately shown in Fig 4.3.14(g)-(l)]

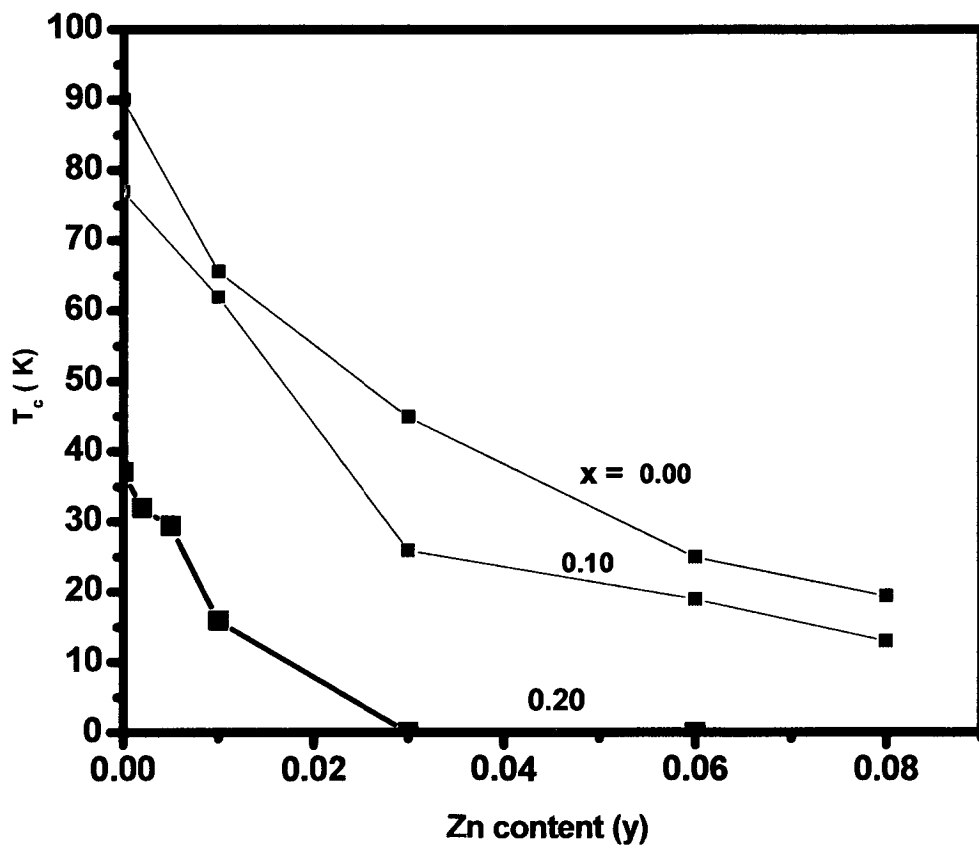


Fig.4.3.13 Plot showing Superconducting Transition temperature as function of Zinc content (y) for $Y_{1-x}Pr_xBa_2[Cu_{1-y}Zn_y]_3O_{7-\delta}$ samples with $x = 0, 0.10, 0.20$

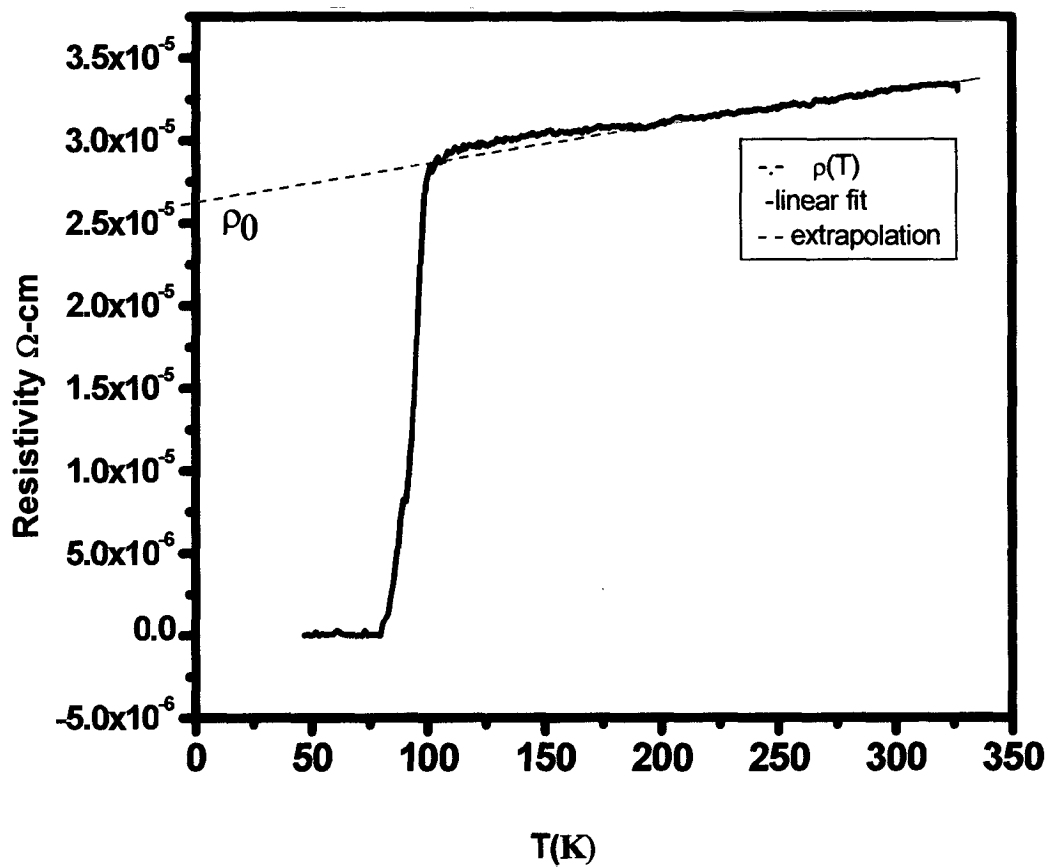


Fig.4.3.14 (a) $\rho(T) - T$ curve for $Y_{1-x}Pr_xBa_2 [Cu_{1-y}Zn_y]_3O_{7-\delta}$

samples showing linear fit for $x = 0.10$ and $y = 0.00$.

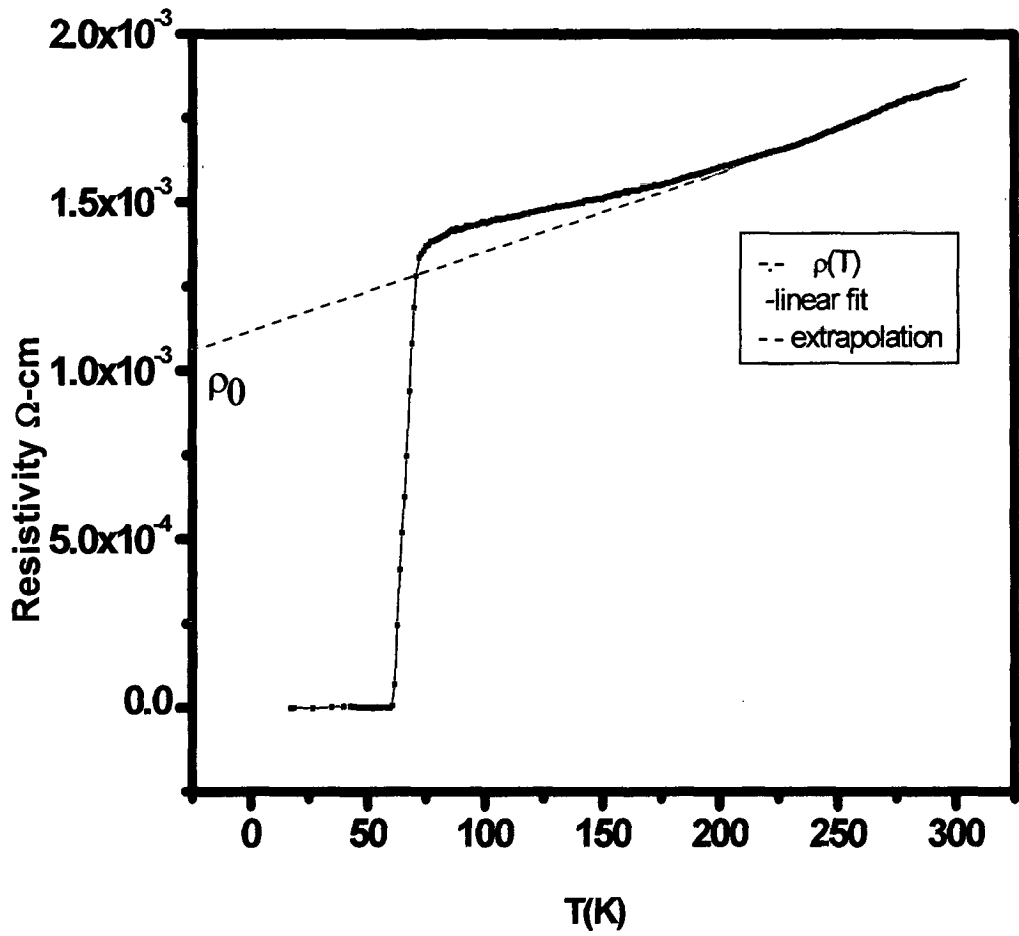


Fig.4.3.14 (b) $\rho(T)$ – T curve for $\text{Y}_{1-x}\text{Pr}_x\text{Ba}_2[\text{Cu}_{1-y}\text{Zn}_y]_3\text{O}_{7-\delta}$ samples showing linear fit for $x = 0.10$ and $y = 0.01$.

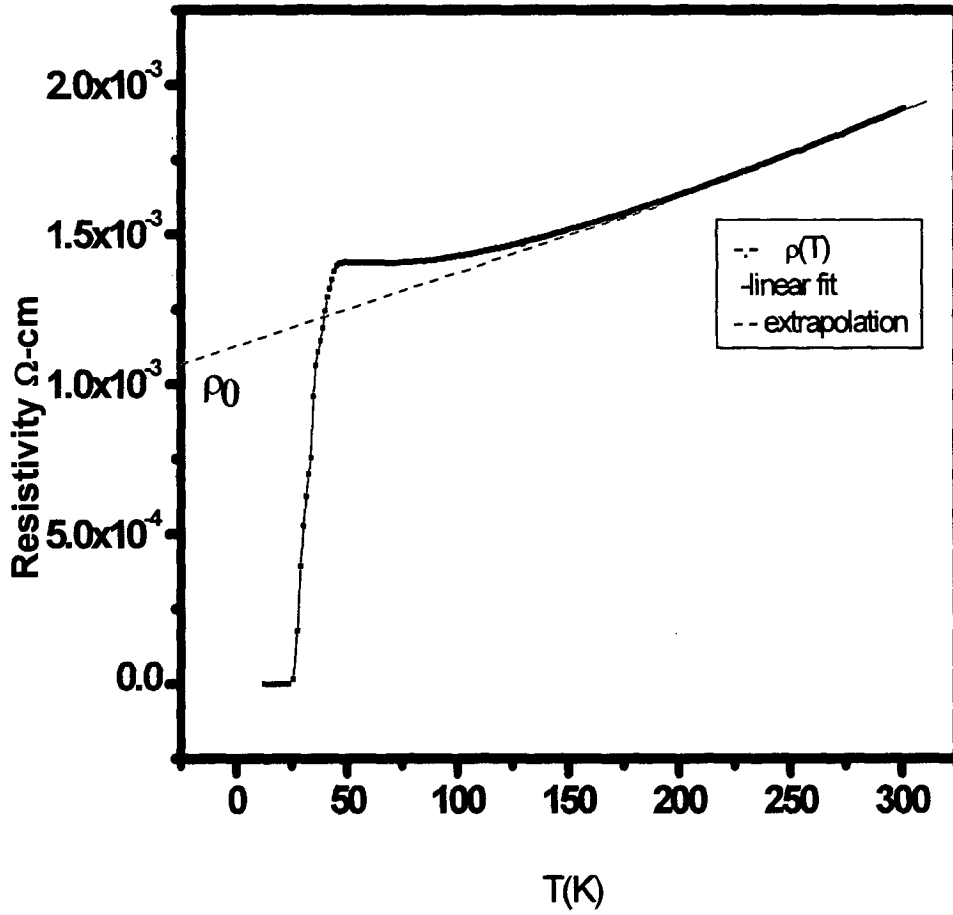


Fig.4.3.14 (c) $\rho(T)$ – T curve for $Y_{1-x}Pr_xBa_2[Cu_{1-y}Zn_y]_3O_{7-\delta}$ samples showing linear fit for $x = 0.10$ and $y = 0.03$.

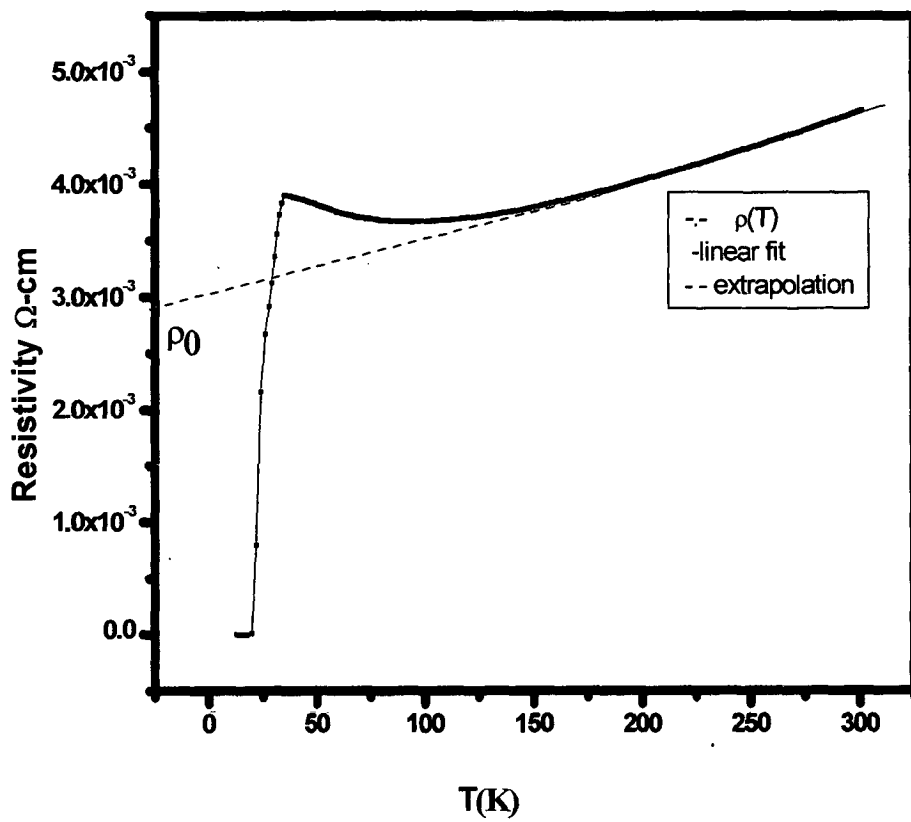


Fig.4.3.14 (d) $\rho(T) - T$ curve for $Y_{1-x}Pr_xBa_2[Cu_{1-y}Zn_y]_3O_{7-\delta}$ samples showing linear fit for $x = 0.10$ and $y = 0.06$.

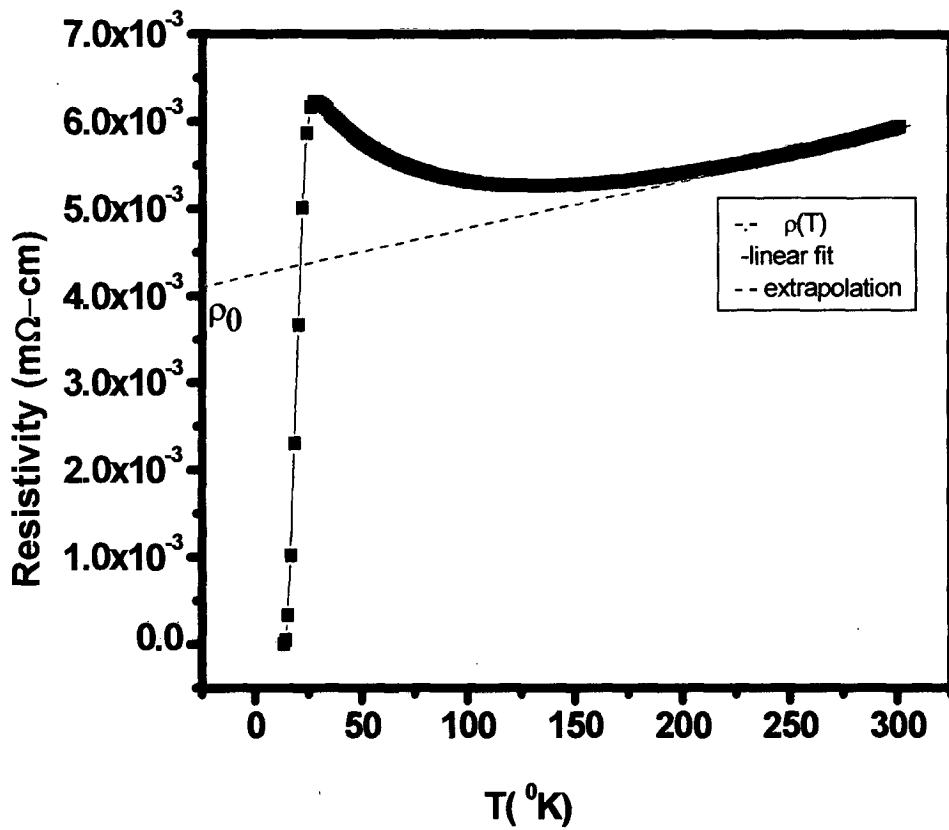


Fig.4.3.14 (e) $\rho(T) - T$ curve for $Y_{1-x}Pr_xBa_2 [Cu_{1-y}Zn_y]_3O_{7-\delta}$ samples showing linear fit for $x = 0.10$ and $y = 0.08$.

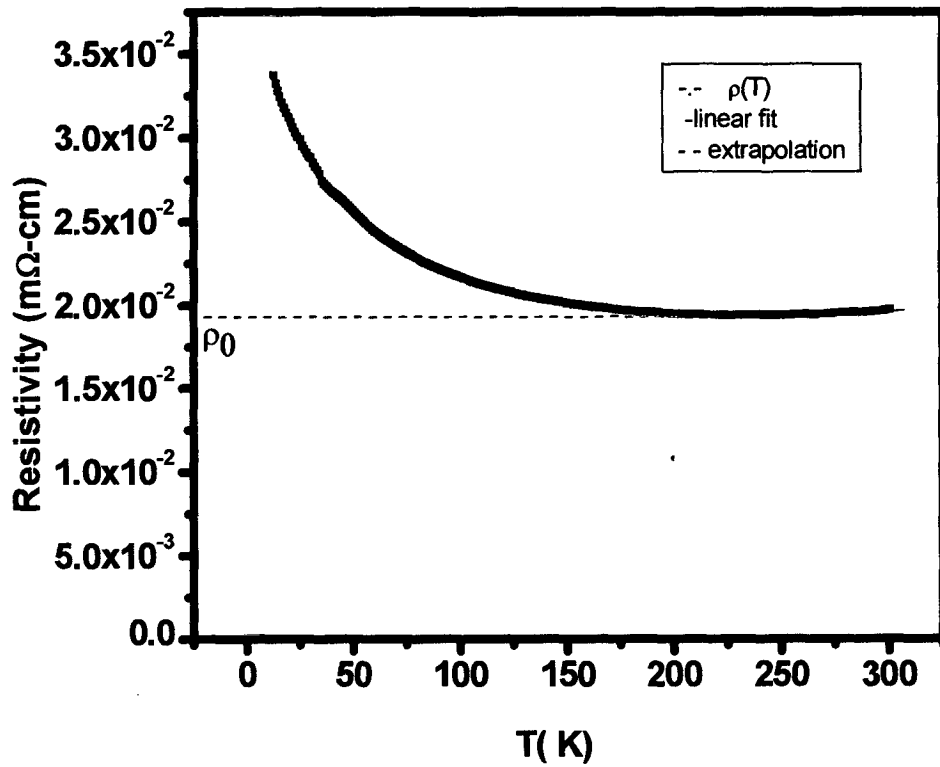


Fig.4.3.14 (f) $\rho(T)$ -T curve for $Y_{1-x}Pr_xBa_2[Cu_{1-y}Zn_y]_3O_{7-\delta}$ samples showing linear fit for $x = 0.10$ and $y = 0.10$.

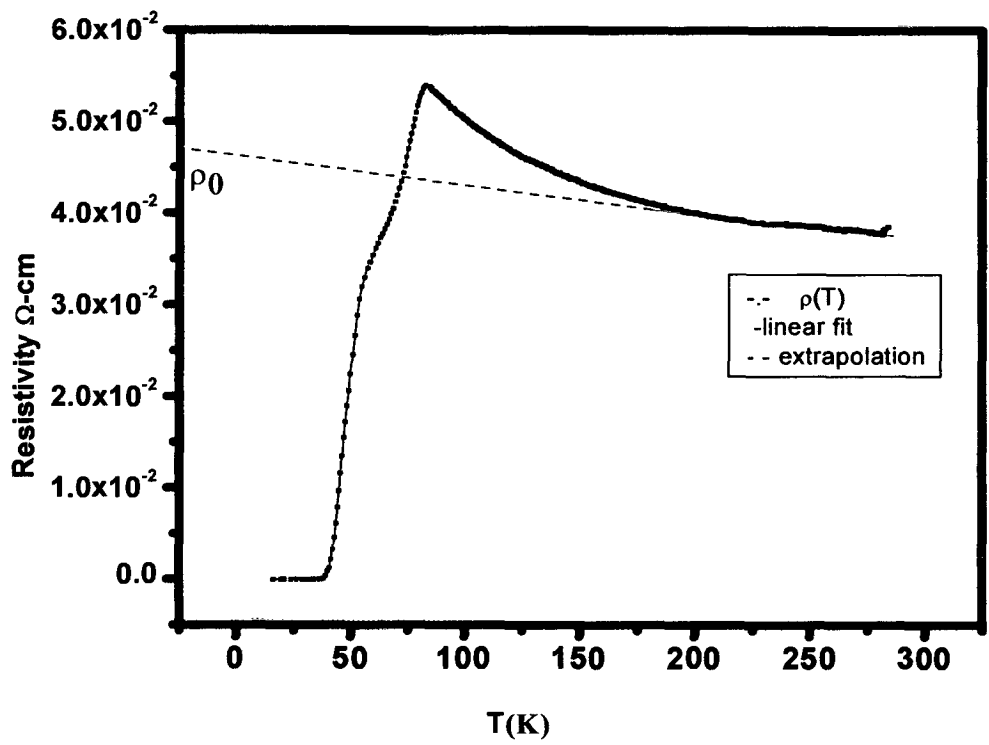


Fig.4.3.14 (g) $\rho(T)$ -T curve for $Y_{1-x}Pr_xBa_2 [Cu_{1-y}Zn_y]_3O_{7-\delta}$ samples showing linear fit for $x = 0.20$ and $y = 0.00$.

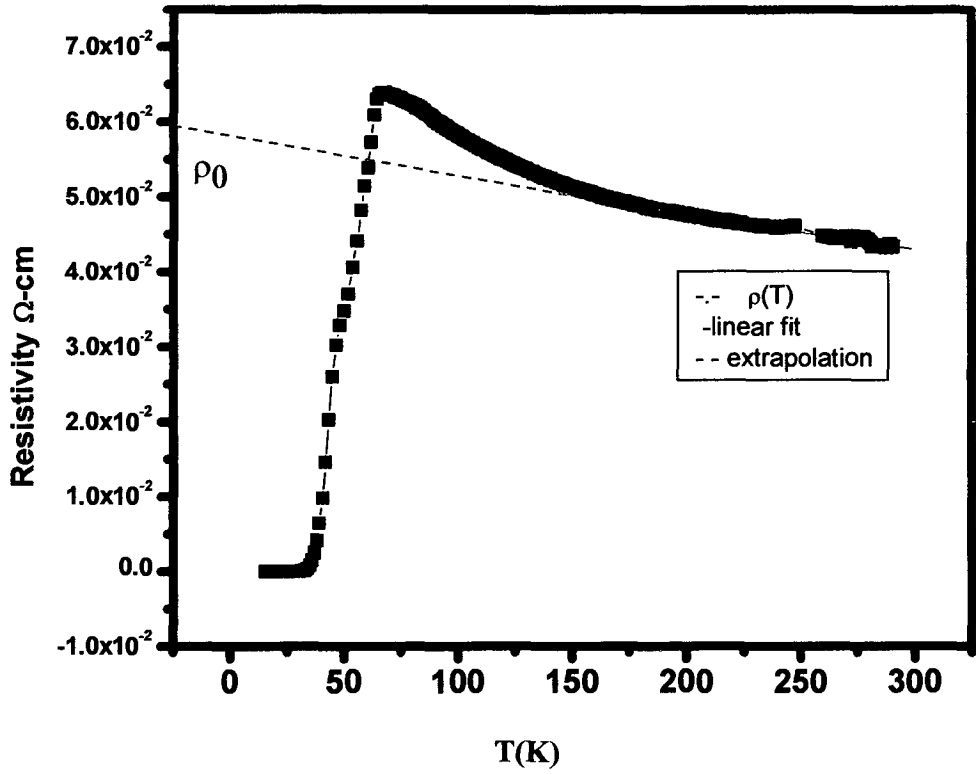


Fig.4.3.14 (h) $\rho(T)$ – T curve for $Y_{1-x}Pr_xBa_2[Cu_{1-y}Zn_y]_3O_{7-\delta}$ samples showing linear fit for $x = 0.20$ and $y = 0.002$.

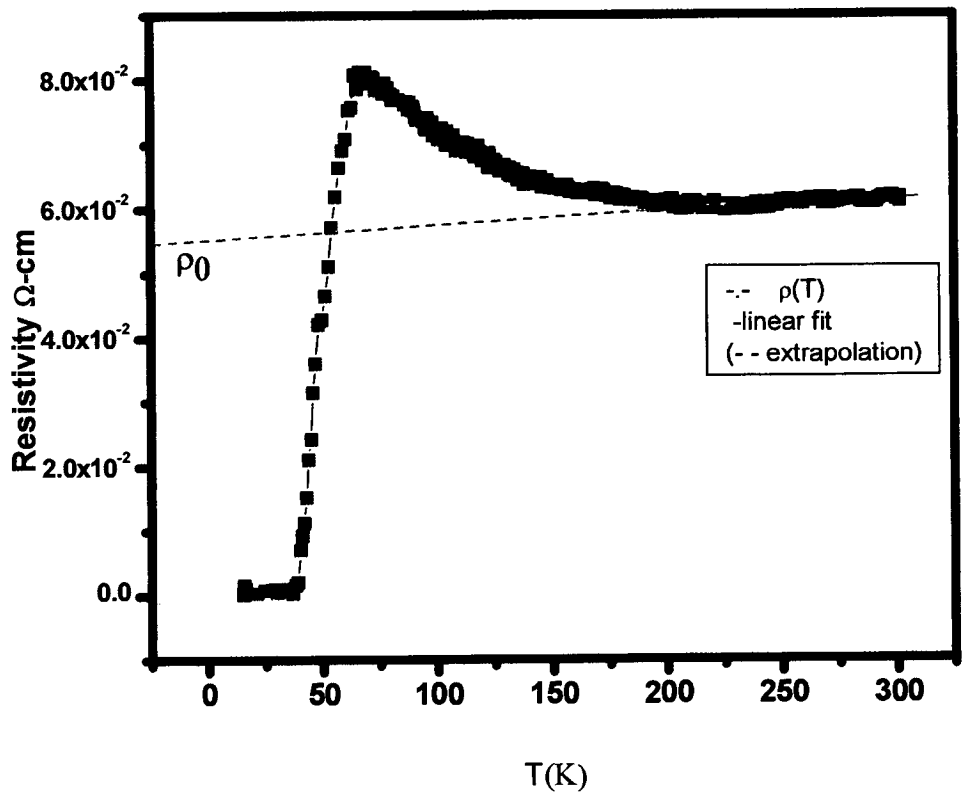


Fig.4.3.14 (i) $\rho(T)$ –T curve for $Y_{1-x}Pr_xBa_2[Cu_{1-y}Zn_y]_3O_{7-\delta}$ samples showing linear fit for $x = 0.20$ and $y = 0.005$.

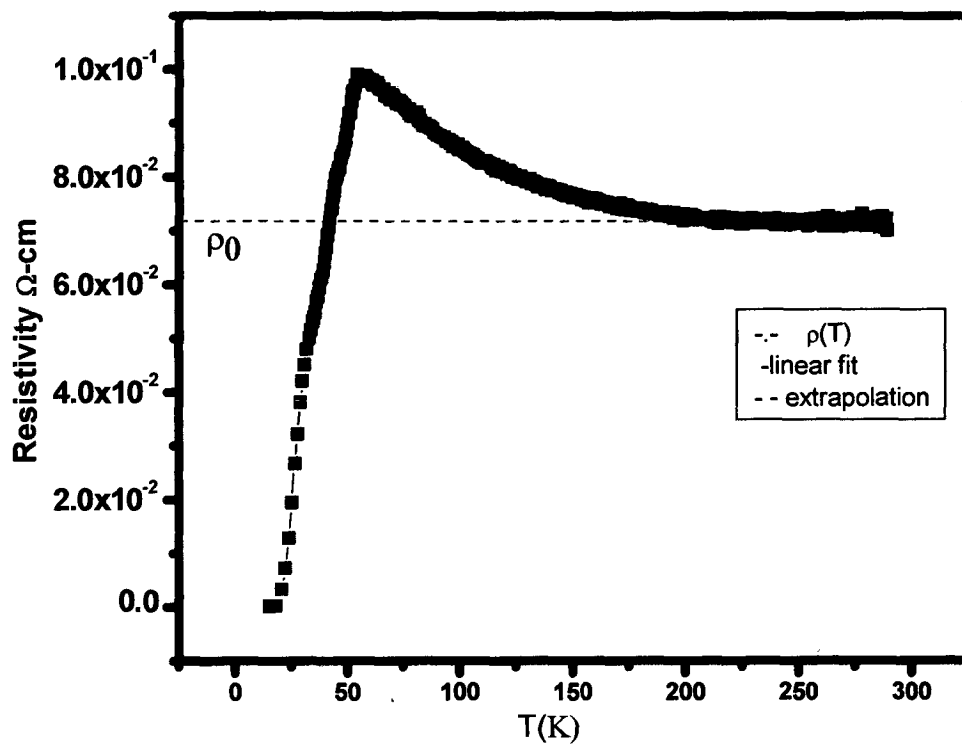


Fig.4.3.14 (j) $\rho(T) - T$ curve for $Y_{1-x}Pr_xBa_2[Cu_{1-y}Zn_y]_3O_{7-\delta}$ samples showing linear fit for $x = 0.20$ and $y = 0.01$.

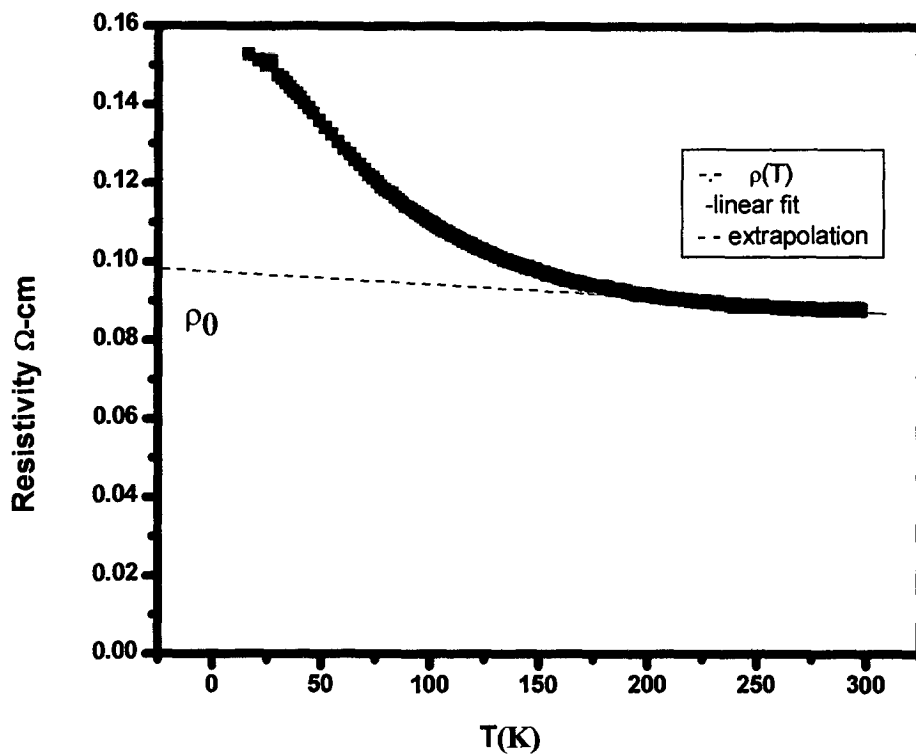


Fig.4.3.14 (k) $\rho(T) - T$ curve for $Y_{1-x}Pr_xBa_2[Cu_{1-y}Zn_y]_3O_{7-\delta}$ samples showing linear fit for $x = 0.20$ and $y = 0.03$.

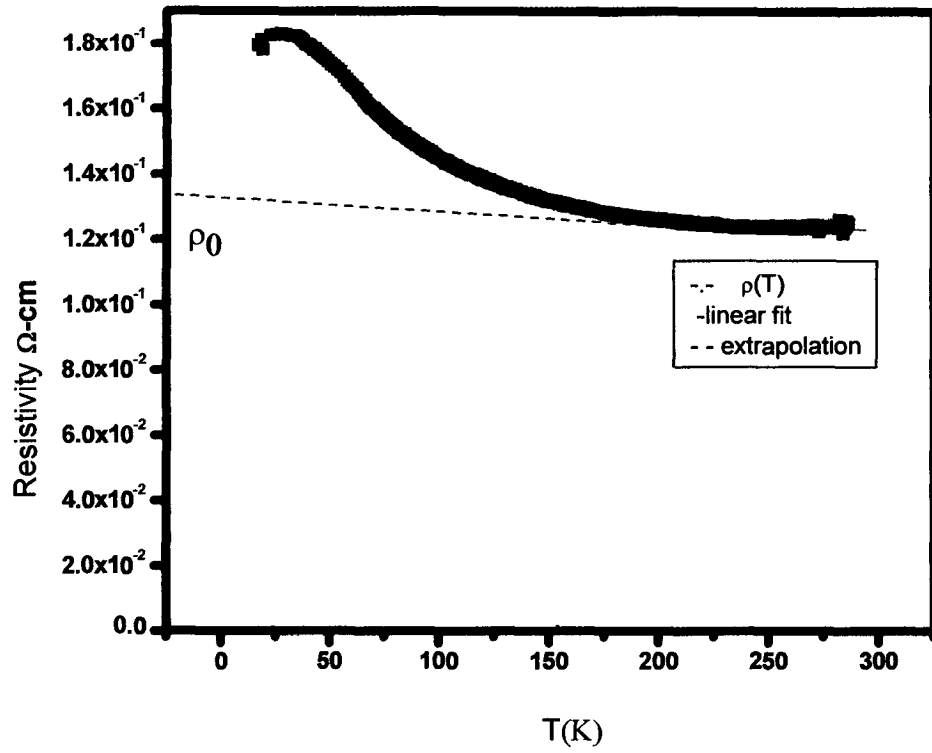


Fig.4.3.14 (I) $\rho(T) - T$ curve for $Y_{1-x}Pr_xBa_2[Cu_{1-y}Zn_y]_3O_{7-\delta}$ samples showing linear fit for $x = 0.20$ and $y = 0.06$.

that for this case T_c falls less rapidly with x in this region implying a depinning effect caused by Pr. The reason for this is that due to Pr substitution the holes starts moving from their planar site to 4f band implying the starting of depinning of charge stripes.

For $x = 0.2$ the hole depletion process is in full swing and the system has made a transition to a new state. As shown in Fig.4.3.13, T_c goes to zero at the Zn concentration $y = 0.03$ and superconductivity is destroyed. Fig 4.3.15(b) shows that ρ_0 becomes very large and Fig.4.3.16(b) shows that $d\rho/dT$ becomes negative. This implies the absence of depinning and a completely pinned charge stripe. It seems that the system has made a transition to the underdoped stage and that just one percent of Zn has made ρ_0 large enough to reach the unitarity value $h/4e^2$ and induces superconductor to insulator transition.

For the two superconducting systems $YBa_2Cu_3O_{7-\delta}$ and $La_{2-x}Sr_xCuO_4$ Uchida et al [43] used the method of determining the resistivity arising from S-wave impurity scattering in two dimensions. We have applied the procedure of Uchida et al [43] and the method of analysis proposed by Chien et al [42] for our system, $Y_{1-x}Pr_xBa_2[Cu_{1-y}Zn_y]_3O_{7-\delta}$ with $x = 0.2$ in order to estimate the the resistivity arising from s-wave impurity scattering in 2D systems using equation (4.2.1). Chemical doping and reflectivity studies [42] show that the carrier density in equation (4.2.1) in the Cu plane is $2.5 \times 10^{21} \text{ cm}^{-3}$ or 0.25 hole per CuO_2 plane. Making a similar assumption like those of Fukuzumi et al that Zn atoms are substituted only on the plane Cu sites, $n_i = \frac{3}{2}y$. Taking the value of $\delta_0 = \pi/2$, we find that ρ_0^{2D} comes close to the unitarity line till $y = 0.01$, when superconducting state exists and thereafter the system becomes insulator. It may be noted that the equation (4.2.1) refers to 2D conductance. In two dimensions, the resistance per square per CuO_2 plane has the dimensions of ohms so that the dimensionality of equation is taken care of.

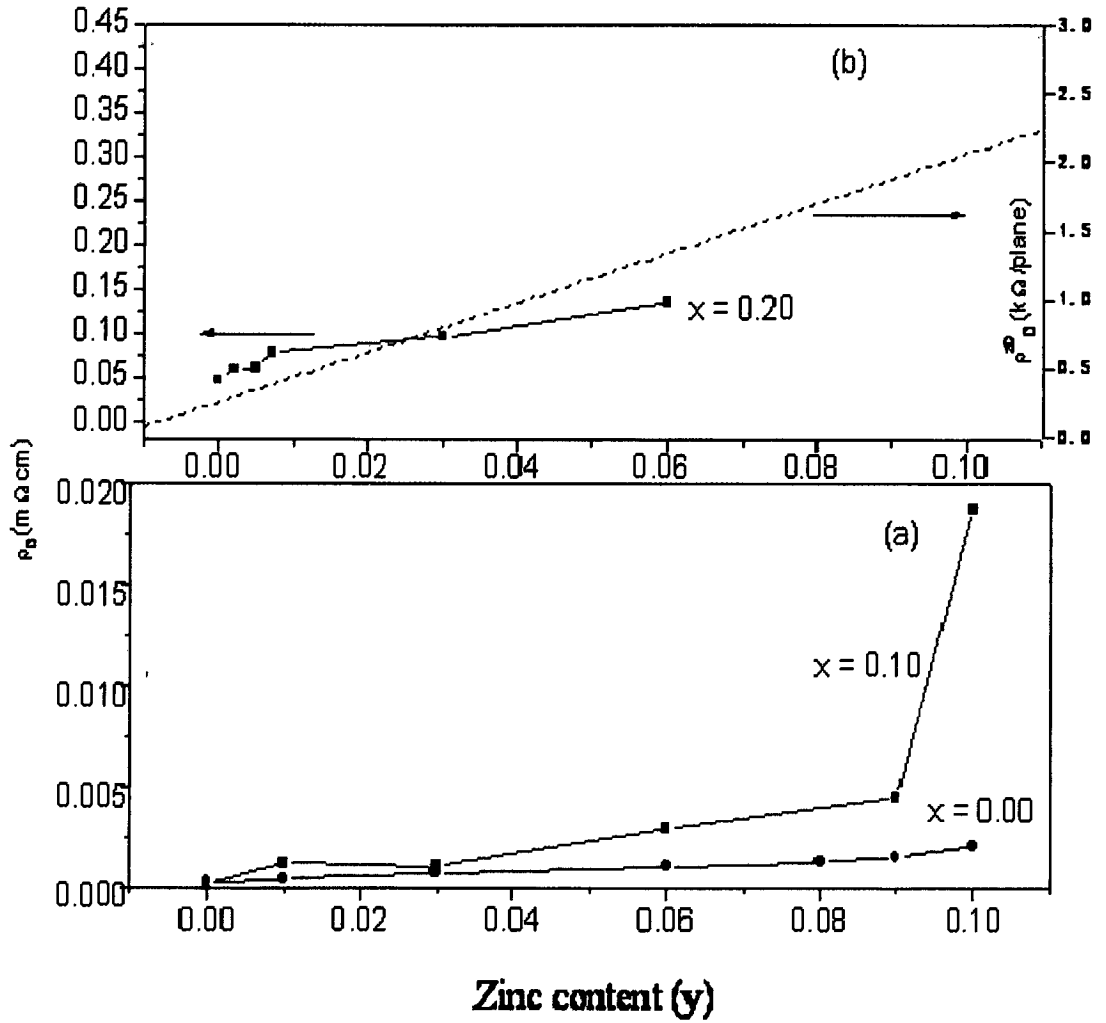


Fig 4.3.15 Variation of residual resistivity ρ_0 as a function of Zn content (y) in $Y_{1-x}Pr_xBa_2[Cu_{1-y}Zn_y]_3O_{7-\delta}$ (a) for $x = 0, 0.10$ and (b) for $x = 0.20$. The dashed line indicates the unitarity limit with the carrier density $n = 0.25$

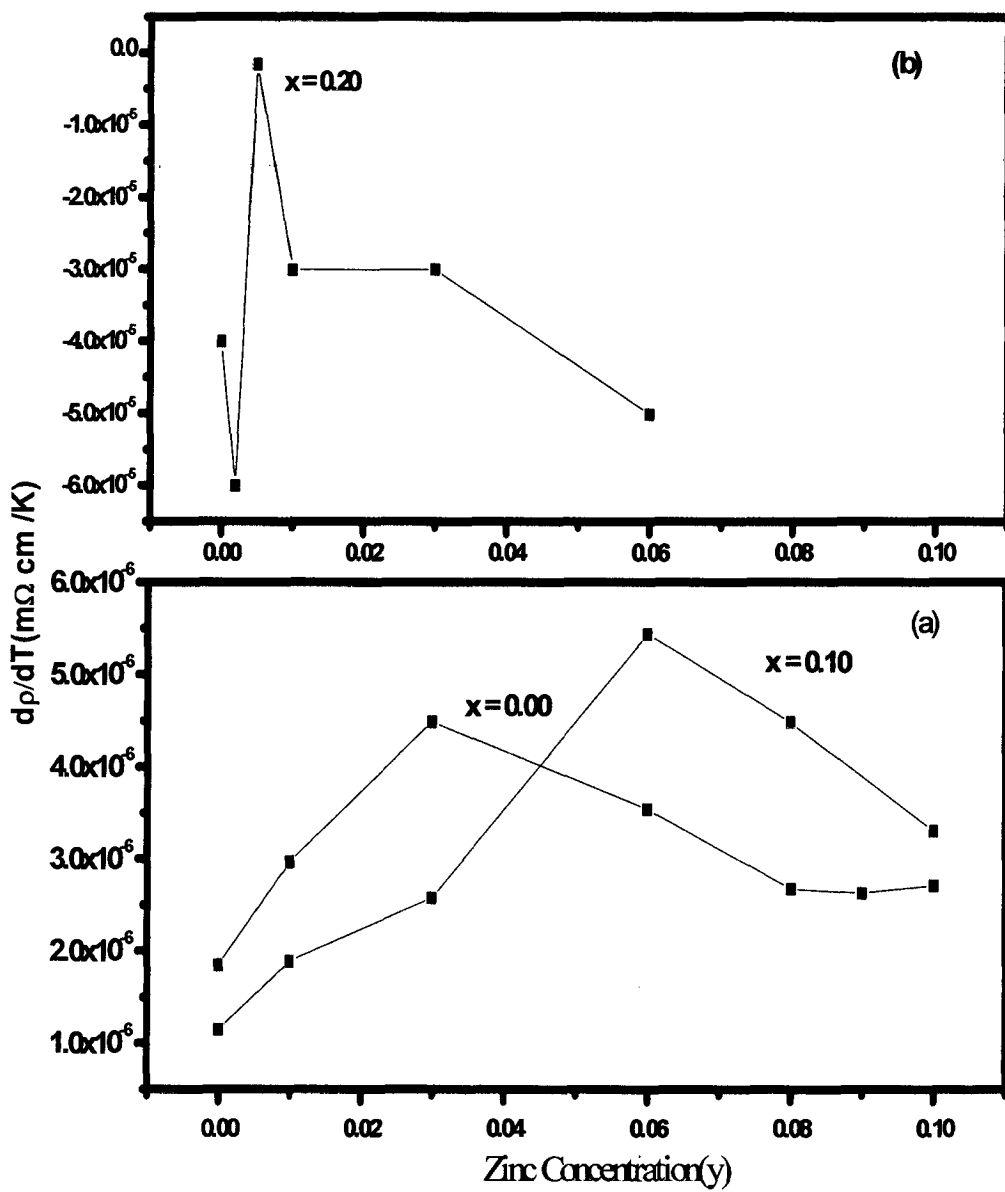


Fig 4.3.16 Slope dp/dT vs Zinc content (y) for different values of

$Y_{1-x}Pr_xBa_2[Cu_{1-y}Zn_y]_3O_{7-\delta}$ for (a) $x = 0, 0.10$ and (b) $x = 0.20$.

4.4 Conclusion

In this chapter we have presented our measurements on electrical resistivity as a function of temperature on samples of composition $Y_{1-x}Pr_xBa_2 [Cu_{1-y}Zn_y]_3O_{7-\delta}$ with $0 < y < 0.1$ and $x=0.1$ and $x=0.2$. The results have been analysed in terms of the superconducting critical temperature T_c , residual resistivity ρ_0 and the resistivity slope dp/dT corresponding to the linear ρ - T region. It is found that for $x = 0.1$ Pr has a minimal influence on the inplane processes for Zn impurity alone and that T_c and ρ_0 are slightly affected. The slope dp/dT becomes larger for the region $0.03 < y < 0.06$ leading to larger depinning effect and hence slower fall of T_c as a function of y . However, we noted for $x = 0.2$ there is a drastic change, ρ_0 becoming abnormally large and dp/dT becomes negative implying thereby the absence of depinning and a totally pinned charge stripes. It is inferred that for $x = 0.2$ the hole depletion is in full swing. We thus conclude that due to the hole depletion process Pr is able to bring the system in the underdoped region so that a small percentage of Zn is able to induce a superconductor-insulator transition. This can be seen by plotting the unitarity line for the case $x = 0.2$ we find that this line lies below $y = 0.01$ thereby suggesting the appearance of superconductor-insulator transition. Such a situation has been observed earlier by Fukuzumi et al [46] for Zn impurity alone by controlling the oxygen content in Y123 system. We feel that it is easier to obtain the same results using Pr, since we can control the charge carrier density easily using the hole depletion mechanism.

Furthermore, it is also observed that the critical transition temperature is reduced while the oxygen content remains constant. This has led to the suggestion that in the cuprate system studied in the present investigation it is not the oxygen content, which is believed to play a role in the suppression of T_c , it is the Pr concentration (i.e. hole concentration) that appears to be responsible for the T_c suppression.

References

1. M. B. Maple, Y. Dalichaouch, J. M. Ferreira, R. R. Hake, B. W. Lee, J. J. Neumeier, M. S. Torikachvili, K. N. Yang, and H. Zhou, *Physica B* **148**, 155 (1987) and references therein.
2. Yunhui Xu and Weiyan Guan, *Appl. Phys. Lett.* **53**, 334(1988).
3. J. K. Liang, X. T. Xu, S. S. Xie, G. H. Rao, X. Y. Shao, and Z. G. Duan, *Z. Phys. B* **69**, 137 (1987); L. Solderhelm, K. Zhang, D.G. Hinks, M. A. Beno, J. D. Jorgensen, C. U. Serge, and I. K. Schuller, *Nature* **328**, 6655 (1987).
4. Y. Dalichaouch, M. S. Torikachvili, E. A. Early, B. W. Lee, C. L. Seaman, K. N. Yang, H. Zhou, and M. B. Maple, *Solid State Commun.* **65**, 1001 (1988).
5. A. Matusuda, K. Kinoshita, T. Ishii, H. Shibata, T. Watanabe, and T. Tamada, *Phys. Rev. B* **38**, 2910 (1988).
6. J. L. Peng, P. Klavins, R. N. Shelton, H. B. Radousky, P. A. Hahn, and L. Bernardez, *Phys. Rev. B* **40**, 4517(1989).
7. A. P. Goncalves, I. C. Santos, E. B. Lopes, R. T. Henriques, and M. Almeida, *Phys. Rev. B* **37**, 7476 (1988).
8. D. W. Cook, R. S. Kwok, R. L. Lichti, T. R. Adams, C. Boekema, W. K. Dawson, A. Kebede, J. Schwegler, J. E. Crow, and T. Mihalisin, *Phys. Rev. B* **41**, 4801 (1990).
9. B. Renker, F. Gompf, E. Gering, G. Roth, W. Reichard, D. Ewert, H. Rietschel, and H. Mutka, *Z. Phys. B* **71**, 437(1988).
10. N. Sanker, V. Sankaranarayanan, L. S. Vaidyanathan, G. Rangarajan, R. Srinivasan, K. A. Thomas, U. V. Varadaraju, and G.V. Subba Rao, *Solid State Commun.* **67**, 391 (1988).

11. U. Neukirch, C. T. Simmons, P. Sladeczac, C. Laubschat, O. Strebel, G. Kaindl, and D. D. Sarma, *Europhys. Lett.* **5**, 167(1988).
12. D. P. Norton, D. H. Lowndes, B. C. Sales, J. D. Budai, B. C. Chakoumakos, and H. R. Kerchner, *Phys. Rev. Lett.* **66**, 1537(1991).
13. R. F. Wood, *Phys. Rev. Lett.* **66**, 829 (1991), and references therein.
14. J. Fink, N. Nucker, H. Romberg, M. Alexander, M. B. Maple, J.J. Neumeier, and J. W. Allen, *Phys. Rev. B* **42**, 4823 (1990).
15. A. A. Abrikosov and L. P. Gor'kov, *Zh. Eksp. Teor. Fiz.* **39**, 1781(1960); *Sov. Phys. JETP* **12**, 1243 (1961).
16. C. Jee, A. Kebede, D. Nichols, J. E. Crow, T. Mihalisin, G. H. Myer, I. Perez, R. E. Salomon, and P. Schlottmann, *Solid State Commun.* **69**, 379 (1989).
17. J. J. Neumeier, T. Björnholm, M. B. Maple, and I. K. Schuller, *Phys. Rev. Lett.* **63**, 2516 (1989).
18. Yunhui Xu and Weiyuan Guan, *Appl. Phys. Lett.* **59**, 2183 (1991); *Phys. Lett. A* **163**, 104(1992).
19. G. Y. Guo and W. M. Temmerman, *Phys. Rev. B* **41**, 6372 (1990).
20. M. B. Maple, C. C. Almasan, C. L. Seaman, S. H. Han, K. Yoshiara, M. Buchgeister, L. M. Paulius, B. W. Lee, D. A. Gajewski, R. F. Jardim, C. R. Fincher, Jr., G. B. Blanchet, and R. P. Guertin, *J. Supercond.* **7**, 97(1994).
21. Yabin Yu, Guanghan Cao and Zhengkuan Jiao, *Phys. Rev. B* **59**, 3845, (1999) .
22. R. Fehrenbacher and T. M. Rice, *Phys. Rev. Lett.* **70**, 3471(1993).
23. A. I. Liechtenstein and I. I. Mazin, *Phys. Rev. Lett.* **74**, 1000(1995).
24. M. Lee, M. L. Stutzman, Y. Suzuki and T. H. Geballe, *Phys. Rev. B* **54**, R3776(1996).

25. H.B. Rodousky, J. Mater. Res. 7 ,1918(1992), and references therein; B. Maple,B. W. Lee , J.J. Neumeier, G. Nieva , L.M. Paulius, C. L. Seaman, J. Alloys Comp. **181**,135(1992).
26. A.V. Narlikar, C.V. Rao, S. K. Agarwal, in studies of “High Temperature Superconductor”, edited by .A.V. Narlikar (Nova Science, New York, 1989), vol.1,p.341.
27. M. Mehbod, P. Wyder, R. Deltour, Ph. Duvigneaud, and G. Maessens,Phys. Rev. B **36**, 8819 (1987).
28. J. M. Tarascon, P. Barboux, P. F. Miceli, L. H. Greene, G. W.Hull, M. Eibschutz, and S. A. Sunshine, Phys. Rev. B **37**, 7458(1988).
29. G. Xiao, M. Z. Cieplak, A. Gavrin, F. H. Streitz, A. Bakhshai, and C. L. Chien,Phys. Rev. Lett. **60**, 1446(1988).
30. Y. Xu, R. L. Sabatini, A. R. Moodenbaugh, Y. Zhu, S. G. Shyu, M. Suenaga, K. W. Dennis, and R. W. McCallum, Physica C**169**, 205 (1990).
31. H. Alloul, P. Mendels, H. Casalta, J. F. Marucco, and J. Arabski, Phys. Rev. Lett. **67**, 3140 (1991).
32. A. J .Millis, S. Sachdev, and C.M. Varma, Phys. Rev. B **37**,4975(1988).
33. Ratan Lal,Phys.Rev.B,**51**,640,(1995).
34. G.V.M. Williams, J. L. Tallon, and R. Meinhold, Phys.Rev.B,**52**,7034(1995).
35. G. D. Liu, Z . X. Zhao, G .C. Che, Solid State Commun. **109**, 495(1999).
36. J. S. Zhou, J. B. Goodenough, and H. Sato, M. Natio, Phy. Rev. B,**59**,3827(1999).
37. T. Katuwal, V. Sadu ,C.C. Almasan , B.J. Taylor and M.B. Maple, Phy. Rev. B **72**,174501 (2005).

38. K. Ishida *et al.*, Physica (Amsterdam) **179C**, 29 (1991); J. Phys. Soc. Jpn. **62**, 2803 (1993).
39. D. A. Bonn *et al.*, Phys. Rev. B **50**, 4051 (1994).
40. H. Alloul *et al.*, Phys. Rev. Lett. **67**, 3140 (1991).
41. K. Kakurai *et al.*, Phys. Rev. B **48**, 3485 (1993).
42. T.R.Chien, Z.Z. Wang, and N.P. Ong, Phys. Rev. Lett. **67**,2088 (1991).
43. S. Uchida, Y. Fukuzumi, K. Mizuhashi, and K. Takenaka, Chinese journal of Physics **34**, 423(1996).
44. D.B. Haviland, Y.Liu, and A.M. Goldman, Phys. Rev. Lett. **62**, 2180 (1989).
45. M.P.A. Fisher, G. Grinstein, and S.M. Girvin, Phys.Rev.Lett. **64**,587(1990).
46. Y. Fukuzumi, K. Mizuhashi, K. Takenaka, and S.Uchida, Phys. Rev. Lett. **76**,684 (1996).
47. Y. Nakamura and S. Uchida, Phys. Rev. B **47**, 8369(1993).
48. K. Takenaka *et al.*, Phys. Rev. B **50**, 6534 (1994).
49. K. Tamasaku *et al.*, Phys. Rev. Lett. **72**, 3088 (1994).
50. I. D.Brown, J.Solid State Chem.**90**,155 (1991); C.C.Almasan *et al* ,Phys. Rev. Lett. **69**,680(1992).
51. A.V. Mahajan *et al* ,Phys.Rev Lett. **72**,3100 (1994).
52. L.S. Borkowski and P.J. Hirschfeld, Phys. Rev.B **49**, 1504 (1994).
53. A.R.Gupta, R.Lal, A. Sedky, A.V. Narlikar, V.P.S.Awana Phys. Rev B **61**, 11752 (2000).

Chapter 5

Normal and Anomalous Pseudogap of Superconducting



5.1 Introduction

The importance of the hole concentration in the copper -oxide superconductors is widely recognised [1]. A number of studies concerning the relationship between the hole concentration (p) and the superconducting temperature (T_c) have been reported [2]. In the $\text{La}_{2-x}\text{Sr}_x\text{CuO}_4$ (La214) system, with increase in Sr content (x), hole concentration (p), increases, T_c increases first to have a maximum and then becomes zero for $x \geq 0.26$. The copper valence is intimately linked with the carrier concentration n , and by studying T_c as a function of n , detailed phase diagrams have been constructed for the Sr or Ba doped La214 system [3, 4]. Attempts have been made to generalise such behaviour to various other families of high T_c cuprates, namely 123 system as well as Bi and Tl based systems [5]. It has been argued that unlike La214 the situation with other cuprates is not so transparent, as the data available are either too scant or not sufficiently unambiguous because of the simultaneous presence of two fluctuating -valence cations [6] such as Cu^{2+} and Bi^{3+} (or Tl^{3+}). In 123 system, the carrier density can be enhanced either by increasing the oxygen stoichiometry or by on-site cationic substitutions with dopants of lower valence state. By increasing the oxygen stoichiometry, the copper valence in general cannot be increased beyond its optimum value, due to structural instability. In such a situation the only alternate strategy left is to realize the objective by substitution of lower -valence -state cations. On this basis, the role of Cu-O chains in 123 system has been debated continuously since the discovery of this material.

Substitutions for different native cations are extensively used to study the mechanism of superconductivity as well as the nature and properties of the normal state in high temperature superconductors [7, 8]. Doping of the $\text{YBa}_2\text{Cu}_3\text{O}_{7-\delta}$ system by nonisovalent impurities affects strongly the charge-carrier system, leading to

significant changes both of electronic and superconducting properties. Despite numerous data on this subject, the mechanism of some substitutions influence is still not completely understood. Besides, it is generally observed [9-13] that any nonisovalent substitution leads to a deviation from the oxygen stoichiometry in different directions depending on the relationship between the valences of the dopant and the replaced element. In particular, substitutions for Cu(1) by transition metals namely Fe, Co, Al or for Ba by rare-earth elements result in increasing oxygen content [14–18].

5.2 Role of Ca doping in Y123 System

Among all dopants calcium plays a special role because the substitution for Y^{3+} by Ca^{2+} is unique in that it induces decreasing oxygen content [19-21] and it is one of the most extensively studied substitutions [22-27]. The results reported in the literature are however varied, which reveal that such substitution creates vacancies [24,27]. Interestingly at same time the X-ray diffraction data of the other workers indicate literally no change in the lattice parameters of the parent material upto 20% of Ca substitution [24,25]. This behaviour remains to be understood. This apart, the T_c decreases with Ca substitution is attributed to the material becoming overdoped [24,27].

The substitution of Ca for Y adds holes to the unit cell. Since Ca has a valence of +2 and hybridizes little, if at all, with the CuO_2 valence band π -states. The most important effect of Ca substitution is to dope the CuO_2 planes with holes because the charge at Y site must balance the charge in the two adjacent CuO_2 planes. The interpretation that substitution at Y site do not result in charge transfer to the chains or a change in their structure.

According to Awana-et-al [28] Ca^{2+} incorporation within the solubility limits in place of Y^{3+} has three main effects (1) decrease in T_c and increase in normal state resistivity, (2) lattice parameters a, b, c remain invariant and (3) effective copper valence essentially remains unchanged while oxygen stoichiometry of the system is decreased.

The invariance of Cu valence with Ca doping is contrary to the general belief that Ca substitution leads to overdoping [24-26] of the 123 system, and thereby lowers T_c . This is reflected in the resistivity measurements [24-26] which shows the increase in normal state resistivity of the system with Ca doping. They found that there is no change in $a, b,$ and c lattice parameters and hence no change in the orthorhombicity of the system. This implies that the oxygen is presumably not removed from the Cu-O chains. No change in c parameters in this system with Ca doping suggests that Ca enters at the Y-site with the same ionic size as Y. The ionic size of Y^{3+} in eightfold coordination is 1.02 \AA , which matches more closely with that of Ca^{2+} in six fold coordination (1.00 \AA) rather than in eightfold coordination (1.12 \AA). This suggests that Ca at a Y-site would prefer six fold coordination instead of eightfold coordination. This would imply creation of oxygen vacancies in the adjoining CuO_2 planes. Since the superconductivity is presumably supposed to reside in these planes, the oxygen disorder thus created is expected to have deleterious effect on T_c , which is observed with Ca substitution. Bottger et-al [29] have carried out a detailed neutron diffraction work on $\text{Y}_{1-x}\text{Ca}_x\text{Ba}_2\text{Cu}_3\text{O}_{7-\delta}$. They have found a correlation between the buckling in the CuO_2 planes and T_c . Charge distribution within the structure via measurement of the Cu-O distances and calculation of bond valence sums have also been determined. From their results they have concluded that the partial substitution for Y^{3+} with Ca^{2+} introduces additional hole carriers in the structure and makes the

system accessible far in to the overdoped region. They have attributed the decrease in T_c to an increase in hole concentration in the CuO_2 planes.

5.3 Codoping Effect of Ca and Pr in Y123 System

Guan and co-workers reported that the superconducting transition temperature, T_c [30] the magnetic ordering temperature of Pr ions, T_N [31] the normal-state resistivity, [32,33] and the Hall number per unit cell n_H in $\text{Y}_{1-x}\text{Pr}_x\text{Ba}_2\text{Cu}_3\text{O}_{7-\delta}$ are all R ion-size dependent [30,33,34]. It was also reported that the Hall number n_H of $\text{Y}_{0.9}\text{Ca}_{0.1}\text{Ba}_2\text{Cu}_3\text{O}_{7-\delta}$ [35] and T_c of $\text{RBa}_2\text{Cu}_{3-x}\text{Ga}_x\text{O}_{7-\delta}$ [36] are also ion-size dependent. It is experimentally shown that upon substituting Pr into the system T_c decreases monotonically and vanishes at a critical concentration $x \sim 0.55$, near the metal insulator transition [37-39] Numerous investigations [30,34] on the system have been carried out. With increasing Pr concentration suppression of superconductivity results from a reduced number of carriers in the CuO_2 sheets.

The valence state of Ca^{2+} is lower than that of Y^{3+} . Such a substitution will generate excess holes and T_c is suppressed by the overdoping effect. On the other hand, it has been known that Ca doping is likely to co-introduce oxygen vacancies, reducing the number of the generated holes. This indicates that doping with Ca ions has a counterbalance effect on the suppression of T_c . Ca doping is able to increase the T_c of the oxygen deficient Y123 [40]. The replacement of 20% Ca ions in tetragonal $\text{YBa}_2\text{Cu}_3\text{O}_6$ induces the superconductivity; whereas the same amount of Ca, in fully oxygenated $\text{RBa}_2\text{Cu}_3\text{O}_{7-\delta}$, lowers T_c from 90 to 78 K. Yakabe et al.[41] showed that there exists a maximum of T_c about 90 K with the variation of the carrier density in single phase $\text{Y}_{1-x}\text{Ca}_x\text{Ba}_2\text{Cu}_3\text{O}_{7-\delta}$. thin films up to 50% Ca concentration. Similar behavior was observed in $\text{Y}_{1-x}\text{Ca}_x\text{Ba}_2\text{Cu}_{2.64}\text{Co}_{0.36}\text{O}_{7-\delta}$. [42] and Y_{1-x}

$x\text{Ca}_x\text{Ba}_2\text{Cu}_{2.5}\text{Fe}_{0.5}\text{O}_{7-\delta}$, [43] These observations indicate that the substitution of Ca^{2+} for Y^{3+} in these compounds compensates the loss of the holes and restores the superconductivity .

The T_c of $\text{Y}_{1-x-z}\text{Pr}_x\text{Ca}_z\text{Ba}_2\text{Cu}_3\text{O}_{7-\delta}$. [44] could be enhanced by Ca doping and there exists a maximum of T_c for varying Ca concentration z . The T_c vs z curves can be resolved into two parts: 1) the counteracting effects of generation and filling of holes on the CuO_2 sheets by Ca^{2+} and Pr^{3+} ions, respectively, and 2) the depairing of superconducting electrons via exchange interaction of mobile holes on the CuO_2 sheets with local Pr magnetic moments.

It was reported that in fully oxygenated Y123, Ca doping is accompanied by the loss of oxygen content [45] ,but it was also found that the oxygen content does not change with Ca concentration in the $\text{Y}_{1-x-z}\text{Pr}_x\text{Ca}_z\text{Ba}_2\text{Cu}_3\text{O}_{7-\delta}$ system. [44] It suggests that the loss of oxygen content, resulting from Ca doping, can be compensated by Pr doping. On the other hand, in oxygen-deficient Y123 [46] the length of the c axis increases progressively with decreasing oxygen content. But it is observed that [47] in $\text{Y}_{1-x-z}\text{Pr}_x\text{Ca}_z\text{Ba}_2\text{Cu}_3\text{O}_{7-\delta}$ samples, the c axis does not increase apparently. Therefore, it is reasonable to assume that the oxygen content does not vary much .

5.4 Codoping effect of Ca and Zn in Y123 System

The normal-state (NS) and superconducting (SC) properties of high- T_c cuprates are extremely sensitive to stoichiometry and the number (p) of added hole carriers per copper oxide plane. In recent years one of the most widely studied phenomena in the physics of high-temperature superconductors (HTS) is the so-called pseudogap (PG) state [48,49] which is observed over a doping range extending from the underdoped (UD) to the slightly overdoped (OD) region. In the pseudogap (PG)-

state various NS and SC anomalies are observed which can be interpreted in terms of a reduction in the effective single particle density of states [50]. Existing theories of the PG, which is believed to be an essential feature of HTS physics, can be classified broadly into two categories. The first is based upon a model of Cooper pair formation of T^* well above the SC transition temperature, T_c , with long-range phase coherence appearing only at $T \leq T_c$ [51–53]. The second model assumes that the appearance of the PG is due to fluctuations of some other type, which compete or coexist with SC. These include antiferromagnetic fluctuations, charge density waves, structural phase transition or electronic phase separation on a microscopic scale (e.g., the stripe scenario) [54-57]. Within this second category the concept of a quantum critical point (QCP) has been mooted to explain the HTS phase diagram [58-60] though its confirmation remains inconclusive [61].

Pure Y123 with full oxygenation is slightly OD and further overdoping can only be achieved by substituting Y^{3+} by Ca^{2+} , while Zn substitution at the in-plane Cu(2) sites increases the planar impurity scattering. The advantages of using Zn are (i) it mainly substitutes the in-plane Cu(2) sites, thus the effects of planar impurity can be studied and (ii) the doping level remains nearly the same when Cu(2) is substituted by Zn enabling one to look at the effects of disorder at almost the same hole concentration [62,64]. Most of the studies on the effect of Zn on charge transport of Y123 are limited to the range of UD to optimum doping levels and at a moderate level of Zn substitution. Therefore, study of the system in the OD region with high levels of planar defects fills an important gap. Here the doping level remains nearly independent of Zn content enabling one to separate the effects of doping and disorder on various NS and SC properties [63-64]. The evolution of the resistivity, $\rho(T, p)$, provides a way of establishing the $T - p$ phase diagram and can give valuable

information about the different crossover regions in the vicinity of a possible quantum critical point [58-60].

From the analysis of $\rho(T, p)$ one can extract UD and OD crossover temperatures, T^* and T^m respectively, above which $\rho(T, p)$ exhibits linear T – dependence and one can also determine the p -dependent exponent m in fits to $\rho = \rho_0 + \rho_1 T^m$ on the overdoped side. Furthermore, the room temperature thermopower, $S[290 \text{ K}]$, has a systematic variation with p for various HTS over the entire doping range extending from very UD to heavily OD regions [65], also $S[290 \text{ K}]$ is insensitive to in-plane disorder like Zn and the crystalline state of the sample [65]. For these reasons $S[290 \text{ K}]$ is a good measure of p even in the presence of strong in-plane electronic scattering by Zn^{2+} ions.

A proper understanding of the normal state has been considered crucial for an insight into the origin of superconductivity in these systems. And that is where the possible role of an impurity affecting the normal state of the cuprate systems becomes indispensable. In the case of the Y123 system the site-dependent disorder is known to produce different effects. For instance, an impurity disorder at the planar CuO_2 site is found to promote localization of charge carriers, while at the Cu-O chain site it affects the dimensionality and the carrier transport along the c direction. With this background we think that a study of the Y123 system with simultaneous doping of two kinds of impurities at Y site and one different impurity at Cu site may provide useful information relevant to the origin of superconductivity. In fact, it may happen that the combined effect of two such kinds of impurities on various properties like residual resistivity, resistivity slope, and superconducting critical temperature comes out to be significantly different from that of the direct summation of the effects of the individual impurities.

In the present Chapter , we have investigated the effect of codoping of Pr, Ca and Zn as impurities in the Y123 system. The reason for the choice of impurities is that, as it is known for this system [47] Pr and Ca substitute at Y site while Zn substitutes at Cu(2) site in the CuO₂ plane. It would therefore be interesting to examine whether simultaneous presence of these impurities at different sites of the Y123 structure alters the normal and superconducting state properties, in comparison to their expected individual effects as studied by earlier workers [47].

5.5 Results and Discussion

5.5.1 X-ray Diffraction and Iodometric Titration

X-ray powder diffraction data were collected on polycrystalline samples of compositions $Y_{0.9-x}Pr_xCa_{0.1}Ba_2[Cu_{1-y}Zn_y]_3O_{7-\delta}$ with different values of x and y ($0 \leq x \leq 0.15$ and $y = 0.02, 0.06$) with Rigaku diffractometer equipped with CuK_{α} radiation. The XRD patterns are presented in Figs. 5.5.1-5.5.2 .The diffraction patterns were refined with Fullprof Rietveld program in the space group Pmmm .The refined lattice parameters , atomic positions and R-factors are listed in Tables 5.5.1-5.5.2 and the fitted diffraction patterns are presented in Figs.5.5.3-5.5.7. The oxygen contents determined from iodometric titration are given in Table 5.5.1 and Table 5.5.2 along with the calculated oxygen contents from equation (3.5.1). The lattice parameters a, b ,c of the samples do not show large variation. It is observed by Narlikar et al [28] that the decrease in oxygen content creates vacancies resulting in a decrease in orthorhombicity when Ca is added to Y123 system. In the present work we have added Pr and Zn together with Ca and we observe that the oxygen contents obtained by iodometry remains almost constant within errors. In this case also, the experimentally determined oxygen content is less than that calculated from c value

equation (3.5.1). This suggests that Ca and Pr enters the Y site with same ionic radius as Y. This results in the creation of vacancies in the CuO_2 planes, because of charge imbalance. . As superconductivity is presumably supposed to reside in these planes, the oxygen disorder thus created is expected to have deteriorious effect on T_c .

It has been is also noted by Awana et al [4] that for Ca with 0.1 concentration in Y123 the system shows tetragonal symmetry. However, our system retains orthorhombicity mostly due to the effect of Zn which localizes the holes.

Table 5.5.1 Rietveld Refinement of XRD data for $Y_{0.9-x}Pr_xCa_{0.1}Ba_2[Cu_{0.98}Zn_{0.02}]_3O_{7-\delta}$.

The space group is Pmmm with $Y(\frac{1}{2}, \frac{1}{2}, \frac{1}{2})$, $Pr(\frac{1}{2}, \frac{1}{2}, \frac{1}{2})$, $Ca(\frac{1}{2}, \frac{1}{2}, \frac{1}{2})$, $Ba(\frac{1}{2}, \frac{1}{2}, z)$, $Cu(1)(0,0,0)$, $Cu(2)(0,0,z)$, $O(1)(0, \frac{1}{2}, 0)$, $O(2)(\frac{1}{2}, 0, z)$, $O(3)(0, \frac{1}{2}, z)$, $O(4)(0,0, z)$. Also shown oxygen content and T_c . The values in the parentheses represents uncertainties in the last digit.

	x = 0.0	x = 0.025	x = 0.075	x = 0.1	x = 0.12
z(Ba)	0.182(2)	0.182(2)	0.182(2)	0.182(2)	0.182(2)
z(Cu2)/z(Zn)	0.360(3)	0.361(3)	0.362(3)	0.363(3)	0.362(3)
z(O2)	0.353(4)	0.365(1)	0.368(1)	0.370(1)	0.371(1)
z(O3)	0.389(1)	0.387(1)	0.379(2)	0.375(3)	0.370(2)
z(O4)	0.162(1)	0.158(3)	0.159(3)	0.160(1)	0.157(3)
a(A ⁰)	3.829(1)	3.830(1)	3.826(2)	3.828(1)	3.829(2)
b(A ⁰)	3.883(1)	3.883(1)	3.882(1)	3.882(1)	3.883(1)
c(A ⁰)	11.667(1)	11.669(1)	11.665(1)	11.667(1)	11.664(1)
R _{wp}	15.9	13.1	15.1	15.0	13.5
R _{exp}	14.3	12.8	13.1	13.6	12.6
R _{Bragg}	25.36	22.3	15.88	12.8	16.27
χ^2	1.24	1.18	1.17	1.20	1.14
Oxygen content as obtained from iodometric titration (7- δ)	6.67±0.03	6.67±0.05	6.67±0.02	6.67±0.03	6.67±0.02
Calculated oxygen content from equation 3.5.1 (7- δ)	6.928±0.01	6.916±0.01	6.940±0.01	6.928±0.01	6.945±0.01
T _c (K)	57.90±1.00	67.43±1.00	58.67±1.00	49.45±1.00	22.66±1.00

Table 5.5.2 Rietveld Refinement of XRD data for $Y_{0.9x}Pr_xCa_{0.1}Ba_2[Cu_{0.94}Zn_{0.06}]_3O_{7-\delta}$.

δ . The space group is Pmmm with $Y(\frac{1}{2}, \frac{1}{2}, \frac{1}{2})$, $Pr(\frac{1}{2}, \frac{1}{2}, \frac{1}{2})$, $Ca(\frac{1}{2}, \frac{1}{2}, \frac{1}{2})$, $Ba(\frac{1}{2}, \frac{1}{2}, z)$, $Cu(1)(0, 0, 0)$, $Cu(2)(0, 0, z)$, $O(1)(0, \frac{1}{2}, 0)$, $O(2)(\frac{1}{2}, 0, z)$, $O(3)(0, \frac{1}{2}, z)$, $O(4)(0, 0, z)$. Also shown oxygen content and T_c .

The values in the parentheses represents uncertainties in the last digit.

	x = 0.0	x = 0.075	x = 0.1	x = 0.12
z(Ba)	0.182(1)	0.183(1)	0.181(1)	0.183(1)
z(Cu2)/z(Zn)	0.360(2)	0.361(2)	0.362(2)	0.362(2)
z(O2)	0.353(3)	0.365(1)	0.369(1)	0.370(1)
z(O3)	0.389(1)	0.370(3)	0.365(5)	0.360(4)
z(O4)	0.162(2)	0.163(2)	0.162(2)	0.161(2)
a(Å)	3.829(1)	3.828(1)	3.826(1)	3.828(1)
b(Å)	3.883(1)	3.882(1)	3.882(1)	3.883(1)
c(Å)	11.667(1)	11.667(1)	11.665(2)	11.668(2)
R_{wp}	15.9	18.2	14.3	15.9
R_{exp}	14.3	13.5	11.2	13.2
R_{Bragg}	25.36	22.3	15.6	14.2
χ^2	1.20	1.25	1.18	1.14
Oxygen content as obtained from iodometric titration (7- δ)	6.67 \pm 0.03	6.67 \pm 0.02	6.67 \pm 0.03	6.67 \pm 0.02
Calculated oxygen content from equation 3.5.1 (7- δ)	6.928 \pm 0.01	6.928 \pm 0.01	6.940 \pm 0.02	6.922 \pm 0.02
T_c (K)	46.05 \pm 1.00	55.43 \pm 1.00	44.66 \pm 1.00	20.79 \pm 1.00

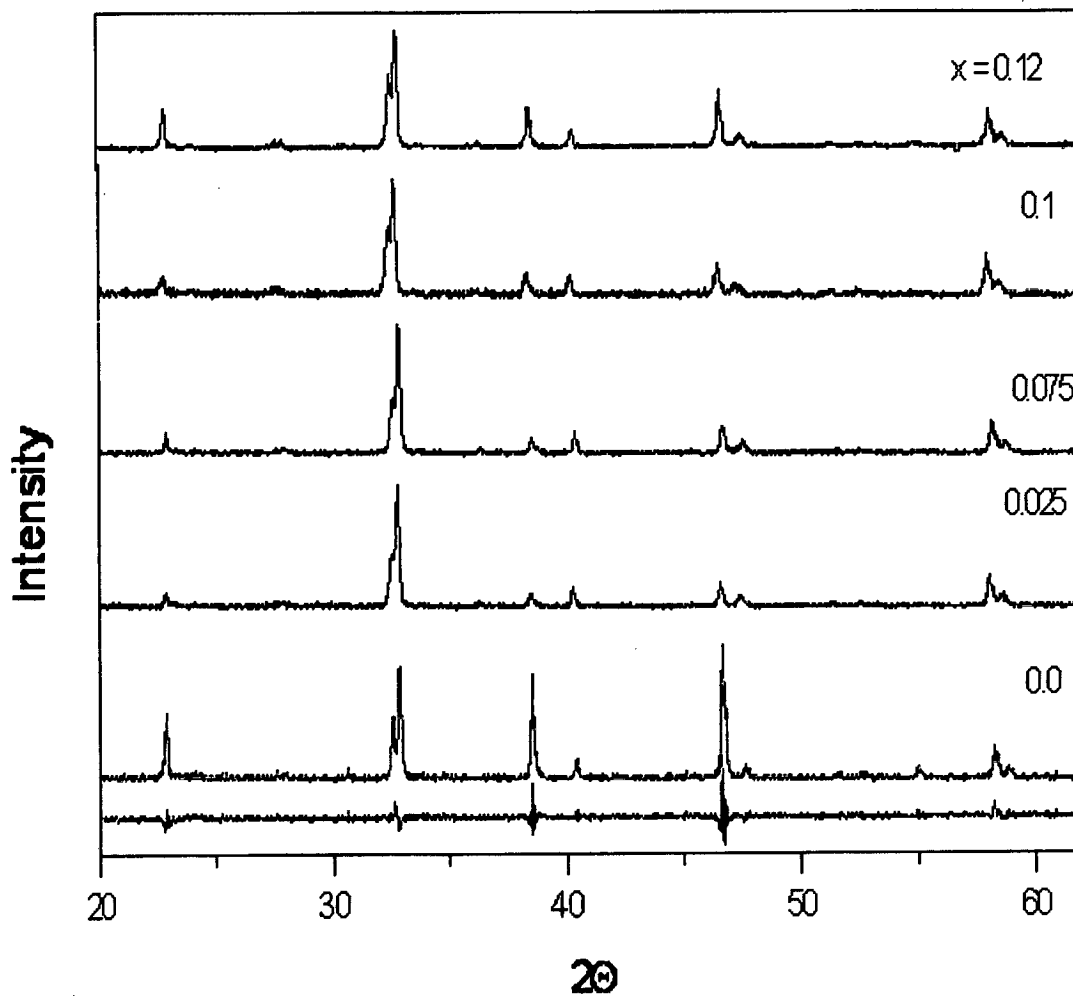


Fig.5.5.1. X-ray diffraction patterns for $Y_{0.9-x}Pr_xCa_{0.1}Ba_2[Cu_{1-y}Zn_y]_3O_{7-\delta}$ samples with different values of Pr concentration and Zinc content $y = 0.02$

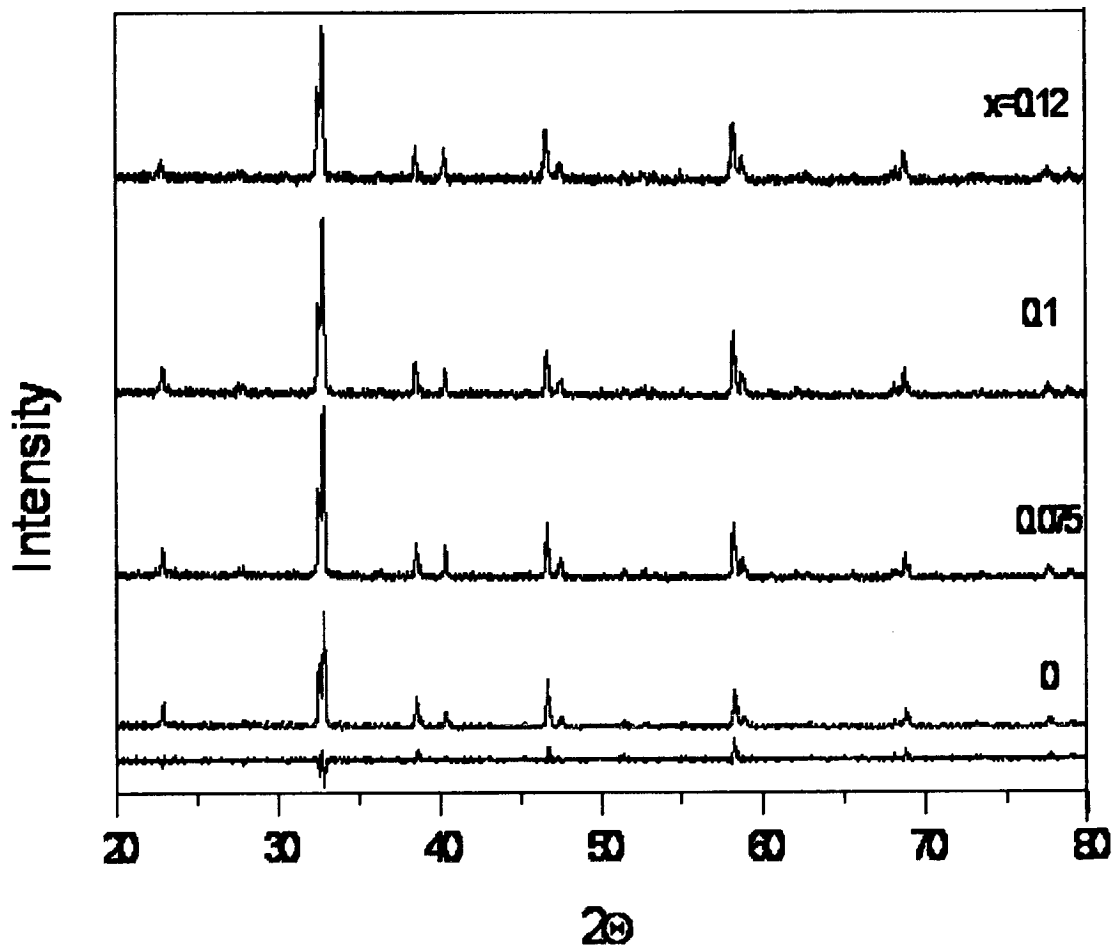


Fig.5.5.2. X-ray diffraction patterns for $Y_{0.9-x}Pr_xCa_{0.1}Ba_2[Cu_{1-y}Zn_y]_3O_{7-\delta}$ samples with different values of Pr concentration and Zn concentration $y = 0.06$

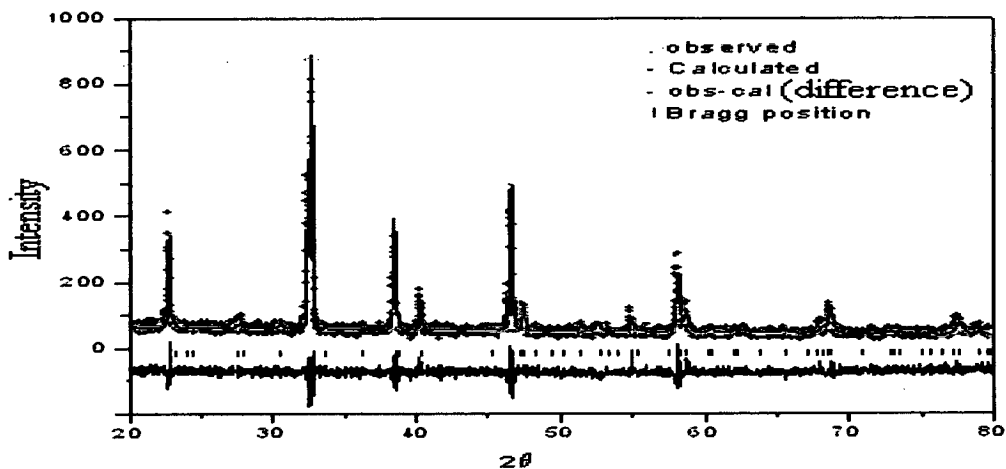


Fig.5.5.3 Rietveld refined diffraction patterns of $Y_{0.9-x}Pr_xCa_{0.1}Ba_2[Cu_{0.98}Zn_{0.02}]_3O_{7-\delta}$ with $x = 0.00$

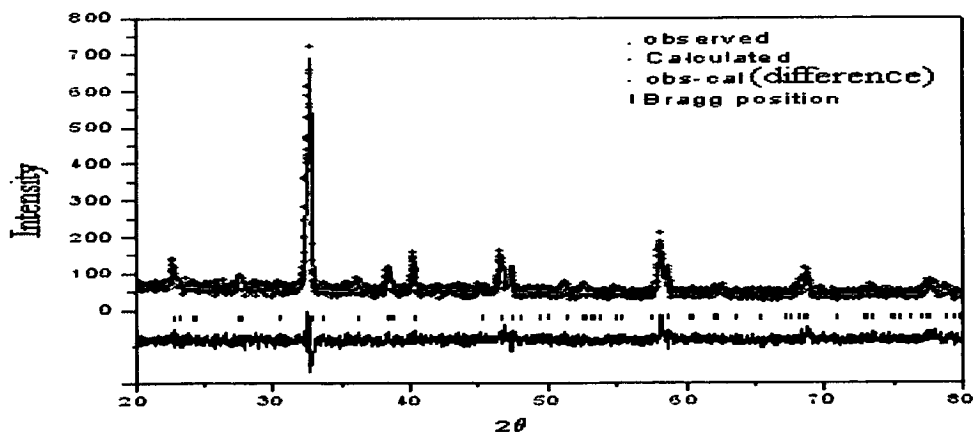


Fig.5.5.4 Rietveld refined diffraction patterns of $Y_{0.9-x}Pr_xCa_{0.1}Ba_2[Cu_{0.98}Zn_{0.02}]_3O_{7-\delta}$ with $x = 0.075$

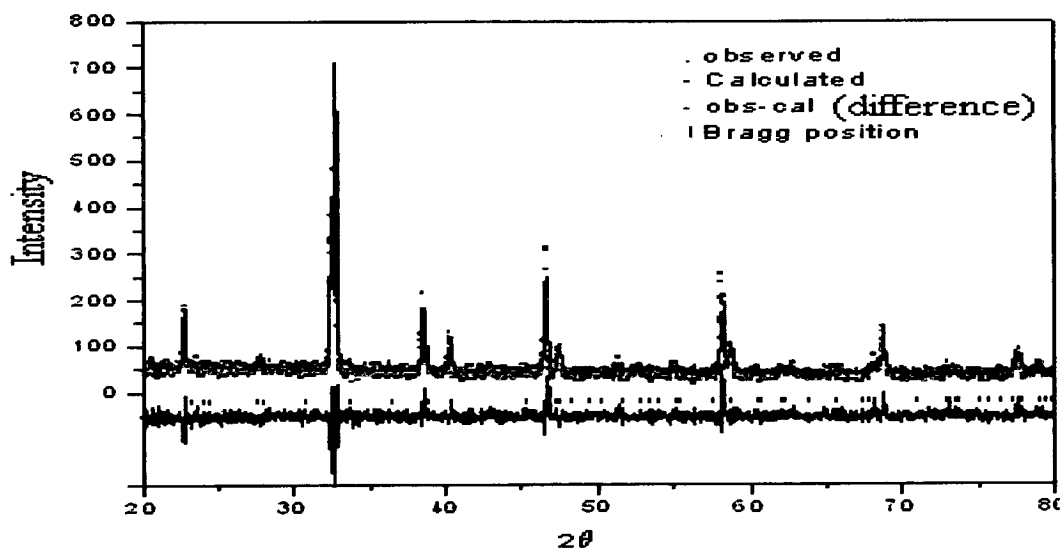


Fig.5.5.5 Rietveld refined diffraction patterns of $Y_{0.9-x}Pr_xCa_{0.1}Ba_2[Cu_{0.98}Zn_{0.02}]_3O_{7.5}$ with $x = 0.10$

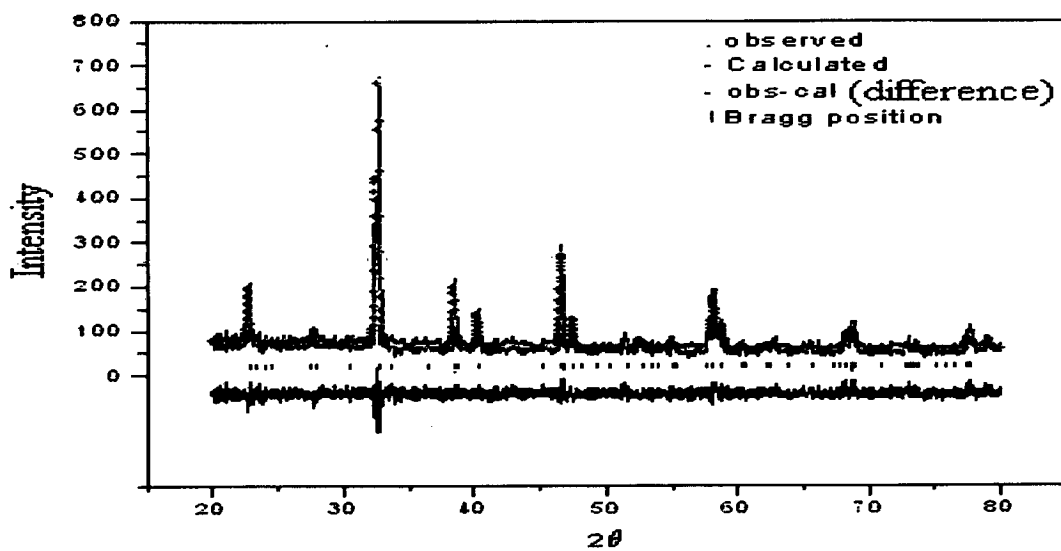


Fig.5.5.6 Rietveld refined diffraction patterns of $Y_{0.9-x}Pr_xCa_{0.1}Ba_2[Cu_{0.94}Zn_{0.06}]_3O_{7.8}$
with $x = 0.00$

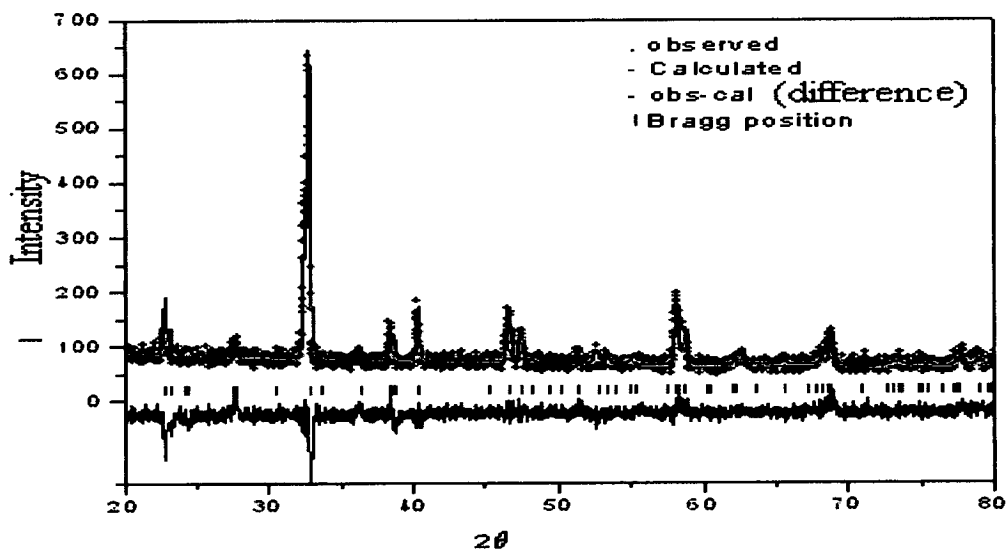


Fig .5.5.7 Rietveld refined diffraction patterns of $Y_{0.9-x}Pr_xCa_{0.1}Ba_2[Cu_{0.94}Zn_{0.06}]_3O_{7.8}$
with $x = 0.075$

5.5.2 Electrical Resistivity

The electrical resistivity measurements were carried out using four probe method in the temperature range 14-300 K. The plots of resistivity versus temperature are given in Figs.5.5.8 - 5.5.9 . The critical temperatures T_c are given in Tables 5.5.1 - 5.5.2 for Zn content $y = 0.02$ and 0.06 . Because of the strong hole density (p) dependence of various non-superconducting and superconducting properties it is important to determine p as accurately as possible. We have estimated p from the room-temperature thermopower, $S[290K]$ using the correlation of Orbetelli et al [61], expressed numerically [61(a)] $S(290K) = 992 \exp(-38.1p) \mu V/K$. These values of p are given in Table 5.5.3 and Table 5.5.4 together with the values of thermopower with errors .

Normal pseudogap has been earlier studied by Naquib -et-al [61- 66] for Ca and Zn doped $YBa_2Cu_3O_{7-\delta}$ (Y123) Compounds. The pseudogap characteristic temperature is T^* . In normal pseudogap state it was established by these workers that T^* decreases linearly as the doping level p increases and goes to zero at $p = 0.19$. This is a universal behaviour, observed in underdoped and optimally doped samples. It was later observed [67] that for Ca based overdoped samples an anomalous behaviour of T^* appeared abruptly in which T^* showed very little or no p dependence.

We have done similar study in which we use Pr substitution along with Ca and Zn. Pr substitutes at the Y site and is responsible for forming a narrow band called FR band near the Fermi energy [68].This band grabs holes from the p-d band in the plane resulting in T_c reduction [69]. As stated earlier in Chapter 4 there are three regions in terms of Pr concentration x . For $0 < x < 0.1$ the system is in the

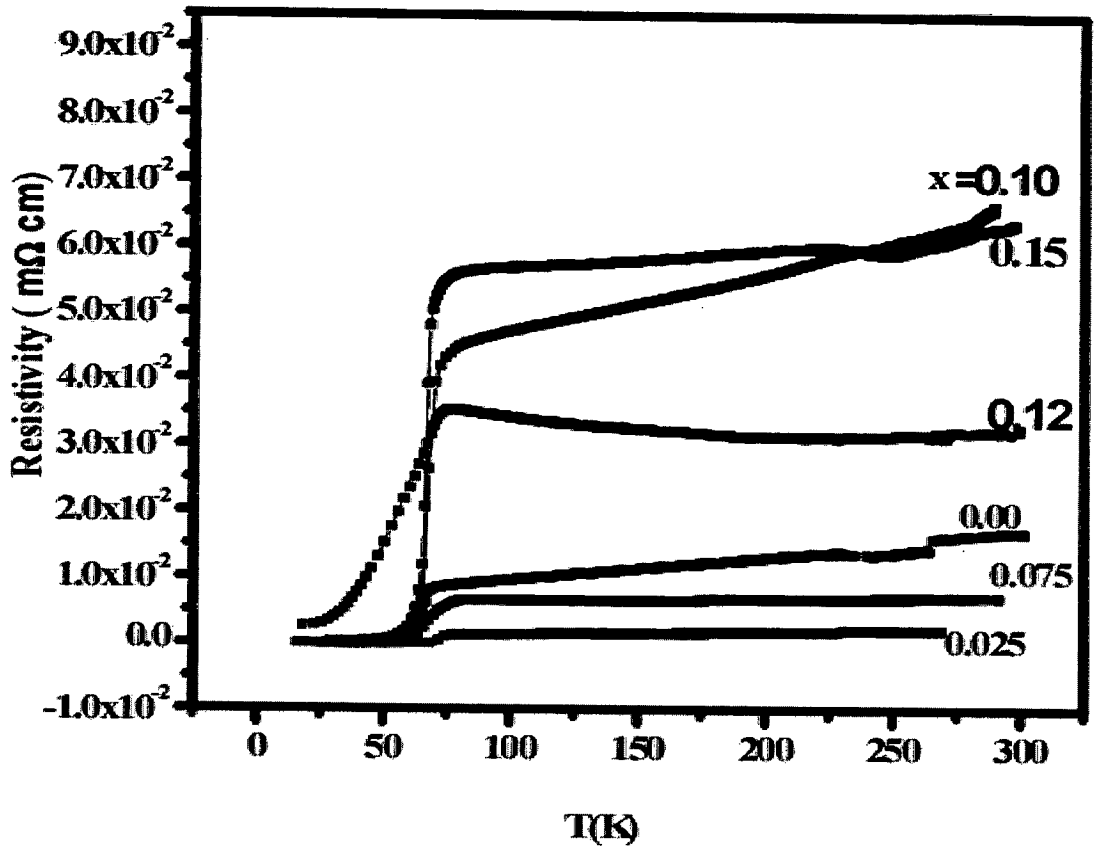


Fig.5.5.8 Resistivity vs temperature curve for $Y_{0.9-x}Pr_xCa_{0.1}Ba_2[Cu_{1-y}Zn_y]_3O_{7-8}$ samples with different values of Zn concentration and $y = 0.02$

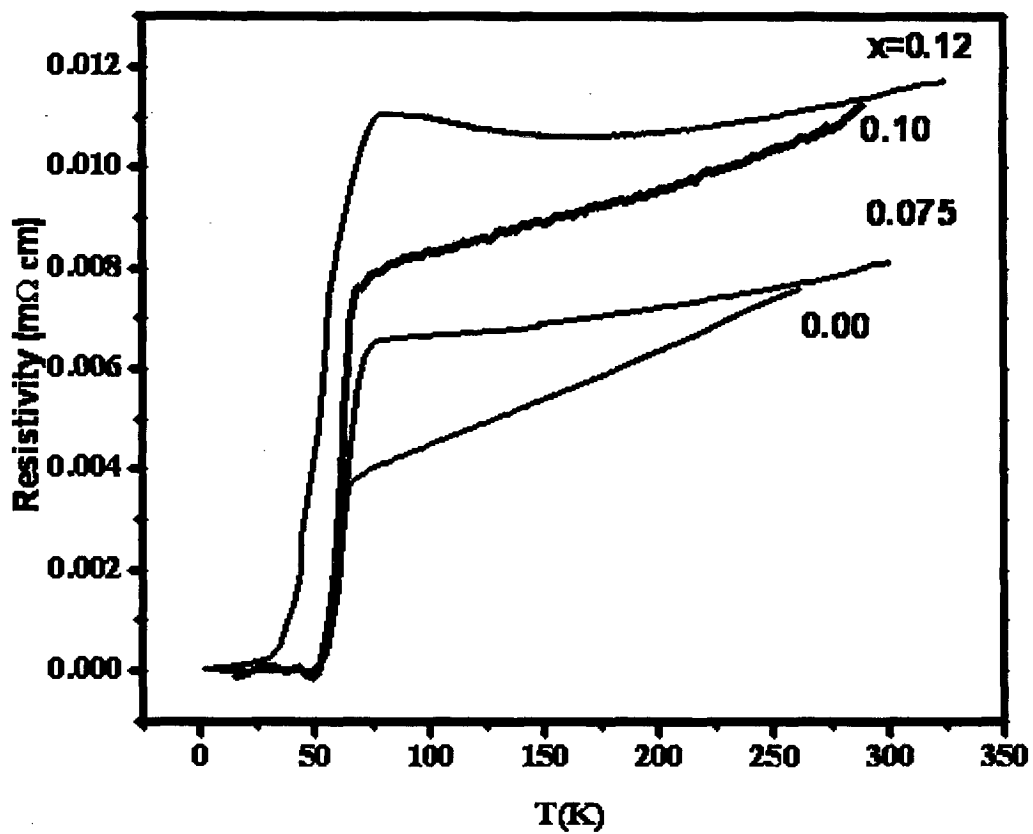


Fig. 5.5.9 Resistivity vs temperature curve for $Y_{0.9-x}Pr_xCa_{0.1}Ba_2[Cu_{1-y}Zn_y]_3O_{7-\delta}$ samples with different values of Pr concentration and $y=0.06$

vicinity of overdoped to underdoped state and T_c as a function of x decreases very slowly. For $0.1 < x < 0.5$ the main process is hole depletion and T_c decreases faste . For $x > 0.5$ there is additional process of magnetic pair breaking and T_c goes to zero rapidly. So to study the underdoped region we have put Ca content zero and for $x = 0.1$ and 0.2 . Zn content is varied . For the overdoped region we put Ca=0.1 and Pr contents are varied from 0 to 0.12 for two values of Zn content 0.02 and 0.06. The doping level p is determined accurately using the thermopower data at 290K, as mentioned above.

5.5.3 Relation between T^* and m with p

As is standard practice [70,71] , the characteristic pseudogap temperature $T^*(p)$ is obtained from the temperature at which downturn in the $\rho(T)$ curve appears. The other method to obtained T^* is from the plots of $d\rho(T)/dT$, this plot gives a more general measure for $T^*(p)$, which is characterized by an increase in the slope of $\rho(T)$ in the vicinity of T^* . We have used both these methods to find T^* values. The values of T^* obtained from these methods are very close to each other. The method of extraction of T^* values from $\rho -T$ and $d\rho(T)/dT$ vs T plots are presented in Fig.5.5.10 for one of the values of the sample with $x = 0.075$ and $y = 0.06$. The values given in Tables 5.5.3 -5. 5.4 are from $\rho -T$ plot. the values of T^* given in these tables are determined when the downturn in $\rho -T$ curve ends and upturn just begins. We have also determined the value of pseudogap temperature T^* in the compounds $YBa_2(Cu_{1-x}Zn_x)_3O_{7-\delta}$, where y varies from 0 to 10 % . Our values agrees with those of Naquib et al [67] and Walker et al [67(a)]. We have therefore not included the values of T^* in the present work. The planar hole concentration p is obtained from the thermopower room temperature data as mentioned above. The results are plotted in

Fig.5.5.11 for the underdoped case and in Fig.5.5.12 for the overdoped case. In the underdoped case $x = 0.1$ and $x = 0.2$ the system is in the hole depletion region and p is varied by increasing Zn concentration as shown in Table 5.5.3. Here it may be noted that Zn acts as pinning the holes in the plane and opposes the action of Pr in removing the holes. Consequently p increases as Zn concentration increases. Fig 5.5.11(a),(b) shows normal pseudogap behaviour i.e. T^* decreases linearly with increasing p . For the overdoped case we have set $y = 0.02$ and $y = 0.06$ and x is varied as shown in Table 5.5.4 and Fig.5.5.12(a),(b). For $y = 0.02$, T^* shows normal behaviour. However, at $y = 0.06$, T^* remains almost constant and is independent of p . Just for comparison we have shown results from Naquib et al [70] in Fig 5.5.12(b) which agree well with our results. These researchers have observed that for overdoped cuprates, the pseudogap temperature show almost no p dependence over a wide range of hole contents extending from the optimally doped to the overdoped regions and that the magnitude of this anomalous $T^*(p)$ depends only on the amount of Zn in the CuO_2 planes.

The abrupt appearance of this anomalous pseudogap-like feature in resistivity as a function of disorder content is indicative of some sort of threshold mechanism in action, consistent with some recent theoretical studies carried out by Bucher et al [72]. For example, in the study by Monthoux [73] it was shown that as quasiparticle lifetime becomes shorter (with increasing scattering by spin fluctuations), it starts to feel long-range magnetic order even when only short-range correlations are present. It is known that [72,73] the quasiparticle mean-free path relative to the correlation length of the short-range antiferromagnetic order determines the size of the pseudogap. As the quasiparticle lifetime decreases with Zn, it is possible that at a certain level of Zn in the CuO_2 plane the scattering rate becomes high enough to

dominate over the more gradual p-dependent scattering. Using the Hubbard model, it was shown that a high scattering rate leads to the removal of low-energy spectral weight [74]. In this scenario the local Coulomb repulsion U becomes an important parameter. Heavy Zn substitution increases the scattering rate, localizes quasiparticles, and effectively enhance U/t (where t is the nearest neighbor hopping energy) globally. Once $U > 8t$ the pseudogap becomes insensitive to U and therefore, shows no significant p dependence [74]. This indicate that the origin of this pseudogap -like feature is in plane disorder.

Following Naquib et al [62] and Takagi et al [75] we have also determined the p dependence of the exponent m , in the fits to the equation $\rho(T) = \rho_o + aT^m$ in our compound. One of such fits of of $Y_{0.9-x}Pr_xCa_{0.1}Ba_2[Cu_{1-y}Zn_y]_3O_{7-\delta}$ for $x = 0.075$ and $y = 0.06$ is shown in Fig 5.5.13. The values of m obtained from these fits are given in Table 5.5.4. In order to see better non-linear dependence of ρ on T , we have also plotted $\ln(\rho - \rho_0)$ versus $\ln T$ in Fig 5.5.13(a). This figure shows better nonlinear dependence of ρ on T than the Fig 5.5.13. Since both T^* and m are measures of the deviation of $\rho(T)$ from linearity, we have plotted T^* and m versus p in Fig 5.5.14. In the same figure we have plotted T_c versus p . This entire plot (Fig.5.5.14) represents an HTS T-P Phase diagram. It is very interesting to find that T^* and m versus p curves cross each other at $p = 0.185 \pm 0.01$ above T_c resembling the existence of system in non-Fermi liquid state It shows the universal behaviour that is with increase in p , T^* decreases whereas m increases with value lower than 2 which is the canonical low-T Fermi liquid value with dominant electron-electron scattering.

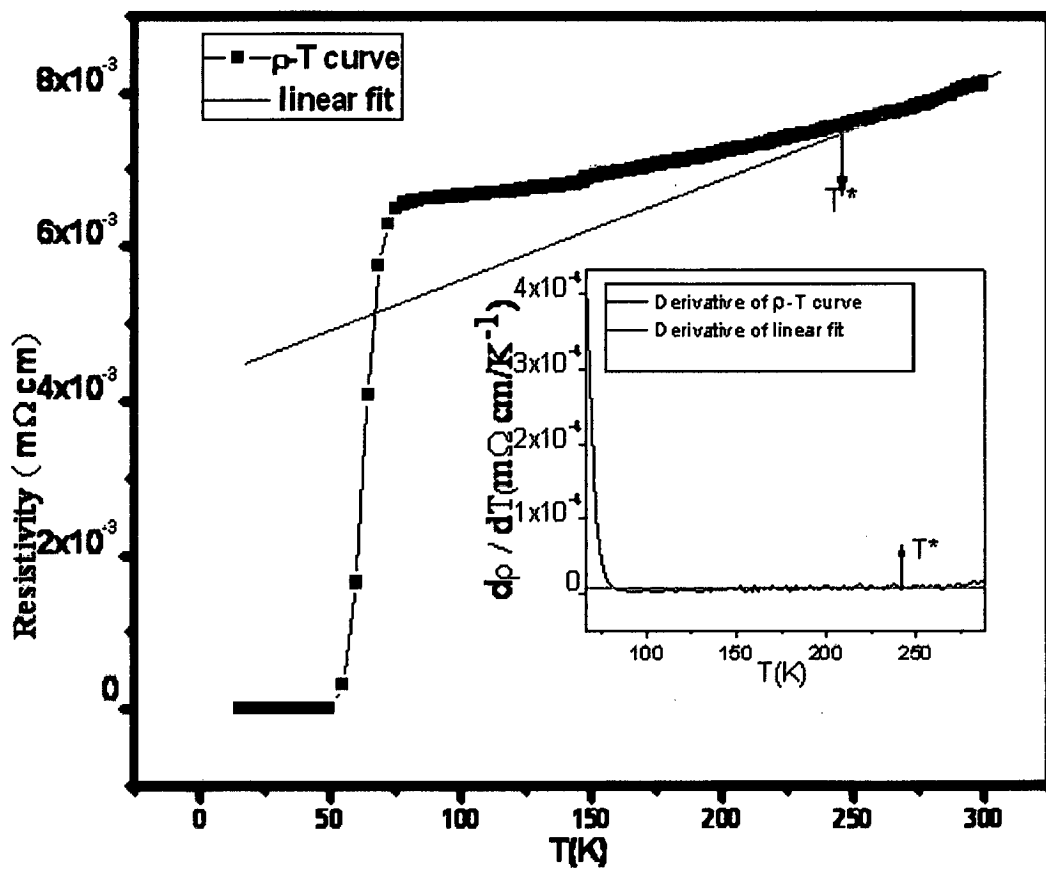


Fig .5.5.10 Methods used for determining T^* of $Y_{0.9-x}Pr_xCa_{0.1}Ba_2[Cu_{1-y}Zn_y]_3O_{7-8}$ for $x = 0.075$ and $y = 0.06$

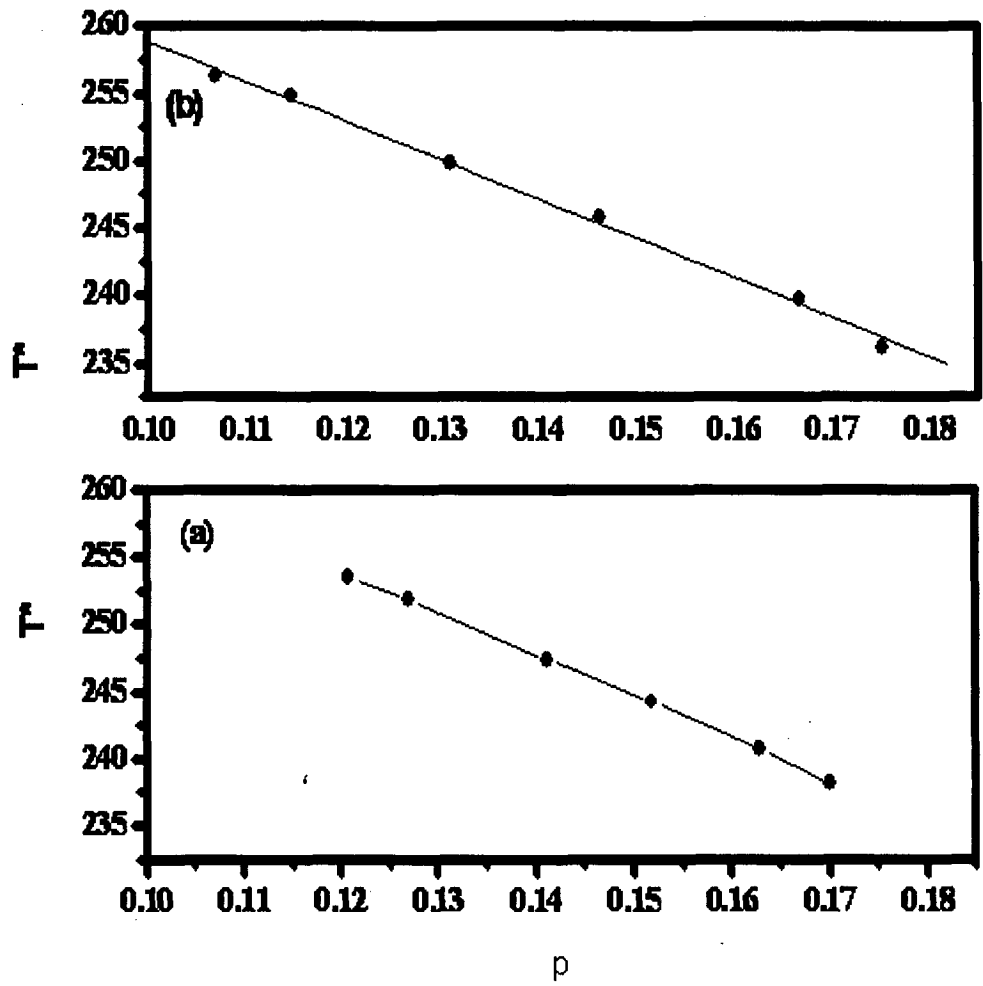


Fig .5.5.11 Plots of T^* against p for $Y_{1-x}Pr_xBa_2(Cu_{1-y}Zn_y)_3O_{7.8}$ samples with $Ca=0$ and for different values of y (a) $x=0.1$, (b) $x=0.2$.

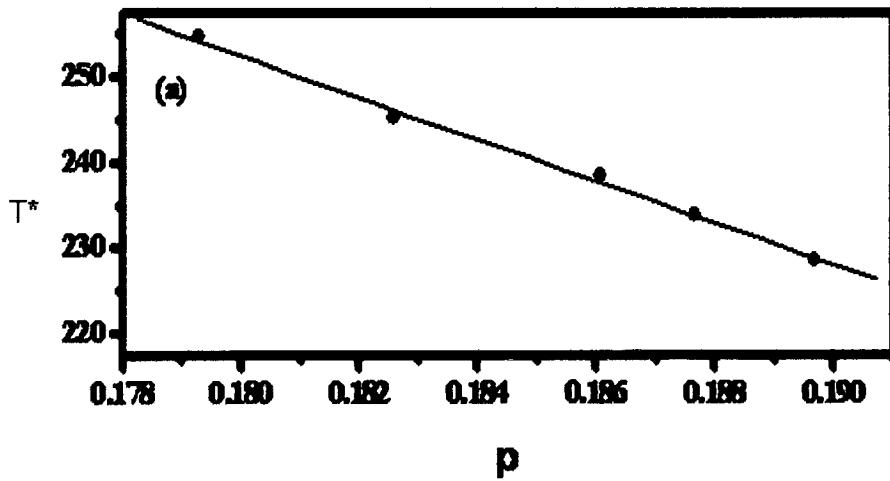
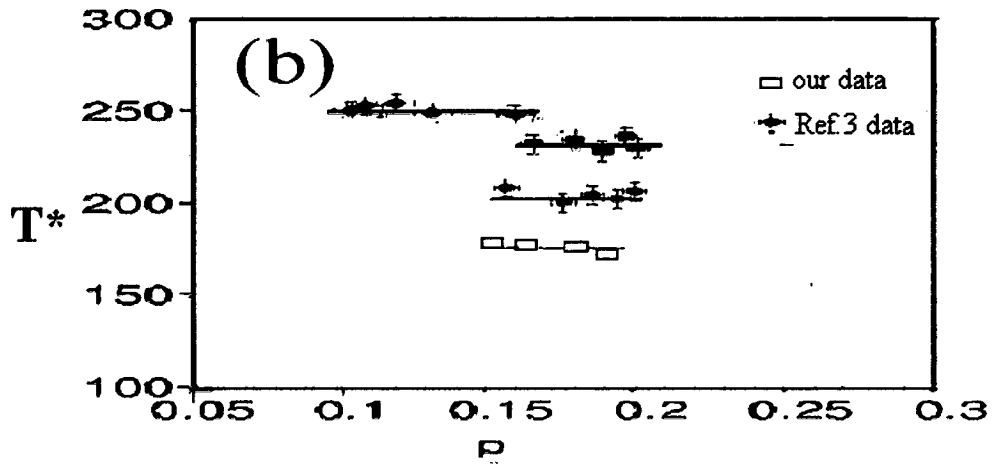


Fig 5.5.12. Plots of T^* against p for $Y_{0.9-x}Pr_xCa_{0.1}Ba_2(Cu_{1-y}Zn_y)_3O_{7.5}$ samples for $y = 0.02$ in Fig(a) and $y = 0.06$ in Fig(b) for varying from 0.00 to 0.15 . Here in Fig (b) data from Naquib et al (Ref.63) is reproduced for comparison.

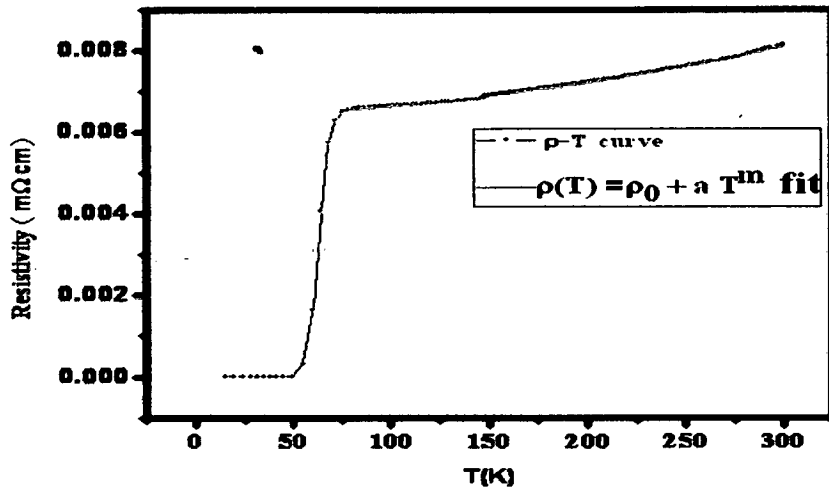


Fig.5.5.13 Plot of resistivity vs T of $Y_{0.9-x}Pr_xCa_{0.1}Ba_2(Cu_{1-y}Zn_y)_3O_{7.8}$ with $x = 0.075$ and $y = 0.06$ showing extraction of m .

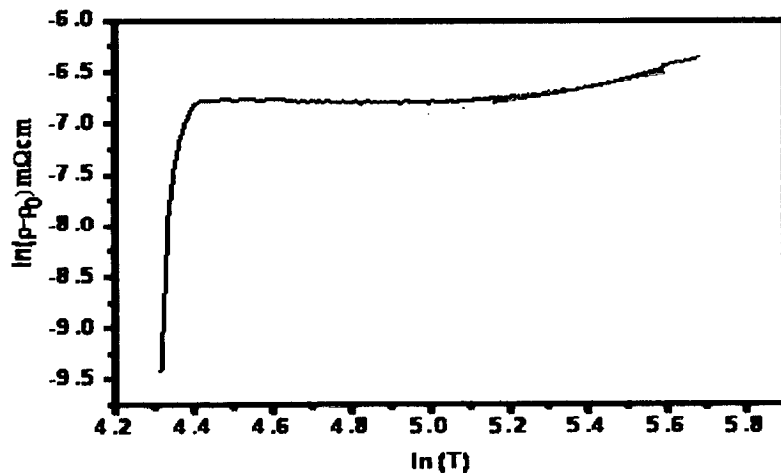


Fig.5.5.13(a) Plot of $\ln(\rho - \rho_0)$ vs $\ln(T)$ of $Y_{0.9-x}Pr_xCa_{0.1}Ba_2(Cu_{1-y}Zn_y)_3O_{7.8}$ with $x = 0.075$ and $y = 0.06$ showing extraction of m .

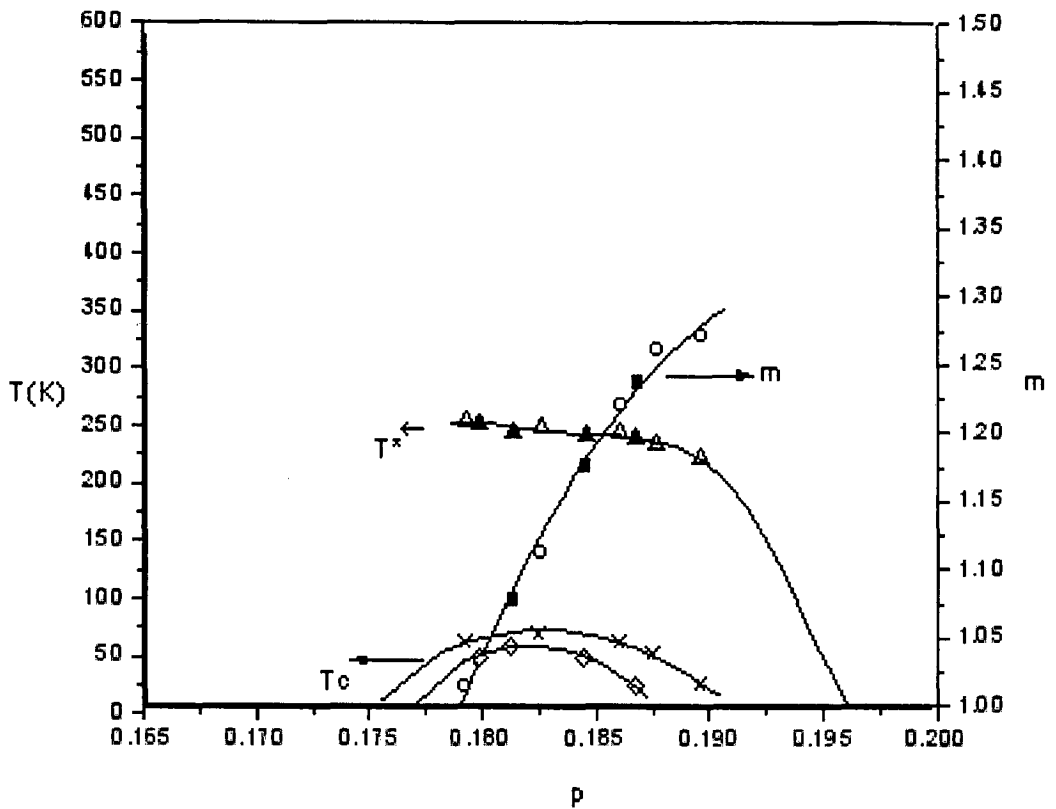


Fig .5.5.14 Phase diagram of $Y_{0.9-x}Pr_xCa_{0.1}Ba_2(Cu_{1-y}Zn_y)_3O_{7-\delta}$

(T^* , m T_c)

O – m vs p for $y=0.02$ and different values of x

■ - m vs p for $y=0.06$ and different values of x

Δ - T^* vs p for $y=0.02$ and different values of x

\blacktriangle - T^* vs p for $y=0.06$ and different values of x

\times - T_c vs p for $y=0.02$ and different values of x

\diamond - T_c vs p for $y=0.06$ and different values of x

Table 5.5.3: The values of T_c , T^* , S and p for the underdoped system $Y_{1-x}Pr_xBa_2(Cu_{1-y}Zn_y)_3O_{7.8}$ for different values of Zn and $x=0.1$, $x = 0.2$.

Concentration of Zn (y)	T_c K ± 1.00 K	$T^*(K)$ ± 2.00 K	$S(290K)$ $(\mu V/K)$	p holes/plane
(a) x = 0.1				
0.00	77.05	253.52	9.87 \pm 0.02	0.121 \pm 0.001
0.01	61.78	251.85	7.85 \pm 0.02	0.127 \pm 0.001
0.03	26.10	247.40	4.60 \pm 0.01	0.141 \pm 0.002
0.06	19.49	244.29	3.21 \pm 0.02	0.152 \pm 0.003
0.08	13.16	240.73	1.54 \pm 0.03	0.163 \pm 0.002
0.10	-	238.18	1.53 \pm 0.02	0.170 \pm 0.001
(b) x = 0.2				
0.00	37.08	256.3	16.82 \pm 0.06	0.107 \pm 0.003
0.002	31.99	254.86	12.40 \pm 0.05	0.115 \pm 0.001
0.005	29.40	249.85	6.74 \pm 0.02	0.131 \pm 0.002
0.01	15.96	245.73	3.81 \pm 0.03	0.146 \pm 0.003
0.03	-	239.77	1.71 \pm 0.04	0.167 \pm 0.002
0.06	-	236.06	1.26 \pm 0.03	0.175 \pm 0.002

Table 5.5.4: Shows the values of T_c , T^* , S and p for the overdoped system

$Y_{1-x}Pr_xCa_{0.1}Ba_2(Cu_{1-y}Zn_y)_3O_{7-\delta}$ for different values of Zn and for Table (a)

$y = 0.02$ and Table (b) $x = 0.06$

Concentration of Pr (x)	T_c K ± 1.00 K	$T^*(K)$ ± 2.00 K	$S(290K)$ ($\mu V/K$)	p (holes/plane)	m
(a) y = 0.02					
0	57.9	254.56	1.08 ± 0.02	0.179 ± 0.002	1.01 ± 0.09
0.025	67.43	250.13	0.97 ± 0.03	0.182 ± 0.003	1.11 ± 0.08
0.075	58.67	243.33	0.83 ± 0.02	0.186 ± 0.002	1.22 ± 0.09
0.1	49.45	233.79	0.78 ± 0.04	0.188 ± 0.001	1.26 ± 0.02
0.12	22.66	221.58	0.77 ± 0.05	0.190 ± 0.002	1.27 ± 0.01
(b) y = 0.06					
0	46.05	256.78	1.04 ± 0.05	0.180 ± 0.003	1.03 ± 0.02
0.075	55.43	243.73	1.00 ± 0.03	0.181 ± 0.001	1.07 ± 0.01
0.1	44.66	249.64	0.86 ± 0.01	0.185 ± 0.002	1.17 ± 0.09
0.12	20.79	253.54	0.80 ± 0.02	0.187 ± 0.001	1.23 ± 0.10

refer to Figs 5.8

5.6 Conclusion

We have carried out measurements on electrical Resistivity of sintered samples of composition $Y_{0.9-x}Pr_xCa_{0.1}Ba_2 [Cu_{1-y}Zn_y]_3O_{7-\delta}$. This technique is a very useful tool as with this single technique we could get the information regarding the characteristic pseudogap temperature T^* . The hole concentrations are found from room temperature thermopower measurement. We have used Pr to obtain the underdoped region while Pr with Ca was used to obtain the overdoped region. We find that for underdoped compound T^* increases with decrease in p thereby showing normal pseudogap. However, for overdoped compound which is attained by doping Ca at higher values of Zn content ($y = 0.06$), T^* remains almost constant showing anomalous pseudogap. Thus our results corroborate the earlier findings of Naquib et al and hence the theoretical explanation given by various researchers can still hold good.

Using the values of T_c , T^* and m we construct the phase diagram following the procedure of Naquib et al .A crossover between T^* and m is obtained at which $p = 0.185 \pm 0.01$ resembling that the system is still in the non-Fermi liquid state. This is in contrast to the findings of by Naquib et al [70]. Phase diagram constructed by these researchers indicates that at $p = 0.19 \pm 0.01$, the pseudogap vanishes and it is a special point called quantum critical point where $\rho(T)$ remains linear in non superconducting state as $T \rightarrow 0$ K.

Our X-ray diffraction studies of $Y_{0.9-x}Pr_xCa_{0.1}Ba_2 [Cu_{1-y}Zn_y]_3O_{7-\delta}$ show that the crystal system is orthorhombic with little or no variation of lattice parameters. The present study contradicts the XRD results obtained by Awana et al. This is because in our study, three dopants are present Pr, Ca,Zn whereas that of Awana et al [4]has only one dopants.viz. Ca . Since Zn localizes the holes in CuO_2 plane as can be seen from

the z parameter for Cu and Zn of Table 5.5.1 and Table 5.5.2, the system retains its orthorhombic crystal structure.

Reference

1. M.W. Shafer, T. Penny and B.L. Olson, Phys. Rev. B **36** , 40474(1987).
2. J. B. Goodenough and A. Manthiram, J. Solid State Chem. **88**,115(1990).
3. J. M. Tarascon, L. H. Greene, W.R. Mckinnon, G. W. Hull,and T. H. Geballe, Science,**235**,1373(1987).
4. V. P. S .Awana, S. K. Agarwal , M. P. Das and A. V. Narlikar , J. Phys Cond.Matter **4**,4971(1992).
5. Hunabo Zhang and Hirasho Sato, Phys. Rev. Lett..**60**,1697 (1993).
6. V.P.S. Awana and A.V. Narlikar Phys. Rev. Lett. **71**, 303(1993).
7. H. Ding et al .Phys Rev. Lett.**74**, 2784 (1995); Z. X. Shen et al. Phys. Rev. Lett. **70** , 1553 (1993).
8. P. chaudhari and S. Y. Lin, Phys. Rev. Lett. **72**, 1084 (1994); D. A. Wollman et al . Phys. Rev. Lett.. **71** , 2134(1993);I.I. Mazin et al. Phys. Rev. Lett..**75**, 2574 (1995).
9. M. Gurvich and A. T. Fiory , Phys. Rev. Lett. **59** ,1337(1987).
10. S. Martin , A. T. Fiory, R. M. Fleming , L.F. Schneemeyer and J. V. Waszczak Phys. Rev. B **41**,846(1990).
11. T. W Jing, N. P. Ong, T. V. Ramkrishnan, J. M. Tarascon and K. Remsching , Phys. Rev. Lett. **67**,761(1991).
12. N.W. Preyer, M.A. Kastner, C. Y. Chen, R. J. Birgeneau and Y. Hidaka, Phys. Rev. B**44**, 407(1991).
13. Y. Ando G.S. Boebinger, A. Passner, T. Kimuraand K. Kishio, Phys. Rev. Lett. **75**, 4662 (1995).
14. J. M. Tarascon, P. Barboux, P. F. Miceli, L. H. Greene, G. W.Hull, M. Eibschutz, and S. A. Sunshine, Phys. Rev. B **37**, 7458,(1988).

15. K. Westerholt, H. J. Wuller, H. Bach, and P. Stauche, *Phys. Rev. B* **39**, 11 680 (1989).
16. Y. Xu, R. Sabatini, A. R. Moodenbaugh, Yi. Zhu, S.-G. Shyu, M. Suenaga, K. W. Dennis, and R. W. McCallum, *Physica C* **169**, 205 (1990).
17. R. Liang, M. Itoh, T. Nakamura, and R. Aoki, *Physica C* **157**, 83 (1989).
18. V. E. Gasumyants, V. I. Kaidanov, and E. V. Vladimirkaya, *Chin. J. Phys.* **31**, 999 (1993).
19. A. Tokiwa, Y. Syono, M. Kikuchi, R. Suzuki, T. Kajitani, N. Kobayashi, T. Sasaki, O. Nakatsu, and Y. Muto, *Jpn. J. Appl. Phys., Part 2* **27**, L1009 (1988).
20. Z. Jirak, J. Hejtmanek, E. Pollert, A. Triska, and P. Vasek, *Physica C* **156**, 750 (1988).
21. M. R. Chandrahod, I. S. Mulla, S. M. Gorwadkar, and A. P. Sinha, *Appl. Phys. Lett.* **56**, 183 (1990).
22. C. Greaves and P. R. Slater, *Supercond. Sci. Technol* **2**, 5 (1989).
23. A. Manthiram and J. B. Goodenough, *Physica C* **159**, 760 (1989).
24. B. Fisher, G. Genissar, C. G. Kuper, L. Patlagan, G. M. Reisner and A. Knizhnik, *Phys. Rev. B* **47**, 6054 (1993).
25. R. G. Buckley, D. M. Pook, J. L. Tallon, M. R. Presland, N. E. Flower, M. P. Staines, H. L. Johnson, M. Meylan, G. V. M. Williams, and M. Wovden, *Physica C* **174**, 383 (1991).
26. J. L. Tallon, N. E. Flower, *Physica C*, **204**, 237 (1993).
27. Kiyotaka Matura, Takihiro Wada, Yuji Yakaeshi, S. Tajima and H. Yamauchi, *Phys. Rev. B* **46**, 11923 (1992).
28. V. P. S. Awana and A. V. Narlikar *Phys. Rev. B* **49**, 6353 (1994).
29. G. Bottger, H. Schwer, E. Kaldis and K. Bente, *Physica C*, **275**, 198 (1997).
30. Yunhui Xu and Weiyan Guan, *Phys. Rev. B* **45**, 3176 (1992).

31. Weiyuan Guan, Yunhui Xu, S. R. Sheen, Y. C. Chen, J. Y. T. Wei, H. F. Lai, and M. K. Wu, *Phys. Rev. B* **49**, 15993 (1994); Weiyuan Guan, Y. C. Chen, J. Y. T. Wei, Y. H. Xu, and M. K. Wu, *Physica C* **209**, 19 (1993).
32. Y. Chen, T. S. Lai, M. K. Wu, and Weiyuan Guan, *J. Appl. Phys.* **78**, 5212 (1995).
33. J. C. Chen, Y. H. Xu, M. K. Wu, and Weiyuan Guan, *Phys. Rev. B* **53**, 5839 (1996).
34. S. K. Malik, C. V. Tomy, and P. Bhargava, *Phys. Rev. B* **44**, 7042(1991).
35. Weiyuan Guan, J. C. Chen, S. H. Cheng, and Y. H. Xu, *Phys. Rev. B* **54**, 6758 (1996); Weiyuan Guan, J. C. Chen, and S. H. Cheng, *ibid.* **54**, 3580 (1996).
36. Yunhui Xu and Weiyuan Guan, *Physica C* **212**, 119 (1993); Yunhui Xu, Weiyuan Guan, Y. F. Chen, S. R. Shen, and M. K. Wu, *Phys. Rev. B* **50**, 1223 (1994); Yunhui Xu, Weiyuan Guan, S. S. Ata-Allah, and Ch. Heiden, *Physica C* **235-240**, 823 (1994).
37. L. Soderholm, K. Zhang, D. G. Hinks, M. A. Beno, J. D. Jorgensen, C. U. Segre, and I. K. Schuller, *Nature* **328**, 604 (1987).
38. H. B. Rodousky, *J. Mater. Res.* **7**, 1918 (1992), and references therein; B. Maple, B.W. Lee, J. J. Neumeier, G. Nieva, L. M. Paulius, C. L. Seaman, *J. Alloys Compd.* **181**, 135 (1992).
39. J. Neumeier, M. B. Maple, and M. S. Torikachvili, *Physica C* **156**, 574 (1990).
40. G. Xiao and N. S. Rebbello, *Physica C* **211**, 433(1993).
41. H. Yakabe, J. G. Wen, Y. Shiohara, and N. Koshizuka, *Physica C* **244**, 256 (1995).
42. E. Surd, A. Maignan, V. Caignaert, and B. Raveau, *Physica C* **200**, 43 (1992).
43. M. G. Smith, J. Chan, and J. B. Goodenough, *Physica C* **208**, 412(1993).
44. J. J. Neumeier, T. Bjornholm, M. B. Maple, and I. K. Schuller, *Phys. Rev. Lett.* **63**, 2516 (1989).

45. B. Fisher, J. Genossar, C. G. Kuper, L. Patlagan, G. M. Reisner, and A. Knizhnik, Phys. Rev. B **47**, 6054 (1993).
46. R. J. Cava, B. Batlogg, S. A. Sunshine, T. Siegrist, R. M. Fleming, K. Rabe, L. F. Schneemeyer, O. W. Murphy, R. B. VanDover, P. K. Gallagher, S. H. Glarum, S. Nakahara, R. C. Farrow, J. J. Krajewski, S. M. Zahurak, J. V. Waszczak, J. H. Marshall, P. Marsh, L. W. Rupp, Jr., W. F. Peck, and E. A. Rietman, Physica C **153-155**, 560(1988).
47. Li-Chun Tung, J. C. Chen, M. K. Wu, and Weiyan Guan Phys. Rev. B **59**,4504(1999).
48. B. Batlogg, C. Varma, Phys. World **13** , 33 (2000).
49. T. Timusk, B. Statt, Rep. Progr. Phys **62** ,61(1999).
50. J.W. Loram, K.A. Mirza, J.R. Cooper, W.Y. Liang, J.M.Wade, J. Supercond. **7** ,243,(1994).
51. V.B. Geshkenbein, L.B. Ioffe, A.I. Larkin, Phys. Rev. B **55**,3173 (1997).
52. V. Emery, S.A. Kivelson, O. Zachar, Phys. Rev. B **56**, 6120 (1997).
53. J. Maly, B. Janko, K. Levin, Phys. Rev. B **59** ,1354 (1999).
54. A.P. Kampf, J.R. Schrieffer, Phys. Rev. B **42** , 7967 (1990).
55. M. Langer, J. Schmalian, S. Grabowski, K.H. Bennemann, Phys. Rev. Lett. **75**, 4508 (1995).
56. J.J. Deisz, D.W. Hess, J.W. Serene, Phys. Rev. Lett. **76**,1312 (1996).
57. J. Schmalian, D. Pines, B. Stojkovic, Phys. Rev. Lett. **80**, 3839 (1998); A.V. Chubkov, D. Pines, J. Schmalian, cond-mat/0201140.
58. J.L. Tallon, J.W. Loram, G.V.M. Williams, J.R. Cooper, I.R. Fisher, J.D. Johnson, M.P. Staines, C. Bernhard, Phys. Status. Solidi. (B) **215** , 531 (1999).
59. C.M. Varma, Phys. Rev. Lett. **83**, 3538 (1999).
60. C. Castellani, C. Di Castro, M. Grilli, Z. Phys. B **103**,137 (1997).

61. S.D. Obertelli, J.R. Cooper, and J.L. Tallon, Phys. Rev. B **46**,14928 (1992).
- 61(a) S.H. Naquib , R.A. Chakalav ,J.R.Cooper,Physica C **407**,73 (2008).
62. S.H. Naquib, J.R. Cooper, J.L. Tallon , C. Panagopoulos Physica C **387**,365 (2003).
63. J. L. Tallon, J. R. Cooper, P. S. I. P. N. de Silva, G. V. M. Williams, and J. W. Loram, Phys. Rev. Lett. **75**, 4114 (1995).
64. K. Mizuhashi, K. Takenaka, Y. Fukuzumi, S. Uchida, Phys. Rev. B **52**, 3884 (1995).
65. H. Alloul, P. Mendels, H. Casalta, J.F. Marucco, J. Arabski, Phys. Rev. Lett. **67**, 3140 (1991).
66. S.H. Naquib, J.R. Cooper, J.L. Tallon, R.S. Islam, R.A. Chakalov , Phys. Rev. B **71**, 054502 ,(2005).
67. S.H. Naquib, J.R. Cooper, J.L. Tallon, R.S. Islam, Phys. Rev. B **71**, 184510 ,(2005)
- 67(a) D.J.C. walker ,A.P. Mackenzie, and J.R. Cooper Phys Rev. B **51**, 15653, (1995)
68. J.L. Tallon and J.W. Loram, Physica C , **349**, 53, (2001).
69. F. R. Fehrenbacher and T. M. Rice, Phys. Rev. Lett. **70**, 3471 (1993).
70. S. H. Naqib, J. R. Cooper, J. L. Tallon, R. S. Islam, and R. A. Chakalov, Phys. Rev. B **71**, 054502 (2005).
71. T. Timusk and B. Statt, Rep. Prog. Phys. **62**, 61 (1999).
72. B. Bucher, P. Steiner, J. Karpinski, E. Kaldis, and P. Wachter, Phys. Rev. Lett. **70**, 2012 (1993).
73. P. Monthoux Phys. Rev. B **68**, 064408 (2003).
74. David Senechal and M. S. Tremblay, cond-mat 0308625 (2004).
75. H. Takagi, b. Batlogg, H.L. Kwo, R.J. cava, J.J. Krajewski, W. F. Peck, Phys. Rev. Lett. **69**, 2975, (1992)

Chapter 6
Summary and Conclusions

6.1 Summary

High- T_c cuprate superconductors are remarkable materials as various strongly correlated electronic ground states are uncovered with increasing the doped hole concentration, (p), in the CuO_2 planes and a nearly parabolic $T_c(p)$ dome is realized in the doping range $0.05 < p < 0.27$ for most of the cuprate families. Over most of the regions of the T - p phase diagram the normal state charge transport and magnetic properties are anomalous in the sense that canonical Fermi-liquid like behavior is only observed in the deeply overdoped region. Besides superconductivity itself, pseudogap and stripe correlations are probably the two of the most widely investigated phenomena. The pseudogap correlation is detected in the T - p phase diagram over a certain doping range, extending from the underdoped to the slightly overdoped regions. In the pseudogap region a number of anomalies are observed both in normal and superconducting states. It is widely believed that understanding the physics of pseudogap is one of the outstanding obstacles in the path of unlocking the mystery of cuprate superconductivity. Considerable debate has ensued as to the nature of the pseudogap and no consequences has been reached yet. On the other hand the charge stripe correlations are only observed in the underdoped cuprates. Some of the existing theoretical models link the origins of both superconductivity and pseudogap to the stripe correlations. It is extremely important to clarify the interplay among these different correlations in order to develop a coherent picture describing the physics of high T_c cuprates.

Among the high- T_c oxide superconductors, the $\text{YBa}_2\text{Cu}_3\text{O}_{7-\delta}$ system has been well studied with regard to structural as well as the physical properties. In the pure $\text{RBa}_2\text{Cu}_3\text{O}_{7-\delta}$ ($R = \text{rare earth}$) system, T_c remains unchanged for all R ions irrespective of their magnetic moments except for $R = \text{Pr}$. However, substitution at the

Cu site by 3d metal ions has a considerable effect on T_c , since the CuO_2 planes are responsible for superconductivity and any substitution at this site suppresses T_c , independent of whether the substituent ion is magnetic or nonmagnetic. Substitutional studies in the $\text{RBa}_2\text{Cu}_{3-x}\text{M}_x\text{O}_7$ ($\text{M} = \text{Fe}, \text{Ni}, \text{Zn}$) system have shown an increase in the solid solubility limits (x) as well as the T_c suppression rates. A similar R ion dependence has been observed in other systems. This has been attributed to the decrease in the spatial extension of the 4f orbitals of the R ion with decrease in the ionic radius. It appears, therefore, that simultaneous substitution of a rare earth ion at the Y site and 3d metal ion at the Cu site modifies the nature of interaction of the 4f orbitals of the R ion with the CuO_2 planes. In the present study, we have carried out systematic substitutional studies on $\text{Y}_{0.9-x}\text{Pr}_x\text{Ca}_x[\text{Cu}_{1-y}\text{Zn}_y]\text{O}_{7-\delta}$ with the following objectives:

- (i) to study the pinning effect which arises due to Zn doping at Cu planar site,
- (ii) to investigate the effect of hole concentration on T_c due to Pr substitution at Y site and
- (iii) to study the pseudogap effect as a consequence of Ca substitution in Pr and Zn doped $\text{YBa}_2\text{Cu}_3\text{O}_{7-\delta}$.

This thesis is divided into six Chapters. Chapter 1 reviews the most important properties of the superconductors, which are essential to understand the structural and electrical properties of the cuprate superconductors studied in this work. Furthermore, it gives a brief account of the state of art knowledge of the high temperature superconductors along with some of the applications related to superconductors. At the end of this Chapter, the scope of present study has been attributed.

In Chapter 2, the experimental techniques used for the investigations carried out in this work are described. The experimental setup and procedure for carrying out

measurements on electrical resistivity, oxygen contents and thermopower are discussed together with the method of preparation of compounds and recording of X-ray diffraction patterns.

In Chapter 3, a detailed crystal structure of $\text{YBa}_2\text{Cu}_3\text{O}_{7-\delta}$ has been described along with general consideration of substitutions at cation sites. Later on effect of Zn doping at Cu(2) site in Y123 system and its structural properties have been discussed on the basis of literature available hitherto. Rietveld analysis of the X-ray diffraction pattern of Zn doped Y123 system with $0 \leq \text{Zn} \leq 0.10$ has been carried out. From these analysis it is found that Zn substitution at Cu(2) site do not affect the orthorhombic structure of parent Y123 system. The results of iodometric titration show that the oxygen content remain invariant thereby confirming the orthorhombicity of the system. From the electrical resistivity measurements superconducting transition temperature, residual resistivity, and resistivity slope have been obtained. It is seen that the transition temperature decreases with increase in Zn content. The resistivity slope increases to a maxima and then decreases. The suppression of T_c with increase in Zn content is attributed to the pinning of dynamically fluctuating stripe phase by impurity scattering based on the assumption that Zn does not change charge carrier density.

The suppression of T_c due to depletion of concentration of mobile holes can be achieved by substituting Pr in Y123 system. In Chapter 4 we present our study on Y123 doped with Pr at Y site and Zn at Cu site, former increases the holes and later localizes these holes in the CuO_2 plane. We have found through the Rietveld analysis of X ray diffraction data that such substitution does not change the orthorhombic symmetry of the system as found in Zn doped Y123 above. The lattice parameters a , and b do not change much. However, c parameter is slightly

affected thereby slightly affecting the $O(4)$ parameter which is responsible for retaining the orthorhombicity of the system. The iodometric measurements suggest that the oxygen content remains invariant as the Pr concentration is increased. As the oxygen content remains unaltered it was interesting to know why there is a reduction in T_c . We, therefore performed the electrical resistivity measurements on these compounds in the temperature range 10-300K. From these measurements, the transition temperature, residual resistivity and the resistivity slope corresponding to linear part of resistivity –temperature curve have been determined. It is that for $x=0.1$ Pr has a minimal influence on the in-plane processes for Zn impurity alone. and that T_c and ρ_0 are slightly affected. The resistivity slope becomes larger for the region for which Zn concentration (y) lies between 0.03 and 0.06 thereby suggesting larger depinning effect and hence slower fall of T_c . However, when the Pr content is increased to 0.2 a drastic change observed in the residual resistivity becoming abnormally large and resistivity slope becomes negative. This implies that the absence of depinning and a totally pinned charge stripes. It is inferred that when Pr content (x) is increased from 0.1 to 0.2 the hole depletion is in full swing. It is concluded that due to the hole depletion process Pr is able to bring the system in the underdoped region so that a small percentage of Zn is able to induce a superconductor –insulator transition. This can be seen by plotting the unitarity line which lies below $y = 0.01$ which suggest that above this line the system goes to insulating state. It is interesting to mention here that, Fukuzumi et al have obtained such situation for Zn impurity by controlling the oxygen content in Y-123 system. We have shown that it is easier to obtain the same results by doping Pr at Y-site since one can control the charge carrier density easily using the hole depletion mechanism.

Another remarkable phenomenon in the field of high T_c cuprate superconductors is the observation of the pseudogap in substituted Y123 and related system. The pseudogap is detected over a certain range of planar hole concentration p i.e. the number of holes in the plane, extending from the underdoped to slightly overdoped state. Chapter 5 deals with the study of this kind of pseudogap. In this study we have prepared Y123 system doped with Ca together with Pr and Zn. Rietveld analysis on X-ray diffraction patterns of these materials shows that when 0.1 Ca is doped in addition to Zn and Pr in Y123, system shows orthorhombicity. This may be due to the presence of Zn which localizes the holes thereby slightly affecting the z parameter for Cu and Zn. Electrical resistivity measurements on such three dopant Y123 were performed for determination of the transition temperature T_c , characteristic pseudogap temperature T^* and the value of exponent m in the fit to resistivity equation, $\rho(T) = \rho_o + aT^m$, where a is constant. Besides, the hole concentration is determined from room temperature thermopower measurements. For underdoped system in absence of Ca, we find that T^* decreases with increasing hole concentration and system shows normal pseudogap effect. This behaviour is also observed in overdoped case when Ca is added and Zn content is kept at 0.02. However, when Zn concentration is increased to 0.06 T^* shows no p dependence taking the system to anomalous pseudogap state. The abrupt appearance of this anomalous pseudogap like feature in resistivity as a function of disorder content is indicative of some sort of threshold mechanism in action consistent with some recent theoretical studies dealing with quasiparticles coupled to spin or charge fluctuations. In this situation the local Coulomb repulsion U becomes important parameter. Higher Zn substitution increases the scattering rate, localises the holes and effectively enhances U/t (where t is the nearest neighbour hopping energy). Once $U > 8t$, the

pseudogap becomes insensitive to U and therefore, shows no p dependence. Using T^* , m and T_c we have constructed a HTS phase diagram. We find a crossover between T^* and m well above T_c at $p = 0.185 \pm 0.01$ indicating that the system is still in the non-Fermi liquid. This is in contrast to the observation made by some of the authors on Zn and Ca doped Y123 system. The finding of these authors that the doping level $p = 0.19 \pm 0.01$ is special and could possibly be a quantum critical point in the sense that a transition between two different states takes place at zero temperature at this doping level. The difference in the results of our work and the work of these researchers may be because of simultaneous presence of Pr and Ca at Y site and Zn at Cu(2) site in Y123 system.

Chapter 6 summarises work carried out in the present study and gives scope for future work on such type of systems.

6.2 Suggestions for Future Work

Today, the investigation of the normal state involves a wide variety of electrical, magnetic, and optical studies. Ironically enough, it is the appearance of superconductivity itself at high temperatures which inhibits a proper study of the normal state down to sufficiently low temperatures. Therefore, it is of interest to study the normal-state properties of the materials. Moreover, systematic studies of the normal-state properties as a function of doping may reveal some interesting insights concerning the evolution of the exotic metallic state from the antiferromagnetic insulating state.

Many experimental techniques have been used to probe the normal state properties of the materials. One such technique is angle resolved photoelectron spectroscopy (ARPES). It is a probe sensitive to the energy and momentum of the

filled electron energy states below the Fermi surface and has been used recently to a great effect in understanding the pseudogap phenomenon . It provides insight into the evolution of pseudogap across T_c and its affect on the spin and charge degrees of freedom. Such study on our system can thus help us in probing the further details of normal state properties

There is a general consensus that the hole states play pivotal role for superconductivity in the p-type cuprate superconductors. Therefore, an understanding of the unoccupied electronic states near the Fermi level of cuprate superconductors is a crucial step toward unveiling the mechanism of superconductivity. X-ray absorption near edge studies (XANES) of O *K* edge using synchrotron radiation has been widely applied to probe the unoccupied states in materials and molecules. In particular, polarization-dependent X-ray absorption measurements are able to provide detailed information about the orbital character of hole states in the p-type cuprates. It would be therefore interesting to study O *K* edge XANES in our Y123 system doped with Ca, Pr and Zn in order to get information about unoccupied electronic states near the Fermi level of these materials. This kind of study will also throw some light on the origin of the ionic size effect.

List Of Publications

1. Normal and Anomalous Pseudogap of Superconducting $Y_{0.9-x}Pr_xCa_{0.1}Ba_2[Cu_{1-y}Zn_y]_3O_{7-\delta}$
M.S.Naik, P.R.Sarode, R.B.Prabhu and K.R.Priolkar
Published online in Journal of Superconductivity and Novel Magnetism on 5th May 2009.
2. Codoping Effect of Pr and Zn on $YBa_2Cu_3O_{7-\delta}$ System
M.S.Naik, P.R.Sarode, R.B.Prabhu, K.R.Priolkar and N.Y.Vasanthacharya
Acta Physica Polonica A, Vol115, 742,(2009)
3. Relationship Between Hole Concentration and Pseudogap Temperature in $YBa_2Cu_3O_{7-\delta}$ System
M.S.Naik, P.R.Sarode, R.B.Prabhu and K.R.Priolkar,
Accepted for Publication in Journal of Low Temperature Physics.
4. Substitutional Effect of Pr and Zn on $YBa_2Cu_3O_{7-\delta}$ System
M.S.Naik, P.R.Sarode, R.B.Prabhu, K.R.Priolkar and N.Y.Vasanthacharya,
Accepted for Publication in Modern Physics Letters B.
5. Phase Diagram of Underdoped and Overdoped $YBa_2Cu_3O_{7-\delta}$ System
M.S.Naik, P.R.Sarode, R.B.Prabhu and K.R.Priolkar
Accepted for Publication in International Journal of Modern Physics B
6. Effect of Zn impurity on Y123
Miskil S.Naik, P.R.Sarode, K.R. Priolkar, R.B. Prabhu, N. Y. Vasantacharya,
and N.P.Lalla
Presented at National Conference on Thermophysical Properties Organized by
Physics Department, Goa University ,Goa in Association with Thermophysical
Society of India during January 20-22, 2004.

Appendix

(Published Papers)

Normal and Anomalous Pseudogap of Superconducting $Y_{0.9-x}Pr_xCa_{0.1}Ba_2[Cu_{1-y}Zn_y]_3O_{7-\delta}$

Miskil S. Naik · K.R. Priolkar · P.R. Sarode · R.B. Prabhu

Received: 29 December 2008 / Accepted: 14 April 2009 / Published online: 5 May 2009
© Springer Science+Business Media, LLC 2009

Abstract Electrical resistivity measurements on the superconducting oxides of the compositions $Y_{0.9-x}Pr_xCa_{0.1}Ba_2[Cu_{1-y}Zn_y]_3O_{7-\delta}$ ($0 \leq x \leq 0.20$ and $0.0 \leq y \leq 0.10$) sintered in oxygen atmosphere were carried out to obtain the normal and anomalous pseudogaps in underdoped and overdoped samples. It is observed that pseudogap temperature T^* decreases with increasing doping level p in the underdoped case. For the overdoped sample with $y = 0.06$, T^* shows no p dependence.

Keywords Superconducting oxides · Pseudogap · Resistivity

PACS 74.62Bf · 74.62Dh · 74.72Bk

1 Introduction

Normal pseudogap has been studied by Naquib et al. [1, 2] in Ca and Zn doped $YBa_2Cu_3O_{7-\delta}$ (Y123) compounds. The T^* is the characteristic temperature above which the resistivity curve takes the upturn. It has been established that [1, 2], T^* decreases linearly as the doping level p increases. This is a universal behavior observed in underdoped and optimally doped samples. It was later observed [3] that for Ca-based overdoped samples, an anomalous behavior of T^* appeared abruptly, showing very little or no p dependence.

In this paper we report our electrical resistivity measurements in under- and overdoped samples of Y123. For this

purpose we use Pr substitution along with Ca. Pr substitutes at the Y site and is responsible for forming a narrow band called Fehrenbacher and Rice (FR) band near the Fermi energy [4]. This band grabs holes from the $p-d$ band in the plane resulting in T_c reduction [5]. There are three regions in terms of Pr concentration x . For $0 < x < 0.1$ the system is in the vicinity of overdoped-to-underdoped state and T_c as a function of x decreases very slowly. For $0.1 < x < 0.5$ the main process is the hole depletion and T_c decreases faster. For $x > 0.5$ there is an additional process of magnetic pair breaking and T_c goes to zero rapidly. For the underdoped region, we have used Pr content, $x = 0.1$ and 0.2 , with various Zn contents and Ca content zero. For the overdoped region, we put Ca = 0.1 and x is varied for two values of Zn content, namely, 0.02 and 0.06. As shown in the results, these two combinations, i.e. of Pr and Ca, lead to the overdoped region. The doping level p is determined accurately using the room temperature (290 K) thermopower data.

2 Experimental Details

The polycrystalline samples with composition of $Y_{0.9-x}Pr_xCa_{0.1}Ba_2[Cu_{1-y}Zn_y]_3O_{7-\delta}$ with different values of x and y ($0 \leq x \leq 0.20$ and $0.0 \leq y \leq 0.10$) were prepared by solid-state reaction method. The ingredients, Y_2O_3 , $CaCO_3$, $BaCO_3$, CuO , ZnO , Pr_6O_{11} of purity 99.99% in the stoichiometric ratio, were thoroughly mixed, grounded and calcined at 920 °C in air for a period of 20–24 h. After four intermediate grindings and calcinations in air the precursors so obtained were reground and pressed into pellets, and sintered in oxygen for 24 h at 940 °C, and then furnace-cooled to below 100 °C with an intervening annealing for 24 h at 600 °C [6]. The samples were then characterized by X-ray diffraction (XRD) using a Rigaku X-ray diffractometer with CuK_{α}

M.S. Naik (✉) · K.R. Priolkar · P.R. Sarode · R.B. Prabhu
Department of Physics, Goa University, Taleigao Plateau,
Goa 403206, India
e-mail: miskilko@rediffmail.com

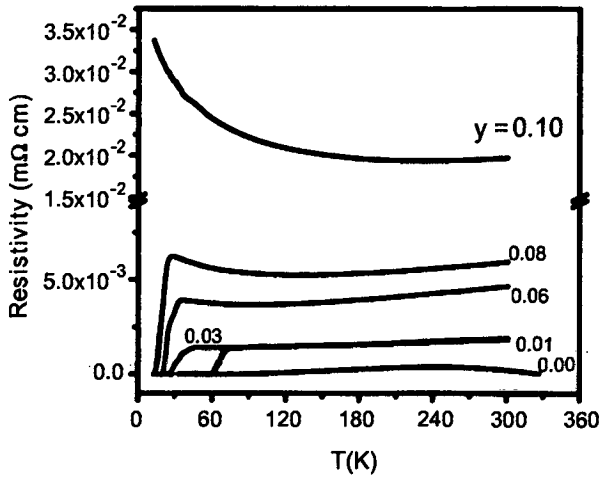


Fig. 1 Resistivity vs. temperature plots for $Y_{1-x}Pr_xBa_2(Cu_{1-y}Zn_y)_3O_{7-\delta}$ samples with $x = 0.10$ and different values of Zn concentration (y)

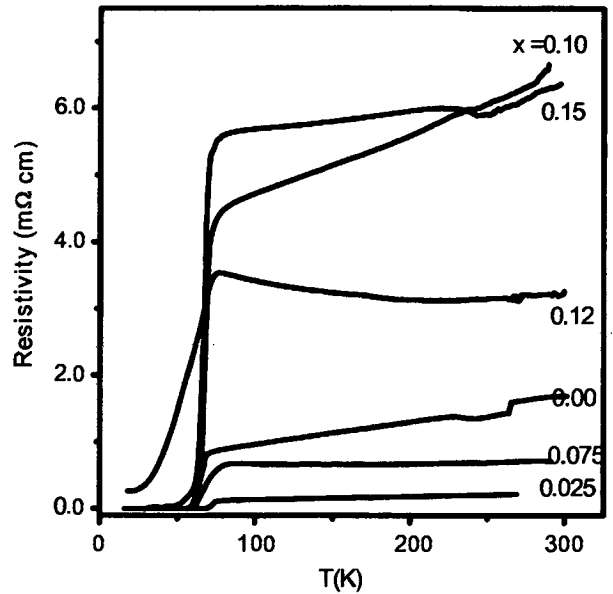


Fig. 3 Resistivity vs. temperature plots of $Y_{0.9-x}Pr_xCa_{0.1}Ba_2(Cu_{1-y}Zn_y)_3O_{7-\delta}$, with $y = 0.02$ and different values of Pr concentration (x)

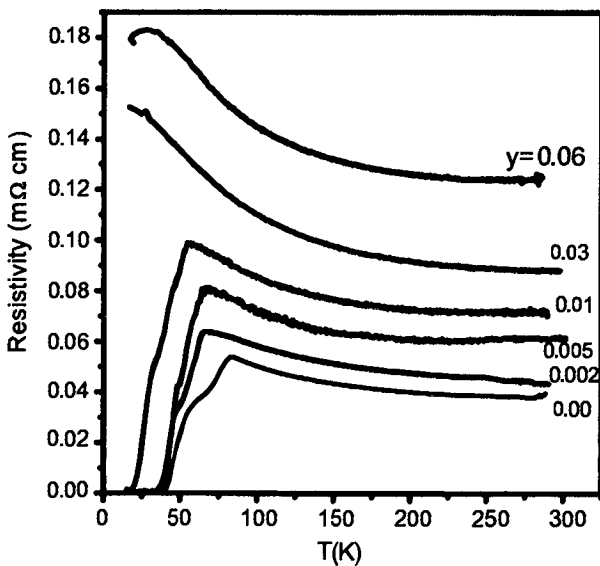


Fig. 2 Resistivity vs. temperature plots for $Y_{1-x}Pr_xBa_2(Cu_{1-y}Zn_y)_3O_{7-\delta}$ samples with $x = 0.20$ and different values of Zn concentration (y)

Table 1 Experimental data on T_c , T^* and p for the underdoped system $Y_{1-x}Pr_xBa_2(Cu_{1-y}Zn_y)_3O_{7-\delta}$ for different values of Zn and $x = 0.1, 0.2$

Concentration of Zn (y)	T_c (K)	T^*	p
(a) $x = 0.1$			
0.00	77	253.52	0.12071
0.01	62	251.85	0.12685
0.03	26	247.40	0.1411
0.06	19	244.29	0.15178
0.08	13	240.73	0.16278
0.10	–	238.18	0.16991
(b) $x = 0.2$			
0.00	37.08	256.3	0.1068
0.002	31.99	254.86	0.11462
0.005	29.4	249.85	0.13107
0.01	15.96	245.73	0.14627
0.03	–	239.77	0.16666
0.06	–	236.06	0.17508

3 Results and Discussion

Figures 1 and 2 represent the resistivity (ρ) vs. T plots for underdoped samples and Figs. 3 and 4 represent resistivity vs. temperature plots for overdoped samples. In Fig. 4(b) we show the ρ vs. T curve taken from Ref. [3] (Naquib et al.) for comparison. We find that the trend in curves 4(a) and 4(b) is almost similar suggesting thereby the constancy of hole concentration. Following Naquib et al. [1] we have

radiation, and the phase purity of the samples was checked using Rietveld Analysis Program DBWS-9411. The structure for all the samples of the series is found to be orthorhombic. The electrical resistivity was measured using standard four-probe method employing silver point contact in the temperature range of 14–300 K using a close cycle refrigerator for temperature variation, as shown in Figs. 1, 2, 3 and 4. The oxygen content of the samples was determined by iodometric titration [7] which is found to be 6.7 ± 0.1 . The thermopower measurements were carried out at room temperature (290 K) in our laboratory.

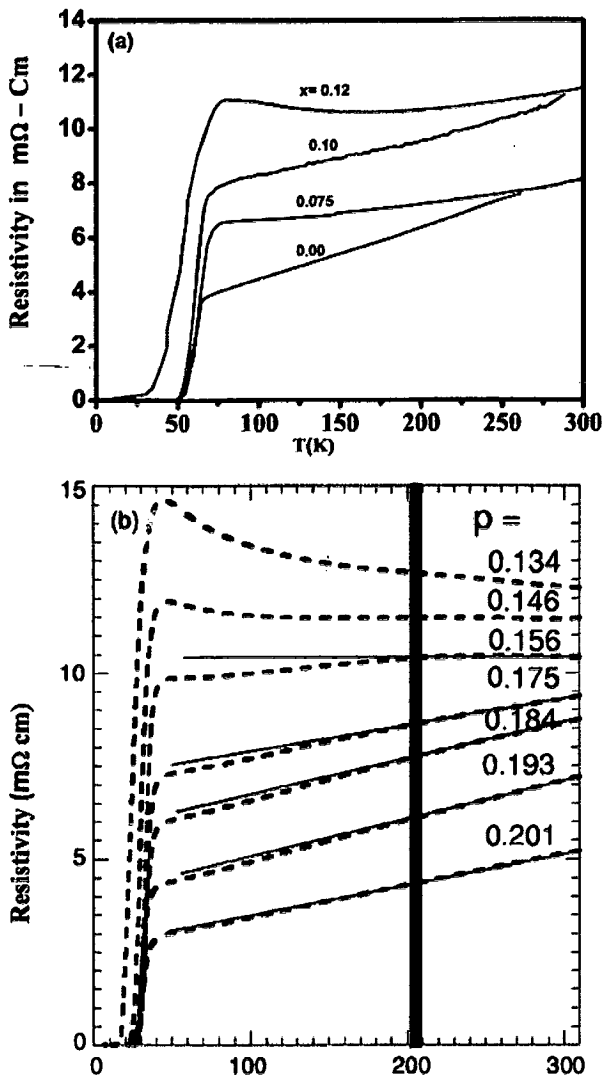


Fig. 4 (a) Resistivity–temperature curves for $Y_{0.9-x}Pr_xCa_{0.1}Ba_2(Cu_{1-y}Zn_y)_3O_{7-\delta}$ with $y = 0.06$ and different values of Pr content (x). (b) Resistivity–temperature curves for sintered $Y_{0.80}Ca_{0.20}Ba_2(Cu_{0.945}Zn_{0.55})_3O_{7-\delta}$ samples, after each oxygen annealing from Ref. [3] shown for comparison

determined T^* from $\rho-T$ at which upturn appears. The hole concentration, p , is obtained from the room temperature thermopower data. Plots of T^* vs. p for the underdoped and overdoped samples are given in Figs. 5 and 6. For the underdoped case at $x = 0.1$ and $x = 0.2$ the system is in the hole depletion region, and p is varied by increasing Zn concentration as shown in Table 1. Here it may be noted that Zn acts as pinning the holes in the plane and opposes the action of Pr in removing the holes. Consequently, p increases as Zn concentration increases, as can be seen from Fig. 5 (a) and (b). Zn is known to suppress T_c faster [8]. The resistivity measurements on the underdoped samples show normal pseudogap behavior, i.e. T^* decreases linearly with increas-

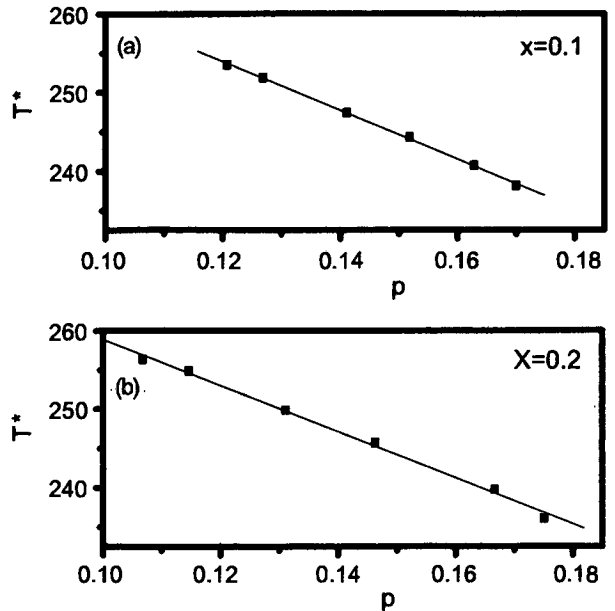


Fig. 5 Plots of T^* against p for $Y_{1-x}Pr_xBa_2(Cu_{1-y}Zn_y)_3O_{7-\delta}$ samples for $x = 0.1$ (a), and $x = 0.2$ (b), for y varying from 0.00 to 0.10

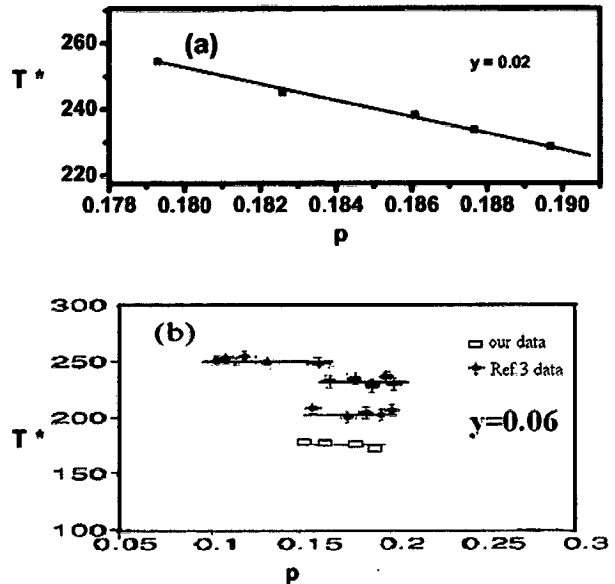


Fig. 6 Plots of T^* against p for $Y_{0.9-x}Pr_xCa_{0.1}Ba_2(Cu_{1-y}Zn_y)_3O_{7-\delta}$ samples for $y = 0.02$ (a), and $y = 0.06$ (b), for x varying from 0.00 to 0.15. Here in (b) the data from Naquib et al. (Ref. [3]) is reproduced for comparison

ing p (see Fig. 5 (a), (b)). For the overdoped case we have set $y = 0.02$ and $y = 0.06$, and x is varied and the measurements are summarized in Table 2, and the T^*-p curves are shown in Fig. 6 (a) and (b). For $y = 0.02$ concentration, T^* shows normal behavior. However, at $y = 0.06$ concentration, T^* remains almost constant and is independent

Table 2 Experimental data on T_c , T^* and p for $Y_{0.9-x}Pr_xCa_{0.1}Ba_2(Cu_{1-y}Zn_y)_3O_{7-\delta}$ with $y = 0.02, 0.06$ and different values of x

Concentration of Pr (x)	T_c (K)	T^*	p
(a) $y = 0.02$			
0	57.9	254.56	0.17928
0.025	67.43	245.13	0.18259
0.075	58.67	238.33	0.18608
0.1	49.45	233.79	0.18766
0.12	22.66	228.58	0.18968
(b) $y = 0.06$			
0	46.05	242.92	0.1799
0.075	55.43	243.73	0.18136
0.1	44.66	242.63	0.18456
0.12	20.79	21.54	0.18682

of p . This is the anomalous pseudogap. Just for comparison we have shown results from Naquib et al. (Ref. [3]) in Fig. 6(b), which agree well with our results. These authors showed that the anomalous behavior appears for $y \geq 0.05$. Our results thus corroborate the earlier results obtained by Naquib et al. [3] and hence the theoretical explanation given by these researchers [3] can still hold good.

Acknowledgements We are thankful to Prof. S.N. Bhatia, Department of Physics, Indian Institute of Technology, Mumbai and Dr. N.Y. Vasanthacharya, Solid State and Structural Chemistry Unit, Indian Institute of Science, Bangalore for providing us with the electrical measurement facility. We are also thankful to Department of Science and Technology, New Delhi and Council of Scientific and Industrial Research, New Delhi for financial support.

References

1. Naquib, S.H., Cooper, J.R., Tallon, J.L., Panagopoulos, C.: *Physica C* **387**, 365 (2003)
2. Naquib, S.H., Cooper, J.R., Tallon, J.L., Islam, R.S., Chakalov, R.A.: *Phys. Rev. B* **71**, 054502 (2005)
3. Naquib, S.H., Cooper, J.R., Tallon, J.L., Islam, R.S.: *Phys. Rev. B* **71**, 184510 (2005)
4. Tallon, J.L., Loram, J.W.: *Physica C* **349**, 53 (2001)
5. Fehrenbacher, R., Rice, T.M.: *Phys. Rev. Lett.* **70**, 3471 (1993)
6. Gupta, A.R., Lal, R., Sedky, A., Narlikar, A.V., Awana, V.P.S.: *Phys. Rev. B* **61**, 11752 (2000)
7. Harris, C.D., Hills, E.M., Hewston, A.T.: *J. Chem. Educ.* **64**, 847 (1987)
8. Narlikar, A.V., Rao, C.V., Agarwal, S.K.: In: Narlikar, A.V. (ed.) *High Temperature Superconductor*, vol. 1, p. 341. Nova Science, New York (1989)

Codoping Effect of Zn and Pr in $\text{YBa}_2\text{Cu}_3\text{O}_{7-\delta}$

M.S. NAIK, P.R. SARODE, R.B. PRABHU, K.R. PRIOLKAR

Department of Physics, Goa University, Taleigao Plateau, Goa 403 206, India

AND N.Y. VASANTHACHARYA

Solid State and Structural Chemistry Unit, Indian Institute of Science

Bangalore 560 012, India

(Received October 10, 2008; revised version December 12, 2008)

In this paper we present the resistivity data for Pr and Zn codoped compound $\text{Y}_{1-x}\text{Pr}_x\text{Ba}_2[\text{Cu}_{1-y}\text{Zn}_y]_3\text{O}_{7-\delta}$ with $0 < y < 0.1$ and $x = 0.0, 0.1$ and 0.2 . The data is analysed in terms of the superconducting critical temperature T_c , residual resistivity ρ_0 and the resistivity slope $d\rho/dT$ corresponding to the linear ρ - T region. It is found that for $x = 0.1$ Pr has a minimal influence on the in-plane processes for Zn impurity alone affecting slightly T_c and ρ_0 . The slope $d\rho/dT$ becomes larger for $0.03 < y < 0.06$ leading to larger depinning effect and hence slower fall of T_c as a function of y . For $x = 0.2$ there is a drastic change, ρ_0 becomes abnormally large, $d\rho/dT$ becomes negative implying absence of depinning and a totally pinned charge stripes. Superconductivity vanishes at $y = 0.03$. It is concluded that for $x = 0.2$ Pr converts the system from overdoped to underdoped region leading to the universal superconductor-insulator transition.

PACS numbers: 74.62.Bf, 74.62.Dh, 74.72.Bk

1. Introduction

Different impurities in cuprate superconductors degrade the critical temperature in different ways. In doing this they shed some light on the electronic state of the superconductor. The joint effect of two different impurities is not the same as the sum of the effects of individual impurities. In this work we report the effect of Pr and Zn in $\text{YBa}_2\text{Cu}_3\text{O}_{7-\delta}$ Y-123 system. It is known that Zn substitutes at Cu(II) [1-6] site in the CuO_2 plane. It is a non-magnetic impurity and degrades T_c by potential scattering [7-9] which results in pinning the charge stripe [10, 11]. Superconductivity vanishes at about ten percent of Zn. On the other hand, Pr substitutes the Y site and is responsible for forming a narrow band called Fehrenbacher and Rice (FR) band [12] near the Fermi energy. This band grabs holes from the p - d band in the plane resulting in T_c degradation [13]. There are three regions in terms of Pr concentration (x). For $0 < x < 0.1$ the system makes transition from overdoped to underdoped state and T_c as a function of x decreases very slowly. For $0.1 < x < 0.5$ the main process is hole depletion and T_c decreases faster. For $x > 0.5$ there is an additional process of magnetic pair breaking and T_c goes to zero rapidly. In this work we present resistivity versus temperature results for varying Zn concentration (y) for two values of Pr concentrations $x = 0.1$ and $x = 0.2$ and study the codoping effects in the two regions mentioned above. The data is analysed in terms of T_c , ρ_0 , $d\rho/dT$.

2. Experimental

The polycrystalline samples with composition of $\text{Y}_{1-x}\text{Pr}_x\text{Ba}_2[\text{Cu}_{1-y}\text{Zn}_y]_3\text{O}_{7-\delta}$ with different values of x

and y ($0 \leq x \leq 0.20$ and $0 \leq y \leq 0.10$) were prepared by solid-state reaction method. The ingredients, Y_2O_3 , BaCO_3 , CuO , ZnO , with/without Pr_6O_{11} of purity 99.99% taken in the stoichiometric ratio were thoroughly mixed, ground and calcined at 920°C in air for a period of 17-20 h. After four intermediate grindings and calcinations in air the precursors so obtained were reground and pressed to pellets, and sintered in oxygen for 24 h at 940°C and then furnace cooled to below 100°C with an intervening annealing for 24 h at 600°C [14]. The samples were characterised by X-ray diffraction (XRD) using $\text{Cu } K_\alpha$ radiation and the phase purity of the samples was checked using the Rietveld refinement. The structure for the entire series is found to be orthorhombic and X-ray diffraction patterns are presented in Fig. 1a-c. The oxygen content was determined by iodometric titration which is found to be 6.7 ± 0.1 [15]. The resistivity was measured in the temperature range 14-300 K, using standard four probe technique coupled with a close cycle refrigerator.

3. Results and discussion

Resistivity curve $\rho(T)$ for $x = 0, 0.1$, and 0.2 samples are presented respectively in Fig. 2a-c. One can see that for $x = 0$, T_c disappears at $y = 0.1$ but the linearity in the curve is retained. Whereas for $x = 0.1$, $\rho(T)$ curve shows non-linear behaviour at $y = 0.1$ and for $x = 0.2$ the non-linearity in $\rho(T)$ curve starts at $y = 0.03$. This behaviour of T_c for different concentration of Zn and Pr is presented in Fig. 3. The linear part of ρ - T curve is fitted to the equation $\rho = \rho_0 + \rho_1 T$. The intercept ρ_0 , called residual resistivity corresponds to the impurity scattering that leads to the pinning of charge stripe [14] and the slope ρ_1

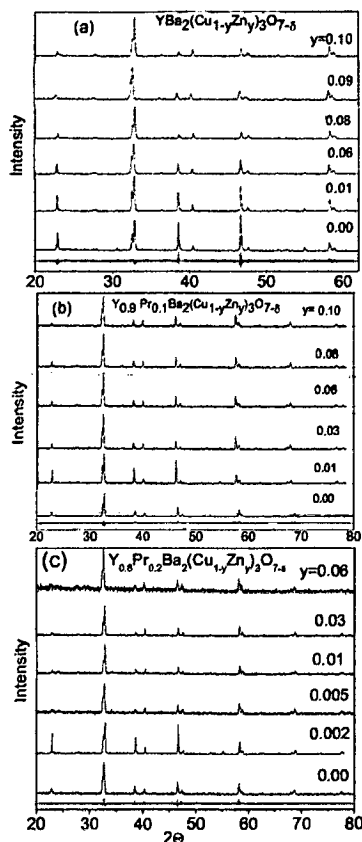


Fig. 1. X-ray diffraction patterns of $\text{Y}_{1-x}\text{Pr}_x\text{Ba}_2[\text{Cu}_{1-y}\text{Zn}_y]_3\text{O}_{7-\delta}$ (a) for $x = 0$, (b) for $x = 0.1$ and (c) for $x = 0.2$.

(i.e., $d\rho/dT$) of this linear part gives the carrier-carrier scattering. Figure 4 shows the behaviour of ρ_0 as function of y for only Zn and Zn plus Pr impurities. Figure 5 shows that $d\rho/dT$ for Zn and Zn plus Pr impurities. We analyse the data for $x = 0.1$ and $x = 0.2$ separately.

Figure 4a shows that for $x = 0.1$ Pr has a very small effect on ρ_0 and hence on pinning of charge stripes. For $x = 0.0$ Zn, $d\rho/dT$ in Fig. 5a, shows a rise up to $y = 0.03$ and then a fall, implying that there is no overall depinning effect which is seen in Fig. 3 which presents the T_c vs. y curve. T_c falls more or less uniformly as y increases. However when Pr is present, Fig. 5a shows that $d\rho/dT$ rises more sharply from $y = 0.02$ to $y = 0.06$. Then Fig. 4 shows that for this case T_c falls less rapidly with y in this region implying a depinning effect caused by Pr. The reason for this is that due to Pr substitution the holes start moving from their planar site to $4f$ band implying the starting of depinning of charge stripes.

For $x = 0.2$ the hole depletion process is in full swing and the system has made a transition to a new state. As shown in Fig. 3, T_c goes to zero at the Zn concentration

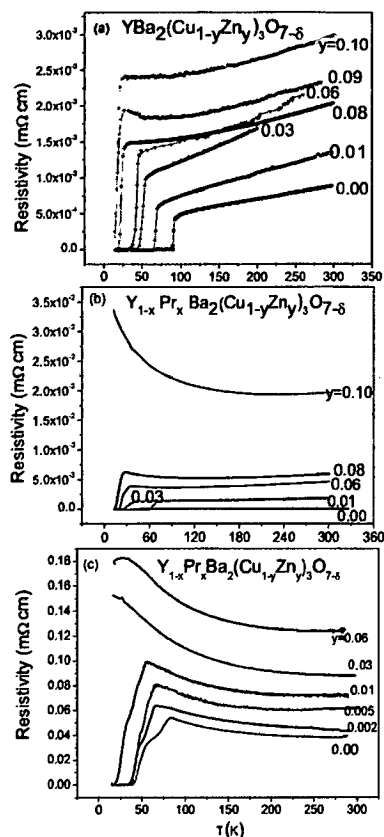


Fig. 2. Resistivity vs. temperature for $\text{Y}_{1-x}\text{Pr}_x\text{Ba}_2[\text{Cu}_{1-y}\text{Zn}_y]_3\text{O}_{7-\delta}$ samples with different values of Zn concentration: (a) for $x = 0$, (b) for $x = 0.1$ and (c) for $x = 0.2$.

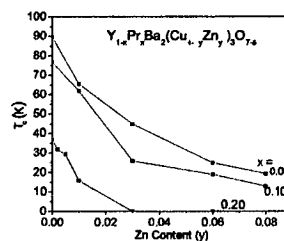


Fig. 3. Superconducting transition temperature T_c as a function of Zn content y for $\text{Y}_{1-x}\text{Pr}_x\text{Ba}_2[\text{Cu}_{1-y}\text{Zn}_y]_3\text{O}_{7-\delta}$ samples with $x = 0, 0.10, 0.20$.

$y = 0.03$ and superconductivity is destroyed. Figure 4b shows that ρ_0 becomes large and Fig. 5b shows that $d\rho/dT$ becomes negative. This implies absence of depinning and a completely pinned charge stripe. It seems that the system has made a transition to underdoped stage and that just three percent of Zn has made ρ_0 large

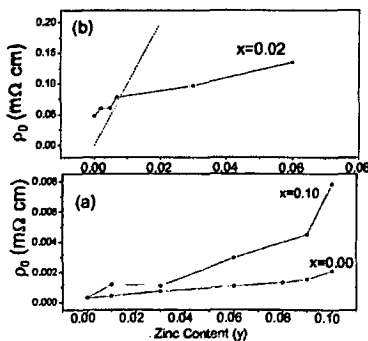


Fig. 4. Variation of residual resistivity ρ_0 as a function of Zn content y in $Y_{1-x}Pr_xBa_2[Cu_{1-y}Zn_y]_3O_{7-\delta}$ samples: (a) for $x = 0, 0.10$ and (b) for $x = 0.20$. The dotted line in (b) indicates the unitarity limit with the carrier density $n = 0.25$.

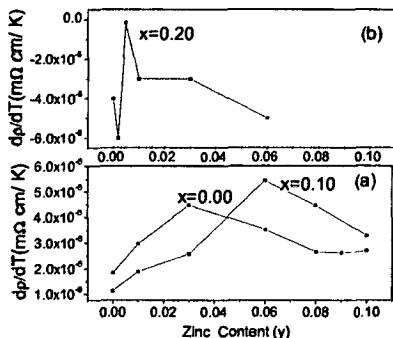


Fig. 5. Slope dp/dT vs. zinc content y for different values of $Y_{1-x}Pr_xBa_2[Cu_{1-y}Zn_y]_3O_{7-\delta}$ samples: (a) for $x = 0, 0.10$ and (b) for $x = 0.20$.

enough to reach the unitarity value of $h/4e^2$ and induces superconductor to insulator transition.

In Fig. 4b we plot the unitarity line besides the ρ_0 vs. y curve using the relation 1 [16]:

$$\rho_0 = \frac{4\hbar n_i}{e^2 n} \sin^2 \delta_0. \quad (1)$$

Here $\delta_0 = \pi/2$, $n_i = (3/2)y$. The value of n , the hole concentration per plane is taken to be 0.25 [16]. It is seen that ρ_0 comes close to the unitarity line till $y = 0.01$ when superconducting state exists.

4. Conclusion

We conclude that due to the hole depletion process Pr is able to bring the system in the underdoped region so that a small percentage of Zn is able to induce a superconductor-insulator transition. Such a situation

has been observed earlier by Fukuzumi et al. [17] for Zn impurity alone by controlling the oxygen content in Y-123 system. We feel that it is easier to obtain the same results using Pr, since we can control the charge carrier density easily using the hole depletion mechanism.

Acknowledgments

Authors thank Prof. S.N. Bhatia, I.I.T. Powai and his research student for providing and help in carrying out four probe resistivity measurements. We extend our thanks to CSIR, UGC and DST New Delhi for providing us financial support under sponsored projects.

References

- [1] A.V. Narlikar, C.V. Rao, S.K. Agarwal, in: *Studies of High Temperature Superconductor*, Ed. A.V. Narlikar, Nova Science, New York 1989, Vol. 1, p. 341.
- [2] M. Mehbod, P. Wyder, R. Deltour, P. Duvigneaud, G. Maessens, *Phys. Rev. B* **36**, 8819 (1987).
- [3] J.M. Tarascon, P. Barboux, P.F. Miceli, L.H. Greene, G.W. Hull, M. Eibschutz, S.A. Sunshine, *Phys. Rev. B* **37**, 7458 (1988).
- [4] G. Xiao, M.Z. Cieplak, A. Gavrin, F.H. Streitz, A. Bakhshai, C.L. Chien, *Phys. Rev. Lett.* **60**, 1446 (1988).
- [5] Y. Xu, R.L. Sabatini, A.R. Moodenbaugh, Y. Zhu, S.G. Shyu, M. Suenaga, K.W. Dennis, R.W. McCallum, *Physica C* **169**, 205 (1990).
- [6] H. Alloul, P. Mendels, H. Casalta, J.F. Marucco, J. Arabshi, *Phys. Rev. Lett.* **67**, 3140 (1991).
- [7] A.J. Millis, S. Sachdev, C.M. Varma, *Phys. Rev. B* **37**, 4975 (1988).
- [8] R. Lal, *Phys. Rev. B* **51**, 640 (1995).
- [9] G.V.M. Williams, J.L. Tallon, R. Meinhold, *Phys. Rev. B* **52**, R7034 (1995).
- [10] G.D. Liu, Z.X. Zhao, G.C. Che, *Solid State Commun.* **109**, 495 (1999).
- [11] J.S. Zhou, J.B. Goodenough, H. Sato, M. Naito, *Phys. Rev. B* **59**, 3827 (1999).
- [12] Y. Yu, G. Cao, Z. Jiao, *Phys. Rev. B* **59**, 3845 (1999).
- [13] R. Fehrenbacher, T.M. Rice, *Phys. Rev. Lett.* **70**, 3471 (1993).
- [14] A.R. Gupta, R. Lal, A. Sedky, A.V. Narlikar, V.P.S. Awana, *Phys. Rev. B* **61**, 11752 (2000).
- [15] C. Daniel, E. Marian, A. Terrell, *J. Chem. Educ.* **64**, 847 (1987).
- [16] T.R. Chien, Z.Z. Wang, N.P. Ong, *Phys. Rev. Lett.* **67**, 2088 (1991).
- [17] Y. Fukuzumi, K. Mizubashi, K. Takenaka, S. Uchida, *Phys. Rev. Lett.* **76**, 684 (1996).